Investigation of Complex Intracellular Dynamics using the Ribosome Flow Model

A Thesis Submitted

in Partial Fulfilment of the Requirements

for the Degree of

DOCTOR OF PHILOSOPHY

by

Aditi Jain

(2018maz0007)

DEPARTMENT OF MATHEMATICS

INDIAN INSTITUTE OF TECHNOLOGY ROPAR

May, 2024

To
My Grandparents

Declaration of Originality

I hereby declare that the work which is being presented in the thesis entitled **"Investigation of Complex Intracellular Dynamics using the Ribosome Flow Model"** has been solely authored by me. It presents the result of my own independent investigation/research conducted during the time period from January 2019 to February 2024 under the supervision of Dr. Arvind Kumar Gupta, Associate Professor at the Department of Mathematics, IIT Ropar.

To the best of my knowledge, it is an original work, both in terms of research content and narrative, and has not been submitted or accepted elsewhere, in part or in full, for the award of any degree, diploma, fellowship, associateship, or similar title of any university or institution. Further, due credit has been attributed to the relevant state-of-the-art and collaborations (if any) with appropriate citations and acknowledgments, in line with established ethical norms and practices. I also declare that any idea/data/fact/source stated in my thesis has not been fabricated/ falsified/ misrepresented. All the principles of academic honesty and integrity have been followed. I fully understand that if the thesis is found to be unoriginal, fabricated, or plagiarized, the Institute reserves the right to withdraw the thesis from its archive and revoke the associated Degree conferred. Additionally, the Institute also reserves the right to appraise all concerned sections of society of the matter for their information and necessary action (if any). If accepted, I hereby consent for my thesis to be available online in the Institute's Open Access repository, inter-library loan, and the title & abstract to be made available to outside organizations.


Signature

Name: Aditi Jain
Entry Number: 2018maz0007
Program: PhD
Department: Mathematics
Indian Institute of Technology Ropar
Rupnagar, Punjab 140001

Date: 10th May, 2024

Acknowledgement

I want to express my heartfelt gratitude to all those who have made diverse contributions, each in their unique way, to the successful completion of this thesis. During my PhD journey, I am fortunate enough to be surrounded by amazing and supportive individuals. The journey entails more than just conducting research papers and publishing them; it encompasses a multitude of experiences beyond mere academia.

First and foremost, I express my sincere gratitude to my PhD advisor, Dr. Arvind Kumar Gupta, for his invaluable guidance, patience, consistent support, and encouragement. His expertise has played a pivotal role in shaping the trajectory of my work. He always understand things and very calmly gives his best advice to me. I really thank him for making me the best version of myself.

I am appreciative of the members of my doctoral committee—Dr. S. C. Martha, Dr. Arun Kumar, Dr. Partha Sharathi Dutta, and Dr. Subhendu Sarkar—for their feedback, valuable suggestions, and continuous evaluation of my research progress. I also express my sincere thanks to the Reviewers—Professor Tamir Tuller and Professor Malay Banerjee for evaluating my thesis and providing positive feedback on it.

I want to extend my sincere gratitude to our collaborator Professor Michael Margaliot for his invaluable suggestions and for providing significant input in my research work. Again thanks to Arun Sir for his helpful insight and advice in collaboration with our research work. I would also like to thank Naman for his patience and help in completing our research problem.

I express my gratitude to IIT Ropar for extending financial support, which has been instrumental in enabling this research. I am also thankful for the provision of essential facilities and a conducive research environment. The research works were partially supported by the FIST program of the Department of Science and Technology, Government of India, Reference No. SR/FST/MS-I/2018/22(C). Furthermore, I appreciate the assistance of Mr. Neeraj Sharma, our office assistant, in handling technical requirements. Additionally, I acknowledge the support of Ms. Jaspreet Kaur in efficiently managing various official tasks and always listening to our not-so-big issues.

My sincere appreciation goes out to the members of my research group – Akriti, Bipasha, Ankita, Nikhil, Naman, Shankha, and Ashish – for engaging in insightful discussions and enjoyable dinner outings. I offer special thanks to Bipasha and Ankita for listening attentively to my issues throughout the PhD journey and always

giving helpful and encouraging advice.

I consider myself fortunate to have had the constant support of wonderful friends throughout my time at IIT Ropar. A heartfelt thank you goes to my close-knit group, including Vikas, Sahil, Monika, Sonam, and Niharika. Your friendship has been a source of joy and support. From shared laughter to navigating challenges, each of you has played a special role in making life's journey more meaningful. I extend my sincere gratitude, with a special acknowledgment to Sonam and Niharika. These two have been my rock, always there for me through thick and thin. Their support means the world to me, and I can't express how grateful I am for their constant presence in my life. They have turned the ups and downs into shared experiences, making this journey incredibly special. I would also like to express my gratitude for the delightful friendships with Amrendra, Taranjot, Surya, Arzoo, Himanshu, Gopika, Kusum, Priya, Ayantika, Swati, Sakshi, Smita, Kapil, Akshay and others. Each of you has added a special touch to my journey, and I truly appreciate the joy you've brought into my life.

In conclusion, I wish to extend profound appreciation to my family. Thank you all for always being there and trusting in my abilities. I feel incredibly fortunate to have such incredible parents and their blessings have always propelled me to reach new heights. I want to express my deep gratitude and love for my brothers – Akshit, Sidham, and Navkar, for their steadfast support throughout my academic journey. The occasional reunions have been imbued with immense joy, thanks to the delightful presence of my sweet and caring younger brother, Navkar. Special thanks to my Nanaji for his wonderful advice and encouragement for always keeping a positive attitude towards life. Lastly, I am grateful to the Divine Entity, Almighty God, whose unfathomable and limitless powers have consistently provided me with the resilience and wisdom required to navigate the challenges of my doctoral endeavors. Thank you God for making things happen at the right place and time.

The successful culmination of this thesis is indebted to the collaborative support and contributions of these individuals and institutions. For this, I extend my heartfelt gratitude.

Finally, I want the reader to believe in these two thoughts:

- Always let your conscience be your guide.
- Choose to be optimistic, it feels better.

Certificate

This is to certify that the thesis entitled **"Investigation of Complex Intracellular Dynamics using the Ribosome Flow Model"**, submitted by **Aditi Jain (2018maz0007)** for the award of the degree of **Doctor of Philosophy** of Indian Institute of Technology Ropar, is a record of bonafide research work carried out under my guidance and supervision. To the best of my knowledge and belief, the work presented in this thesis is original and has not been submitted, either in part or full, for the award of any other degree, diploma, fellowship, associateship or similar title of any university or institution.

In my opinion, the thesis has reached the standard fulfilling the requirements of the regulations relating to the Degree.

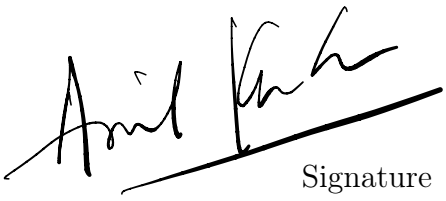

Signature

Dr. Arvind Kumar Gupta
Department of Mathematics
Indian Institute of Technology Ropar
Rupnagar, Punjab 140001

Date: 15th May 2024

Abstract

Movement is an important part of life. For example, in a central and fundamental process known as gene expression, there is a movement of biological particles called RNA polymerases on the DNA strand to produce messenger RNA (mRNA). Then, ribosomes move sequentially along an mRNA molecule and decode it to produce functional proteins. In intracellular transport within living organisms, motor proteins move along microtubules to transport cargo from one location to another. Another prominent example is the vehicular traffic in a city, where people or goods are transported to another place via pathways. Understanding these complex transport phenomena has been a significant area of research in mathematics, biology, and physics. It requires developing appropriate mathematical and computational models to analyze the flow of particles in these systems. Over the years, the Ribosome Flow Model (RFM), obtained via a mean-field approximation of a stochastic model called the Totally Asymmetric Simple Exclusion Process (TASEP), has provided a rigorous mathematical framework for the analysis. It is a deterministic, continuous-time model for analyzing the flow of interacting particles, and its dynamics are described by ordinary differential equations (ODEs). It is amenable to both mathematical and numerical analysis. The results of the RFM analysis can be used to model and engineer gene expression.

In this thesis, we rely on the framework of RFM to model and analyze the dynamical flow of particles along an ordered chain of sites encapsulating various biologically observed features. We specifically focus on formulating a system of non-linear ordinary differential equations, where the densities of each site on a lattice serve as the state variables and understand their asymptotic behavior. Exploring cooperative irreducible systems of ODEs with a first integral exhibiting positive gradient, we leverage results on the global phase portrait of such systems in our proposed models. Additionally, contraction theory proves to be a powerful tool for establishing asymptotic properties, such as convergence to steady-state and entrainment to a periodic excitation.

There are certain types of uncertainties present in the system leading to variability in the parameters modeling the dynamics. In this direction, we develop a framework to understand the flux of particle flow in the transport system having different site capacities. Next, drawing inspiration from complex cellular processes like intracellular transport where particles having extended length interact through binding and repelling actions and can detach along the microtubule, we investigate the impact of interactions and detachment phenomena on the output rate. Further, motivated by experimental studies on collision-stimulated abortive termination of

ribosomes, we develop a modeling framework to analyze the production rate under various circumstances. Next, we derive a network model for large-scale translation in the cell that encapsulates important cellular properties like ribosome drop-off and attachment. We explore the effects of ribosome drop-off on production rates to understand how drop-off influences the total production rate in the system. Moving ahead, we develop a closed network system modeling simultaneous particle movement along tracks with varying capacities in a resource-limited environment. This facilitates the study of competition for shared resources and the development of network models with feedforward and feedback connections between the tracks. Inspired by real-world systems where entry rates into a lane are influenced by nearby pools' occupancy, we develop a model where parallel lanes are strategically connected to multiple finite pools. This model takes into account the distribution of particles in a local neighborhood.

In summary, we develop mathematical models that capture intricate features of several biological and physical systems. These frameworks yield deeper insights into how parameters influence system dynamics, enhancing our comprehension of the underlying processes.

Keywords: Transport Phenomena; Mathematical Modeling; Ribosome Flow Model; Ordinary Differential Equations; Cooperative Theory; Contraction Theory; Steady-State.

Publications

- **Articles from the content embodied in this thesis**

1. Aditi Jain, Michael Margaliot, and Arvind Kumar Gupta. "Large-scale mRNA translation and the intricate effects of competition for the finite pool of ribosomes." *Journal of the Royal Society Interface* 19(188): 20220033, 2022.
2. Aditi Jain and Arvind Kumar Gupta. "Modeling transport of extended interacting objects with drop-off phenomenon." *Plos one* 17(5): e0267858, 2022.
3. Aditi Jain and Arvind Kumar Gupta. "Modeling mRNA translation with ribosome abortions." *IEEE/ACM Transactions on Computational Biology and Bioinformatics* 20(2): 1600-1605, 2022.
4. Aditi Jain, Arun Kumar, and Arvind Kumar Gupta. "A theoretical framework to analyse the flow of particles in a dynamical system with stochastic transition rates and site capacities." *Royal Society Open Science*, 9(10): 220698, 2022.
5. Aditi Jain and Arvind Kumar Gupta. "Large-scale closed and generalized networks of ribosome flow model with different site sizes." *Physica D: Nonlinear Phenomena* 455: 133881, 2023.
6. Aditi Jain and Arvind Kumar Gupta. "A mathematical framework for analyzing particle flow in a network with multiple pools." *Royal Society Open Science* 11: 231588, 2024.

- **Other publications**

1. Aditi Jain and Arvind Kumar Gupta. "A closed network of RNA polymerase flow models for analyzing intracellular transport" (under review).
2. Naman Krishna Pande, Aditi Jain, Arun Kumar, and Arvind Kumar Gupta. "Conservative deep neural networks for modeling competition of ribosomes with extended length" (under review).

Contents

List of Figures

List of Symbols

$\mathbb{R}$	The set of real numbers
$\mathbb{R}_+$	The set of non-negative real numbers
$\mathbb{R}^+$	The set of positive real numbers
$\mathbb{R}^n$	The set of n-dimensional real vectors
$\mathbb{R}^n_+$	The set of n-dimensional non-negative real vectors
$\mathbb{R}^n_{++}$	The set of n-dimensional positive real vectors
$\mathbb{R}^{n\times n}$	The set of matrices having dimension n with real entries
$\mathbb{R}^{n\times n}_+$	The set of matrices having dimension n with non-negative real entries
C^n	n-dimensional closed unit cube
$\text{int}(C^n)$	The interior of C^n
∂C^n	The boundary of C^n

Chapter 1

Introduction

1.1 Transport phenomena

Over the years, unraveling the intricate dynamics of transport phenomena has remained a focal point for scientists and engineers in various research domains such as Mathematics, Physics, Biology, and more. Understanding the underlying mechanisms driving these transport processes is crucial in analyzing their respective dynamics. Many natural or man-made transport processes can be viewed as non-equilibrium systems where 'particles' move along a one-dimensional lattice of ordered 'sites'. The concepts of self-driven and field-driven dynamics describe two different mechanisms by which particles move within these systems. Self-driven dynamics involve internal forces propelling particles autonomously, while field-driven dynamics result from external fields exerting forces on particles. There is a non-zero particle flux present in these systems which allows the particles to flow preferentially in a particular direction. Hence, to analyze the collective movement of particles in such systems, it is important to gain insights about the non-equilibrium steady-states.

A pivotal and fundamental process within this realm is gene expression, which converts genetic information into proteins [1]. Gene expression comprises two primary stages: transcription and translation. In transcription [2], biological particles known as RNA polymerases (RNAPs) move to interpret the instructions encoded in specific regions of the DNA strand, generating messenger-RNA (mRNA) (see Fig. 1.1a). The mRNA consists of codons, with each codon corresponding to a specific amino acid. In the subsequent translation stage [3], ribosomes sequentially traverse the mRNA and the successive tRNA molecules bring amino acids to the ribosome, and the growing polypeptide chain is formed through peptide bond formation, ultimately yielding functional proteins (see Fig. 1.1b). The polypeptide chain, in turn, represents the initial linear form of a protein, with its final structure and function determined by the specific sequence of amino acids.

Another notable example involves intracellular transport [2], where molecular motors facilitate the movement of cargo between the cell's center and periphery (see

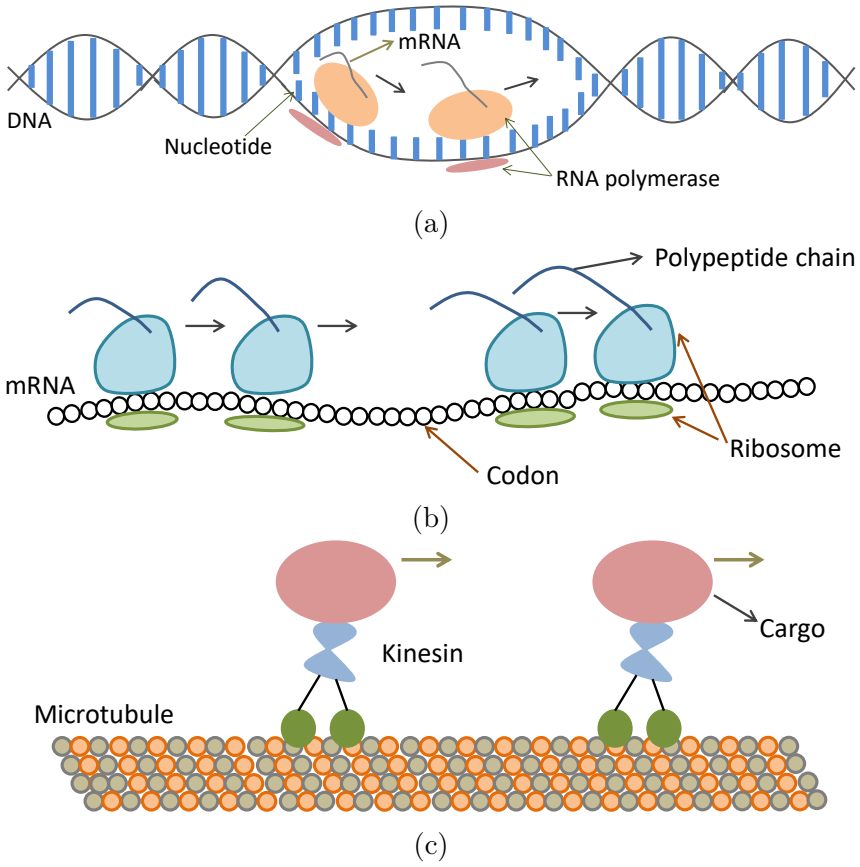

Figure 1.1: Biological processes: a) DNA transcription into mRNAs by RNA polymerases. b) mRNA translation to produce polypeptide chains by ribosomes. c) Intracellular transport to deliver cargo by kinesin.

Fig. 1.1c). These motors navigate along microtubule pathways, utilizing the energy generated through adenosine triphosphate (ATP) hydrolysis [4]. Additionally, the transportation of goods in a city's vehicular traffic serves as another instance, illustrating the movement of vehicles from one location to another [5]. Linear communication networks provide yet another example, where data packets traverse a structured arrangement of buffers [6].

The analysis of these transportation processes commonly involves employing a model depicting the flow of particles along an ordered sequence of sites known as a lattice or track. The particles' movement may exhibit either unidirectional flow, as seen in gene translation [7], or bidirectional flow, as observed in gene transcription [8, 9]. To enhance the overall flow, multiple particles often traverse the same lattice simultaneously. For instance, several ribosomes concurrently decode the same mRNA molecule to increase protein production [10, 11]. In general, these moving particles possess volume and are unable to pass through a particle positioned in front of them. This leads to adherence to a simple exclusion principle, asserting that along the lattice, two particles cannot occupy the same site simultaneously.

Consequently, a stalled particle can trigger the formation of "traffic jams" behind it. Substantial evidence supports the existence of traffic jams involving ribosomes, RNAPs, and motor proteins [10, 12, 13].

The proper functioning of these transport processes is crucial for the survival of any living organism. For example, specific mutations in molecular motor components can give rise to various neurological conditions, such as Alzheimer's disease, viral transport issues, and kidney diseases [14]. Additionally, research indicates that ribosome drop-off may lead to potentially non-functional proteins, contributing to developmental defects [15]. The consequences of traffic jams are also of significant interest in understanding how particle density relies on system parameters [16, 17]. Despite years of in vivo and in vitro studies on these transport processes, certain properties remain inadequately analyzed due to experimental constraints. Consequently, there is a need to develop suitable models to scrutinize the movement of biological particles within the realms of biotechnology and synthetic biology.

In investigating cellular transport phenomena, scientists employ mathematical and computational models to analyze both qualitatively and quantitatively [18, 19, 20, 21]. Mathematical models are becoming increasingly significant in understanding particle flow dynamics because they can be used to make qualitative and quantitative predictions about the effects of changing parameters on system dynamics [22, 23, 24, 25]. Models with a steady state or several steady states are useful in numerous studies in system biology [26]. This is so as the steady state has been used to accurately predict several features of the biological experiments that are generally performed in a very specific experimental environment [27, 28]. These models aid in the identification of useful control parameters and in understanding the influence of system structure and parameters on the particle density along the chain. Another objective involves determining optimal parameter values that lead to achieving an optimal production rate. Their significance is notably pronounced in synthetic biology, wherein biological modules undergo modification or redesign [29].

1.2 Totally asymmetric simple exclusion process

The conventional model of translation is the totally asymmetric simple exclusion process (TASEP) introduced by Mac-Donald *et al* [30]. It is a stochastic model for modeling the unidirectional flow of particles along an ordered lattice. The term "simple exclusion" represents that the particles hop forward with some probability to a neighboring site provided it is empty. This describes the fact that the particles cannot overtake each other due to their volume constraint. In TASEP with open

boundary conditions, the particles enter the chain from the environment and exit the chain into the environment. Fig. 1.2 depicts the topology of TASEP with open boundary conditions along the chain having n sites. The input rate into the chain is denoted by $\alpha > 0$, the hopping rate from site i to site $i+1$ is denoted by $\gamma_i > 0$, and the exit rate from the chain is denoted by $\beta > 0$. During a short time interval $[t, t + \Delta T]$, a particle enters the chain with probability $\alpha \Delta T$, provided the first site is empty, hop from site i to site $i+1$ with probability $\gamma_i \Delta T$, provided site $i+1$ is empty, and exit the chain with probability $\beta \Delta T$.

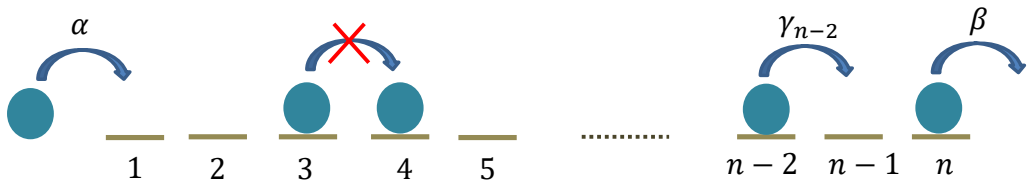

Figure 1.2: TASEP with open boundary conditions.

The TASEP has been used to study a large number of transport phenomena ranging from intracellular transport to pedestrian dynamics [22, 31, 32]. However, due to the indirect interactions between the particles, rigorous analysis of TASEP is still a challenge, and closed-form results exist only in the case of the homogeneous TASEP or in particular cases such as when only one or two rates differ from all the others. In the non-homogeneous case, one resort to extensive and time-consuming Monte Carlo simulations [33, 34, 35]. Several mathematical models, such as those based on Petri nets and probabilistic Boolean networks, have been proposed, but they often entail lengthy and laborious calculations [36, 37].

Reuveni *et al.* introduced a dynamical model called the ribosome flow model (RFM) for translation and it has been used extensively to study transport in cell biology with many applications [38]. It is a deterministic dynamical model for describing the evolution of particle densities in a finite chain with unidirectional movement that obeys the 'soft' version of the simple exclusion principle. The dynamics of the RFM are described by nonlinear ordinary differential equations (ODEs) [39].

The next section describes the dynamics of the RFM.

1.3 Ribosome flow model

The RFM is a continuous-time model for analyzing the flow of particles along n consecutive sites [39]. During modeling the flow of ribosomes in the translation process, mRNA molecules are coarse-grained into a lattice consisting of n sites of

codons. The entry of particles from the environment to the first site of the lattice is regulated by a transition rate λ_0. The flow of particles from site i to site $i+1$ is regulated by a transition rate λ_i for $i = 1, 2, \ldots, n-1$. The transition rate at which particles exit the lattice is regulated by λ_n. The rates λ_i, $i = 0, 1, \ldots, n$ are positive numbers and has units of 1/time. The exact values of λ_i's can be determined based on the biophysical properties of the phenomena modeled by the RFM. For example, in the translation process, these properties include the tRNA pool of the organism, the codon composition of each site, the local folding of mRNA molecule, and the number of free available ribosomes [38, 40]. The occupancy or density level of site i at time t is represented by a state variable $x_i(t) : \mathbb{R}_+ \to [0, 1]$, for $i = 1, 2, \ldots, n$. Here, $x_i(t) \in [0, 1]$ represents the probability how occupied site i is, where $x_i(t) = 0$ [$x_i(t) = 1$] means that site i is completely empty [completely occupied] at time t. The topology of the RFM is described in Fig. 1.3.

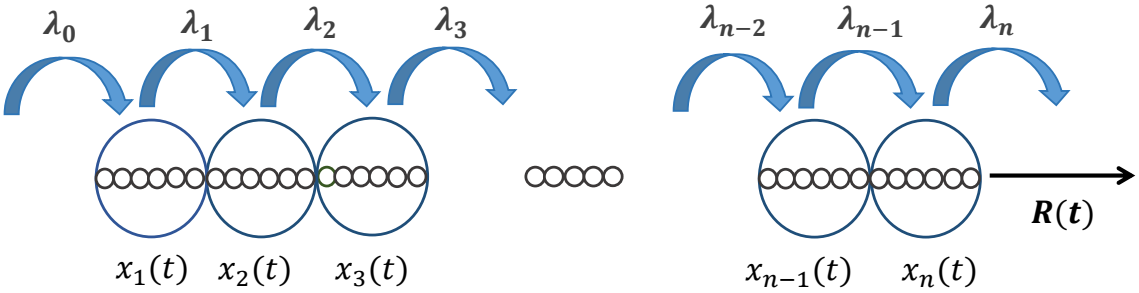

Figure 1.3: The RFM models unidirectional flow along a chain of n sites. The density at site i at time t is represented by $x_i(t) \in [0, 1]$. The transition rate from site i to site $i+1$ is regulated by a parameter $\lambda_i > 0$, with λ_0 and λ_n regulating the initiation and termination rates, respectively. $R(t)$ denotes the output rate at time t.

The dynamics of the RFM is given by n nonlinear first-order ODEs:

$$\begin{aligned}
\dot{x}_1 &= \lambda_0(1 - x_1) - \lambda_1 x_1(1 - x_2), \\
\dot{x}_2 &= \lambda_1 x_1(1 - x_2) - \lambda_2 x_2(1 - x_3), \\
&\vdots \\
\dot{x}_n &= \lambda_{n-1} x_{n-1}(1 - x_n) - \lambda_n x_n.
\end{aligned} \tag{1.1}$$

Defining $x_0(t) \equiv 1$ and $x_{n+1}(t) \equiv 0$ allows to write the above equations more succinctly:

$$\dot{x}_i = \lambda_{i-1} x_{i-1}(1 - x_i) - \lambda_i x_i(1 - x_{i+1}), \quad i \in \{1, \ldots, n\}. \tag{1.2}$$

The flow of particles from site i to site $i+1$ increases with the occupancy level of

particles at site i and decreases as site $i+1$ becomes fuller. This corresponds to a "soft" version of the simple exclusion principle in TASEP. Hence, the rate of flow of particles from site i to site $i+1$ is proportional to x_i and $(1-x_i)$ [vacancy level at site $i-1$] and is given by $\lambda_i x_i(1-x_{i+1})$. Thereby, Eq. (1.2) states that the change in the state variable x_i as a function of time t is equal to the flow entering from site $i-1$ to site i minus the flow leaving from site i to site $i+1$. The rate of flow of particles out of the system is the output rate given by $R(t) := \lambda_n x_n$. In the case of mRNA translation, the output rate of ribosomes from the mRNA is also called translation (protein production) rate. Since the state variables represent normalized density levels, the state-space of the RFM is $C^n := [0,1]^n$.

Thus, RFM is a nonlinear compartmental system, where each x_i represents a normalized amount of "material" in the ith compartment and the dynamics describe the flow of material from one compartment to another (see Fig. 1.4). Compartmental systems play an important role in various biological domains including cellular growth, pharmacokinetics, and epidemiology [41, 42].

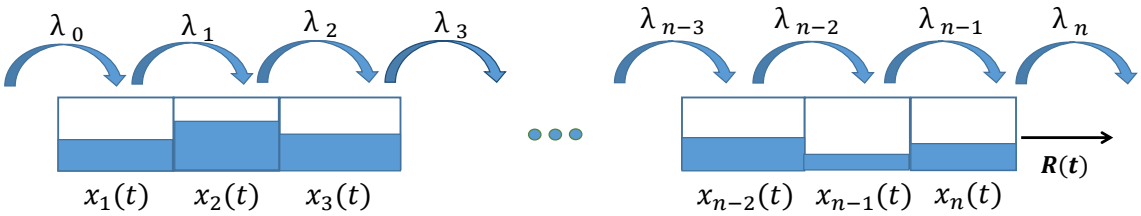

Figure 1.4: The RFM as a compartmental system where $x_i(t)$ denote the normalized amount of "material" in compartment i at time t.

The RFM can be derived via a mean-field approximation for the occupation probabilities of the sites of TASEP with open boundary conditions. The advantage of this model is that it is highly amenable to rigorous numerical and mathematical analysis using tools from systems and control theory [39]. The theory of TASEP focuses on phase transitions [23], domain wall theory [43], etc., which is different from the control-theoretic approach used to analyze RFM. Also, the analysis of the RFM provides results that are valid for any number of sites n. In contrast, the analysis of the TASEP provides approximate results that become more accurate as n is taken to be very large. Furthermore, the analysis of the RFM holds for any set of feasible rates including the case where the rates differ from one another. From modeling intricate dynamics to analyzing stability, predicting future states, and optimizing processes, the application of RFM theory significantly contributes to the understanding of complex transport phenomena [44, 45, 46].

We next address the relevant concepts and results that describe the dynamical properties of the RFM.

1.4 Dynamical properties of RFM

For two vectors $a, b \in \mathbb{R}^n$, we write $a \leq b$ if $a_i \leq b_i$ for all $i = 1, \ldots, n$, $a < b$ if $a_i \leq b_i$ and $a_i < b_i$ for some i, and $a \ll b$ if $a_i < b_i$ for all $i = 1, \ldots, n$. Similarly, for two control function $u, v : \mathbb{R}_+ \to \mathbb{R}_+$, we write $u \leq v$ if $u(t) \leq v(t)$ for all $t \geq 0$. Let $x(t, a)$ denote the solution of Eq. (1.1) at time $t \geq 0$ for the initial condition $a \in C^n$.

1.4.1 Invariance

Defining an invariant set is an important aspect of analyzing dynamical systems. The existence of an invariant set entails bounds for the solution's behavior [47]. In this thesis, the main focus lies on modeling cellular transport through dynamical systems generated by a system of nonlinear differential equations. Therefore, it is important to consider such state spaces that form an invariant set for the system.

Definition 1.4.1. A set C is invariant if a solution starts in C and stays in it for all $t \geq 0$.

Proposition 1.4.1 ([39])**.** *The state space C^n is an invariant set for the dynamics of the RFM, i.e., if $a \in C^n$ then $x(t, a) \in C^n$ for all $t \geq 0$.*

In other words, every trajectory emanating from any initial condition in the state space remains in it for all $t \geq 0$.

1.4.2 Repelling boundaries and persistence

Consider a time-varying dynamical system:

$$\dot{y} = f(t, y), \tag{1.3}$$

whose trajectories evolve on $\Omega = I_1 \times I_2 \cdots \times I_N \subset \mathbb{R}^n$, where each I_k is an interval of the form $[0, c], c > 0$ or $[0, \infty)$, $t \in [0, \infty)$ is the time, and f is nonlinear vector field which is continuously differentiable. Let $y(t, a)$ denote the solution of (1.3) at t for the initial condition a.

Definition 1.4.2 ([48])**.** The vector field f has the *boundary repelling* (BR) property if given any $\epsilon > 0$ and each sufficiently small $\Delta > 0$, there exists $M = M(\epsilon, \Delta)$ such that for each $i \in \{1, 2, \ldots, n\}$ and each $t \geq 0$, the condition

$$y_i(t) \leq \Delta \quad \text{and} \quad y_j \geq \epsilon \quad \text{for every} \quad j \in \{1, 2, \ldots, i-1\} \tag{1.4}$$

implies that

$$f_i(t, y) \geq M. \tag{1.5}$$

In other words, every $y_i(t)$ is separated from zero after an arbitrarily short time.

Definition 1.4.3 ([49]). The vector field f has the *cyclic boundary repelling* (CBR) property if given any $\epsilon > 0$ and each sufficiently small $\Delta > 0$, there exists $M = M(\epsilon, \Delta)$ such that for each $i \in \{1, 2, \ldots, n\}$ and each $t \geq 0$, the condition

$$y_i(t) \leq \Delta \quad \text{and} \quad y_{i-1} \geq \epsilon \quad (\text{where} \quad y_0 \equiv y_n) \tag{1.6}$$

implies that

$$f_i(t, y) \geq M. \tag{1.7}$$

In particular, if system (1.3) have a first integral then this property is important to conclude that the trajectories get repelled from the boundaries.

Proposition 1.4.2 ([48, 49]). *Suppose that vector field f satisfies BR (CBR) property and for any $\tau > 0$, $x_i(\tau) > 0$ implies that $x_i(t) > 0$, for all $i \in \{1, 2, \ldots, n\}$ and all $t \geq \tau$. Then given any $\delta > 0$ there exists $\epsilon = \epsilon(\delta) > 0$, with $\epsilon(\delta) \to 0$ as $\delta \to 0$, such that every solution $y(t, a)$ satisfies*

$$y_i(t, a) \geq \epsilon, \quad \textit{for all} \quad t \geq \delta \quad \textit{and} \quad i \in \{1, 2, \ldots, n\}. \tag{1.8}$$

The following result shows that trajectories of (1.1) that emanate from an initial condition in C^n become uniformly separated from the boundary of C^n.

Proposition 1.4.3 ([48]). *Consider the RFM. For any $\delta > 0$ there exists $\epsilon = \epsilon(\delta) > 0$, with $\epsilon(\delta) \to 0$ as $\tau \to 0$, such that for any $a \in C^n \setminus \{0\}$ we have*

$$\epsilon \leq x_i(t, a) \leq 1 - \epsilon, \quad \textit{for all} \quad t \geq \delta \quad \textit{and} \quad i \in \{1, 2, \ldots, n\}. \tag{1.9}$$

In other words, after an arbitrarily short time, each state variable is in the range $[\epsilon, 1 - \epsilon]$. This implies that, after an arbitrarily short time $\tau > 0$, every site along the lattice is neither completely empty nor completely full.

To explain the usefulness of Proposition 1.4.3, consider the Jacobian $J(x)$ of the vector field of the RFM given by

$$\begin{bmatrix} -\lambda_0 - \lambda_1(1-x_2) & \lambda_1 x_1 & 0 & \dots & 0 \\ \lambda_1(1-x_2) & -\lambda_1 x_1 - \lambda_2(1-x_3) & \lambda_2 x_2 & \dots & 0 \\ & & \ddots & & \\ 0 & 0 & 0 & \dots & \lambda_{n-1}x_{n-1} \\ 0 & 0 & 0 & \dots & -\lambda_n x_n \end{bmatrix}.$$

For any $x \in C^n$, all the entries of $J(x)$ are non-zero and it may become reducible for values x on the boundary of $[0,1]^n$. However, $J(x)$ is irreducible for all $x \in (0,1)^n$. Thus, Proposition 1.4.3 is useful in guaranteeing that after an arbitrarily short time, the matrix J becomes an irreducible matrix. This property is important in analyzing the asymptotic properties of the RFM.

1.4.3 Monotonicity

Let $\Omega \subset \mathbb{R}^n$ be an open set. Consider a system of n ODEs:

$$\dot{y} = f(y), \tag{1.10}$$

where $f : \Omega \to \mathbb{R}^n$ is a continuously differentiable function. We assume that the solution exists for all $t \geq 0$. Let $y(t,a)$ denote the solution of (1.10) at time t for the initial condition a.

Definition 1.4.4 ([50], Chapter 3)**.** Let $<_R$ denote any of relations $\leq$, $<$ and $\ll$. The vector field $f : \Omega \to \mathbb{R}^n$ is said to satisfy the *Kamke* condition if for any vectors $a, b \in \Omega$ satisfying $a <_R b$, we have $f_i(a) <_R f_i(b)$.

The next result implies that the flow is monotone.

Theorem 1.4.1 ([50], Chapter 3)**.** *Suppose that the vector field f satisfies the Kamke condition. Then for $a <_R b$, we have*

$$y(t,a) <_R y(t,b), \quad \textit{for all} \quad t \geq 0. \tag{1.11}$$

One way to verify that the Kamke condition holds is based on the sign structure of the Jacobian matrix J whose ij entry is $\frac{\partial f_i}{\partial y_{ij}}$.

Definition 1.4.5 ([51])**.** System (1.10) is called *cooperative* if for each $y \in \Omega$, $\frac{\partial f_i}{\partial y_j}(y) \geq 0$ for any $i \neq j$. If a cooperative system satisfies $\frac{\partial f_i}{\partial y_j}(y) = 0$ for any $|i-j| > 1$, then it is called a *tridiagonal cooperative system*. Furthermore, if $\frac{\partial f_i}{\partial y_j}(y) > 0$ for any $|i-j| = 1$, then it is called *strongly cooperative tridiagonal system* (SCTS).

Proposition 1.4.4. *For a cooperative system defined on an open convex set Ω, the resulting local flow is monotone.*

Proof. By the fundamental theorem of calculus for line integrals [52], we have

$$f_i(b) - f_i(a) = \int_0^1 \frac{\partial f_i}{\partial y_j}(a + (b-a)r)(b_j - a_j)dr. \tag{1.12}$$

We have $\frac{\partial f_i}{\partial y_j}(y) \geq 0$ for any $i \neq j$, therefore the above equation implies $f_i(a) \leq f_i(b)$. Hence, by Theorem 1.4.1 the flow of (1.10) is monotone. □

Proposition 1.4.5 ([39])**.** *For any $a, b \in C^n$ with $a <_R b$, the solution of the RFM satisfy*

$$x(t,a) <_R x(t,b), \quad \textit{for all} \quad t \geq 0. \tag{1.13}$$

This has the following interpretation. If $b_i \geq a_i$ for all i, we say that a density profile b is "more occupied" than a. The above proposition guarantees that this relation between the corresponding density profiles of the RFM remains true for all time.

1.4.4 Contractivity

Contraction theory is a potent tool for analyzing the behavior of certain nonlinear dynamical systems [53]. It is a powerful tool for proving asymptotic properties of the system including convergence to equilibrium and entrainment to a periodic excitation [54, 55].

We consider a general deterministic dynamical system of the form:

$$\dot{y} = f(t, y), \tag{1.14}$$

where $y(t) \in \Omega \subset \mathbb{R}^n$ is the state variable, $t \in [0, \infty)$ is the time and f is nonlinear vector field which is continuously differentiable. Let $y(t, a)$ denote the solution of (1.14) at t for the initial condition a. Given a vector norm $|.| : \mathbb{R}^n \to \mathbb{R}^+$, the induced matrix norm $||.|| : \mathbb{R}^{n\times n} \to \mathbb{R}^+$ is $||A|| = \max_{|y|=1} |Ay|$ and the induced matrix measure $\mu : \mathbb{R}^{n\times n} \to \mathbb{R}$ is $\mu(A) = \lim_{h\to 0} \frac{1}{h}(||I + hA|| - 1)$.

Definition 1.4.6 ([53])**.** The system (1.14) is called *contractive* if there exists a vector norm $|.|$ and $c > 0$ such that

$$|y(t,a) - y(t,b)| \leq \exp(-ct)|a - b|, \tag{1.15}$$

for any $a, b \in \Omega$ and all $t \geq 0$.

We focus here on the matrix measures to prove that the trajectories converge to each other exponentially.

Definition 1.4.7 ([55]). The given system (1.14) is said to be infinitesimally contracting on Ω if there exists a norm $||.||$ on Ω, with associated matrix measure μ, such that for some positive constant c (contraction rate) it holds that

$$\mu(J(t,y)) \leq -c, \quad \text{for all} \quad y \in \Omega \quad \text{and all} \quad t \geq 0. \tag{1.16}$$

The next result states that infinite contractivity implies global contractivity.

Theorem 1.4.2 ([55]). *Let Ω be convex and an invariant set of the dynamics of (1.14). Suppose that f is infinitesimally contracting on Ω with respect to a norm, $||.||$, with contraction rate c. Then for any two solutions $y_1(t)$ and $y_2(t)$, it holds that:*

$$||y_1(t) - y_2(t)|| \leq \exp(-ct)|y_1(0) - y_2(0)|, \quad \textit{for all} \quad t \geq 0. \tag{1.17}$$

Certain dynamical systems from system biology are not contracting with respect to any norm but become eventually contractive after arbitrarily short transients in time or amplitude. Indeed, the study of contraction after initial transients seems reasonable as this notion is usually used to prove asymptotic properties of the dynamical system. We next define two forms of *generalized contractive systems*(GCSs).

Definition 1.4.8 ([56]). The system (1.14) is said to be *contractive after a small overshoot and short transient* (SOST) on Ω with respect to a norm $|.|$ if given any $\epsilon > 0$ and $\tau > 0$ there exists $c = c(\tau, \epsilon) > 0$ such that

$$|y(t+\tau, a) - y(t+\tau, b)| \leq (1+\epsilon)\, \exp(-ct)\, |a-b|, \tag{1.18}$$

for all $t \geq 0$ and all $a, b \in \Omega$.

The definition of SOST states that the system contracts at an exponential rate but only after an arbitrarily small time τ and with an arbitrarily small overshoot $(1+\epsilon)$.

Definition 1.4.9 ([56]). The system (1.14) is said to be *contractive after a small overshoot* (SO) on Ω with respect to a norm $|.|$ if given any $\epsilon > 0$ and $\tau > 0$ there exists $c = c(\tau, \epsilon) > 0$ such that

$$|y(t, a) - y(t, b)| \leq (1+\epsilon)\, \exp(-ct)\, |a-b|, \tag{1.19}$$

for all $t \geq 0$ and all $a, b \in \Omega$.

The definition of SO states that the system contracts at an exponential rate with an arbitrarily small overshoot $(1+\epsilon)$ and there is no time transient.

Note that SO implies SOST. The next definition provides a sufficient condition to show that system (1.14) is SOST with respect to a norm.

Definition 1.4.10 ([56]). The system (1.14) is said to be *nested contractive* (NC) on Ω with respect to a norm $|.|$ if there exist a convex set $\Omega_\xi \subset \Omega$ and norms $|.|_\xi : \mathbb{R}^n \to \mathbb{R}_+$, where $\xi \in (0, 1/2]$, such that the following conditions holds.

1. $\bigcup_{\xi\in(0,1/2]} \Omega_\xi = \Omega$, and $\Omega_{\xi_1} \subset \Omega_{\xi_2}$, for all $\xi_1 \geq \xi_2$.
2. For every $\tau > 0$ there exists $\xi(\tau) \in (0, 1/2]$, with $\xi(\tau) \to 0$ as $\tau \to 0$ such that $x(t, a) \in \Omega_\xi$, for all $a \in \Omega$ and all $t \geq 0$.
3. It is contractive on Ω_ξ with respect to a norm $|.|_\xi$.
4. The norms Ω_ξ converge to $|.|$ as $\xi \to 0$, i.e., for every $\xi > 0$ there exist $\delta = \delta(\xi) > 0$ with$\delta(\xi) \to 0$ as $\xi \to 0$ such that $(1-\delta)|w| \leq |w|_\xi \leq (1+\delta)|w|$, for all $w \in \Omega$.

Theorem 1.4.3 ([56]). *If the system (1.14) is NC with respect to a norm $|.|$ then it is SOST with respect to a norm.*

Also, it is interesting to know that under what conditions SO and SOST are equivalent. The following definition addresses this aspect.

Definition 1.4.11 ([56]). A system (1.14) is said to be *weakly expansive* (WE) if for any $\epsilon > 0$ there exist $\tau > 0$ such that

$$|y(t, a) - y(t, b)| \leq (1+\epsilon)|a - b|, \tag{1.20}$$

for all $a, b \in \Omega$ and all $t \geq \tau$.

Proposition 1.4.6 ([56]). *Suppose that the system (1.14) is WE. Then (1.14) is SO if and only if it is SOST.*

Let $|.|_1 : \mathbb{R}^n \to \mathbb{R}_+$ denote the L_1 norm, i.e., for $x \in \mathbb{R}^n$, $|x|_1 = |x_1| + |x_2| + \cdots + |x_n|$. The next result shows that the solutions of the RFM are contracting after an arbitrarily small overshoot.

Proposition 1.4.7 ([48]). *Given any $\epsilon > 0$ there exist $\gamma = \gamma(\epsilon) > 0$ such that the solutions of the RFM satisfy*

$$|x(t, a) - x(t, b)|_1 \leq (1+\epsilon)\ \exp(-\gamma t)|a - b|_1, \tag{1.21}$$

for all $a, b \in C^n$ *and all* $t \geq 0$.

Proof: It can be proved that the RFM satisfies SOST property by referring to Definition 1.4.10. It can be easily observed that RFM is WE (see Ref. [39]). Hence, by Proposition 1.4.6, RFM satisfies SO property.

The above contraction result is useful in implying that the RFM satisfies several useful and important asymptotic properties.

1.4.5 Global asymptotic stability

Theorem 1.4.4 ([51]). *Consider the system* (1.10) *to be a SCTS defined on* Ω. *Then either: a)* $\lim_{t\to\infty} y(t,a)$ *exists and is a steady-state point of the dynamics, or b) as* $t \to \infty$, $y(t,a)$ *eventually leaves any compact set.*

The following Brouwer Fixed-Point theorem guarantees the existence of the steady-state point of the system (1.1).

Theorem 1.4.5 ([57]). *Given that set* Ω *is compact and convex, and that function* $f : \Omega \to \Omega$ *is continuous, then there exists some* $k \in \Omega$ *such that* $f(k) = k$.

Theorem 1.4.6 ([39]). *The RFM admits a unique steady-state point* $e \in \text{int}(C^n)$ *that is globally asymptotically stable, i.e.,*

$$\lim_{t\to\infty} x(t,a) = e, \quad \textit{for all} \quad a \in C^n. \tag{1.22}$$

Proof: The proof can be concluded by combining the fact that the RFM is a strongly cooperative tridiagonal system with the above theorems. Also, the framework of contraction theory provides a tool to conclude the existence of a steady state for the RFM.

Thus, any set of transition rates λ_i, $i = 0, 1, \ldots, n$ induces a unique steady-state value and any trajectory of the RFM converges to this value, regardless of the initial point. The next simple example demonstrates the dynamical behavior of the RFM.

Example 1.4.1. Consider the RFM with dimension $n = 3$, rates $\lambda_0 = 1.1654$, $\lambda_1 = 1.0426$, $\lambda_2 = 1.0249$, and $\lambda_3 = 1.2086$. Fig. 1.5 depicts trajectories for six different initial conditions $[0.5 \;\; 0 \;\; 0]'$, $[0 \;\; 0.5 \;\; 0]'$, $[1 \;\; 0 \;\; 0]'$, $[0 \;\; 1 \;\; 1]'$, $[1 \;\; 0 \;\; 1]'$, and $[1 \;\; 1 \;\; 1]'$. It can be seen that the three solutions converge to the same point.

1.4.6 Entrainment

Many biological systems are excited by periodic signals, for example, the 24-hour solar day. Proper functioning requires biological mechanisms to synchronize with

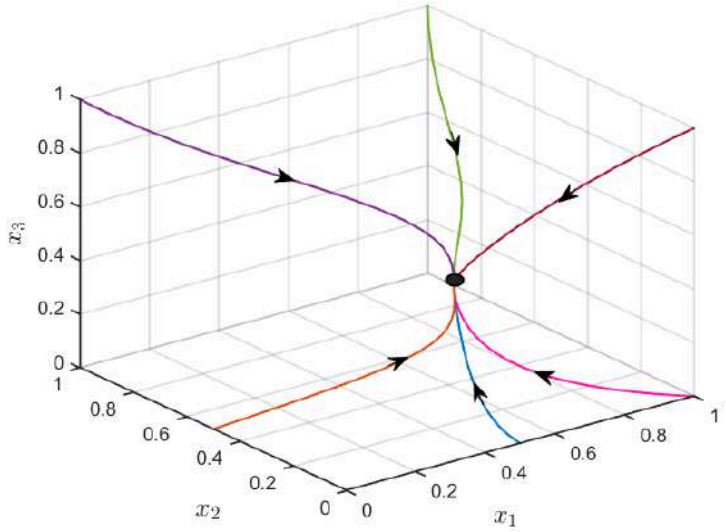

Figure 1.5: Trajectories of the RFM in Example 1.4.1 for six different initial points in $\text{int}(C^n)$. The unique steady-state point is marked by an ellipse.

the periodic excitations. An important question is whether the system converges to a periodic pattern with the same period as the excitation. It is well-known that stable linear time-invariant systems entrain [58]. There are nonlinear systems that may not entrain, for example, their trajectories may display a chaotic pattern rather than converge to a periodic pattern [59]. There are however two important classes of nonlinear systems that do entrain: contraction systems and cooperative systems that admit a first integral.

The next theorem is an important result that proves entrainment to a periodic excitation.

Theorem 1.4.7 ([56]). *Suppose that the system (1.14), with state y evolving on a compact and convex state-space Ω, is SOST and that the vector field f is T-periodic. Then it admits a unique periodic solution $\phi : [0, \infty) \to \Omega$ with period T and $y(t, a)$ converges to ϕ for any $a \in \Omega$.*

To study entrainment in the RFM, assume that the parameters λ_i are not constant, but are time-varying functions that are all jointly periodic with a period $T > 0$. More precisely, we assume that

- There exists a (minimal) $T > 0$ such that all the rate functions $\lambda_i(t)$ are non-negative, continuous and T-periodic.
- There exists $0 < \delta_1 \leq \delta_2$ such that $\lambda_i(t) \in [\delta_1, \delta_2]$, for all i and all $t \in [0, T)$.

We then refer to the network as the *periodic RFM*(PRFM). Note that a constant function is T-periodic for any T.

The next result shows that the PRFM entrains.

Theorem 1.4.8 ([48]). *The PRFM admits a unique function* $\phi : \mathbb{R}_+ \to \text{int}(C^n)$, *i.e., T-periodic and for any initial condition* $a \in C^n$, *the solution* $x(t, a)$ *of the PRFM converges to* ϕ *as* $t \to \infty$.

The next simple example demonstrates that the RFM entrains to the periodic excitations.

Example 1.4.2. Consider a PRFM with dimension $n = 4$, $\lambda_0 = 1$, $\lambda_i = 1$, $\lambda_2(t) = 2 + \sin(\pi t)$, $\lambda_3(t) = 3 + \sin(\pi t)$, and $\lambda_4 = 1$. Note that all the rates are periodic with a common minimal period $T = 2$. It can be seen from Fig. 1.6 that all the trajectories converge to the periodic solution with period $T = 2$.

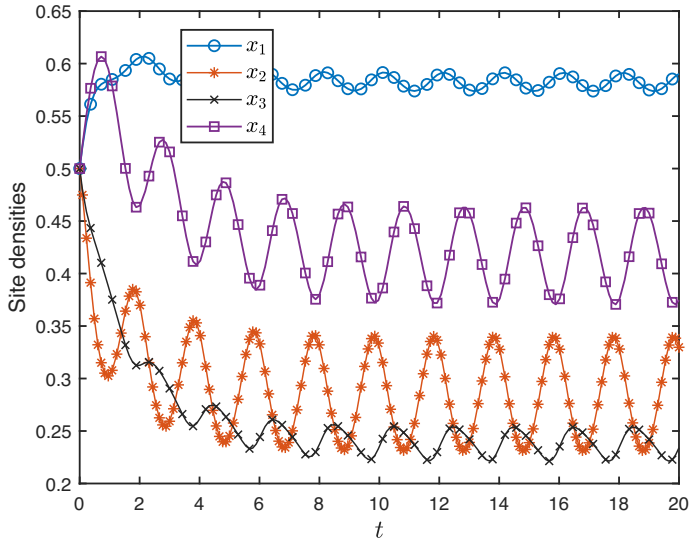

Figure 1.6: State variables x_i as a function of t in Example 1.4.2. Note that each state variable converges to a periodic function with a period $T = 2$.

1.4.7 Spectral representation of RFM

At the steady state, the time derivative of the state variables in Eq. (1.1) is zero, and this gives

$$\lambda_i e_i(1 - e_{i+1}) = R, \quad \text{for} \quad i = 0, 1, \ldots, n, \tag{1.23}$$

where $e_0 := 1$ and $e_{n+1} := 0$. Solving the above set of nonlinear equations is not trivial. However, there exists a spectral representation of the mapping from the λ_i's

to R [60]. Define the $(n+2)\times(n+2)$ tridiagonal matrix given by

$$A_n := \begin{bmatrix} 0 & \lambda_0^{-1/2} & 0 & \dots & 0 \\ \lambda_0^{-1/2} & 0 & \lambda_1^{-1/2} & \dots & 0 \\ 0 & \lambda_1^{-1/2} & 0 & \dots & 0 \\ & & \ddots & & \\ 0 & \dots & 0 & 0 & \lambda_n^{-1/2} \\ 0 & \dots & 0 & \lambda_n^{-1/2} & 0 \end{bmatrix}.$$

It has been proved that there is a simple maximal eigenvalue $\sigma > 0$, and let $\zeta \in \mathbb{R}^{n+2}_{++}$ be the corresponding eigenvector. It has been analyzed that steady-state densities satisfy

$$e_i = \frac{\zeta_{i+2}}{\lambda_i^{1/2}\zeta_{i+1}}, \quad \text{for all} \quad i \in \{1, 2, \dots, n\} \tag{1.24}$$

and

$$R = \frac{1}{\sigma^2}. \tag{1.25}$$

1.5 Simulations

Direct simulation. We numerically solve the equation in Matlab to obtain the set of steady-state occupancy probabilities and the steady-state rate of protein synthesis, R. We start from an mRNA strand which is empty of ribosomes, $x(0) = 0$. The densities are then found for a set of later times using Eq. (1.1) and Matlab's ordinary differential equation solver. The process stops when the vector $x(t)$ converges to the vector of steady-state density. More accurately, $x(t)$ is constant (up to we stop the process for a time t^* for which some prefixed numeric error threshold) for every $t > t^*$. The vector of steady state density and the protein production rate are then $x = e$ and $R = \lambda_n e_n$.

Stochastic simulation. Since the RFM is a mean-field approximation of TASEP, we ran MATLAB simulations of this process. A simulation begins with an empty chain of dimension n and continues for 10^7 time steps i.e., total simulation time. Each site can accommodate atmost one particle and a particle can only hop unidirectionally to a consecutive site if it is empty. Every site i, $i = 1, 2, \dots, n$ in the chain is associated with hopping rates λ_i's, where the next hopping event time $t_k + \epsilon_k$ is generated randomly. For site i, ϵ_k are random variables drawn from the exponential distribution with mean rate λ_i. If hopping time is equal to the simulation time, then the particle at site i hops to site $i+1$, provided site $i+1$ is empty. The occupancy at each site is averaged throughout the simulations with the first 10^3 time steps discarded from the calculations to obtain the average steady-state

reader density of each site.

To verify that the high correlation between the model and Monte Carlo simulations holds for a large set of parameters, we ran 400 tests, wherein each test a new set of rates are drawn randomly.

Example 1.5.1. Consider an RFM having dimensions $n = 40$. Assume that $\lambda_i = 1 + \theta_i$ where θ_i is a random variable uniformly distributed in the interval $(-\frac{1}{4}, \frac{1}{4})$. Fig. 1.7 depicts the correlations between the steady-state mean densities (ρ) of the RFMs and the steady-state mean densities (σ) calculated through Monte Carlo simulations. It can be seen that the correlation between the two is high ($r \simeq 0.93484$).

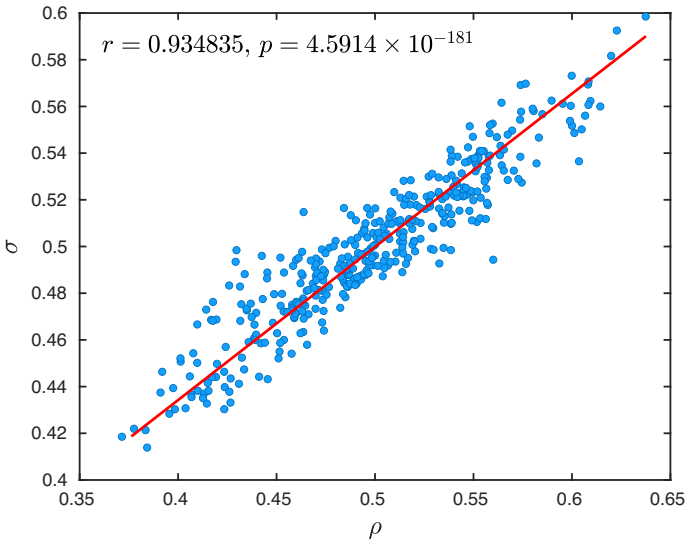

Figure 1.7: Steady-state mean densities (numerically simulated ρ and Monte Carlo simulated σ) and the corresponding Pearson's correlation coefficient r and p-value in Example 1.5.1.

Hence, Monte Carlo simulations support the modeling of dynamical aspects of translation using RFM.

1.6 Generalizations of the RFM

The RFM primarily analyzes the dynamical flow of ribosomes along the mRNA molecule during the translation process. Many important aspects: the effect of ribosome recycling [61], optimizing the protein production rate subject to convex constraints on the rates [44, 62, 63], stochastic variability in translation [64], and more have also been analyzed using tools from the theory of continued partial fractions [65] and random matrix theory [66]. Several generalizations of the RFM have been used to model numerous cellular central processes incorporating more

sophisticated and more realistic features into the dynamical systems modeling the movement of particles along the tracks. This includes ribosome flow model network with a pool (RFMNP) to study the impact of competition for the limited resources [49], excluded flow with local repelling and binding model (EFRBM) to model the flow of motor proteins along a one-dimensional lattice of sites with nearest-neighbor interactions between the motors [67], ribosome flow model with Langmuir kinetics (RFMLK) that models attachment and detachment of ribosomes along the mRNA molecule [68], the ribosome flow model with extended objects (RFMEO) that models the unidirectional flow of ribosomes that cover several site units [69], ribosome flow model with different site sizes (RFMD) that models the unidirectional flow of particles along a lattice having different site sizes [70], and many more. Next, we briefly review the dynamical properties of the enlisted models above.

1.6.1 Ribosome flow model network with a finite pool

Naturally, as cellular resources are finite, the cellular components available are in a limited amount, for example, it was estimated that there are approximately 24×10^4 ribosomes and 6×10^4 mRNA molecules in a yeast cell [71]. Biological evidence suggests that there is an indirect coupling between the mRNAs as they compete with each other for the limited availability of ribosomes [72]. Competition for shared finite resources is a substantial aspect of studying the biophysics of the cell. The investigation of the effect of a finite pool of ribosomes has been done by a model called RFMNP introduced by Raveh *et al.* using a mean-field TASEP approximation [49]. This is the very first model of a network composed of interconnected RFMs. In this model, a set of m RFMs with input are considered to represent different mRNA molecules parallelly competing for ribosomes. These are interconnected through a pool of free ribosomes. An important property of the RFMNP is that it is a closed system, so the total number of ribosomes remains conserved for all $t \geq 0$. Let $z(t)$ denote the pool density of free ribosomes at time t. The ith RFM has dimension n_i, transition rates $\lambda_j^i > 0$, an input measurable function G_i and output function y^i. The dynamics of the ith RFM in the network is thus given by:

$$\begin{aligned}
\dot{x}_1^i &= \lambda_0^i G_i(z)(1 - x_1^i) - \lambda_1^i x_1^i (1 - x_2^i), \\
\dot{x}_2^i &= \lambda_1^i x_1^i (1 - x_2^i) - \lambda_2^i x_2^i (1 - x_3^i), \\
&\vdots \\
\dot{x}_{n_i}^i &= \lambda_{n_i-1}^i x_{n_i-1}^i (1 - x_{n_i}^i) - \lambda_{n_i}^i x_{n_i}^i, \\
y^i &= \lambda_{n_i}^i x_{n_i}^i.
\end{aligned} \tag{1.26}$$

The output of each RFM is fed into the pool. Hence, the pool dynamics is given by:

$$\dot{z} = \sum_{i=1}^{m} y^i - \sum_{i=1}^{m} \lambda_0^i G_i(z)(1 - x_1^i). \tag{1.27}$$

In other words, all the ribosomes that exit the mRNAs feed the pool and the pool feeds the initiation sites in all the mRNAs (see Fig. 1.8).

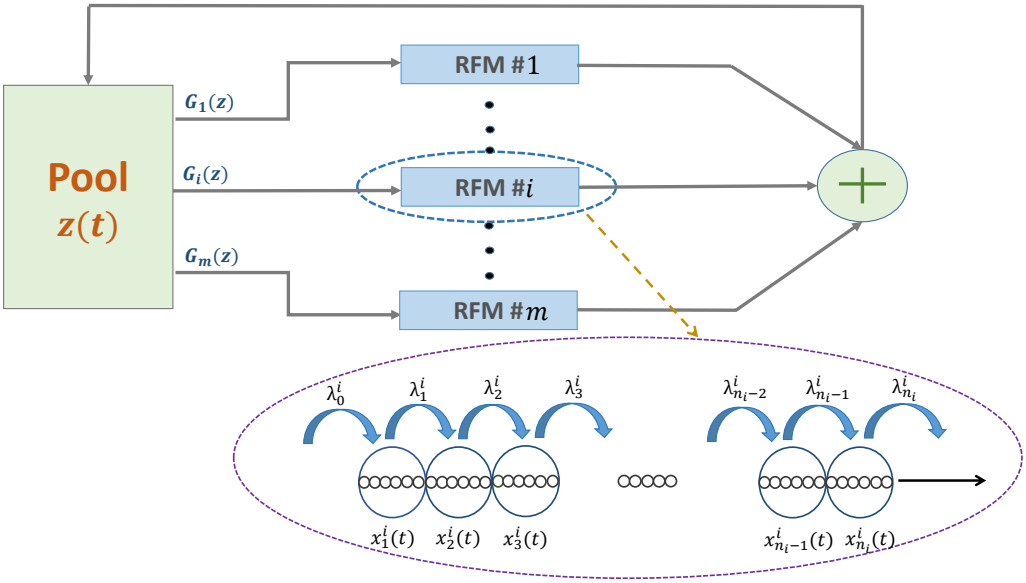

Figure 1.8: Each mRNA is described by an RFM with input and output. The output of each RFM is fed into the pool and the pool feeds the initiation rates of each RFM. The function G_i describes the likelihood that the particles from the pool will attach to the ith RFM.

Recall that every state variable x_j^i denotes the probability how occupied is the site j of ith mRNA molecule and the pool variable z represents an average number of free ribosomes in the pool. Therefore, the relevant state space of the RFMNP is:

$$\Omega := [0,1]^{n_1} \times \cdots \times [0,1]^{n_m} \times [0,\infty).$$

Let

$$H(t) := z(t) + \sum_{i=1}^{m} \sum_{j=1}^{n_i} x_j^i(t).$$

This is the total number of ribosomes in the system at time t. Thus, H is a first integral of the dynamics. Let $d := n_1 + \cdots + n_m + 1$, and let 1_d denote a column vector of d ones. For $s \geq 0$, let $L_s := \{a \in \Omega : 1_d' a = s\}$, i.e., the s level set of the first integral H. The next stability result provides a rigorous framework for analyzing the effect of competition by analyzing the steady-state behavior of the network after a change in the parameters.

Theorem 1.6.1 ([49]). *Every level set L_s contains a unique steady-state point e_{L_s} of the RFMNP and for any initial condition $a \in L_s$, the solution of the RFMNP converges to e_{L_s}.*

In other words, the RFMNP admits a continuum of steady-state points and every trajectory converges to a steady state.

1.6.2 Ribosome flow model with extended objects

In many biological flows, the particles are larger than their step sizes. For example, in DNA transcription, each RNAP typically covers between 42 and 51 nucleotides [73] and in mRNA translation, each ribosome typically covers about 10 to 11 codons [2]. In the RFM, mRNA molecules are coarse-grained into sites of consecutive codons. However, how to coarse-grain the mRNA in a systematic way to obtain the best fidelity between the model and the biological reality is still not clear. To encapsulate the feature that every ribosome occupies the codon it is translating and codons after it, a model called RFMEO was introduced [69]. The RFMEO is a continuous-time model that describes the unidirectional flow of ribosomes where every ribosome covers ℓ site units, with $1 \leq \ell \leq n$ [69]. The part of the ribosome translating the codon is referred to as the "reader".

The transition rates $\lambda_i > 0$ represent the flow of ribosomes from one codon to another, where λ_0 represents the rate at which the ribosomes start attaching to the mRNA, and λ_n represents the rate at which ribosomes stop translating the mRNA. Each codon on the n-dimension mRNA has a normalized reader density $x_k(t) \in [0,1]$ and a coverage density $y_k(t) \in [0,1]$ given by

$$y_k(t) = \sum_{i=\max\{1,k-\ell+1\}}^{k} x_i(t), \quad k = 1, 2, \ldots, n. \tag{1.28}$$

The dynamical equations describing the RFMEO are:

$$\begin{aligned}
\dot{x}_1 &= \lambda_0(1 - y_\ell) - \lambda_1 x_1(1 - y_{\ell+1}),\\
\dot{x}_2 &= \lambda_1 x_1(1 - y_{\ell+1}) - \lambda_2 x_2(1 - y_{\ell+2}),\\
&\vdots\\
\dot{x}_n &= \lambda_{n-1} x_{n-1}(1 - y_{\ell+n-1}) - \lambda_n x_n(1 - y_{\ell+n}),
\end{aligned} \tag{1.29}$$

with $y_k \equiv 0$ for all $k > n$.

More succinctly, we can write the above equations as follows:

$$\dot{x}_i = f_{i-1}(x) - f_i(x), \quad i = 1, 2, \ldots, n, \tag{1.30}$$

where

$$f_i(x) := \lambda_i x_i(1 - y_{i+\ell}), \quad i = 0, 1, \ldots, n, \tag{1.31}$$

with $x_i(t) \equiv 0$ and $y_i(t) \equiv 0$ for all $i < 1$ and $i > n$. The term $x_i(1-y_{i+\ell})$ represents that the reader flow from site i to site $i+1$ increases with the reader density at site i and decreases with the coverage occupancy level at site $i+\ell$ (see Fig. 1.9). Also, note that the equations describing the flow in the last sites are linear ones as the ribosome decoding the last ℓ codons can move without any hindrance towards the exit end of the mRNA.

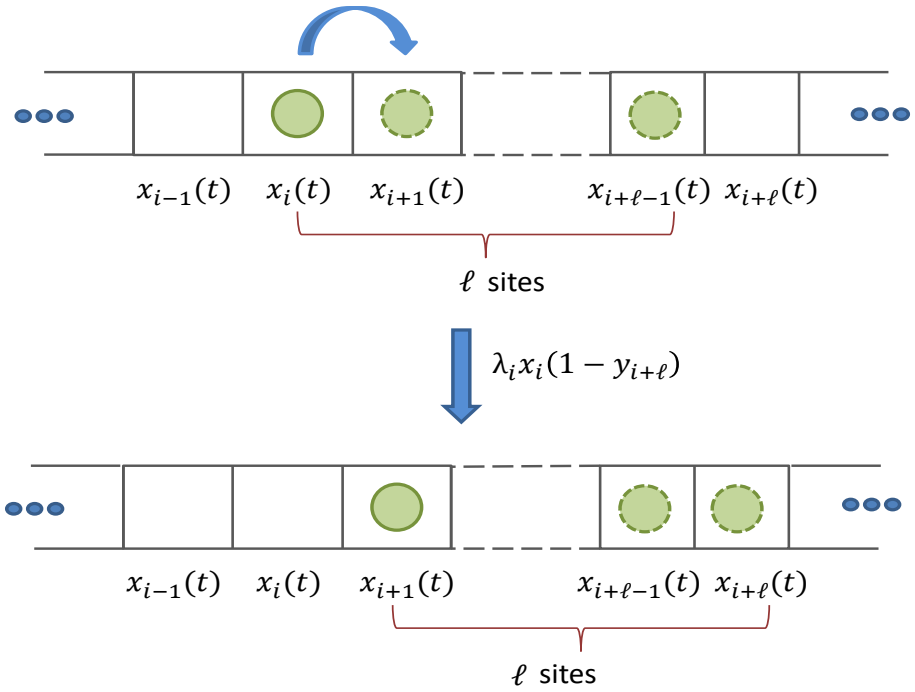

Figure 1.9: Ribosomes that cover ℓ sites scan the mRNA from left to right. The solid circle represents the reader location of the ribosome and the sites $i, i+1, \ldots, i+\ell-1$ are covered by the ribosome. The flow of ribosomes from site i to site $i+1$ is given by $\lambda_i x_i(1 - y_{i+\ell})$, where $y_{i+\ell}(t) = \sum_{k=i+1}^{i+\ell} x_k(t)$.

The RFMEO, unlike the RFM, is not a cooperative dynamical system. The RFM is a special case of RFMEO, with $\ell = 1$. Further, as x_k and y_k are densities, the state space is given as:

$$\Psi = \{x \in \mathbb{R}^n : x_k \in [0, 1] \text{ and } y_k \in [0, 1]\}. \tag{1.32}$$

The next result shows that the solutions of the RFMEO are contracting after an arbitrarily small overshoot and short transient.

Proposition 1.6.1 ([69]). *Given any $\epsilon > 0$ and each $\tau > 0$, there exist $\gamma = \gamma(\epsilon) > 0$*

such that the solutions of the RFMEO satisfy

$$|x(t+\tau,a)-x(t+\tau,b)|_1 \leq (1+\epsilon)\ \exp(-\gamma t)|a-b|_1, \tag{1.33}$$

for all $a, b \in \Psi$ *and all* $t \geq 0$.

The following theorem states for fixed parameters in the system, the trajectories corresponding to different initial states all converge to a unique steady-state point.

Theorem 1.6.2 ([69]). *The RFMEO admits a global asymptotically stable steady-state point* $e \in \text{int}(\Psi)$ *i.e.,*

$$\lim_{t\to\infty} x(t,a) = e, \quad \textit{for all} \quad a \in \Psi. \tag{1.34}$$

1.6.3 Ribosome flow model with Langmuir kinetics

Biological observations suggest that ribosomes may detach from the mRNA before reaching the stop codon due to different reasons such as the presence of premature codon, depletion in the concentration of tRNAs, or ribosome stalling [74, 75]. Also, it is known that ribosomes may get attached to a codon via internal ribosome entry sites (IRES), or due to leaky scanning [76]. To encapsulate all these features, a deterministic, nonlinear, and continuous-time model called ribosome flow model with Langmuir kinetics (RFMLK) was introduced [68]. The RFMLK is a coarse-grained mean-field approximation of TASEP with open boundary conditions and Langmuir kinetics. The RFMLK describes the flow of ribosomes along n consecutive sites of an mRNA molecule. It contains three sets of parameters:

- $\lambda_i > 0$, $i = 0, 1, \ldots, n$, controls the transition rate from site i to site $i+1$,
- $\alpha_i \geq 0$, $i = 1, \ldots, n$, controls the detachment rate from site i, and
- $\beta_i \geq 0$, $i = 1, \ldots, n$, controls the attachment rate to site i.

Each parameter has units of 1/time. The probability that how occupied site i is at time t is represented by a state variable $x_i(t)$. The dynamical equations describing the RFMLK are:

$$\begin{aligned}
\dot{x}_1 &= \lambda_0(1-x_1) - \lambda_1 x_1(1-x_2) + \beta_1(1-x_1) - \alpha_1 x_1,\\
\dot{x}_2 &= \lambda_1 x_1(1-x_2) - \lambda_2 x_2(1-x_3) + \beta_2(1-x_2) - \alpha_2 x_2,\\
&\vdots\\
\dot{x}_n &= \lambda_{n-1} x_{n-1}(1-x_n) - \lambda_n x_n + \beta_n(1-x_n) - \alpha_n x_n.
\end{aligned} \tag{1.35}$$

The term $\alpha_i x_i$ represents the detachment of particles from site i to the environment, whereas $\beta_i(1-x_i)$ represents the attachment of particles from the environment to site i. The topology of the RFMLK is depicted in Fig. 1.10. By setting some of the α_i's and β_i's to positive values and the others to zero, it is possible to model drop-off and internal entry of ribosomes at specific sites.

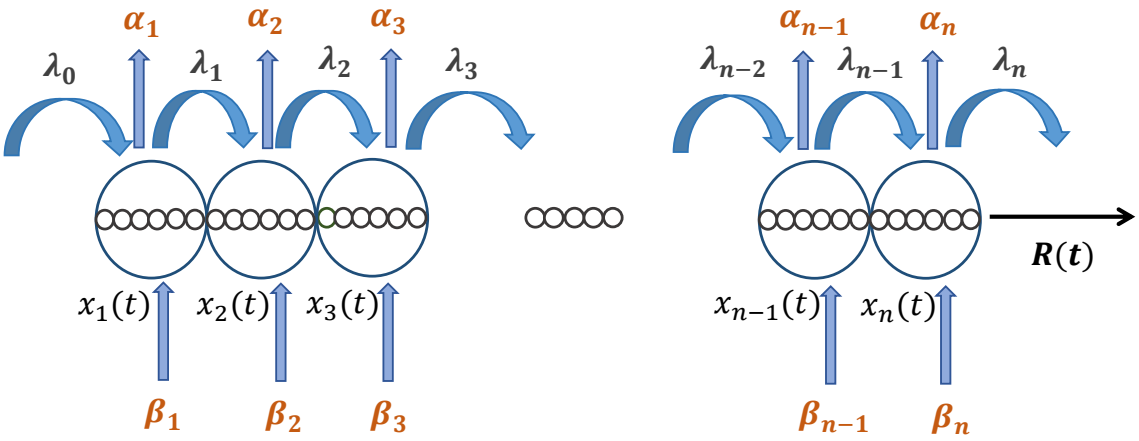

Figure 1.10: The RFMLK models unidirectional flow along a chain of n sites. The density at site i at time t is represented by $x_i(t) \in [0,1]$. The transition rate from site i to site $i+1$ is regulated by a parameter $\lambda_i > 0$, with λ_0 and λ_n regulating the initiation and termination rates, respectively. The parameter $\alpha_i \geq 0$ [$\beta_i \geq 0$] controls the drop-off [attachment] rate from [to] site i. $R(t)$ denotes the output rate at time t.

The RFMLK, just like RFM, is a nonlinear tridiagonal compartmental model and the dynamical equations describe the flow between these compartments and also with the cellular environment. If $\alpha_i = \beta_i = 0$ for all i, then the model reduces to the RFM. The following contraction property helps to deduce the global behavior of the dynamical equations.

Proposition 1.6.2 ([68]). *Given any $\epsilon > 0$, there exist $\gamma = \gamma(\epsilon) > 0$ such that the solutions of the RFMLK satisfy*

$$|x(t,a) - x(t,b)|_1 \leq (1+\epsilon)\ \exp(-\gamma t)|a-b|_1, \tag{1.36}$$

for all $a, b \in C^n$ and all $t \geq 0$.

The next theorem implies that any solution of the RFMLK converges to a unique steady-state density.

Theorem 1.6.3 ([68]). *The RFMLK admits a unique steady-state $e \in \mathrm{int}(C^n)$ that is globally asymptotically stable, i.e.,*

$$\lim_{t\to\infty} x(t,a) = e, \quad \textit{for all} \quad a \in C^n. \tag{1.37}$$

In particular the output (production) rate $R := \lambda_n x_n + \sum_{i=1}^{n} \alpha_n x_n$ converges to a steady-state. The RFMLK demonstrates the effect of the drop-off of ribosomes on the mRNA translation process. It is intuitive to expect that detachment of ribosomes from a jammed site may reduce congestion and hence increase the flow. This is not true as drop-off results in truncated and non-functional proteins that are of no use in cellular activities. The next result shows that detachment always decreases the steady-state output R.

Proposition 1.6.3 ([68]). *Suppose we modify RFMLK by changing α_j to $\bar{\alpha}_j$, with $\alpha_j < \bar{\alpha}_j$, for any $j \in \{1, 2, \ldots, n-1\}$. Let $\bar{R}$ denote the steady-state output rate in the modified RFMLK. Then $\bar{R} < R$.*

1.6.4 Excluded flow with local repelling and binding model

Experimental investigations exhibit that intracellular transport phenomena are influenced by the presence of interactions between the particles. Transport by kinesins-1 along microtubules is an example of such behavior where kinesins-1 remains longer attached to the microtubule in the presence of neighboring motor proteins [77]. An extension of the RFM called excluded flow with local repelling and binding model (EFRBM) was introduced to include the nearest-neighbor interactions between the particles by incorporating two "force" interactions: repelling and binding forces with parameters r and q [67]. The EFRBM with n sites includes the following parameters:

- $\lambda_i > 0$, $i = 0, 1, \ldots, n$, controls the transition rate from site i to site $i+1$,
- $r \geq 0$ is the attachment/detachment force between the two existing neighbors,
- $q \geq 0$ is the attachment/detachment force between the two new neighbors.

Let

$$z_i(t) := \begin{cases} x_i(t) & i = 1, 2, \ldots, n, \\ 0 & \text{otherwise.} \end{cases} \tag{1.38}$$

The dynamical equations describing the EFRBM are as follows:

$$\dot{x}_i = f_{i-1}(x) - f_i(x), \quad i = 1, 2, \ldots, n, \tag{1.39}$$

where

$$f_i(x) := \lambda_i x_i (1 - x_{i+1})(1 + (q-1)z_{i+2})(1 + (r-1)z_{i-1}), \quad i = 1, 2, \ldots, n. \tag{1.40}$$

Eq. (1.39) implies that the change in the reader density at site i is the inflow $f_{i-1}(x)$ from site $i-1$ to site i minus the outflow $f_i(x)$ to site $i+1$. The term $(1+(q-1)z_{i+2})$ represents that the flow from site i to site $i+1$ also depends upon the density at site $i+2$ and increases [decreases] if $q>1$ [$q<1$]. The particle at site $i+2$ will attract [$q>1$] or repel [$q<1$] the particle that move from site i to $i+1$. Similarly, the term $(1+(r-1)z_{i-1})$ represents that the flow into site $i+1$ also depends upon the density at site $i-1$. The topology of the EFRBM is depicted in Fig. 1.11.

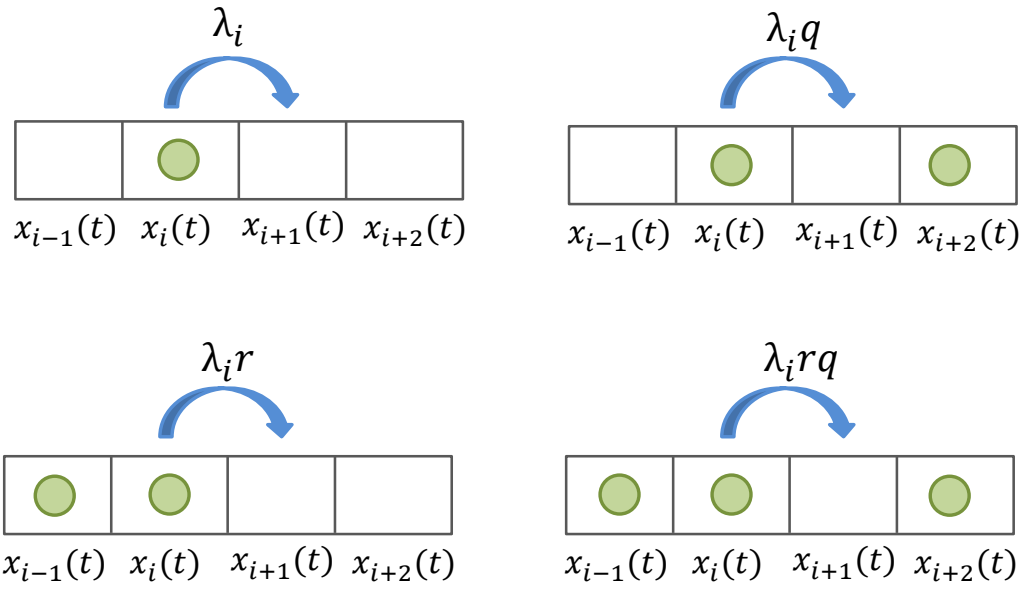

Figure 1.11: Schematic explanation of the transition flow from site i to site $i+1$ in the EFRBM. Upper-left: the transition rate is λ_i when both sites $i-1$ and $i+2$ do not contain particles. Upper-right: the transition rate is $\lambda_i q$ when site $i-1$ does not contain particle and site $i+2$ does. Lower-left: the transition rate is $\lambda_i r$ when site $i-1$ does contain particle and site $i+2$ does not. Lower-right: the transition rate is $\lambda_i rq$ when both sites $i-1$ site $i+2$ do contain particles.

The EFRBM, unlike the RFM, is not a cooperative dynamical system and if $r=q=1$ for all i, then the model reduces to the RFM. The following contraction property after a small overshoot helps to deduce the global behavior of the dynamical equations.

Proposition 1.6.4 ([67]). *Given any $\epsilon>0$, there exist $\gamma=\gamma(\epsilon)>0$ such that the solutions of the EFRBM satisfy*

$$|x(t,a)-x(t,b)|_1 \leq (1+\epsilon)\ \exp(-\gamma t)|a-b|_1, \tag{1.41}$$

for all $a,b\in C^n$ and all $t\geq 0$.

The next theorem implies that any solution of the EFRBM converges to a unique

steady-state density that depends on the rates λ_i, r, q, and is independent of the initial conditions.

Theorem 1.6.4 ([67]). *Assume that $r, q > 0$. The EFRBM admits a unique steady-state $e \in \text{int}(C^n)$ that is globally asymptotically stable, i.e.,*

$$\lim_{t\to\infty} x(t,a) = e, \quad \textit{for all} \quad a \in C^n. \tag{1.42}$$

1.6.5 Ribosome flow model with different site sizes

In the previous generalizations of the RFM, the capacity of each site or compartment is taken to be equal. However, each site along the compartment can have a different size, for example, if we consider the flow of vehicles down a road, then the capacity changes depending on the number of parallel lanes. A dynamical model called ribosome flow model with different site sizes (RFMD) was introduced to analyze the effect of different site capacities on the dynamics of the flow [70]. To incorporate the feature of different site sizes each particle in this model hops forward to the next site not only if it is vacant, but also if it is ready to accept the particle. The model contains two sets of parameters:

- $\lambda_i > 0$, $i = 0, 1, \ldots, n$ controls the transition rate from site i to site $i+1$, and
- $q_i \in (0, 1]$ describes the capacity at site i.

The dynamics of the RFMD is given by the set of n nonlinear ordinary differential equations:

$$\begin{aligned}
\dot{x}_1 &= \lambda_0(q_1 - x_1) - \lambda_1 x_1(q_2 - x_2),\\
\dot{x}_2 &= \lambda_1 x_1(q_2 - x_2) - \lambda_2 x_2(q_3 - x_3),\\
&\vdots\\
\dot{x}_n &= \lambda_{n-1} x_{n-1}(q_n - x_n) - \lambda_n x_n.
\end{aligned} \tag{1.43}$$

The state variable $x_i(t) : \mathbb{R}_+ \to [0, q_i]$ describes the normalized occupancy level of site i at time t where $x_i(t) = 0$ $[x_i(t) = q_i]$ means that site i is completely empty [full] (see Fig. 1.12). The RFMD, just like RFM, is a nonlinear tridiagonal compartmental model where compartments can have different capacities and the dynamical equations describe the flow between these compartments. In the particular case, when $q_i = 1$ for all i, RFMD becomes the RFM.

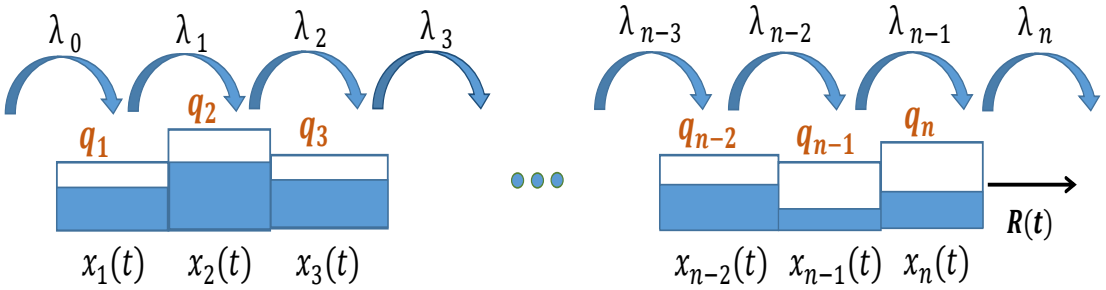

Figure 1.12: The RFM with different site sizes models the unidirectional flow along a chain of n sites. The density at site i at time t is represented by $x_i(t) \in [0, q_i]$, where $q_i \in (0, 1]$ represents the maximal possible capacity at site i. The transition rate from site i to site $i+1$ is regulated by a parameter $\lambda_i > 0$, with λ_0 and λ_n regulating the initiation and termination rates, respectively. $R(t)$ denotes the output rate at time t.

The state-space of the RFMD is:

$$C := \{x \in \mathbb{R}^n : \quad x_i \in [0, q_i], \quad i = 1, 2, \ldots, n\}.$$

The next theorem states that the transition rates and site sizes determine a unique steady-state e and any solution arising from different initial conditions in C converges to it.

Theorem 1.6.5 ([70]). *The RFMD admits a unique $e \in \text{int}(C)$ such that*

$$\lim_{t\to\infty} x(t, a) = e, \quad \textit{for all} \quad a \in C.$$

1.7 Aims and objectives

This thesis aims to predict the translation rates of ribosomes on a complex network, which otherwise is difficult to predict through experiments. This will give future directions to experimentalists for the further investigation of protein synthesis. These mathematical models can serve as an effective tool for designing synthetic biological circuits and have ramifications for biotechnology and human health. In addition, they can also be useful for modeling and analyzing vehicular flow, molecular traffic flow, pedestrian dynamics, and more. This thesis seeks to resolve unanswered questions by developing dynamical models that capture realistic biological phenomena occurring in cellular processes, specifically gene expression. The following are the main objectives of this thesis:

- To obtain a framework for analyzing a complex transport model that involves the flow of particles with stochastic transitions and stochastic site

capabilities. Certain types of randomness or uncertainty are always present in many nonlinear systems. The main goal of the model is to investigate the steady-state particle flux under the notion that parameters are random variables by using tools from the random matrix theory. The analysis can be generalized and applied to study the flow of particles in numerous transport systems in scenarios where rates depend on local factors.

- Examining the impact of interactions and detachment phenomena during the flow of particles having extended length along the track. The stimulation to do this problem comes from the fact that in many complex cellular processes such as intracellular transport carried by motor proteins, the particles are larger than their step sizes and they usually interact with one another by binding and repelling actions based on the state of its neighboring particles [78]. The methods rely on the theory of dynamical systems to predict properties of the steady state and its ratification through the numerical solution of the equations on selected examples.

- Understanding flow of ribosomes having extended length moving along mRNA, including the possibility of detachment of the particles due to several reasons like ribosome-ribosome collisions [79]. Motivated by the recent experimental studies on collision-stimulated abortive termination of the ribosomes [80, 79], we develop a deterministic modeling framework and analyze the steady state production rate under different circumstances, such as, with and without collisions with the neighboring ribosomes on the lattice. The formalism developed is general and can be applied to different scenarios by considering appropriate parameter values.

- Analyzing and developing a better understanding of large-scale simultaneous mRNA translation incorporating the possibility of attachment/detachment of ribosomes from the mRNA. Translation is the most energetically consuming process in the cell and the phenomena of ribosome drop-off from a single mRNA result in a decrease in production rate [81]. In the context of simultaneous translation of mRNA molecules: does drop-off still decrease the production rate? This work is motivated by the fact to analyze the effect of ribosome drop-off as this may perhaps increase the total production rate in the entire system, as it allows ribosomes to detach from slow sites, and then attach to the initiation sites of other mRNA molecules.

- Building a closed network system that can model the simultaneous movement of particles along tracks having sites of different capacities in a resource-limited environment. Thus, it allows for studying the important topic of competition

for shared resources. Moreover, developing a network model with feedforward and feedback connections between the tracks facilitates modeling a network of interconnected roads, where the flow out of one road may enter another road in the network or re-enter the same road.

- To analyze the dynamics of several parallel lanes connected strategically to multiple finite pools. This work is inspired by the fact that in many real-world systems, the entry rate of particles into a lane is affected by the occupancy of nearby pools. The main goal of the model is to investigate the effect of parameters on the system properties. As per our knowledge, there is no existing work in the context of RFM models that addresses the possibility of distinct pools that mimic various physical transport processes.

1.8 Outline of the thesis

In this thesis, various generalizations of the RFM-based models are presented that play a key role in understanding the different biophysical aspects of many complex transport phenomena including intracellular transport. These models capture several dynamical features of the phenomena which were not examined previously. Models with a steady-state or several steady-states are very useful in various studies not only related to system biology but also in other areas e.g., physical systems. In this respect, using tools from contraction theory and cooperative theory, we prove that the model admits a unique steady state. Secondly, we study the effect of a small increase/decrease in any of the parameters on the steady-state profile. Monte Carlo simulations are also performed supporting the modeling of intracellular processes using the dynamical system. We present the work into eight chapters that include the introductory (Chapter 1), six main chapters (from Chapter 2 to 7), and a conclusive chapter (Chapter 8). The summary of the contents of each main chapter is provided below.

Chapter 1: Introduction

This chapter briefs various important intracellular transport processes that require developing appropriate mathematical and computational models to analyze the flow of biological particles in the context of biotechnology and synthetic biology. Then we discuss an important deterministic model called the ribosome flow model (RFM). We provide a comprehensive insight into the dynamical properties of the RFM which include persistence, contractivity, cooperativity, stability, and entrainment. Next, we show that the RFM correlates with TASEP, supporting the modeling of intracellular processes such as translation and transcription using the RFM. Further, various generalizations of the RFM are reviewed that encapsulate several

other realistic features of the biological processes and further serve as the basis for developing more sophisticated and more realistic models.

Chapter 2: A theoretical framework to analyze the flow of particles in a dynamical system with stochastic transition rates and site capacities
In this chapter, we first study several dynamical properties of the RFMD which models the unidirectional movement of particles controlled by transition rates along a lattice having different site sizes. There are various types of stochasticity present in the systems due to several reasons such as experimental noise, uncertainty, etc. Therefore, we speculate the RFMD model in the stochastic environment to understand it in a better way. This work models the parameters as random variables with known distributions and investigates the steady-state flow rate under this notion by using tools from the random matrix theory. Some closed-form theoretical results are derived for the steady-state flow rate under some restrictive assumptions such as random variables being independent and identically distributed. Furthermore, for arbitrary but bounded stochastic transition rates, stochastic site capacities, or both, we establish bounds for the steady-state flow rate.

Chapter 3: Modeling transport of extended interacting objects with drop-off phenomenon
This chapter considers a deterministic model of cellular transport on a one-dimensional chain. The main novelty of the model is the inclusion of interactions between the extended objects. The study focuses on characterizing the steady state of the system under different circumstances, putting special emphasis on the steady outflow. The methods rely on the theory of dynamical systems to predict properties of the steady state and its ratification through the numerical solution of the equations on simple examples. The main result is an existence and uniqueness proof for the steady state. This work also shows examples of non-trivial behaviors such as detachment rates may help in increasing the steady-state flow by alleviating traffic jams that can exist due to several reasons like bottleneck rate or interactive forces between the particles. We also analyze the special case of our model, when there are no forces exerted by neighboring particles, and study the sensitivity of its steady-state to variations in the parameters.

Chapter 4: Modeling mRNA translation with ribosome abortions
The contents of this chapter are motivated by the recent experimental studies on collision-stimulated abortive termination of the ribosomes. We propose a deterministic mathematical model for the process of mRNA translation described by the flow of ribosomes having extended length moving along a one-dimensional track i.e., mRNA, including the possibility of detachment of the particles due to several reasons like ribosome-ribosome collisions. We prove that the model admits a

unique steady-state profile. Furthermore, we study the effect of parameters on the steady state through a theoretical framework in some cases. We also demonstrate that in some cases, the predictions of the proposed model are consistent with the previously proposed computational-based kinetic models. This work is important in the context of studying dynamical processes involving abortions due to collisions.

Chapter 5: Large-scale mRNA translation and the intricate effects of competition for the finite pool of ribosomes

In this chapter, we present a network model called RFM with Langmuir kinetics network (RFMLKN) that encapsulates important biological phenomena such as competition of a finite number of ribosomes leading to an indirect coupling between the mRNA molecules and also the possibility of attachment/detachment of ribosomes from the mRNA. In this work, we prove that the network always converges to a steady state and entrains periodic excitations in any of its rates. Next, we study its sensitivity to variations in parameters. Among our results, we study the effect of change in a hopping rate in an mRNA molecule on the network. This yields a local effect: an increase or decrease in the translation rate of this mRNA, and also the global effect: the translation rate of the other mRNA molecules either all increase or decrease. Next, we analyze that an increase in detachment [attachment] rate in one of the RFMLKs increases [decreases] the steady-state pool density and consequently increases [decreases] the density in each site in all the other RFMLKs.

Chapter 6: Large-scale closed and generalized networks of ribosome flow model with different site sizes

This chapter describes and analyzes in detail two mathematical models for the flow of "particles" along a set of "trails" e.g., ribosomes along a set of mRNA molecules. The models are deterministic and use ordinary differential equations to describe the occupancy levels at each site. The first large-scale network model that is introduced and analyzed is RFMDNP - RFMDs network with a pool. This is a closed system that can model the simultaneous movement of particles along tracks having sites of different capacities in a resource-limited environment. Thus, it allows for studying the important topic of competition for shared resources like ribosomes. Next, we introduce a generalized network of RFMDs called RFMDN. This models a network with feedforward and feedback connections between the RFMDs. For both models, we prove various analytical properties related to stability, entrainment, convexity, and more. Also, both models have been analyzed using the tools from the theory of cooperative systems. We also present plenty of useful synthetic examples to comprehend the results.

Chapter 7: A mathematical framework for analyzing particle flow in a network with multiple pools

This chapter studies a network of deterministic mathematical model ribosome flow models that are interconnected via multiple pools, where RFM provides a useful framework to model the flow of particles along a one-dimensional chain of sites. It captures the scenario where the particles in the vicinity of the lanes compete for entry into them. Firstly, we study a minimal model ribosome flow model network with two pools (RFMNTP) and then illustrate the methodology to study a network with multiple pools. Using the powerful theory of a cooperative dynamical system with a first integral, we prove that the network always converges to a unique steady state in every level set. Sensitivity analysis of the parameter's variation is also performed to understand overall the network behavior. This work provides results that will be useful in the context of analyzing networks of dynamical processes in which the entry rates of particles to a compartmental system are affected only by the nearby local density.

Chapter 8: Conclusion and future scopes

The concluding chapter contains the summary of the results discussed in the aforementioned main chapters of the thesis. We also consider some future directions that might aid in understanding the transport processes more deeply and thoroughly.

Chapter 2

A theoretical framework to analyze the flow of particles in a dynamical system with stochastic transition rates and site capacities

In this chapter[1], we study the stochasticity in an RFMD that models the unidirectional movement of particles controlled by transition rates along a lattice having different site sizes. The parameters are considered as random variables with known distributions and some closed-form theoretical results are derived for the steady-state flow rate under some restrictive assumptions such as random variables being independent and identically distributed. Furthermore, the bounds for the steady-state flow rate are established for arbitrary but bounded stochastic transition rates, stochastic site capacities, or both.

2.1 Introduction

In reality, there are various types of stochasticity present in transport systems due to several reasons such as intrinsic factors, experimental noise, uncertainty, etc. For example, in many cellular transport processes, chemical reactions are stochastic due to variability in the concentrations of the input factors and can produce probabilistic outcomes [82]. Therefore, it is necessary to speculate on these transport processes in the stochastic environment to understand them in a better way. A key factor to analyze is the flow rate and hence, it is of considerable interest to understand how this rate is affected under stochasticity in these processes. Generally, the stochastic effects are modeled by considering the parameters drawn from the probability distributions following certain physical arguments.

The RFMD is an important dynamical model for analyzing the movement of

[1]The content of this chapter is published as: "Aditi Jain, Arun Kumar, and Arvind Kumar Gupta. A theoretical framework to analyse the flow of particles in a dynamical system with stochastic transition rates and site capacities. *Royal Society Open Science*, 9(10): 220698, 2022."

particles along a one-dimensional track and encapsulates an important dynamical feature of different site sizes [70] (for details refer to Chapter 1). Therefore, it is crucial to understand this model with variable rates due to various levels of stochasticity. In this chapter, we characterize the notion of randomness in the RFMD in the sense that the parameters are random variables with known distributions and analyze the steady-state flow rate in the RFMD through a theoretical approach under this assumption. In particular, this also models the transport phenomena having stochastic variations in the transition rates and fixed site sizes. Our main results also include some closed-form results under restrictions such as rates are independent and identically distributed (i.i.d.) random variables. The analysis can be applied to study the flow of particles in numerous transport systems in the stochastic environment.

The content of the chapter is organized as follows. The next section recalls the dynamical properties of the RFMD that are relevant in our context. Section 2.3 describes our main theoretical results that are derived for the steady-state flow rate. In Section 2.4, we summarize the findings and finally present the proofs of all the theoretical results in Section 2.5.

2.2 Dynamical properties of the RFMD

Consider an RFMD with dimension n, having transition rates $\lambda_i \in \mathbb{R}_{++}$ for $i = 0, 1, \ldots, n$, site sizes $q_i \in (0, 1]$ for $i = 1, 2, \ldots, n$, and $q_{n+1} \coloneqq 1$.

More succinctly, the dynamical equations (1.43) describing the RFMD can be written as:

$$\dot{x}_i = \lambda_{i-1} x_{i-1}(q_i - x_i) - \lambda_i x_i (q_{i+1} - x_{i+1}), \quad i = 1, \ldots, n, \tag{2.1}$$

where $x_0(t) \coloneqq 1$ and $x_{n+1}(t) \coloneqq 0$.

Let $x(t, a)$ denote the solution of the RFMD at time t for the initial condition $x(0) = a$. Recall that the relevant state space is: $C \coloneqq \{x \in \mathbb{R}^n : \quad x_i \in [0, q_i], \quad i = 1, 2, \ldots, n\}$. It has been proved that there exists a unique $e \in \text{int}(C)$ such that for any initial condition in C, the solution belongs to $\text{int}(C)$ for all $t > 0$ and $\lim_{t\to\infty} x(t, a) = e$ [70].

At the steady-state, for $x = e$, we have

$$\begin{aligned}\lambda_0(q_1 - e_1) &= \lambda_1 e_1(q_2 - e_2)\\ &= \lambda_2 e_2(q_3 - e_3)\\ &\vdots\\ &= \lambda_{n-1} e_{n-1}(q_n - e_n)\\ &= \lambda_n e_n.\end{aligned}$$

To put it another way, at the steady state, the flow into and out of each site is equal. Let $R := \lambda_n e_n$ denote the steady-state flow or output rate. It is clear that obtaining the solution of nonlinear equations in (2.1) is not straightforward in general. However, it has been recently proved in Ref. [70] that the steady-state flow rate can be obtained from the spectral properties of a suitable tridiagonal matrix. Define $A_n : \mathbb{R}_+ \to \mathbb{R}^{(n+2)\times(n+2)}$ by

$$A_n(r) := \begin{bmatrix} 0 & \lambda_0^{-1/2} & 0 & \dots & 0\\ \lambda_0^{-1/2} & (1-q_1)r & \lambda_1^{-1/2} & \dots & 0\\ 0 & \lambda_1^{-1/2} & (1-q_2)r & \dots & 0\\ & & \ddots & & \\ 0 & \dots & 0 & (1-q_n)r & \lambda_n^{-1/2}\\ 0 & \dots & 0 & \lambda_n^{-1/2} & 0 \end{bmatrix}.$$

The above matrix $A_n(r)$ has real eigenvalues as it is symmetric. Further, each element of $A_n(r)$ is non-negative and $A_n(r)$ is irreducible implying that it has a simple maximal positive eigenvalue for each r [83]. It was shown in Ref. [70] that there exists a unique value $r^* \in (0, \infty)$ such that

$$\sigma(A_n(r^*)) = r^* \tag{2.2}$$

and the steady-state flow rate satisfies

$$R = \frac{1}{(\sigma(A_n(r^*)))^2}. \tag{2.3}$$

The spectral representation above shows that the steady-state flow rate in the RFMD depends on the transition rates and site capacities. This spectral representation has various useful theoretical implications. It has been used to obtain results on the sensitivity analysis and quasi-concavity of the steady-state flow rate. It also allows determining the upper and lower bounds of R when the rates are random variables with some known distributions using tools from probability theory.

The main results on the steady-state flow rate in the RFMD given random transition rates or random site capacities are presented in the next section.

2.3 Main results

Let $(\Omega, \mathcal{F}, \mathbb{P})$ be a probability space, and all random variables in the next subsections are defined on this common probability space. We call random variable X to be almost sure bounded if there exists $0 \leq c < \infty$ such that $\mathbb{P}[|X| \leq c] = 1$. Let $M_X := \inf_{c \geq 0} \{\mathbb{P}[|X| \leq c] = 1\}$ and $m_X := \sup_{c \geq 0} \{\mathbb{P}[c \leq |X|] = 1\}$. Let $\mathbb{R}_{\geq \delta} := \{x \in \mathbb{R} : \ x \geq \delta > 0\}$. The steady-state flow rate in the n-site RFMD is denoted by R_n.

We analyze the value of R_n given the random transition rates or the site capacities. In Subsection 2.3.1, we provide results on the value of R_n by assuming that the transition rates are random variables and the site capacities are deterministic. Subsection 2.3.2 deals with the case when the site capacities are random variables and the transition rates are deterministic. The last subsection analyzes R_n given the variability in all the rates.

2.3.1 The RFMD with stochastic transition rates

In this subsection, we consider randomness only in the transition rates i.e., we assume that the size of all the compartments is fixed and tackle stochasticity or uncertainties in the transition rates by assuming them as random variables with some known distributions. This situation may model, for example, variations in the speed of the vehicles due to different human behaviors along a multi-lane road where there is a change in the number of lanes along the road.

The random variable $Z := X^{-1/2}$ is almost sure bounded for X supported on $\mathbb{R}_{\geq \delta}$. We further examine the steady-state flow rate by investigating two cases: homogeneous and non-homogeneous site capacities. In the first case, we assume that all the site capacities are equal. This assumption is certainly restrictive and is required in order to derive some closed-form theoretical outcomes.

Case 1: The homogeneous compartment sizes ($q_i = q$)

Firstly, we consider an RFMD with all the q_i's equal and denote their common value as q. The following result assumes that the rates are i.i.d. random variables.

Theorem 2.3.1. *Assume that rates λ_i in the RFMD with dimension n are independent copies of a random variable X having support on $\mathbb{R}_{\geq \delta}$. Then $R_n \xrightarrow{p} q^2(2M_{X^{-1/2}})^{-2}$ as $n \to \infty$ i.e., R_n approaches the value $q^2(2M_{X^{-1/2}})^{-2}$ with probability one, as $n \to \infty$.*

The above result states that as the dimension of the RFMD increases, the steady-state flow rate converges with unit probability to a fixed value depending upon the constant site size q and on the minimal possible value (with probability one) that the random variable X attains. Clearly, for $q = 1$, we retrieve the case of variability in the rates in the RFM [64].

Example 2.3.1. Suppose that X follows a half-normal distribution with mean having a value of 2 and standard deviation having a value of 0.1. Note that $M_{X^{-1/2}} = 1/\sqrt{2}$. Let $q_i = 0.5$ for all i. In this case as n goes to infinity, $R_n \xrightarrow{p} 0.125$ by Theorem 2.3.1. A histogram of the results for $n \in \{50, 500, 1000\}$ is shown in Fig. 2.1.

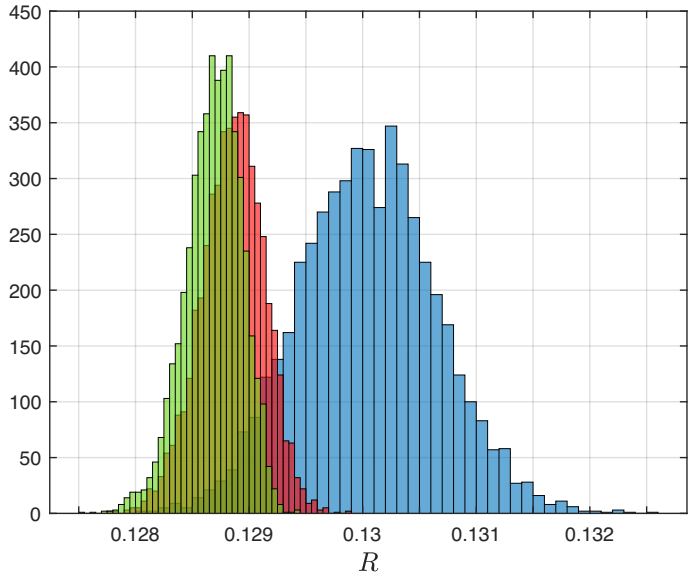

Figure 2.1: Histograms showing 5000 distinct values each for RFMD with dimension 50, 500 and 1000 colored in blue, red and green, respectively for the steady-state flow rate in the RFMD with the parameters considered in Example 2.3.1. Our theoretical result predicts that as n goes to infinity, the steady-state flow rate converges to 0.125 with probability one.

We now investigate the cases where the restrictive assumption of rates being i.i.d. random variables is a little bit relaxed. Our first case considers that the random variables X_i could be non-identical, but all independent and having the same support. In this case also, the analysis of the proof of Theorem 2.3.1 proves that the steady-state flow rate asymptotically approaches the same value as in Theorem 2.3.1. The next example exhibits this.

Example 2.3.2. Let $n + 1$ independent random variables X_0, $X_1, \ldots$, $X_{\frac{n}{2}-1}$ be distributed using the half-normal distribution with mean having value 1 and standard deviation having value 0.1 and $X_{\frac{n}{2}}$, $X_{\frac{n}{2}+1}, \ldots$, X_n distributed uniformly on $[1, 2]$. Note that $M_{X_i^{-1/2}} = 1$ for all i. Let $q_i = 0.3$ for all i. The theory

predicts that as n goes to infinity, $R_n \xrightarrow{p} 0.0225$. A histogram of the results for $n \in \{50, 500, 1000\}$ is depicted in Fig. 2.2.

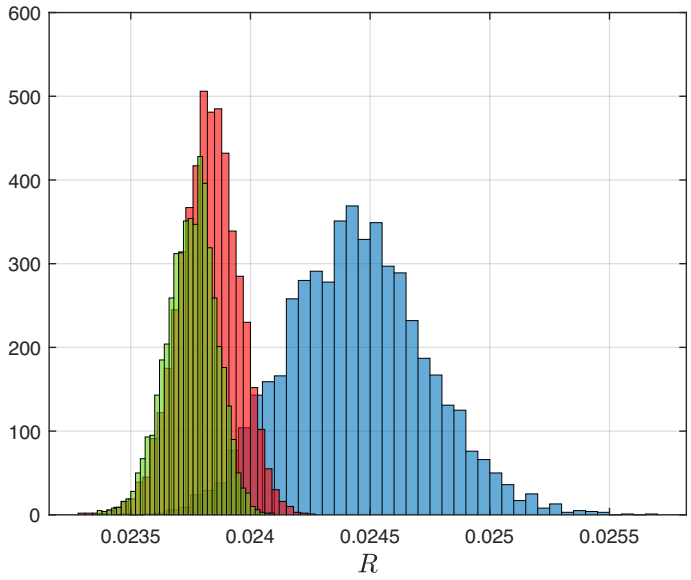

Figure 2.2: Histograms showing 5000 distinct values each for RFMD with dimension 50, 500 and 1000 colored in blue, red and green, respectively for the steady-state flow rate in the RFMD with the parameters considered in Example 2.3.2. The theory predicts that as n goes to infinity, the steady-state flow rate converges to 0.0225 with probability one.

In the second case, we allow a growing (but still tiny) number of random variables having support different from the other random variables. We use the notation S^n to denote the set of permutations on $\{1, 2, \ldots, n\}$. Consider a permutation $\pi \in S^n$, and let $Y^\pi \triangleq \pi \circ Y = (Y_{\pi(1)}, Y_{\pi(2)}, \ldots, Y_{\pi(n)})$. Let Y_i^π denote the ith element in Y^π. The next result is a generalization of the theorem stated for $q = 1$ in Ref. [64].

Theorem 2.3.2. *Let $d = d(n) > 0$ be an integer which has the property $\lim_{n\to\infty} \frac{d(n)}{n} = 0$. Let $\{X_i\}_{i=0}^{n-d}$ is a collection of $(n - d + 1)$ independent random variables having support on $\mathbb{R}_{\geq\delta}$, and satisfies*

$$M_{X_0^{-1/2}} = M_{X_1^{-1/2}} = \cdots = M_{X_{n-d}^{-1/2}}. \tag{2.4}$$

Let $\{X_i\}_{n-d+1}^{n}$ is a collection of d random variables having support on the positive semi-axis and satisfies

$$M_{X_j^{-1/2}} \leq \delta^{-1/2}, \quad j = n - d + 1, \ldots, n. \tag{2.5}$$

Denote $Y = (X_0, X_1, \ldots, X_n)$. Fix a permutation $\pi \in S^{n+1}$. Let each rate λ_i in the RFMD with dimension n is a copy of the random variable Y_i^π, for $0 \leq i \leq n$ and λ_i's are independent. Then $R_n \xrightarrow{p} q^2(2M_{X_0^{-1/2}})^{-2}$ as $n \to \infty$.

The above result shows that the steady-state flow rate asymptotically approaches the same value as in Theorem 2.3.1. We shall now describe the results on the steady-state flow rate given the non-homogeneous site capacities.

Case 2: The non-homogeneous compartment sizes

Secondly, we consider the case when some (or all) q_i's are non-identical. Let q_ℓ and q_L denote the minimum and maximum value of $\{q_i : i = 1, \ldots, n\}$, respectively. For given $\epsilon > 0$, define $a(\epsilon) := \mathbb{P}\{X^{-1/2} \geq M_{X^{-1/2}} - \epsilon\}$. The next result analyzes the bounds of R_n for the finite dimension n of the RFMD.

Theorem 2.3.3. *Assume that rates λ_i in the RFMD are independent copies of a random variable X having support on $\mathbb{R}_{\geq\delta}$. Consider two sequences of positive integers (n_i) with $n_j < n_i$ for $j < i$ and (s_i) with $s_j < s_i$ for $j < i$ and satisfying $s_i < n_i - 1$ for all i. Also, consider a decreasing sequence of positive scalars ϵ_i, with $\epsilon_i \to 0$. Then R_{n_i} in the RFMD with dimension n_i, for any i, satisfies*

$$(q_\ell)^2(2M_{X^{-1/2}})^{-2} \leq R_{n_i} \leq (q_L)^2(2M_{X^{-1/2}})^{-2}\big(1 + O(\epsilon_i + s_i^{-2})\big), \tag{2.6}$$

with probability atleast

$$1 - \exp\left(-\left\lfloor \frac{n_i - 2}{s_i} \right\rfloor (a(\epsilon_i))^{s_i}\right). \tag{2.7}$$

The following general result examines the case where we have bounded but arbitrary X_i's. The set of all possible s consecutive integers from the set $\{1, 2, \ldots, n-1\}$ is denoted by $\mathcal{J}_s^{n-1}$.

Theorem 2.3.4. *Assume that each rate λ_i in the RFMD with dimension n is a copy of a random variable X_i having support on $\mathbb{R}_{\geq\delta_i}$, for $0 \leq i \leq n$. Then R_n satisfies*

$$(q_\ell)^2\big(\max_{1\leq i\leq n} X_{i-1}^{-1/2} + X_i^{-1/2}\big)^{-2} \leq R_n \leq (q_L)^2\left(2\max_{1\leq s\leq n-1}\cos\left(\frac{\pi}{s+2}\right)\max_{J_s\in\mathcal{J}_s^{n-1}}\min_{i\in J_s} X_i^{-1/2}\right)^{-2}, \tag{2.8}$$

with probability one.

The above result shows that the steady-state flow rate may not approach a deterministic value in this scenario, but rather it is constrained by two random values above and below. Given several possible distributions of random transition rates, this result gives a notion of a range of output rates. The steady-state flow rate is examined in the next subsection, given deterministic transition rates and variability in site capacities.

2.3.2 The RFMD with stochastic compartment sizes

In this subsection, we consider randomness only in the site sizes i.e., we assume that the transition rates are fixed and tackle fluctuations in the size of compartments by assuming them as random variables with some known distributions. This may model processes like the packet flow in communication networks. In the context of linear communication networks, the data packets are the moving particles and buffers are the sites [45]. Due to many reasons such as run-down communication infrastructure or interference, there could be fluctuations in the capacity of the buffers holding the data packets [84]. The approach used here can be generalized to analyze the flow of packets in such networks.

We further analyze the steady-state flow rate by considering the cases of homogeneous and non-homogeneous transition rates. We assume that all the transition rates are equal in the first case. Of course, this assumption is limiting, yet it is required to derive some closed-form theoretical results. However, it has some empirical support, for example, the rate of data packet transmission in a communication network can be the same under similar conditions.

Case 1: The homogeneous transition rates ($\lambda_i = \lambda$)

Firstly, we consider the case when all the λ_i's are equal and denote their common value by λ. The next result assumes that the site capacities are i.i.d. random variables.

Theorem 2.3.5. *Assume that site capacities q_i in the RFMD with dimension n are independent copies of a random variable Q having support on $[\beta, \gamma]$, where $0 < \beta < \gamma \leq 1$. Then $R_n \xrightarrow{p} (m_Q)^2\lambda/4$ as $n \to \infty$.*

The above result states that the steady-state flow rate asymptotically approaches a constant value with probability one that depends on the constant transition rate λ and the minimal possible value (with probability one) of the random variable Q as the RFMD's dimension grows.

Example 2.3.3. Assume that Q has a uniform distribution in the range $[0.8, 1]$. Take note of $m_Q = 0.8$. For all i, let $\lambda_i = 1$. In this case, Theorem 2.3.5 implies that as n approaches infinity, $R_n \xrightarrow{p} 0.16$. A histogram of the results for $n \in \{50, 500, 1000\}$ is shown in Fig. 2.3.

Likewise, in the first subsection, we now examine the cases, where we allow some relaxations in the assumption that the site capacities are i.i.d. random variables. Our first case considers the random variables Q_i that might be non-identical, but all independent and they all have the same minimum bound. The following example

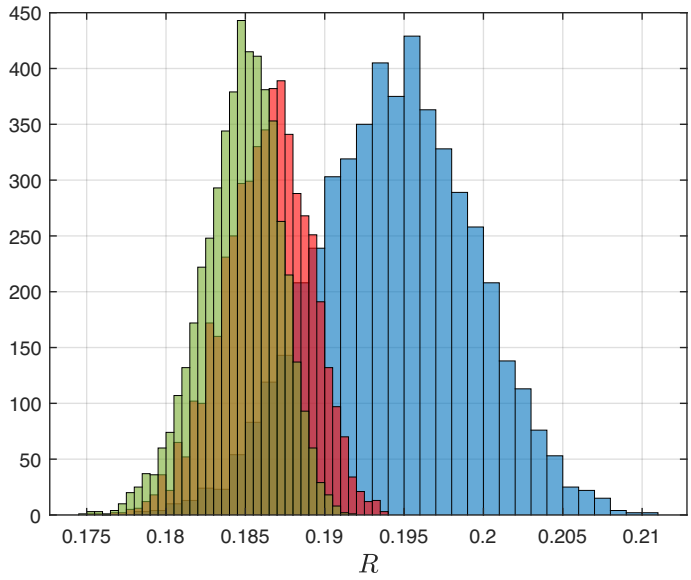

Figure 2.3: Histograms showing 5000 distinct values each for RFMD with dimension 50, 500 and 1000 colored in blue, red and green, respectively for the steady-state flow rate in the RFMD with the parameters considered in Example 2.3.3. Our theoretical result shows that as n goes to infinity, the steady-state flow rate converges to 0.16 with probability one.

shows that if each site capacity q_i is taken from the Q_i distribution, then again the steady-state flow rate approaches the same value as given in Theorem 2.3.5.

Example 2.3.4. Let n independent random variables $Q_1, \ldots, Q_{\frac{n}{2}}$ distributed uniformly on $[0.7, 0.9]$ and $Q_{\frac{n}{2}+1}, \ldots, Q_n$ distributed uniformly on $[0.7, 0.8]$. Note that $m_{Q_i} = 0.7$ for all i. Let $\lambda_i = 1$ for all i. Thus, our theory predicts that as n approaches infinity, $R_n \xrightarrow{p} 0.125$. A histogram of the results for $n \in \{50, 500, 1000\}$ is depicted in Fig. 2.4.

We consider an increasing (but small in comparison to n) number of random variables modeling site sizes to have different support than the rest of the other random variables in the next result.

Theorem 2.3.6. *Consider an integer $d = d(n) > 0$ with the property $\lim_{n\to\infty} \frac{d(n)}{n} = 0$. Let $\{Q_i\}_{i=1}^{n-d}$ is a collection of $(n-d)$ independent random variables having support on $[\beta, \gamma]$, where $0 < \beta < \gamma \leq 1$ and satisfies*

$$m_{Q_1} = m_{Q_2} = \cdots = m_{Q_{n-d}}. \tag{2.9}$$

Let $\{Q_i\}_{n-d+1}^{n}$ is a collection of d random variables having support on $[\mu_i, \tau_i]$, where $0 < \mu_i < \tau_i \leq 1$, for $i = n-d+1, \ldots, n$ and satisfies

$$m_{Q_j} \geq \beta, \quad j = n-d+1, \ldots, n. \tag{2.10}$$

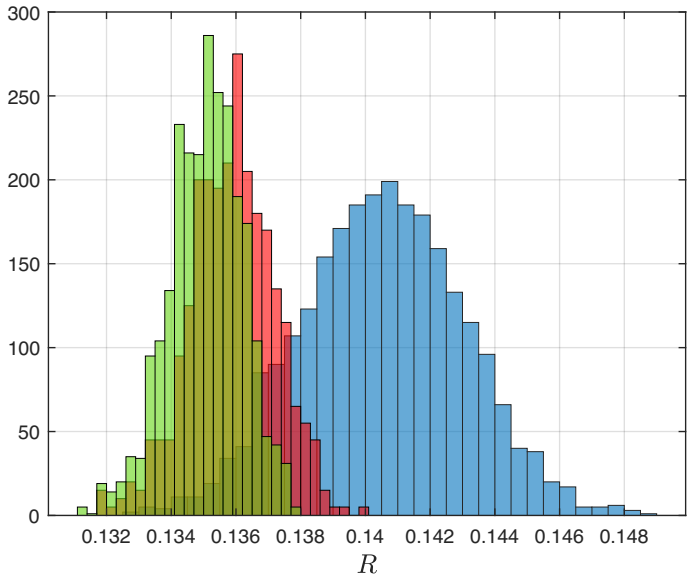

Figure 2.4: Histograms showing 2500 distinct values each for RFMD with dimension 50, 500 and 1000 colored in blue, red and green, respectively for the steady-state flow rate in the RFMD with the parameters considered in Example 2.3.4. The theory forecasts that as n goes to infinity, the steady-state flow rate converges to 0.125 with probability one.

Denote $Y = (Q_1, Q_2, \ldots, Q_n)$. *Consider a permutation* $\pi \in S^n$. *Let each site capacity* q_i *in the RFMD with dimension* n *is a copy of the random variable* Y_i^π, *for* $1 \le i \le n$ *and* q_i*'s are independent. Then* $R_n \xrightarrow{p} (m_{Q_1})^2\lambda/4$ *as* $n \to \infty$.

The above result shows that the steady-state flow rate approaches the same value as n goes to infinity as in Theorem 2.3.5. Next, we shall discuss the case of non-homogeneous transition rates.

Case 2: The non-homogeneous transition rates

Secondly, we consider the case when some (or all) λ_i's are non-identical. Let λ_ℓ and λ_L denote the minimum and maximum value of $\{\lambda_i^{-1/2} : i = 0, 1, \ldots, n\}$, respectively. For $\eta > 0$, define $b(\eta) := \mathbb{P}\{Q \le m_Q + \eta\}$. The following result provides the bounds of R_n for the finite dimension n of the RFMD.

Theorem 2.3.7. *Let us assume that site capacities* q_i *in the RFMD are independent copies of a random variable* Q *having support on* $[\beta, \gamma]$, *where* $0 < \beta < \gamma \le 1$. *Choose two positive integer sequences* (n_i) *with* $n_j < n_i$ *for* $j < i$ *and* (s_i) *with* $s_j < s_i$ *for* $j < i$ *and satisfying* $s_i < n_i$ *for all* i, *and a decreasing sequence of positive scalars* η_i, *with* $\eta_i \to 0$. *Then* R_{n_i} *in the RFMD with dimension* n_i, *for any* i, *satisfies*

$$(m_Q)^2(2\lambda_L)^{-2} \le R_{n_i} \le (m_Q)^2(2\lambda_\ell)^{-2}\left(1 + \frac{\eta_i^2}{m_Q} + \frac{2\eta_i}{m_Q}\right)\left(1 + O(s_i^{-2})\right), \qquad (2.11)$$

with probability atleast

$$1 - \exp\left(-\left\lfloor \frac{n_i - 1}{s_i} \right\rfloor (b(\eta_i))^{s_i}\right). \tag{2.12}$$

Notably, the convergence rate (2.11) to the value given for homogeneous transition rate in Theorem 2.3.5 as n increases is slower than the rate of convergence (2.6) to the value given for homogeneous site size in Theorem 2.3.1. The following result deals with the situation, where Q_i's are arbitrary yet bounded. They don't have to be independent or identical.

Theorem 2.3.8. *Suppose that every site capacity q_i in the RFMD with dimension n is a copy of a random variable Q_i having support on $[\beta_i, \gamma_i]$, where $0 < \beta_i < \gamma_i \leq 1$, for $1 \leq i \leq n$. Then R_n satisfies*

$$\left(\min_{1\leq i\leq n} Q_i\right)^2 (2\lambda_L)^{-2} \leq R_n \tag{2.13}$$

and

$$\max_{1\leq s\leq n}\left(2\lambda_\ell \cos\left(\frac{\pi}{s+1}\right) + \max_{J_s\in\mathcal{J}_s^n}(1 - \max_{i\in J_s} Q_i)\frac{1}{(R_n)^{1/2}}\right) \leq \frac{1}{(R_n)^{1/2}}. \tag{2.14}$$

The above theorem shows that the steady-state flow rate is explicitly bounded below by a random quantity and the other bound follows an implicit relationship. In the above subsections, we derive the theoretical results where we allow assumptions on the transition rates as random variables and the site capacities are deterministic, and vice-versa. However, in the following subsection, we provide the bounds for the steady-state flow rate in the most general scenario, when the capacities of the sites and the values of the transition rates are random.

2.3.3 The Stochastic RFMD

We state our last result where we assume that all the parameters are arbitrary random variables but bounded and they need not be independent or identical. For $J_s \in \mathcal{J}_s^{n-1}$, let H_s is the set $\{J_s \cup (\ell(J_s)+1)\}$, where $\ell(J_s)$ denotes the last entry of the set J_s.

Theorem 2.3.9. *Assume that each rate λ_i in the RFMD with dimension n is a copy of a random variable X_i having support on $\mathbb{R}_{\geq\delta_i}$, for $0 \leq i \leq n$. Suppose that each site capacity q_i in the RFMD is a copy of a random variable Q_i having support*

on $[\beta_i, \gamma_i]$, *where* $0 < \beta_i < \gamma_i \leq 1$, *for* $1 \leq i \leq n$. *Then* R_n *satisfies*

$$\left(\min_{1\leq i\leq n} Q_i\right)^2 \left(\max_{1\leq i\leq n} X_{i-1}^{-1/2} + X_i^{-1/2}\right)^{-2} \leq R_n \tag{2.15}$$

and

$$\max_{1\leq s\leq n-1} \max_{J_s\in\mathcal{J}_s^{n-1}} \left(2\cos\left(\frac{\pi}{s+2}\right) \min_{i\in J_s} X_i^{-1/2} + (1 - \max_{i\in H_s} Q_i)\frac{1}{(R_n)^{1/2}}\right) \leq \frac{1}{(R_n)^{1/2}}. \tag{2.16}$$

The above result states that the steady-state flow rate is bounded by two random quantities: the lower bound is explicit and the other bound follows an implicit relationship. The theoretical result stated here is the most general result that holds for variability or fluctuations both in the transition rates and the site capacities. We state an example to demonstrate the above theorem.

Example 2.3.5. Consider an RFMD with dimension $n = 3$. Let the transition rates λ distributed uniformly on $[1, 2]$ and the site sizes q distributed uniformly on $[0.5, 0.7]$. We have by calculation, $0.0625 \leq R_n \leq 0.49$. Fig. 2.5 depicts a histogram for $n = 3$.

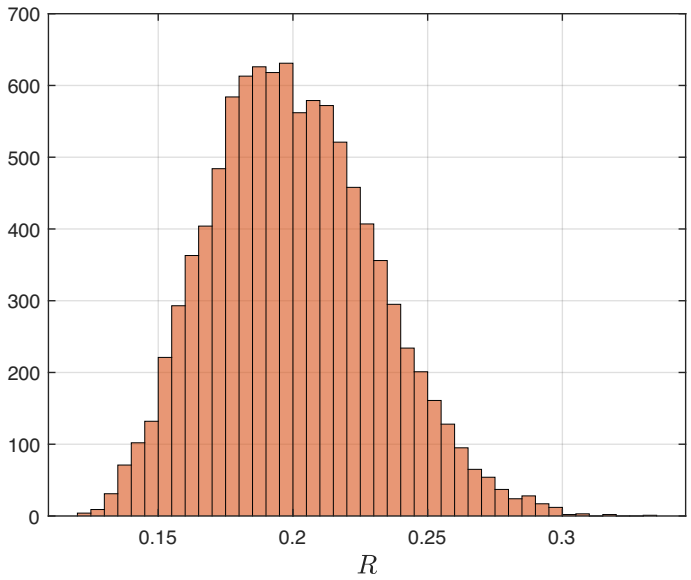

Figure 2.5: Histogram of 10,000 different values for RFMD with dimension 3 for the steady-state flow rate in the RFMD with the parameters considered in Example 2.3.5. The theory predicts that the steady-state flow rate lies between 0.0625 and 0.49.

Note: Even though both the transition rates and the site capacities themselves are i.i.d. random variables, the steady-state flow rate does not converge to a

deterministic value in this situation, contrary to our earlier theoretical conclusions. This can be explained as follows. Suppose that each rate λ_i is generated using the distribution of a random variable X that takes values in the interval $[a, b]$, where $a > 0$. Consider that every site capacity q_i is selected using the distribution of a random variable Q taking values in the interval $[c, d]$, where $0 < c < d \leq 1$. In this respect, we have

$$\frac{1}{\sqrt{b}} \leq \frac{1}{\sqrt{X}} \leq \frac{1}{\sqrt{a}} \tag{2.17}$$

and

$$c \leq Q \leq d. \tag{2.18}$$

From Eq. (2.15), we have

$$\frac{c^2\ a}{4} \leq R_n. \tag{2.19}$$

From Eq. (2.16), we have

$$2\ \cos\left(\frac{\pi}{s+2}\right)\frac{1}{\sqrt{b}} + (1-d)\frac{1}{\sqrt{R_n}} \leq \frac{1}{\sqrt{R_n}} \tag{2.20}$$

$$\implies R_n \leq \frac{d^2\ b}{4\ (\cos(\frac{\pi}{s+2}))^2}. \tag{2.21}$$

As $n \to \infty$, we can choose s large enough such that

$$R_n \leq \frac{d^2\ b}{4}. \tag{2.22}$$

Eqs. (2.19) and (2.22) implies

$$\frac{c^2\ a}{4} \leq R_n \leq \frac{d^2\ b}{4}. \tag{2.23}$$

Thus, the steady-state flow rate is bounded above and below by two different deterministic values as $n \to \infty$.

2.4 Discussion

Analyzing the flow of particles along the tracks is of paramount importance to understand the dynamics of transport processes including the flow of biological machines like motor proteins along filaments, the evacuation dynamics, etc. Various models both deterministic and stochastic have been proposed to model the movement of particles along the lattice. The RFM is a recent area of research to rigorously analyze such processes. This is a deterministic, synchronous, and continuous-time mathematical model that is an approximation of TASEP.

The RFMD is a generalized version of the RFM that models an important feature of sites having different sizes that were not incorporated in the RFM. The RFMD analyzes the motion of particles in a preferred direction along a lattice through a system of nonlinear ordinary differential equations. The dynamics always converge to a steady-state density thus implying a constant flow rate eventually. Certain types of randomness or uncertainties are always present in many nonlinear systems. An important question in this context is how the steady-state flow rate in the RFMD is affected by these fluctuations.

In this chapter, we analyze the stochasticity in RFMD through the consideration of randomness in all the parameters by assuming them as random variables. Our analysis includes some closed-form theoretical results under restrictive assumptions such as rates are i.i.d. random variables. We show that, given a constant homogeneous site size, the steady-state flow rate ultimately depends on the site size and the minimal value of the random variables modeling the transition rates as the number of sites increases. This scenario also holds where the assumption on the random variables as i.i.d. is relaxed a bit. This may explain that the steady-state flow rate can be maintained inspite of some variations in the transition rates. Furthermore, we derive bounds for the steady-state flow rate in the case of a finite dimension of the RFMD having rates as i.i.d. variables and also in the case where transition rates are drawn from arbitrary but bounded random variables.

Next, we analyze the steady-state flow rate in the case of deterministic transition rates and stochastic site capacities. Similarly, we prove that given a fixed homogeneous transition rate, as the number of sites increases, the steady-state flow rate depends on the transition rate and the minimum value that the random variable modeling the site sizes attains. Our results also provide bounds on the steady-state flow rate given the general case of arbitrary site capacities. In the last and most general result, we derive bounds on the steady-state flow rate given different distributions of the transition rates or the site sizes.

In conclusion, our work provides some asymptotic results and bounds on the output of the RFMD and our observations are not dependent on the specific statistical distribution. For further research, one can develop a different approach to derive results for the convergence of the steady-state flow rate to the limiting value in the case of stochasticity in all the parameters in the RFMD. Moreover, one can analyze the steady-state flow rate in the RFMD by assuming transition rates and site capacities as dependent random variables. We believe that the results described here will be useful for analyzing systems modeled through the RFMD with rates subject to uncertainties or fluctuations. For example, to analyze the performance of wireless line networks or multi-receiver diversity with random-varying connectivity.

2.5 Appendix: Proofs

Firstly, we recall a result stated in Ref. [64] that will be used later on in proving Theorem 2.3.1.

Proposition 2.1. Suppose that $\{U_i\}_{i=1}^n$ are i.i.d. random variables such that they are almost sure bounded. Let $\epsilon > 0$. Consider an integer $1 \leq s \leq n$ and let S be the event that there exists an index $1 \leq k \leq n-s+1$ such that $U_k, \ldots, U_{k+s-1} \geq M_{U_1} - \epsilon$. Then the probability of S converges to one as $n \to \infty$.

Proof: Let $f := M_{U_1} - \epsilon$. For $k \in \{1, \ldots, n-s+1\}$, let $S(\ell)$ denote the event: $U_\ell, \ldots, U_{\ell+s-1} \geq f$. Then

$$\mathbb{P}(S) \geq \mathbb{P}\big(S(1) \cup S(s+1) \cup S(2s+1) \cup \cdots \cup S(hs+1)\big),$$

where h is the largest integer such that $(h+1)s \leq n$. We have the i.i.d. U_i's and thus we get

$$\mathbb{P}(S) \geq 1 - \big(1 - (\mathbb{P}(U_1 \geq f))^s\big)^{h+1}.$$

Since, the probability $\mathbb{P}(U_1 \geq f)$ is positive, when $n \to \infty$, we have $\mathbb{P}(S) \to 1$.

Proof of Theorem 2.3.1: For ease of notation, let $Z_i := \lambda_i^{-1/2}$ and each random variable Z_i is a copy of $X^{-1/2}$. Then $A_n : \mathbb{R}_+ \to \mathbb{R}^{(n+2)\times(n+2)}$ can be written as

$$A_n(r) := \begin{bmatrix} 0 & Z_0 & 0 & \ldots & 0 \\ Z_0 & (1-q)r & Z_1 & \ldots & 0 \\ 0 & Z_1 & (1-q)r & \ldots & 0 \\ & & \ddots & & \\ 0 & \ldots & 0 & (1-q)r & Z_n \\ 0 & \ldots & 0 & Z_n & 0 \end{bmatrix}.$$

The maximum eigenvalue of any symmetric matrix A having non-negative elements is bounded above by the maximum of the row sums of A [83], i.e.,

$$\lambda_{max}(A) \leq \max_{1 \leq i \leq n} \sum_{j=1}^{n} a_{ij}. \tag{2.24}$$

Given $A_n(r)$ is a symmetric matrix with non-negative elements and hence,

$$\lambda_{max}(A_n(r)) \leq \max_{1 \leq i \leq n-1} (Z_i + Z_{i+1}) + (1-q)r. \tag{2.25}$$

Also, we have $Z_i \leq M_{Z_i}$ for all i, which implies

$$\lambda_{max}(A_n(r)) \leq 2M_{Z_1} + (1-q)r \tag{2.26}$$

with probability one. By Eqs. (2.2) and (2.3), we get

$$\frac{q^2}{(2M_{Z_1})^2} \leq R_n. \tag{2.27}$$

Let G_s denote the $(s+1) \times (s+1)$ symmetric tridiagonal matrix

$$G_s := \begin{bmatrix} 0 & 1 & 0 & \dots & 0 \\ 1 & 0 & 1 & \dots & 0 \\ 0 & 1 & 0 & \dots & 0 \\ & & \ddots & & \\ 0 & \dots & 0 & 0 & 1 \\ 0 & \dots & 0 & 1 & 0 \end{bmatrix}.$$

It is known that the maximal eigenvalue of the above matrix is $\lambda_{max}(G_s) = 2\cos(\frac{\pi}{s+2})$ [85]. Let $f := M_{Z_1} - \epsilon$. By Proposition 2.1, we have an index k such that $Z_k, \dots, Z_{k+s-1} \geq f$. We shall consider $k = 1$ and the other cases can be handled similarly. Let $B_n(r)$ be the matrix obtained by replacing the $(s+1)\times(s+1)$ principal minor corresponding to the indices $2, 3, \dots, s+2$ of $A_n(r)$ by $fG_s + (1-q)rI_{s+1}$. Hence $B_n(r)$ is given by

$$\begin{bmatrix} 0 & Z_0 & 0 & 0 & \dots & \dots & \dots & 0 \\ Z_0 & (1-q)r & f & 0 & \dots & \dots & \dots & 0 \\ 0 & f & (1-q)r & f & 0 & \dots & \dots & 0 \\ & & \ddots & & & & & \\ 0 & \dots & 0 & f & (1-q)r & Z_{s+1} & \dots & 0 \\ 0 & \dots & 0 & 0 & Z_{s+1} & (1-q)r & \dots & 0 \\ & & \ddots & & & & & \\ 0 & \dots & \dots & & \dots & 0 & (1-q)r & Z_n \\ 0 & \dots & \dots & & \dots & 0 & Z_n & 0 \end{bmatrix}.$$

Then $A_n(r) \geq B_n(r)$ (the inequality is componentwise) and hence $\lambda_{max}(A_n(r)) \geq \lambda_{max}(B_n(r))$. Utilizing Cauchy's interlacing theorem, we have that the largest eigenvalue of $B_n(r)$ is larger or equal to the largest eigenvalue of any of its principal minors. Thus,

$$\lambda_{max}(B_n(r)) \geq f\lambda_{max}(G_s) + (1-q)r \tag{2.28}$$

$$\implies \lambda_{max}(A_n(r)) \geq 2f\cos\left(\frac{\pi}{s+2}\right) + (1-q)r. \tag{2.29}$$

By Eq. (2.2), we get

$$r^* \geq 2f\cos\left(\frac{\pi}{s+2}\right) + (1-q)r^*. \tag{2.30}$$

By Eq. (2.3), we get

$$R_n \leq \frac{q^2}{\left(2f\cos\left(\frac{\pi}{s+2}\right)\right)^2}. \tag{2.31}$$

Since, this holds for any $\epsilon > 0$ and any integer s, and by Eq. (2.27), the proof of the theorem is completed.

Proof of Theorem 2.3.2: By the pigeonhole principle, there exist a subsequence of Y^π of length atleast $\frac{n}{d}$, which consists of consecutive X_i's. In the proof of Proposition 2.1, the range of parameter h becomes $(h+1)s \leq \lfloor \frac{n}{d} \rfloor$ and we have $\frac{n}{d} \to \infty$ which implies $h \to \infty$ as well. The lower bound also holds due to the condition in Eq. (2.5). Hence, by applying the arguments used in the proof of the Theorem 2.3.1, we get the result.

Proof of Theorem 2.3.3: Let $\epsilon > 0$. Consider an integer $1 \leq s \leq n-1$. Let $a(\epsilon) \coloneqq \mathbb{P}\{Z_1 \geq M_{Z_1} - \epsilon\}$. The arguments in the proof of Theorem 2.3.1 imply that

$$r^* \geq \frac{2(M_{Z_1} - \epsilon)}{q_L}\cos\left(\frac{\pi}{s+2}\right) \tag{2.32}$$

with probability $\mathbb{P}(S) \geq 1 - \left(1-(a(\epsilon))^s\right)^{\lfloor \frac{n-1}{s} \rfloor} \geq 1 - \exp\left(-\left\lfloor \frac{n-1}{s} \right\rfloor (a(\epsilon))^s\right)$. By Eq. (2.32), we get

$$\begin{aligned} R_{n_i} &\leq (q_L)^2 \left(2(M_{Z_1} - \epsilon_i)\cos\left(\frac{\pi}{s_i+2}\right)\right)^{-2} \\ &= (q_L)^2(2M_{Z_1})^{-2}\left(1 + \frac{\epsilon_i}{M_{Z_1}} + o(\epsilon_i)\right)\left(1 + \frac{\pi^2}{(s_i+2)^2} + o(s_i^{-2})\right) \\ &= (q_L)^2(2M_{Z_1})^{-2}\left(1 + O(\epsilon_i + s_i^{-2})\right). \end{aligned}$$

The lower bound can be attained as in Theorem 2.3.1 and hence, this completes the proof of the theorem.

Proof of Theorem 2.3.4: From Eq. (2.24), we have

$$\lambda_{max}(A_n(r)) \leq \max_{1 \leq i \leq n}(X_{i-1}^{-1/2} + X_i^{-1/2}) + (1-q_\ell)r. \tag{2.33}$$

By Eq. (2.3), we have

$$r^* \leq \frac{\max\limits_{1\leq i\leq n}(X_{i-1}^{-1/2}+X_i^{-1/2})}{q_\ell} \tag{2.34}$$

$$\implies \frac{(q_\ell)^2}{\left(\max\limits_{1\leq i\leq n}(X_{i-1}^{-1/2}+X_i^{-1/2})\right)^2} \leq R_n. \tag{2.35}$$

For $1 \leq s \leq n-1$, let $J_s \in \mathcal{J}_s^{n-1}$. Let $B_n(r)$ be the matrix obtained by replacing $(s+1)\times(s+1)$ principal minor corresponding to the indices J_s of $A_n(r)$ by $G_s \min\limits_{i\in J_s} X_i^{-1/2}$. Thus,

$$\begin{aligned}\lambda_{max}(A_n(r)) &\geq \lambda_{max}(G_s \min_{i\in J_s} X_i^{-1/2}) + (1-q_L)r \\ &\geq 2\cos\left(\frac{\pi}{s+2}\right)\min_{i\in J_s} X_i^{-1/2} + (1-q_L)r.\end{aligned}$$

Since this holds for any choice of $1 \leq s \leq n-1$ and $J_s \in \mathcal{J}_s^{n-1}$, therefore we get the upper bound given in Eq. (2.8).

Proof of Theorem 2.3.5: Let $m_X := \sup\limits_{c\geq 0}\{\mathbb{P}[c \leq |X|] = 1\}$. We shall state a Proposition that has proof similar to the proof of Proposition 2.1.

Proposition 2.2. Suppose that $\{V_i\}_{i=1}^n$ are i.i.d. random variables and are almost sure bounded. Let $\eta > 0$. Consider an integer $1 \leq s \leq n$ and let S be the event that there exists an index $1 \leq k \leq n-s+1$ such that $V_k, \ldots, V_{k+s-1} \leq m_{V_1} + \eta$. Then the probability of S converges to one as $n \to \infty$.

Now, using Proposition 2.2 and the arguments in the proof of Theorem 2.3.1 completes its proof.

Proof of Theorem 2.3.6: Utilizing the arguments given in Theorem 2.3.2 and in the proof of the Theorem 2.3.5, completes the proof.

Proof of Theorem 2.3.7: Let $\eta > 0$. Consider an integer $1 \leq s \leq n$. Let $b(\eta) := \mathbb{P}\{Q \leq m_Q + \eta\}$. Using the arguments as in the proof of the Theorem 2.3.5, we have

$$r^* \geq \frac{2\lambda_\ell}{(m_Q+\eta)}\cos\left(\frac{\pi}{s+2}\right), \tag{2.36}$$

with probability $\mathbb{P}(S) \geq 1 - \left(1-(b(\eta))^s\right)^{\lfloor \frac{n}{s} \rfloor} \geq 1 - \exp\left(-\left\lfloor \frac{n}{s} \right\rfloor (b(\eta))^s\right)$.

By Eq. (2.36), we get the upper bound. Similarly, the lower bound can be attained as in Theorem 2.3.1, and hence, the proof of the theorem can be concluded.

Proof of Theorems 2.3.8 and 2.3.9: The proofs are based on the same approach used in Theorem 2.3.4 and thus omitted.

Chapter 3

Modeling transport of extended interacting objects with drop-off phenomenon

The chapter[1] provides a deterministic framework for modeling transport phenomena involving interacting particles having an extended length. The model also incorporates the realistic feature that particles may detach along the track. We study its asymptotic behavior and analyze the effect of the nearest-neighbor interactions on its density profile.

3.1 Introduction

There are many important biological transport phenomena where the driving force for the movement of particles depends upon the constant source of energy [86]. One of the most known examples of such a system is intracellular transport carried out by motor proteins. Experimental investigations show that in many complex cellular processes such as mRNA translation by ribosomes or intracellular transport carried by motor proteins, the particles are larger than their step sizes and they usually function in large groups and interact with one another by binding and repelling actions based on the state of its neighboring particles [31]. Also, it has been seen that in many of these transport processes, the biological particles may get detached along the tracks. For example, kinesin-family motor proteins get detached from the microtubule after every power stroke or when their path is blocked [87, 88]. Defects in kinesin-linked transport may disrupt the functioning of nerve cells and can cause many serious diseases [14]. The neuron-wide system requires intracellular transport of cargo throughout complex neuronal morphologies and its transport malfunction is one of the indications of some neuronal diseases like Alzheimer's [78]. Therefore, deriving mathematical models of these dynamical biological phenomena

[1]The content of this chapter is published as: "Aditi Jain and Arvind Kumar Gupta. Modeling transport of extended interacting objects with drop-off phenomenon. *Plos one* 17(5): e0267858, 2022."

is important and crucial for understanding the collective behavior of the movement of particles and unraveling its biophysical aspects in the context of synthetic biology and biomedical applications.

In this chapter, we introduce a model called the excluded flow of extended interacting objects with drop-off effect (EFEIOD) to include the fact biological "particles" cover several sites and are susceptible to detach at various sites along the lattice. Using the theory of contractive dynamical systems, we prove that EFEIOD always converges to a steady state. This steady state depends on the length of the lattice n, the particle size ℓ, transition rates λ_i's, detachment rates α_i's, and the interaction parameters q and r but not on the initial conditions. We also prove that it entrains to periodic excitations in the transition/detachment rates and the interaction parameters. This is important for the proper functioning of the biological processes that are excited by the periodic events. Analysis and simulations highlight the role of the effect of interactions on the steady-state flow. For example, in the case of strong attractions from the neighboring particle at site $i-\ell$, the flow of particles from site i to $i+1$ gets reduced, therefore an increase in detachment rate of particles at site $i-\ell$ leads to an easy steady-state flow. In the absence of interactions, we analyzed mRNA translation with ribosome drop-off and called it RFMEOD. We also show using simulations that the RFMEOD correlates well with the TASEP with extended objects including the drop-off phenomenon.

The EFEIOD, presented here, is more general than the EFRBM as it includes biologically observed features such as particles with extended length and phenomena of dissociation of particles along the tracks. For details about EFRBM, the reader can refer to Chapter 1.

This chapter is organized as follows. Section 3.2 describes the mathematical model. The next section presents our main theoretical results and the effects of the nearest-neighbor interactions on the steady-state behavior. In Section 3.4, we describe the application of the EFEIOD to model mRNA translation with ribosome drop-off and understand how a change in one of the parameters affects protein production. Section 3.5 concludes and summarizes the chapter. Furthermore, to increase readability we have placed all the proofs in the Appendix.

3.2 Model

The EFEIOD is a nonlinear, continuous time, compartmental model for the unidirectional flow of biological "particles" of size ℓ directed from left to right on a one-dimensional chain of n consecutive compartments or sites along the track.

The EFEIOD contains the following sets of $2n+3$ non-negative parameters:

1. $\lambda_i > 0$, $i = 0, 1, \ldots, n$ controls the transition rate from site i to $i+1$.

2. $\alpha_i \geq 0$, $i = 1, \ldots, n$ controls the detachment rate from site i to the environment.

3. $r \geq 0$, is the attachment/detachment force between any two existing consecutive particles.

4. $q \geq 0$, is the attachment/detachment force between any two new consecutive particles.

Each parameter λ_i and α_i has units of 1/time. A parameter q controls the repelling or binding forces between two new neighbors and a parameter r between two existing neighbors. In many studies, creating and breaking of bonds between the nearest neighbors has been viewed as opposite chemical reactions [89]. So, it is assumed that $\frac{q}{r} = \exp(\frac{E}{K_B\ T})$, where E denotes the interaction energy, by applying the detailed balance arguments.

The position of the particle along the lattice is denoted by the site covered by the leftmost end of it and this part is referred to as the reader. Thus, 'the reader is at site i' means that the particle is located at site i and covers the sites $i, i+1, \ldots, i+\ell-1$. Let $x_i(t) \in [0, 1]$ denote the normalized reader density of the biological particle at site i at time t, and let $y_i(t) \in [0, 1]$ denote its normalized coverage density at site i at time t, i.e.,

$$y_i(t) = \sum_{j=max\{1,i-\ell+1\}}^{i} x_j(t), \quad i = 1, 2, \ldots, n. \tag{3.1}$$

The term 'normalized' here means that each $x_i(t)$ and each $y_i(t)$ takes value in the interval $[0, 1]$ for all $t \geq 0$. The value zero [one] corresponds to completely empty [full]. The schematic explanation of a particle with size ℓ on the lattice is shown in Fig. 3.1.

Eq. (3.1) implies that the total particle coverage at any site i is the summation of the reader densities of ℓ consecutive sites left to site i. The state variables $x_i(t)$ and $y_i(t)$ can be interpreted as the probability that site i is occupied and covered, respectively at time t. Hence, x_i and y_i are dimensionless. Fig. 3.2 depicts the possible transition scenarios from site i to site $i+1$.

To state the dynamical equations describing the EFEIOD, we introduce more

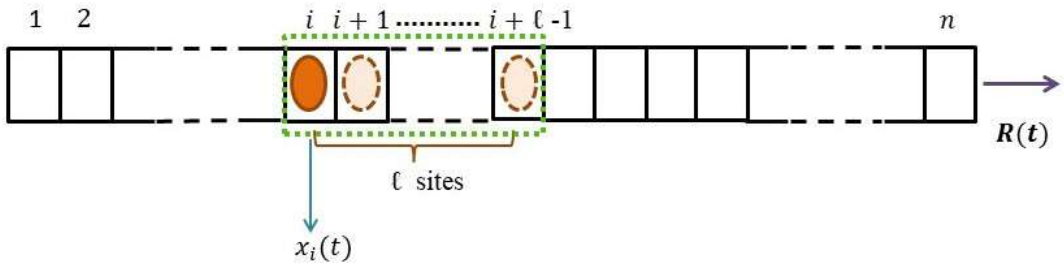

Figure 3.1: A schematic view of a single particle of size ℓ at site i covering sites $i, i+1, \ldots, i+\ell-1$ on the lattice of dimension n. The state variable $x_i(t)$ describes the reader density of particle at site i at time t. $R(t)$ denotes the output rate at time t.

notation for simplicity. Let

$$z_i(t) := \begin{cases} x_i(t) & i = 1, 2, \ldots, n, \\ 0 & \text{otherwise}, \end{cases} \tag{3.2}$$

and

$$w_i(t) := \begin{cases} y_i(t) & i = 1, 2, \ldots, n, \\ 0 & \text{otherwise}. \end{cases} \tag{3.3}$$

The dynamics of the EFEIOD is described by n nonlinear first-order ordinary differential equations:

$$\dot{x}_i = f_{i-1}(x) - f_i(x) - g_i(x), \quad i = 1, 2, \ldots, n, \tag{3.4}$$

where

$$f_0(x) := \lambda_0(1 - w_\ell)(1 + (q-1)z_{\ell+1}), \tag{3.5}$$

$$f_i(x) := \lambda_i x_i(1 - w_{i+\ell})(1 + (q-1)z_{i+\ell+1})(1 + (r-1)z_{i-\ell}), \quad i = 1, 2, \ldots, n, \tag{3.6}$$

and

$$g_i(x) := \alpha_i x_i(1 + (r-1)z_{i+\ell})(1 + (r-1)z_{i-\ell}), \quad i = 1, 2, \ldots, n. \tag{3.7}$$

Eq. (3.4) implies that the change in the reader density at site i is the inflow $f_{i-1}(x)$ from site $i-1$ to site i minus the outflow $f_i(x)$ to site $i+1$ minus the outflow $g_i(x)$ to the cell environment.

Eq. (3.6) can be explained as follows. The term x_i represents that the reader flow from site i to site $i+1$ increases with the reader density at site i. The term $(1-w_{i+\ell})$ represents a "soft" version of the simple exclusion principle which implies that the flow increases with the 'vacancy' level at site $i+\ell$ i.e., as the density in any of the ℓ

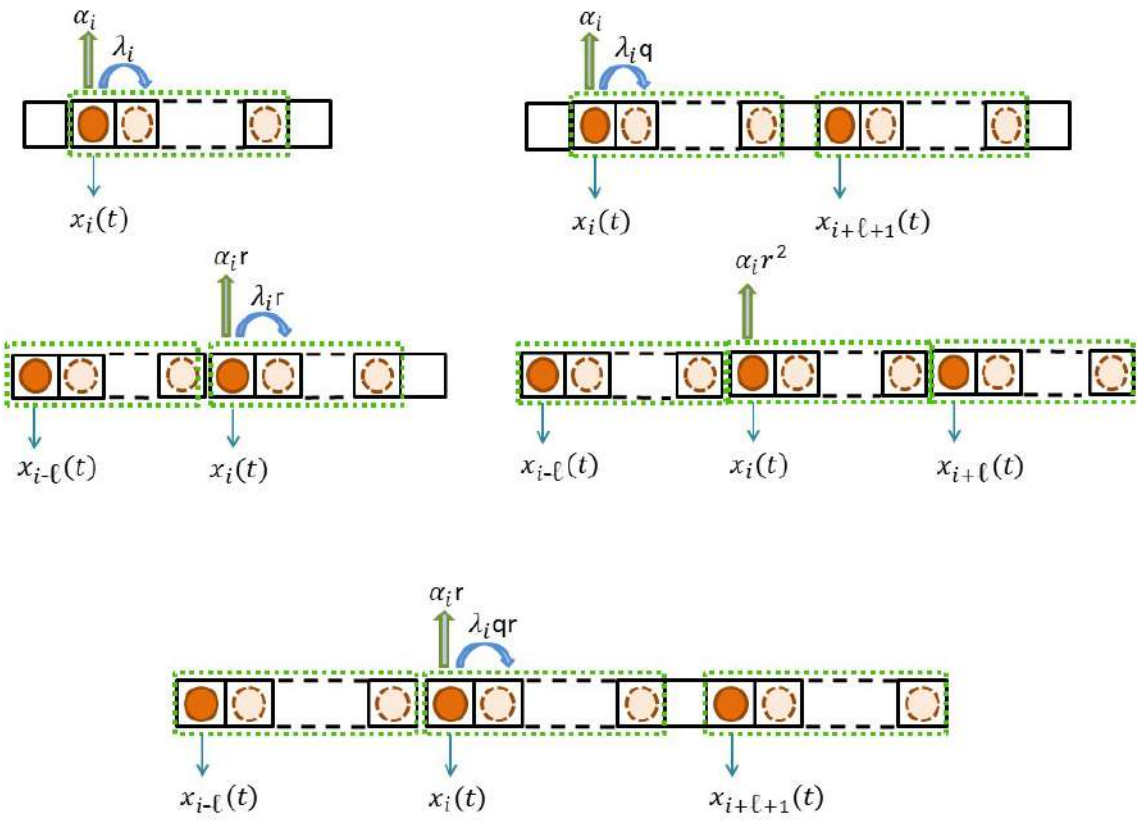

Figure 3.2: The particle covers ℓ sites and the dark red label denotes the reader location. Schematic explanation of the transition flow from site i to site $i+1$ in the EFEIOD: Upper-left: When there are no readers at sites $i-\ell$, $i+\ell$ and $i+\ell+1$, the transition rate is λ_i and detachment rate is α_i. Upper-right: When there is a reader at site $i+\ell+1$ and site $i-\ell$ does not have, the transition rate is $\lambda_i q$ and detachment rate is α_i. Middle-left: When there is reader at site $i-\ell$ and no readers at sites $i+\ell$ and $i+\ell+1$, the transition rate is $\lambda_i r$ and detachment rate is $\alpha_i r$. Middle-right: When there are readers at sites $i-\ell$ and $i+\ell$, detachment rate is $\alpha_i r^2$. Lower-part: When there are readers at sites $i-\ell$ and $i+\ell+1$, the transition rate is $\lambda_i qr$, and detachment rate is $\alpha_i r$.

consecutive sites increases the reader flow from site i to site $i+1$ gradually decreases. The term $(1+(q-1)z_{i+\ell+1})$ represents that the reader flow from site i to site $i+1$ also depends upon the reader density at site $i+\ell+1$ and increases [decreases] if $q>1$ [$q<1$]. The particle at site $i+\ell+1$ will attract [$q>1$] or repel [$q<1$] the particle that move from site i to $i+1$. Similarly, the term $(1+(r-1)z_{i-\ell})$ represents that the flow into site $i+1$ also depends upon the reader density at site $i-\ell$.

The term $g_i(x)$ in Eq. (3.7) represents the detachment of particles from the site i to the cell environment. If $r>1$ [$r<1$], then the particles at sites $i-\ell$ and $i+\ell$ repel [attract] the particle at site i and increases [decreases] its detachment from

site i.

The output rate from site n at any time t is given by:

$$R(t) = (\lambda_n + \alpha_n)x_n(t)(1 + (r-1)x_{n-\ell}). \tag{3.8}$$

Note that in the particular case, $r = 1$, $q = 1$, $\ell = 1$, and $\alpha_i = 0$, the model gets reduced to the RFM [38]. Clearly, in the case when the length of the biological particle is equal to the lattice length, i.e., $\ell = n$, there is no role of interaction forces in the system. The splitting of interaction energy E between the creation and breaking processes is not unique. Like in [89], we also assume that E is equally split between the rates r and q, where

$$q = \exp\left(\frac{E}{2K_BT}\right), \quad r = \exp\left(\frac{-E}{2K_BT}\right) \tag{3.9}$$

Note that Eq. (3.9) implies $r = 1/q$ and has a simple physical meaning. If $E > 0$, then there are attractive interactions in the system, i.e., the particle moves faster creating a new pair $[q > 1]$ and the process of breaking out of the pair is slowed down $[r < 1]$. Similarly, $E < 0$ implies that there are repulsive interactions in the system. The case $E = 0$ corresponds to the fact that there are no interactions in the system and then we have $q = r = 1$.

The next section analyzes the EFEIOD using tools from systems and control theory and in particular contraction theory.

3.3 Main results

Note that the state variable x_i at any time t represents a reader density in the range $[0, 1]$. The next example shows that C^n is not an invariant set of the EFEIOD.

Example 3.3.1. Consider a EFEIOD with dimension $n = 6$, particle size $\ell = 2$, rates $\lambda_0 = 0.01$, $\lambda_i = 1$, $\alpha_i = 0.1$, for $i = 1, 2, \ldots, n$, $r = 2$, and $q = 1/2$. Consider an initial condition $x(0) = [1 \quad 0.9 \quad 0.5 \quad 1 \quad 1 \quad 1]'$. It has been observed that at some time t we have $x(t) = [1.0033 \quad 0.8907 \quad 0.4993 \quad 1.0744 \quad 0.6954 \quad 0.9084]'$ (all numbers are four digit accurate).

Now, we define a state space which is an invariant set of dynamics. We assume that any initial condition belongs to the state space:

$$\Psi := \{x \in \mathbb{R}^n : x \in C^n \text{ and } y \in C^n\}.$$

Note that the set Ψ is a compact and convex set. Let $x(t, a)$ denote the solution of

Eq. (3.4) at time $t \geq 0$ for the initial condition $a \in \Psi$.

3.3.1 Invariance and persistence

The following result shows that Ψ is an invariant set for the dynamics of the EFEIOD.

Proposition 3.3.1. *If $a \in \Psi$ then the solution of EFEIOD satisfies $x(t,a) \in \Psi$, for all $t \geq 0$. For any $a \in \partial\Psi$, $x(t,a) \in \text{int}(\Psi)$ for $t > 0$.*

This implies that the trajectories that emanate from the boundary of Ψ 'immediately' enter the interior of Ψ. The next proposition is useful because it shows that the solutions of the EFEIOD get 'immediately' uniformly separated from the boundary of Ψ.

Proposition 3.3.2. *For any $\tau > 0$, there exists a compact and convex set Ψ_τ that is strictly contained in Ψ such that for any $a \in \Psi$, $x(t,a) \in \Psi_\tau$, for all $t \geq \tau$.*

This means, in particular, for any $\tau > 0$ there exists $d = d(\tau) \in (0, \frac{1}{2})$ such that, $d \leq x_i(t,a), y_i(t,a) \leq 1-d$, for all $t \geq \tau$, for all i and all $a \in \Psi$.

This property is useful in analyzing the asymptotic properties of the system dynamics.

3.3.2 Contraction

Differential analysis provides a very useful way to study the behavior of certain nonlinear dynamical systems. In particular, contraction theory is based on analyzing the time evolution of the distance between the trajectories that emanate from different initial conditions and have its applications to synchronization and reaction-diffusion partial differential equations [53, 55]. However, for our proposed model, we needed a generalized version of contraction theory that has been defined in Chapter 1.

Let $|.|_1 : \mathbb{R}^n \to \mathbb{R}_+$ denote the L_1 norm, i.e., for $x \in \mathbb{R}^n$, $|x|_1 = |x_1| + |x_2| + \cdots + |x_n|$.

Proposition 3.3.3. *The EFEIOD is SOST with respect to the L_1 norm, i.e., for each $\epsilon > 0$ and each $\tau > 0$ there exists $c = c(\tau, \epsilon) > 0$ such that*

$$|x(t+\tau,a) - x(t+\tau,b)|_1 \leq (1+\epsilon)\ \exp(-ct)|a-b|_1, \quad \text{for all}\ \ t \geq 0\ \ \text{and all}\ \ a,b \in \Psi. \tag{3.10}$$

This means that the EFEIOD is contractive after an arbitrarily small time transient τ and with an arbitrarily small overshoot $(1+\epsilon)$. This implies that any

two initial feasible densities in the EFEIOD evolving in time become 'more similar' to each other at an exponential rate.

3.3.3 Global asymptotic stability

Since the convex and compact set Ψ is an invariant set of the dynamics, it contains atleast one steady-state e [57]. By Proposition 3.3.1, we have $e \in \text{int}(\Psi)$. Using Eq. (3.10) with $b = e$, yields the following result.

Theorem 3.3.1. *Assume that $q, r > 0$. The EFEIOD admits a globally asymptotically stable steady-state density $e \in \text{int}(\Psi)$, i.e., $\lim_{t\to\infty} x(t, a) = e$, for all $a \in \Psi$.*

This means that, regardless of the initial density, all trajectories emanating from different initial conditions converge to the unique steady-state density that depends on the system parameters: transition rates λ_i's, detachment rates α_i's, interactions determined by q and r, particle size ℓ, and length of the chain n. The next example demonstrates that the assumption $q, r > 0$ is necessary.

Example 3.3.2. Consider the EFEIOD with dimension $n = 3$ and particle size $\ell = 1$.
For $q = r = 0$, we have:

$$\begin{aligned}
\dot{x}_1 &= \lambda_0(1-x_1)(1-x_2) - \lambda_1 x_1(1-x_2)(1-x_3) - \alpha_1 x_1(1-x_2),\\
\dot{x}_2 &= \lambda_1 x_1(1-x_2)(1-x_3) - \lambda_2 x_2(1-x_1)(1-x_3) - \alpha_2 x_2(1-x_1)(1-x_3),\\
\dot{x}_3 &= \lambda_2 x_2(1-x_1)(1-x_3) - \lambda_3 x_3(1-x_2) - \alpha_3 x_3(1-x_2).
\end{aligned} \tag{3.11}$$

Also, for $q = 1$ and $r = 0$, we have:

$$\begin{aligned}
\dot{x}_1 &= \lambda_0(1-x_1) - \lambda_1 x_1(1-x_2) - \alpha_1 x_1(1-x_2),\\
\dot{x}_2 &= \lambda_1 x_1(1-x_2) - \lambda_2 x_2(1-x_1)(1-x_3) - \alpha_2 x_2(1-x_1)(1-x_3),\\
\dot{x}_3 &= \lambda_2 x_2(1-x_1)(1-x_3) - \lambda_3 x_3(1-x_2) - \alpha_3 x_3(1-x_2).
\end{aligned} \tag{3.12}$$

Eqs. (3.11) and (3.12) admits a continuum of steady-states, here $[1 \quad 1 \quad v]'$ is a steady-state for all v. Therefore, the assumption that $q, r > 0$ cannot be dropped.

The next example demonstrates the global asymptotic property, i.e., trajectories starting from different initial conditions in Ψ asymptotically converge to a unique density profile along the lattice.

Example 3.3.3. Consider the EFEIOD with dimension $n = 3$, particle size $\ell = 2$, rates $\lambda_i = 1$, $\alpha_i = 0.01$, $q = 1$, and $r = 1$. Fig. 3.3 depicts trajectories for

three different initial conditions $[1 \quad 0 \quad 0]'$, $[0 \quad 1 \quad 0]'$, and $[0 \quad 0 \quad 1]'$ in Ψ. It can be seen that the three solutions converge to the same steady state point $e = [0.4959 \quad 0.2483 \quad 0.2459]'$.

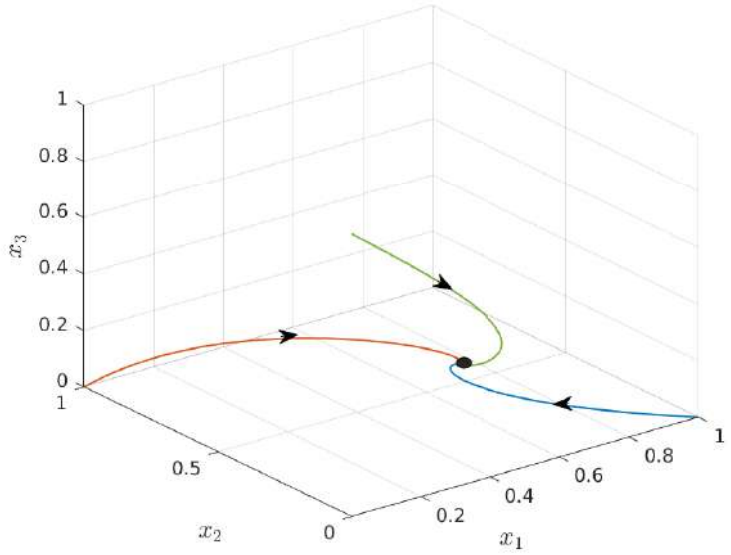

Figure 3.3: Trajectories of EFEIOD for three initial conditions given in Example 3.3.3 as a function of time. The steady-state point is marked by an ellipse.

The next subsection analyzes how the various parameters in the proposed model affect the steady-state output rate.

3.3.4 Analysis of the steady-state

At steady state for $x = e$, the left-hand side of all the equations in (3.4) is zero, so

$$f_{i-1}(e) = f_i(e) + g_i(e), \quad i = 1, 2, \ldots, n. \tag{3.13}$$

It follows from Eq. (3.13) that if we multiply parameters λ_i's and α_i's by a scalar constant $c > 0$ then e will not change, i.e., $e(cp) = e(p)$ where $p = [\lambda_0, \lambda_1, \ldots, \lambda_n, \alpha_1, \alpha_2, \ldots, \alpha_n]$. Also, $R(cp) = cR(p)$, i.e., the output rate is homogeneous of order one w.r.t. the parameters λ_i's and α_i's. By Eq. (3.13), we have:

$$R = f_n(e) + g_n(e) = f_i(e) - \sum_{k=i+1}^{n-1} g_k(e), \quad i = 0, 1, \ldots, n-1. \tag{3.14}$$

However, solving Eq. (3.14) in general, is non-trivial.

The next result shows that the derivatives of the steady state point coordinates with respect to the rates exist and are well-defined. Let the mapping from the parameters to the unique steady state point be denoted by η, i.e., $\eta_i(\gamma) = e_i$, for all $i = 1, 2 \ldots, n$ and $\gamma = [\lambda_0 \;\; \lambda_1 \;\; \cdots \;\; \lambda_n \;\; \alpha_1 \;\; \alpha_2 \;\; \cdots \;\; \alpha_n \;\; r \;\; q]'$.

Proposition 3.3.4. *The derivative* $(\partial/\partial\gamma_j)\eta_i(\gamma)$ *exists for all* i, j.

The above result allows us to calculate the derivatives of the steady-state density if some of the parameters in the system are changed. This is useful to study the sensitivity of the steady-state w.r.t. small changes in the rates.

3.3.5 Effect of interactions

We demonstrate with several simulations the non-trivial effect of interactions on the steady state of the EFEIOD.

The example below demonstrates that in the presence of strong attractive interactions, the detachment of particles could be useful for increasing the flow of particles along the lattice.

Example 3.3.4. Consider the EFEIOD with dimension $n = 9$, particle size $\ell = 3$, rates $\lambda_0 = 1$, $\lambda_i = 1$, and $\alpha_i = \alpha$. Fig. 3.4 depicts that increasing the detachment rate increases the steady-state output for the higher values of q.

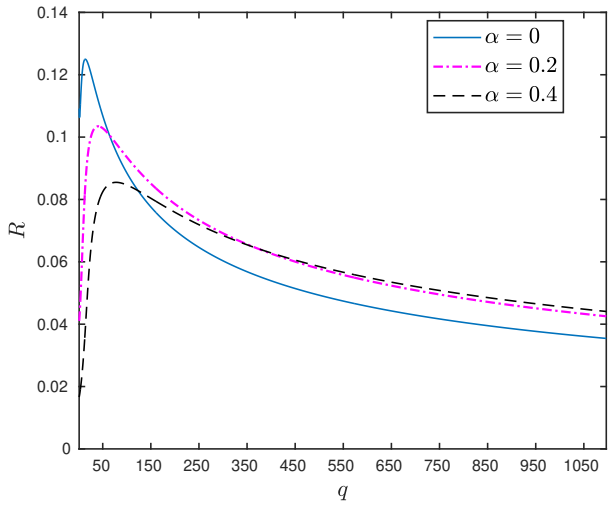

Figure 3.4: The steady-state output rate R as a function of q for a EFEIOD with $n = 9$, $\ell = 3$, $\lambda_0 = 1$, $\lambda_i = 1$, and $\alpha_i = \alpha$, for all i.

The above example suggests that for larger values of attractive interactions, there could be a regulatory mechanism to increase the flow of particles in the system by

allowing the particles to detach from the sites. The next example shows the positive role of increasing the detachment rate in the presence of a bottleneck rate at a site.

Example 3.3.5. Consider the EFEIOD with dimension $n = 9$, particle size $\ell = 2$, rates $\lambda_0 = 1$, $\lambda_i = 1$, for all i except $\lambda_5 = 0.01$, and $\alpha_i = 0$. Note that λ_5 is the bottleneck rate. We vary the parameter α_3, i.e., detachment rate of particles at site 3. It can be seen in Fig. 3.5 that for $q > 1$, i.e., $r < 1$, increasing α_3 increases the steady-state output rate. However, for $q = 1$, i.e., $r = 1$, increasing α_3 decreases the steady-state output rate.

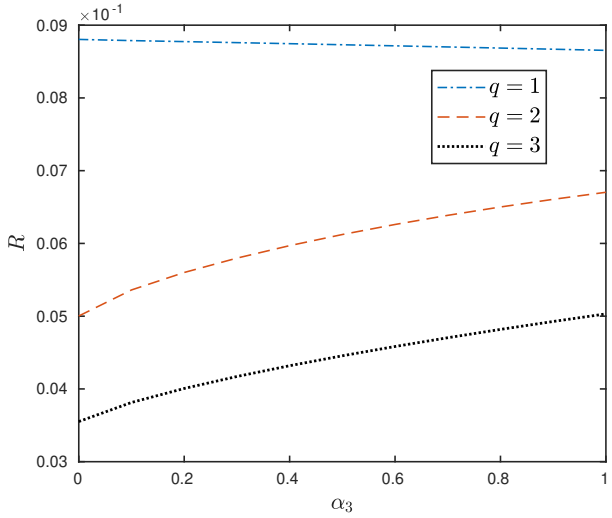

Figure 3.5: The steady-state output rate R as a function of α_3 for a EFEIOD with $n = 9$, $\ell = 2$, $\lambda_0 = 1$, $\lambda_i = 1$, for all i except $\lambda_5 = 0.01$, $\alpha_i = 0$, and $r = 1/q$.

This can be explained as follows: for $r < 1$, a particle at site 5 will tend not to hop forward as there is strong attraction from a particle at site 3. Therefore, allowing particles to detach from site 3, leads to an easy flow of particles from site 5 and this increases the flow. This is important to study as the interactions from the neighboring particles at the bottleneck rate further deteriorate the flow of particles along the lattice. In the case of no interactions i.e., $q = 1$ [$r = 1$], it can be seen that increasing the detachment rate leads to a decrease in the steady-state flow which is always true as we theoretically analyze this special case in the next section.

The example above demonstrates that in the case of interactions, locally controlled detachment can avoid bottlenecks and can lead to faster movement of particles, hence increasing the flow and alleviating the "traffic jams" [90]. One may perhaps think that increasing the particle size leads to a decrease in the steady-state output rate, but steady-state densities follow complicated behavior in the presence of interactions. It has been shown that when $q = r = 1$ and α_i's$= 0$, the steady-state

output rate for $\ell > 1$ is always less than the steady-state output rate for the RFM [69]. But in the presence of interactions, increasing length does not always decrease the output rate as shown in the example below.

Example 3.3.6. Consider the EFEIOD with dimension $n = 9$, rates $\lambda_0 = 1$, $\lambda_i = 1$, and $\alpha_i = 0$, for all i. We vary the particle size ℓ. It can be seen in Fig. 3.6 that for $q = 13$: when $\ell = 1$, we have $R = 0.0808$, when $\ell = 2$, we have $R = 0.1442$, and when $\ell = 3$, we have $R = 0.1249$.

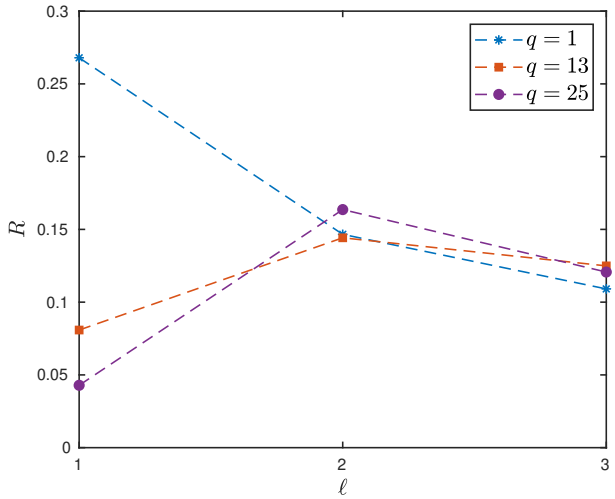

Figure 3.6: The steady-state output rate R as a function of $\ell \in \{1, 2, 3\}$ for a EFEIOD with $n = 9$, $\lambda_0 = 1$, $\lambda_i = 1$, $\alpha_i = 0$, for all i, and $r = 1/q$.

Furthermore, in the thermodynamical limit, i.e., as number of sites goes to ∞, the homogeneous case of TASEPEO with strong repulsions and particle size ℓ, and with entry and exit rates equal to one is in the maximal current phase, where the steady-state mean reader density is $1/(\ell + 1 + \sqrt{\ell + 1})$ and the steady-state output rate is $1/((1 + \sqrt{\ell + 1})^2)$[91]. This implies that as ℓ goes to ∞, the steady-state output and mean reader density go to zero. The next example shows that this is consistent with the results of our model. We define the steady-state mean reader density by $\rho = (1/n) \sum_{i=1}^{n} e_i$.

Example 3.3.7. Consider EFEIOD with dimension $n = 100$, rates $\lambda_0 = 1$, $\lambda_i = 1$, for all i, $\alpha_i = 0$, $q = 0.01$, $r = 100$, and particle size ℓ. Fig. 3.7a depicts that output rate R decrease with ℓ. Also, the steady-state mean reader density ρ decreases with ℓ as seen in Fig. 3.7b.

The next example shows that in the presence of interactions, an increase in an initiation rate does not always lead to an increase in the output rate. However, in

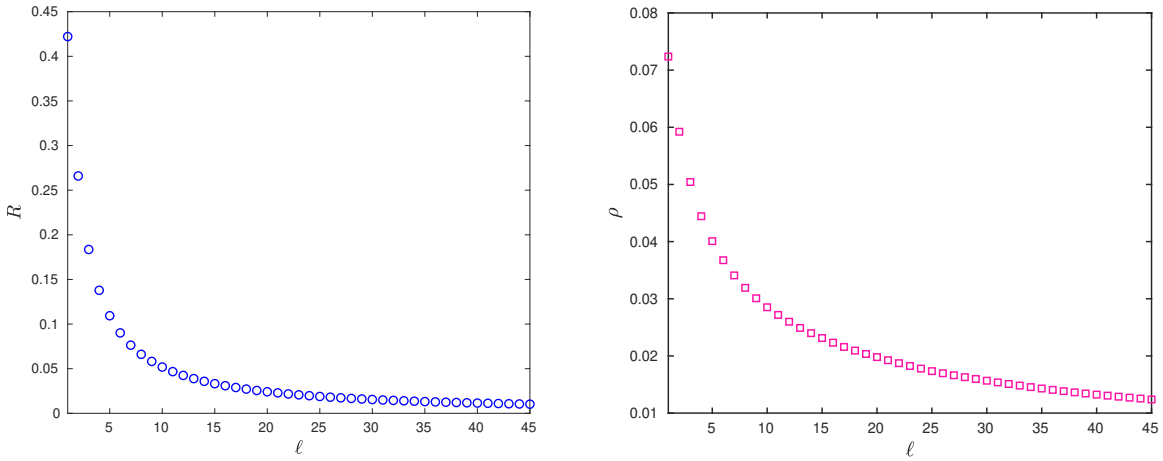

(a) (b)

Figure 3.7: a) The steady-state output rate R as a function of $\ell \in \{1, 2, \ldots, 45\}$ for a EFEIOD with $n = 100$, $\lambda_0 = 1$, $\lambda_i = 1$, $\alpha_i = 0$, for all i, $q = 0.01$, and $r = 1/q$. b) The steady-state mean reader density ρ as a function of $\ell \in \{1, 2, \ldots, 45\}$ for a EFEIOD with $n = 100$, $\lambda_0 = 1$, $\lambda_i = 1$, $\alpha_i = 0$, for all i, $q = 0.01$, and $r = 1/q$.

the case of no interactions, i.e., $q = 1$ $[r = 1]$, an increase in an initiation rate due to feedback or due to an increase in the number of 'free' biological particles leads to an increase in the steady-state output rate as we theoretically analyze this special case in the next section.

Example 3.3.8. Consider the EFEIOD with dimension $n = 6$, $\ell = 2$, rates $\lambda_i = 1$, for all i except $\lambda_4 = 0.1$, and $\alpha_i = 0$. We vary the initiation rate λ_0. It can be seen in Fig. 3.8a that the steady-state output rate decreases with an increase in λ_0. Fig. 3.8b depicts that the steady-state output rate increases with an increase in λ_0.

Now, we analyze the effect of increasing the length of a particle in the case $q \to \infty$.

Example 3.3.9. Consider the EFEIOD with dimension $n = 3$, $\lambda_0 = 1$, $\lambda_i = 1$, $\alpha_i = \alpha$, for all i. Fig. 3.9a depicts that when $q \to \infty$, the steady-state output rate decreases to zero. Fig. 3.9b depicts that when $q \to \infty$, the steady-state output rate saturates to a non-zero constant value depending on the value of α, i.e., $R = 0.1910$ for $\alpha = 0$, $R = 0.1720$ for $\alpha = 0.5$, and $R = 0.1267$ for $\alpha = 1$.

A high value of q corresponds to a strong attachment between existing neighbors (small r) and a high tendency for creating new neighbors (large q), resulting in traffic jams and leading to a sharp decrease in the output rate. Therefore, the length of the particle has an interesting role to play in order to maintain a non-zero constant steady-state output rate in the case of weak repulsions.

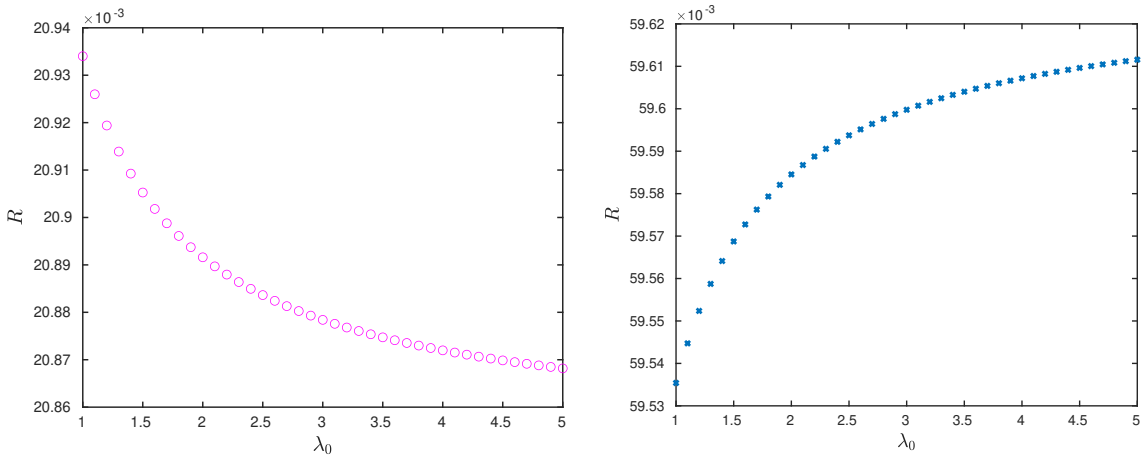

(a) (b)

Figure 3.8: a) The steady-state output rate R as a function of λ_0 for a EFEIOD with $n = 6$, $\ell = 2$, $\lambda_0 = 1$, $\lambda_i = 1$, except $\lambda_4 = 0.1$, $\alpha_i = 0$, for all i, $q = 7$, and $r = 1/7$. b) The steady-state output rate R as a function of λ_0 for a EFEIOD with $n = 6$, $\ell = 2$, $\lambda_0 = 1$, $\lambda_i = 1$, except $\lambda_4 = 0.1$, $\alpha_i = 0$, for all i, $q = 1$, and $r = 1$.

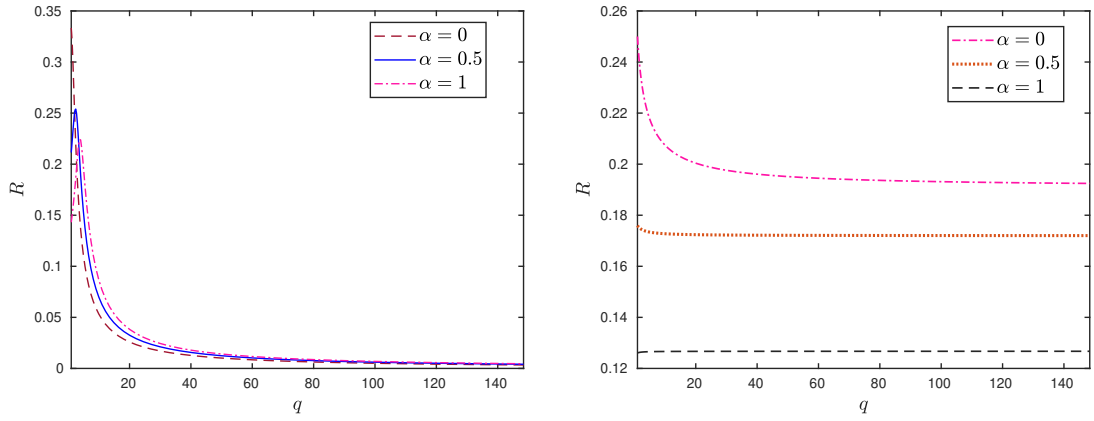

(a) (b)

Figure 3.9: a) The steady-state output rate R as a function of E for a EFEIOD with $n = 3$, $\ell = 1$, $\lambda_0 = 1$, $\lambda_i = 1$, $\alpha_i = \alpha$, for all i, and $r = 1/q$. b) The steady-state output rate R as a function of E for a EFEIOD with $n = 3$, $\ell = 2$, $\lambda_0 = 1$, $\lambda_i = 1$, $\alpha_i = \alpha$, for all i, and $r = 1/q$.

3.3.6 Entrainment

Many biological processes are periodic [92], for example, in translation-elongation mechanism; tRNA molecules [93], ATP levels [94], ribosome drop-off rate [95], translation initiation and elongation factors [96], oscillations in mRNA levels [97], and more may vary in a periodic manner and this results into the periodicity of the rates in the system. For the proper functioning of our body, certain biological systems must be in sync with the periodic changes induced due to the continuously changing environment [98, 99]. Entrainment also plays an important part in

designing extracellular biomedical systems [100]. An important question is: will the state variables of EFEIOD preserve the property of entrainment w.r.t. the parameters λ_i's, α_i's, q, and r?

Assume that the λ_i's, α_i's, q and r are non-negative, uniformly bounded time-varying continuous functions satisfying:

- There exists a (minimal) $T > 0$ such that every λ_i's, α_i's, q, and r is a T-periodic function.
- There exists $0 < \delta_1 < \delta_2$ such that $\lambda_i(t) \in [\delta_1, \delta_2]$, for all $i = 0, 1, \ldots, n$ and all $t \geq 0$.

This model has been referred to as periodic EFEIOD (PEFEIOD). The next result follows from the fact that EFEIOD is SOST on Ψ and the known results on entrainment [54].

Theorem 3.3.2. *The PEFEIOD admits a unique function $\phi : \mathbb{R} \to \text{int}(\Psi)$, that is T-periodic and for any initial condition $a \in \Psi$, the trajectory $x(t, a)$ converges asymptotically to ϕ.*

The above theorem implies that the state variables entrain to the periodic excitations in the parameters. The next example illustrates the behavior of PEFEIOD.

Example 3.3.10. Consider a PEFEIOD with dimension $n = 3$, ribosome size $\ell = 2$, $\lambda_0 = 1$, $\lambda_i = 1$, except for $\lambda_2(t) = 0.5 + 0.25 \sin(\pi t/2)$, $\alpha_i = 0.01$, $r = 5$, and $q = 1/5$. Note, that there is a single time-varying periodic rate in the network and all these rates are periodic with a common minimal period $T = 4$. We have taken two different initial conditions $[0 \quad 0 \quad 0]'$ and $[0.2 \quad 0.2 \quad 0.2]'$ in Ψ. It can be seen from Fig. 3.10 that all the trajectories converge to the periodic solution with period $T = 4$.

In general, describing the effect of parameters on the system dynamics by a theoretical framework is cumbersome, as analyzing the set of nonlinear equations that define the steady state is not trivial. However, for a special case $q = r = 1$, the steady-state output rate sensitivity to variations in the parameters of the system can be answered rigorously. Moreover, the proposed general model was representative of the biology of molecular motors whereas this special case is important in the context of studying the ribosome flow and provides a tool for developing a better understanding and analyzing the factors that can affect this dynamical process of translation.

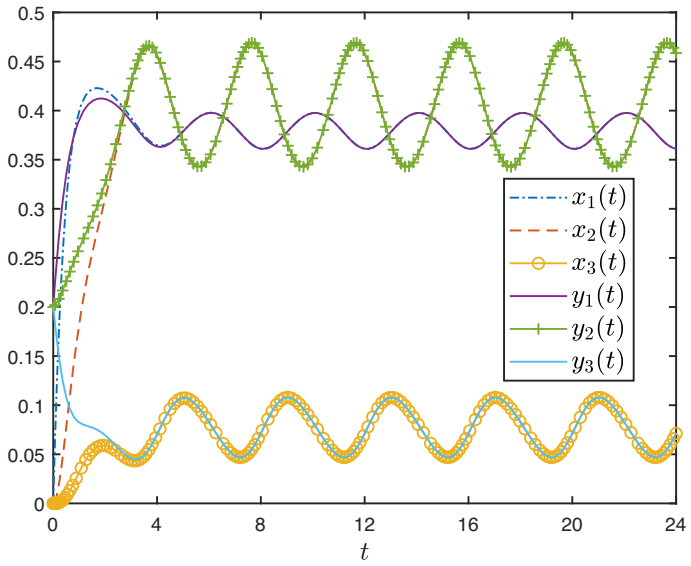

Figure 3.10: Trajectories of PEFEIOD in Example 3.3.10 as a function of time (t). Here, $x_i(t)$ and $y_i(t)$ are the trajectories of PEFEIOD corresponding to initial conditions $[0 \;\; 0 \;\; 0]'$ and $[0.2 \;\; 0.2 \;\; 0.2]'$, respectively.

3.4 Ribosome flow model with extended objects and ribosome drop-off

The synthesis of protein as directed by the mRNA template consisting of codons is carried out by ribosome and the process is referred to as translation [2]. The process broadly takes place in three steps: initiation where ribosomal complex assembles at the start codon of an mRNA chain; elongation where it moves along the mRNA in a forward series of steps forming a polypeptide chain of amino acids, and termination where it releases the chain that folds into functional protein and unbinds from the mRNA. Translation is a fundamental cellular process that occurs in all living beings at all times [1] and is known to consume most of the cell's energy [101]. Therefore, it is crucial to understand its dynamical aspects through mathematical modeling.

It is known from previous studies that the footprint of the ribosome on the mRNA is 10 to 20 codons [102, 103, 104]. Many ribosomes can simultaneously move on the same mRNA template, blocking the movement of other ribosomes behind it [105], resulting in traffic-like movement on the template, and these "traffic jams" are more severe in genes that are lowly expressed [106]. The ribosomes that initiate translation of mRNA sequence may not successfully complete it and hence fail to produce a full-length protein product [107, 108]. Hence, there are translational errors that can disrupt cellular fitness and can cause diseases [109]. Such errors can have multiple causes like ribosomal traffic jams, reading frameshifts [110], non-availability of tRNAs [111], misreading of codon, premature stop codons

[112, 113, 114], etc. These errors often result in ribosome dissociating from the mRNA before reaching the stop codon called ribosome drop-off event, resulting in incomplete or incorrect peptides that are mostly non-functional, and possibly toxic to the cell. The translational error due to premature translation termination seems to represent more than two-thirds of the overall errors and thus have a strong impact on protein formation [115, 81]. Therefore, modeling mRNA translation with ribosome drop-off is important in analyzing the effect on the translation phenomena as it leads to a reduction in the rate of protein production.

To gain insights into these dynamical aspects of translation, we consider a special case of our model when $q = r = 1$ and we refer to this case as the ribosome flow model of extended objects with drop-off effect (RFMEOD). In this model, mRNA is treated as a one-dimensional lattice of length n, where n denotes the number of sites (codons) and every ribosome covers ℓ sites, where $1 \leq \ell \leq n$. The sites 1 and n represent the start and stop codons, respectively. The position of the ribosome along the mRNA is denoted by the site covered by the leftmost end of it. At any time t, if the leftmost edge of the ribosome is at site i, it means the reader is located at site i and the ribosome is translating site i and sites $i, \ldots, i + \ell - 1$ are covered by this ribosome. Ribosomes move unidirectionally from left to right by only one site on the template and no two ribosomes can occupy or cover the same site simultaneously.

The dynamics of RFMEOD is given by:

$$\begin{aligned}
\dot{x}_1 &= \lambda_0(1 - y_\ell) - \lambda_1 x_1(1 - y_{\ell+1}) - \alpha_1 x_1, \\
\dot{x}_2 &= \lambda_1 x_1(1 - y_{\ell+1}) - \lambda_2 x_2(1 - y_{\ell+2}) - \alpha_2 x_2, \\
&\vdots \\
\dot{x}_{n-\ell+1} &= \lambda_{n-\ell} x_{n-\ell}(1 - y_n) - \lambda_{n-\ell+1} x_{n-\ell+1} - \alpha_{n-\ell+1} x_{n-\ell+1}, \\
\dot{x}_{n-\ell+2} &= \lambda_{n-\ell+1} x_{n-\ell+1} - \lambda_{n-\ell+2} x_{n-\ell+2} - \alpha_{n-\ell+2} x_{n-\ell+2}, \\
&\vdots \\
\dot{x}_n &= \lambda_{n-1} x_{n-1} - \lambda_n x_n - \alpha_n x_n.
\end{aligned} \tag{3.15}$$

The term $\lambda_{i-1} x_{i-1}(1 - y_{i+\ell-1})$ represents the reader flow from site $i - 1$ to site i. The flow increases with density level of readers at site $i - 1$ and decreases with coverage density $y_{i+\ell-1} = x_i + x_{i+1} + \cdots + x_{i+\ell-1}$. The term $\alpha_i x_i$ represents the detachment of particles from the site i to the cell environment. Also, the equations describing the last $n - \ell + 2$ equations are linear, as a ribosome reading the last ℓ codon is the last particle and hence it moves without any hindrance towards the last(stop) codon.

The output rate from site n at any time t, which is the protein production rate is

given by:

$$R(t) = (\lambda_n + \alpha_n)x_n(t). \tag{3.16}$$

3.4.1 Analysis of the steady-state

Eq. (3.15) can be written as:

$$\dot{x}_i = f_{i-1}(x) - f_i(x) - g_i(x_i), \quad i = 1, 2, \ldots, n, \tag{3.17}$$

where

$$\begin{aligned} f_0(x) &:= \lambda_0(1 - y_\ell), \\ f_i(x) &:= \lambda_i x_i(1 - y_{i+\ell}),\ i = 1, \ldots, n-1, \\ f_n(x) &:= \lambda_n x_n, \\ g_i(x_i) &:= \alpha_i x_i. \end{aligned} \tag{3.18}$$

Also, $y_i = 0$, for all $i \geq n+1$. At steady state, the left-hand side of Eq. (3.17) is zero, so

$$f_{i-1}(e) = f_i(e) + g_i(e_i), \quad i = 1, 2, \ldots, n. \tag{3.19}$$

Let $R = (\lambda_n + \alpha_n)e_n$ denote the steady-state output rate. From Eq. (3.19), we get

$$R = f_n(e) + g_n(e_n) = f_i(e) - \sum_{k=i+1}^{n-1} g_k(e_k), \quad i = 0, 1, \ldots n-1. \tag{3.20}$$

This yields the following set of $n+1$ equations in the $n+1$ unknowns: $e_1, \ldots, e_n, R$:

$$\begin{aligned} e_n &:= \frac{R}{\lambda_n}, \\ e_i &:= \frac{R + \sum_{k=i+1}^{n-1} g_k(e_k)}{\lambda_i(1 - y_{i+\ell})},\ i = n-1, \ldots, 1, \quad \text{and} \\ y_\ell &:= \frac{\lambda_0 - R - \sum_{k=1}^{n-1} g_k(e_k)}{\lambda_0}. \end{aligned} \tag{3.21}$$

Solving Eq. (3.21) is in general non-trivial. Nevertheless, it can be solved in closed form in some special cases. Note that when $\alpha_i = 0$, for all i, RFMEOD gets reduced to RFMEO [69].

Example 3.4.1. Consider an RFMEOD with dimension n and with particle size $\ell = n$. Consider homogeneous rates; $\lambda_i = \lambda$, for $i = 0, 1, \ldots, n$ and $\alpha_i = \alpha$, for

$i = 1, 2, \ldots, n$. We have

$$R = \frac{\lambda}{1 + \frac{\lambda}{\lambda+\alpha} + (\frac{\lambda+\alpha}{\lambda})(\sum_{i=1}^{n-1} \sum_{j=0}^{n-i-1} \binom{n-i-1}{j} (\frac{\alpha}{\lambda})^j)}, \tag{3.22}$$

and

$$e_i = \frac{\sum_{j=0}^{n-i-1} \binom{n-i-1}{j} (\frac{\alpha}{\lambda})^j}{1 + \frac{\lambda}{\lambda+\alpha} + (\frac{\lambda+\alpha}{\lambda})(\sum_{i=1}^{n-1} \sum_{j=0}^{n-i-1} \binom{n-i-1}{j} (\frac{\alpha}{\lambda})^j)}. \tag{3.23}$$

In case of totally homogeneous rates $\lambda = \alpha$, we have

$$R = \frac{2\ \lambda}{2^{n+1} - 1}, \quad \text{and} \quad e_i = \frac{2^{n-i}}{2^{n+1} - 1}. \tag{3.24}$$

Eq. (3.20) can be used to prove various theoretical results. The next result shows that increasing any of the α_i's, $i \neq n$ decreases R. In other words, increasing any of the internal detachment rate decreases the steady-state protein production rate.

Proposition 3.4.1. *Consider an RFMEOD with dimension n and particle size ℓ. Then $(\partial/\partial\alpha_i)R < 0$, for all $i = 1, 2, \ldots, n-1$.*

The next result shows that increasing any of the λ_i's increases R. In particular, increasing the initiation rate always leads to an increase in the protein synthesis rate. This result is consistent with a proposed canonical model of eukaryotic translation exhibiting a relation between initiation rate and protein expression [116].

Proposition 3.4.2. *Consider an RFMEOD with dimension n and particle size ℓ. Then $(\partial/\partial\lambda_i)R > 0$, for $i = 0, 1, 2, \ldots, n$.*

Consider the case where all $\lambda_i = \lambda$ and $\alpha_i = \alpha$. In this case, we can say more about steady-state densities.

Proposition 3.4.3. *Consider an RFMEOD with dimension n, particle size ℓ, $\lambda_i = \lambda$, and $\alpha_i = \alpha$ $(\neq 0)$. Then*

$$e_i = \left(\frac{\lambda + \alpha}{\lambda}\right)^{n-i} e_n, \quad \textit{for} \quad i = n - \ell + 1, \ldots, n, \tag{3.25}$$

$$e_1 > e_2 > \cdots > e_{n-\ell+1} > e_{n-\ell+2} > \cdots > e_n, \tag{3.26}$$

and

$$y_\ell > y_{\ell+1} > \cdots > y_n. \tag{3.27}$$

This implies that the steady-state reader densities decrease between sites 1 and n and last ℓ sites reader density is given by Eq. (3.25). The next example demonstrates this.

Example 3.4.2. The steady-state reader densities of the RFMEOD with dimension $n = 16$, for three particle sizes $\ell = 2, 4, 8$ and $\lambda_0 = 1$, $\lambda_i = 1$, and $\alpha_i = 0.1$, are depicted in Fig. 3.11. It may be observed that steady-state reader densities monotonically decrease along the mRNA.

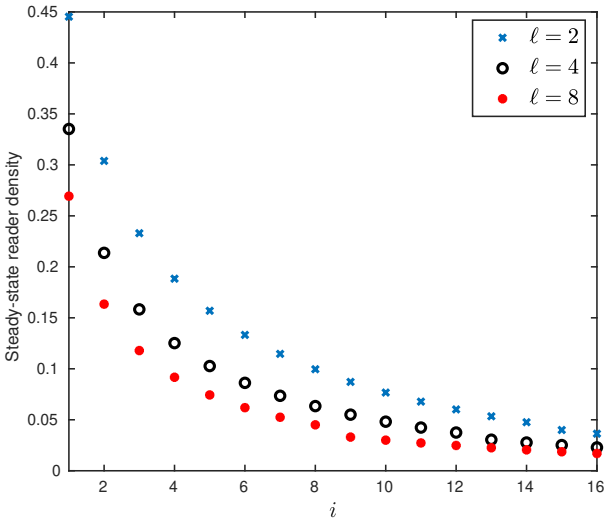

Figure 3.11: The steady-state reader densities as a function of i for a RFMEOD with $n = 16$, $\lambda_0 = 1$, $\lambda_i = 1$, and $\alpha_i = 0.1$, for $i = 1, 2, \ldots, 16$, for different values of ℓ.

It has been seen that for fixed rates, the steady-state protein production rate in the RFMEO with $\ell > 1$ is always less than the steady-state protein production rate with $\ell = 1$ [69]. We also observed and investigated through simulations that this seems to hold even in the case of the presence of a drop-off phenomenon.

Example 3.4.3. Consider a RFMEOD with $n = 300$ sites, ribosome size ℓ and rates $\lambda_0 = 0.8$, $\lambda_i = 1$, $\alpha_i = 0.01$, for all i. It can be seen that in Fig. 3.12, R monotonically decreases with ℓ.

3.4.2 RFMEOD with positive feedback

In eukaryotes, mRNA molecules sometimes form circular structures that promote recycling of the ribosomal subunits [117, 118, 74]. Therefore, it is biologically evident to include the fact that the translation initiation rate is affected by the premature and complete translation termination rate. This model can be used to fine-tune the rate of protein production by ribosome recycling in the case of changing ribosomal availability due to environmental stress [119]. We analyze the behavior of the RFMEOD as a control system after closing the loop from the output of ribosomes to the input with positive linear feedback.

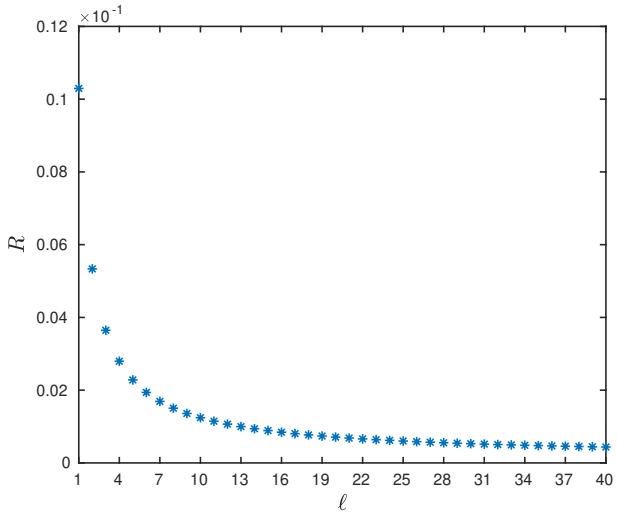

Figure 3.12: The steady-state output rate R as a function of $\ell \in \{1, 2, \ldots, 40\}$ for a RFMEOD with $n = 300$, $\lambda_0 = 0.8$, $\lambda_i = 1$, and $\alpha_i = 0.01$, for all i.

Consider the RFMEOD with feedback:

$$\begin{aligned}
\dot{x}_1 &= (k_1 + k_2(\lambda_n x_n + \sum_{i=1}^{n} \alpha_i x_i))(1 - y_\ell) - \lambda_1 x_1(1 - y_{\ell+1}) - \alpha_1 x_1, \\
\dot{x}_2 &= \lambda_1 x_1(1 - y_{\ell+1}) - \lambda_2 x_2(1 - y_{\ell+2}) - \alpha_2 x_2, \\
&\vdots \\
\dot{x}_{n-\ell+1} &= \lambda_{n-\ell} x_{n-\ell}(1 - y_n) - \lambda_{n-\ell+1} x_{n-\ell+1} - \alpha_{n-\ell+1} x_{n-\ell+1}, \\
\dot{x}_{n-\ell+2} &= \lambda_{n-\ell+1} x_{n-\ell+1} - \lambda_{n-\ell+2} x_{n-\ell+2} - \alpha_{n-\ell+2} x_{n-\ell+2}, \\
&\vdots \\
\dot{x}_n &= \lambda_{n-1} x_{n-1} - \lambda_n x_n - \alpha_n x_n,
\end{aligned} \tag{3.28}$$

where $k_1 > 0$ and $k_2 \geq 0$.

Here, the parameter k_1 represents the diffusion of ribosomes to the start codon of a mRNA molecule that is not related to the recycling of ribosomes. The term $k_2(\lambda_n x_n + \sum_{i=1}^{n} \alpha_i x_i)$ represents the feedback due to recycling of ribosomes that have finished (partially or completely) the process of translating the mRNA as depicted in Fig. 3.13.

This is a generalization of the original RFMEOD as it includes both a term related to initiation rate with and without recycling of ribosomes. The next theorem proves that trajectories from any initial condition in Ψ will always converge to a unique steady state point in Ψ.

Theorem 3.4.1. *The set Ψ includes a unique steady-state density e of the*

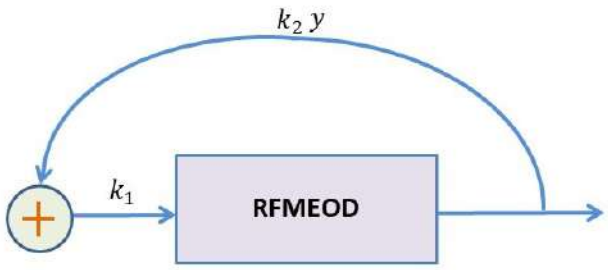

Figure 3.13: The EFEIOD with feedback where parameters k_1 and k_2 represent the constant source and recycling rate of ribosomes, respectively. The term $y = \lambda_n x_n + \sum_{i=1}^{n} \alpha_i x_i$ denotes the output of ribosomes from the system.

closed-loop system (3.28). This point is globally asymptotically stable in Ψ*, i.e.,* $\lim_{t\to\infty} x(t,a) = e$ *for any initial condition* $a \in \Psi$.

Example 3.4.4. Consider the closed loop system (3.28) with dimension $n = 3$, $\ell = 2$, $\lambda_i = 1$, $\alpha_i = 0.01$, $k_1 = 1$ and $k_2 = 100$. Fig. 3.14 depicts trajectories for three different initial conditions $[1 \quad 0 \quad 0]'$, $[0 \quad 1 \quad 0]'$, and $[0 \quad 0 \quad 1]'$ in Ψ.

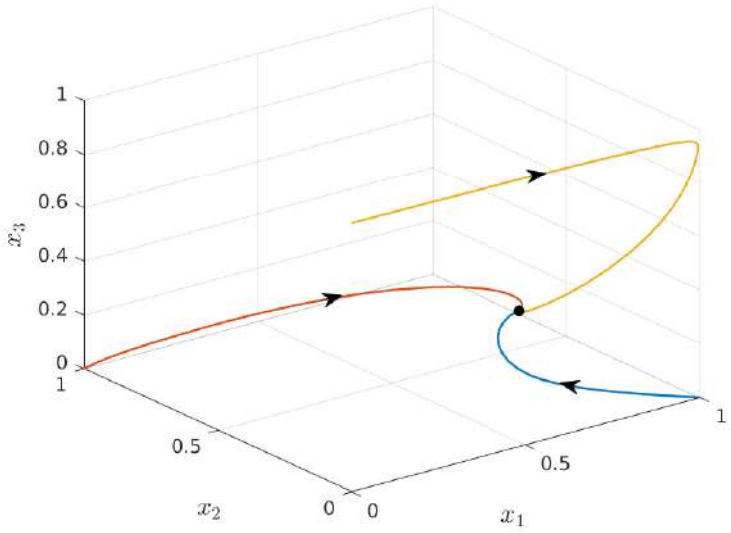

Figure 3.14: Trajectories of RFMEOD for three initial conditions given in Example 3.4.4 as a function of time. The steady-state point is marked by a ellipse.

The next result provides information on the change of e w.r.t. the control parameters k_1 and k_2.

Proposition 3.4.4. *Suppose that the* λ_i*'s and* α_i*'s are fixed. Let* e *and* $\bar{e}$ *correspond to the control parameters* (k_1, k_2) *and* $(\bar{k}_1, \bar{k}_2)$*, respectively. If* $k_1 = \bar{k}_1$*, then* $e_n < \bar{e}_n$ *if and only if* $k_2 < \bar{k}_2$*. If* $k_2 = \bar{k}_2$*, then* $e_n < \bar{e}_n$ *if and only if* $k_1 < \bar{k}_1$.

From a biophysical point of view, the above result inferred the intuitive result that increasing any of the control parameters leads to an increase in the protein production rate. This result may be useful in the context of biotechnology in order to improve the levels of proteins in the host.

3.4.3 Validation through Monte Carlo simulations

Since the RFMEOD is a mean-field approximation of TASEP with extended objects and includes an additional detachment rate at every site of the lattice, we ran MATLAB simulations of this process. A simulation begins with an empty chain of dimension n and continues for 10^8 time steps i.e., total simulation time. Each site can accommodate atmost one particle and a particle can only hop unidirectionally to a consecutive site if it is empty. The leftmost site that the particle is covering is referred to as the reader. Every site i, for $i = 1, 2, \ldots, n$ in the chain is associated with hopping rates λ_i's and detachment rates α_i's where the next hopping event time $t_k + \epsilon_k$ or the next detachment event time $t_k + \delta_k$ is generated randomly. For site i, ϵ_k and δ_k are random variables drawn from the exponential distribution with mean rate λ_i and α_i, respectively. If hopping time is equal to the simulation time, then the reader at site i hops to site $i + 1$, provided site $i + \ell$ is empty. Similarly, if the detachment event time is equal to the simulation time then the reader dissociates from site i. The occupancy at each site is averaged throughout the simulations with the first 10^6 time steps discarded from the calculations to obtain the average steady-state reader density of each site.

In the example below, we show that simulations support the modeling of dynamical aspects of translation using RFMEOD.

Example 3.4.5. Consider the RFMEOD with dimension $n = 15$, particle size $\ell = 3$, rates $\lambda_0 = 0.1$, $\lambda_i = 1$, for $i = 1, 2, \ldots, n-1$, $\lambda_n = 0.8$, and $\alpha_i = 0$ except for $\alpha_8 = 0.01$. Fig. 3.15 depicts steady-state reader density e and ρ for RFMEOD and TASEP-detachment, respectively.

3.5 Discussion

In many biological processes like translation, cellular transport, gene transcription, and many more, 'particles' move along one-dimensional "tracks". We studied a deterministic model called EFEIOD for the flow of particles along an ordered lattice of sites that encapsulates important cellular properties like detachment of particles from any site, nearest-neighbor interactions, and the fact that most particles cover more than one site along the lattice. We analyzed this model using tools from systems and control theory, in particular contraction theory.

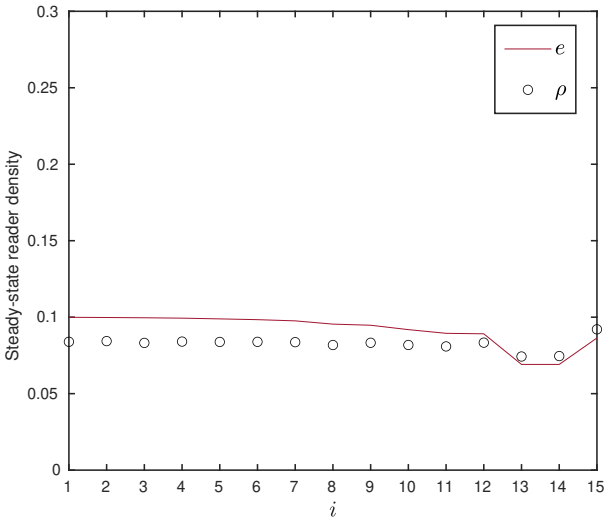

Figure 3.15: Steady-state reader density as a function of site number i given in Example 3.4.5.

We proved that the EFEIOD converges to a unique steady-state density for any set of feasible parameters. In other words, EFEIOD is robust to the initial conditions. Moreover, we prove that if one or more of the parameters are time-varying periodic functions with a common period T, then the steady-state densities also converge to a periodic solution with period T. We demonstrate through simulations of the EFEIOD several useful observations. For example, increasing the particle size may sometimes lead to an increase in the output rate in the presence of weak repulsions. Surprisingly, we also show that increasing the detachment rate does not always decrease the output rate as elucidated in Ref. [90]. It is also important to note that several known models like RFM with positive feedback [61], RFMEO [69], and the model used in [75] for mRNA translation are special cases of the proposed model.

We also rigorously analyzed a special case of the EFEIOD, when $q = r = 1$ and called it RFMEOD to analyze the effects of ribosome drop-off on the translation process. The ribosome drop-off is important to study as it could significantly deteriorate the fitness of the host. We proved that increasing any one of the transition (detachment) rates of the RFMEOD always increases (decreases) the steady-state protein production and that in the homogeneous case, i.e., when all the transition rates are equal and all the detachment rates are equal, the reader density monotonically decreases along the lattice. We also modeled the observed phenomenon that many eukaryotic ribosomes may translate mRNA in multiples by including positive linear feedback in the RFMEOD.

The results reported can shed light on many biophysical properties of intracellular transport and may prove useful for applications in synthetic biology. One may consider integrating another realistic feature of cellular transport such as the attachment of biological particles at different sites along the tracks in our model. Another research topic is studying the networks of EFEIOD and considering various phenomena like competition of resources in the network. We believe that the EFEIOD can be generalized to model and analyze more natural and artificial processes. Examples include coordination of large groups of organisms, traffic control, and more.

3.6 Appendix: Proofs

Proof of Proposition 3.3.1 and 3.3.2: The fact that Ψ is an invariant set of the dynamics and has a repelling boundary follows from the equations from the EFEIOD. Let

$$\eta_i(t) := \lambda_i(1+(q-1)z_{i+\ell+1})(1+(r-1)z_{i-\ell}), \quad i=0,1,\ldots,n \tag{3.29}$$

and

$$\delta_i(t) := \alpha_i(1+(r-1)z_{i+\ell})(1+(r-1)z_{i-\ell}), \tag{3.30}$$

with the z_i's defined in Eq. (3.2). Therefore, EFEIOD can be written as:

$$\dot{x}_1 = \eta_0(t)\ (1-w_\ell) - \eta_1(t)\ x_1(t)\ (1-w_{\ell+1}) - \delta_1\ x_1 \quad \text{and} \tag{3.31}$$

$$\dot{x}_i = \eta_{i-1}(t)\ x_{i-1}(t)\ (1-w_{i+\ell-1}) - \eta_i(t)\ x_i(t)\ (1-w_{i+\ell}) - \delta_i\ x_i \quad i=2,3,\ldots,n, \tag{3.32}$$

with the w_i's defined in Eq. (3.3).

Note that for $r,q>0$, all the time-varying transition rates $\eta_i(t)$ are uniformly separated from zero and uniformly bounded and all the time-varying detachment rates are non-negative and uniformly bounded. Now, the proof of proposition follows from the results in Refs. [69] and [48].

Proof of Proposition 3.3.3 : Let

$$\psi_i(t) := \eta_i(t)\ \frac{(1-w_{i+\ell}(t))}{(1-x_{i+1}(t))}, \quad i=0,1,\ldots,n-1 \tag{3.33}$$

and

$$\psi_n(t) := \eta_n(t)\ (1-w_{n+\ell}(t)). \tag{3.34}$$

Now, combining the representations in Eqs. (3.33) and (3.34) with the Eqs. (3.31)

and (3.32), we get

$$\dot{x}_1 = \psi_0\ (1 - x_1) - \psi_1\ x_1(1 - x_2) - \delta_1\ x_1, \tag{3.35}$$

$$\dot{x}_i = \psi_{i-1}\ x_{i-1}(1 - x_i) - \psi_i\ x_i(1 - x_{i+1}) - \delta_i\ x_i, \quad i = 2, \ldots, n-1, \quad \text{and} \tag{3.36}$$

$$\dot{x}_n = \psi_{n-1}\ x_{n-1}(1 - x_n) - \psi_n\ x_n - \delta_n\ x_n. \tag{3.37}$$

Proposition 3.3.1 and the equations above imply that that EFEIOD can be interpreted as time-varying MFALK system with no backward and attachment dynamics with the well defined rates for all $t > 0$. Write the time-varying MFALK as $\dot{x} = f(x, t)$ with transition rates $\psi_i(t)$ and detachment rates $\delta_i(t)$. A calculation shows that the Jacobian of f is $J(t, x) = L(t, x) + D(t)$, where L is the matrix

$$\begin{bmatrix} -\psi_1(1-x_2) & \psi_1 x_1 & 0 & \ldots & 0 \\ \psi_1(1-x_2) & -\psi_1 x_1 - \psi_2(1-x_3) & \psi_2 x_2 & \ldots & 0 \\ 0 & \psi_2(1-x_3) & -\psi_2 x_2 - \psi_3(1-x_4) & \ldots & 0 \\ & & \ddots & & \\ 0 & 0 & \ldots & \psi_{n-1}(1-x_n) & -\psi_{n-1}x_{n-1} \end{bmatrix}$$

and D is the diagonal matrix

$$D = \mathrm{diag}(-\psi_0 - \delta_1, -\delta_2, \ldots, -\delta_{n-1}, -\psi_n - \delta_n). \tag{3.38}$$

Hence, Proposition 3.3.2 and the results in Ref. [68] and [48] imply that the EFEIOD is SOST on Ψ and this completes the proof.

Proof of Proposition 3.3.4: It follows from the results in Ref. [68] and the argument used in the proof of Proposition 3 in Ref. [67].

Proof of Proposition 3.4.1: Consider two RFMEODs both with same dimension n, particle size ℓ, rates λ_i for all $i = 0, 1, \ldots, n$, and α_i for $i = 1, 2, \ldots, n$, except for any one $j \in \{1, 2, \ldots, n-1\}$ such that

$$\alpha_j < \bar{\alpha}_j. \tag{3.39}$$

Therefore, the first RFMEOD admits a steady-state production rate R and the second one admits $\bar{R}$. We have to prove that $\bar{R} < R$. We shall prove it by contradiction.

Let us assume that

$$R \leq \bar{R}, \tag{3.40}$$

which implies that

$$e_n \leq \bar{e}_n. \tag{3.41}$$

From Eqs. (3.40), (3.41), and (3.20), we have

$$e_{n-1} \leq \bar{e}_{n-1}. \tag{3.42}$$

We start with the case $j = n - 1$. From Eqs. (3.20) and (3.40), we have

$$\lambda_{n-2}\ e_{n-2} - \alpha_{n-1}\ e_{n-1} \leq \lambda_{n-2}\ \bar{e}_{n-2} - \bar{\alpha}_{n-1}\ \bar{e}_{n-1}. \tag{3.43}$$

Now, Eqs. (3.39) and (3.43) implies that

$$\lambda_{n-2}\ e_{n-2} - \bar{\alpha}_{n-1}\ e_{n-1} \leq \lambda_{n-2}\ \bar{e}_{n-2} - \bar{\alpha}_{n-1}\ \bar{e}_{n-1}, \tag{3.44}$$

which implies that

$$e_{n-2} < \bar{e}_{n-2}. \tag{3.45}$$

Continuing this way, we have

$$e_j \leq \bar{e}_j, \quad \text{for} \quad j = n - \ell + 1, \ldots, n - 2. \tag{3.46}$$

This means that

$$y_n < \bar{y}_n. \tag{3.47}$$

Now, from Eqs. (3.20), (3.39), and (3.40), we have

$$\lambda_{n-\ell}\ e_{n-\ell}\ (1 - y_n) - \sum_{i=n-\ell+1}^{n-1} \alpha_i\ e_i \leq \lambda_{n-\ell}\ \bar{e}_{n-\ell}\ (1 - \bar{y}_n) - \sum_{i=n-\ell+1}^{n-1} \alpha_i\ \bar{e}_i. \tag{3.48}$$

Combining this with Eqs. (3.42), (3.46), and (3.47), we have

$$e_{n-\ell} < \bar{e}_{n-\ell}. \tag{3.49}$$

Continuing this way, we have

$$e_j < \bar{e}_j, \quad \text{for} \quad j = 1, \ldots, n - 2, \tag{3.50}$$

which implies that

$$y_\ell < \bar{y}_\ell. \tag{3.51}$$

From Eqs. (3.20) and (3.39), consider

$$\lambda_0\ (1 - y_\ell) - \sum_{i=1}^{n-1} \alpha_i\ e_i \leq \lambda_0\ (1 - \bar{y}_\ell) - \sum_{i=1}^{n-1} \alpha_i\ \bar{e}_i. \tag{3.52}$$

From Eqs. (3.41) and (3.52), we have

$$y_\ell \geq \bar{y}_\ell, \tag{3.53}$$

which is the contradiction to Eq. (3.51) resulting in $\bar{R} < R$ in the case $\alpha_{n-1} < \bar{\alpha}_{n-1}$.

Hence, using the same approach for any $j \in \{1, 2, \ldots, n-1\}$, we can conclude that $\bar{R} < R$.

Proof of Proposition 3.4.2: The proof is similar to the proof of Proposition 3.4.1 above and is thus omitted.

Proof of Proposition 3.4.3: From Eq. (3.20), we have

$$\lambda\ e_{n-1} = (\lambda + \alpha)\ e_n \implies e_{n-1} = \left(\frac{\lambda + \alpha}{\lambda}\right)\ e_n. \tag{3.54}$$

Similarly, we have

$$e_j = \left(\frac{\lambda + \alpha}{\lambda}\right)^{n-j}\ e_n, \quad \text{for} \quad j = n - \ell + 1, \ldots, n \tag{3.55}$$

Since $(\lambda + \alpha) > \lambda$, we have

$$e_{n-\ell+1} > e_{n-\ell+2} > \cdots > e_n. \tag{3.56}$$

From Eq. (3.20), consider

$$\lambda\ e_{n-\ell}\ (1 - y_n) - \sum_{i=n-\ell+1}^{n-1} \alpha\ e_i = \lambda\ e_{n-\ell+1} - \sum_{i=n-\ell+2}^{n-1} \alpha\ e_i, \tag{3.57}$$

which implies

$$\lambda\ e_{n-\ell}\ (1 - y_n) = \lambda\ e_{n-\ell+1} + \alpha\ e_{n-\ell+1}. \tag{3.58}$$

Therefore,

$$e_{n-\ell}\ (1 - y_n) > e_{n-\ell+1} \implies e_{n-\ell} > e_{n-\ell+1}. \tag{3.59}$$

From Eq. (3.56),

$$e_{n-\ell} > e_{n-\ell+1} > e_{n-\ell+2} > \cdots > e_n. \tag{3.60}$$

Now, consider

$$y_{n-1} - y_n = e_{n-\ell} - e_n > 0 \implies y_{n-1} > y_n. \tag{3.61}$$

Now, from Eq. (3.20),

$$\lambda\ e_{n-\ell-1}\ (1 - y_{n-1}) = \lambda\ e_{n-\ell}\ (1 - y_n) + \alpha\ e_{n-\ell}. \tag{3.62}$$

which implies

$$e_{n-\ell-1}\ (1 - y_{n-1}) > e_{n-\ell}\ (1 - y_n). \tag{3.63}$$

From Eq. (3.61), we have

$$e_{n-\ell-1} > e_{n-\ell} \tag{3.64}$$

and thus

$$y_{n-2} > y_{n-1}. \tag{3.65}$$

Continuing in this way completes the proof.

Proof of Theorem 3.4.1: Clearly, Ψ is an invariant set of the dynamics. Note that this system is RFMEOD with a time-varying initiation rate which is uniformly bounded and uniformly separated from zero, i.e.,

$$0 < k_1 + k_2(\lambda_n x_n + \sum_{i=1}^{n} \alpha_i x_i) < M. \tag{3.66}$$

Now, the proof follows by Theorem 3.3.1.

Proof of Proposition 3.4.4: We have equations for the RFMEOD with feedback at steady-state as follows:

$$\begin{aligned} e_n &:= \frac{R}{\lambda_n}, \\ e_i &:= \frac{R + \sum_{k=i+1}^{n-1} g_k(e_k)}{\lambda_i(1 - y_{i+\ell})},\ i = n-1, \ldots, 1, \quad \text{and} \\ y_\ell &:= 1 - \frac{R + \sum_{k=1}^{n-1} g_k(e_k)}{\lambda_0\ (k_1 + k_2(\lambda_n e_n + \sum_{i=1}^{n} \alpha_i e_i))}. \end{aligned} \tag{3.67}$$

Suppose that $k_1 = \bar{k}_1$ and $k_2 < \bar{k}_2$. We have to prove that $e_n < \bar{e}_n$. We shall prove it by contradiction. Assume

$$\bar{e}_n \leq e_n, \tag{3.68}$$

which implies that

$$\bar{R} \leq R, \tag{3.69}$$

which further implies from Eq. (3.67) that

$$\bar{e}_i \leq e_i, \quad \text{for all} \quad i = 1, 2, \ldots, n-1. \tag{3.70}$$

Therefore,

$$\bar{y}_\ell \leq y_\ell. \tag{3.71}$$

From Eq. (3.67) and simplifying calculations we have,

$$\begin{aligned} y_\ell - \bar{y}_\ell = k_1\ (\lambda_n + \alpha_n)\ (\bar{e_n} - e_n) + (k_2 - \bar{k}_2)\ (\lambda_n\ (\lambda_n + \alpha_n)\ \bar{e}_n + \alpha_n\ (\lambda_n + \alpha_n)\ e_n\ \bar{e}_n) \\ + (k_2 - \bar{k}_2)\ \Big((\lambda_n + \alpha_n)\ \sum_{i=1}^{n-1}(\bar{e}_i\ e_n + e_i\ \bar{e}_n) + \Big(\sum_{i=1}^{n-1} \alpha_i\ e_i\Big)\ \Big(\sum_{i=1}^{n-1} \alpha_i\ \bar{e}_i\Big)\Big). \end{aligned} \tag{3.72}$$

The fact that $k_2 < \bar{k}_2$ and Eqs. (3.68) and (3.72) implies that

$$y_\ell < \bar{y}_\ell \tag{3.73}$$

which is a contradiction to Eq. (3.71) and hence $e_n < \bar{e}_n$, and the other part follows the same arguments.

Chapter 4

Modeling mRNA translation with ribosome abortions

This chapter[1] introduces a deterministic mathematical model for the flow of extended length particles along the track encapsulating the fact that particles may detach due to the collision with the neighboring particles. In particular, we study ribosome flow along a mRNA molecule and provide insight into the effects of premature termination due to abortions on protein expression.

4.1 Introduction

Gene translation is a process during which complex macromolecules called ribosomes decode the information inscribed in an mRNA molecule unidirectionally codon by codon to yield a functional protein [2]. One of the major errors in translation is abortion, i.e., premature detachment of ribosomes from the mRNA strand resulting in non-functional truncated proteins [115]. Even in non-stressed conditions, a certain minimal abortion rate is observed [81]. Various mechanisms are known to cause translation abortion. For example, ribosome collisions at stalls stimulate abortive termination of the leading ribosome or can correspond to mutual abortion [116], a false stop codon resulting from frameshift [120], and local depletion of tRNA molecules etc. [74, 121, 122]. Translation is a central and one of the most energy consuming processes in the cell and thus, modeling translation by encapsulating the feature of ribosome abortions that can affect this process has important implications to cell's functioning, human health, evolution, and biotechnology [1].

The RFMLK analyzes mRNA translation with ribosome drop-off [68]. Yet, it does not take into account the feature of detachment of ribosomes due to collisions between them. As such, both the RFM and the RFMLK inherit the property that the site size is equal to the size of the particle.

In this chapter, we introduce a deterministic mathematical model called ribosome

[1]The content of this chapter is published as: "Aditi Jain and Arvind Kumar Gupta. Modeling mRNA translation with ribosome abortions. *IEEE/ACM Transactions on Computational Biology and Bioinformatics* 20(2):1600-1605, 2022."

flow model with extended objects and abortions (RFMEOA) to analyze mRNA translation with fundamental phenomena of ribosome drop-off from the mRNA. It models several reasons that could lead to detachment of ribosomes along a mRNA molecule such as collisions between ribosomes or depletion of the concentration of elongation factors. Using tools from the contraction theory, we prove that RFMEOA always converges to a steady state. In other words, the density profile of ribosomes and the protein production rate always converge to a unique steady state.

The chapter is organized as follows. The next two sections describe the model and present our main results, respectively. Section 4.4 studies the effect of parameters on the steady-state output rate. Section 4.5 summarizes the chapter and finally, the proofs of the results are given in Section 4.6.

4.2 Model

The RFMEOA is a set of n first-order nonlinear ordinary differential equations, where n denotes the number of sites along the mRNA. We assume that every ribosome covers $1 \leq \ell \leq n$ site units and is translating the left-most site it is covering and refer to this part of the ribosome as the *reader*. Thus, 'the ribosome is at site i' implies that the ribosome is located at site i and is translating it while all the sites $i,\ i+1,\ldots,\ i+\ell-1$ remain covered by it simultaneously. Hence, the ribosome that is located upto ℓ sites left to the site i contributes to the total ribosome coverage at site i. Let $x_i(t)$ denote the 'normalized' reader density at site i at time t (see Fig. 4.1).

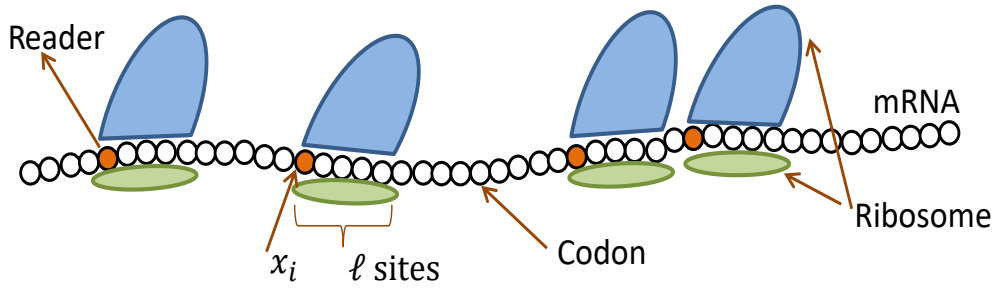

Figure 4.1: The RFMEOA as a chain of n sites of codons. Each ribosome occupies ℓ sites and each site is described by a reader density $x_i(t) \in [0, 1]$.

Let $y_i(t)$ denote the 'normalized' coverage density at site i at time t, i.e.,

$$y_i(t) = \sum_{j=max\{1,i-\ell+1\}}^{i} x_j(t), \quad i = 1, 2, \ldots, n. \tag{4.1}$$

The term 'normalized' implies that each variable $x_i(t)$ and $y_i(t)$ takes value in the

interval $[0,1]$ for all $t \geq 0$. The value zero [one] means that site i is completely free [full]. Now, we consider a state-space Ψ for the RFMEOA such that values of x_i's and y_i's are between zero and one. Let

$$\Psi := \{x \in \mathbb{R}^n : x \in C^n \text{ and } y \in C^n\}.$$

Note that the 'vacancy' level at site i is $(1-y_i)$, where y_i denotes the total ribosome coverage at site i.

The dynamics of the RFMEOA with n sites is given by:

$$\dot{x}_i = f_{i-1}(x) - f_i(x) - g_i(x), \quad i = 1, 2, \ldots, n, \tag{4.2}$$

where

$$f_i(x) := \lambda_i x_i (1 - y_{i+\ell}), \quad i = 0, 1, \ldots, n, \tag{4.3}$$

and

$$g_i(x) := \alpha_i x_i (a_i + b_i\ x_{i-\ell})(c_i + d_i\ x_{i+\ell}), \quad i = 1, 2, \ldots, n, \tag{4.4}$$

with $x_i(t) \equiv 0$ and $y_i(t) \equiv 0$ for all $i < 1$ and $i > n$. Here, the non-negative parameters α_i, a_i, b_i, c_i and d_i controls the detachment from site i to the environment. Each parameter λ_i, α_i, a_i, b_i, c_i and d_i has units 1/time.

The term $f_i(x)$ represents that the *reader* flow from site i to site $i+1$ is proportional to the reader occupancy level at site i $[x_i]$ and to the 'vacancy' level at site $i+\ell$ $[1-y_{i+\ell}]$ [69]. This is a 'soft' version of the exclusion principle which implies that the rate of movement decreases as the density in any of the ℓ consecutive sites increases.

The term $g_i(x)$ represents that the detachment of ribosomes from site i to the environment is proportional to its reader occupancy level and to the reader occupancy level of the neighboring ribosomes. Note that the neighboring ribosomes of a ribosome at site i are ribosomes at sites $i-\ell$ and $i+\ell$. The term $(a_i + b_i\ x_{i-\ell})$ represents the fact that the detachment of ribosomes at site i is stimulated by the collision with the preceding ribosome, i.e., the preceding ribosome must be at site $i-\ell$. Similarly, the term $(c_i + d_i\ x_{i+\ell})$ represents the fact that the detachment of ribosomes at site i is stimulated by the collision with the succeeding ribosome. To further explain Eq. (4.4), consider the case $i = 4$, $\ell = 2$, $b_4 \neq 0$ and $d_4 \neq 0$ (assume that $n \geq 6$). Then Eq. (4.4) yields

$$g_4(x) = \alpha_4 x_4 (a_4 + b_4\ x_2)(c_4 + d_4\ x_6). \tag{4.5}$$

The term $a_4 + b_4 x_2$ and $c_4 + d_4 x_6$ represents the fact that the detachment from site 4

also depends on the reader density at site 2 and at site 6, respectively, which means that the detachment of ribosome at site 4 is stimulated by the collisions with the neighboring ribosomes.
The output rate of ribosomes from site n at time t, which is also called the protein translation rate or production rate, is denoted by

$$R(t) := \lambda_n x_n(t) + \alpha_n x_n(t)(a_n + b_n\ x_{n-\ell}(t)). \tag{4.6}$$

Remark 1. The case when $a_i = 1$, $b_i = 0$, $c_i = 1$ and $d_i = 0$ models the situation where ribosomes detach due to kinetic competition between normal elongation and premature termination (see Fig. 4.2(a)). This kind of situation can be viewed as a simple abortive termination (SAT) model [116].
Remark 2. The case when $a_i = 1$, $c_i = 1$ and $d_i = 0$ for all i and $b_i \neq 0$ for some i models the situation where the leading ribosomes undergo premature termination after getting hit by the trailing ribosome (see Fig. 4.2(b)). This kind of situation can be viewed as a collision-stimulated abortive termination (CSAT) model [116].
Remark 3. The case when $a_i = 1$, $b_i = 0$ and $c_i = 0$ for all i and $d_i \neq 0$ for some i models the situation where the ribosomes after a collision with the leading ribosomes will stop processing the mRNA transcript (see Fig. 4.2(c)). This kind of situation can be viewed as a collide and abortive termination (CAT) model [116].
In the particular case where $\alpha_i = 0$ for all i, the RFMEOA becomes the RFMEO, i.e., a dynamic mean-field approximation of TASEPEO [69]. The next section analyzes the dynamical behavior of the RFMEOA theoretically.

4.3 Main results

Let $x(t, a)$ denote the solution of Eq. (4.2) at time $t \geq 0$ for the initial condition $a \in \Psi$.

4.3.1 Invariance and persistence

The next result shows that Ψ is an invariant set of the dynamics and the reader/coverage densities enter and remain in the interior of Ψ after an arbitrarily short time.

Proposition 4.3.1. *If $a \in \partial\Psi$ then the solution of RFMEOA satisfies $x(t, a) \in \text{int}(\Psi)$ for all $t > 0$. For any $\tau > 0$, there exists a compact and convex set Ψ_τ that is strictly contained in Ψ such that for any $a \in \Psi$, $x(t, a) \in \Psi_\tau$, for all $t \geq \tau$.*

From a biological point of view, this means that if the system is initiated such

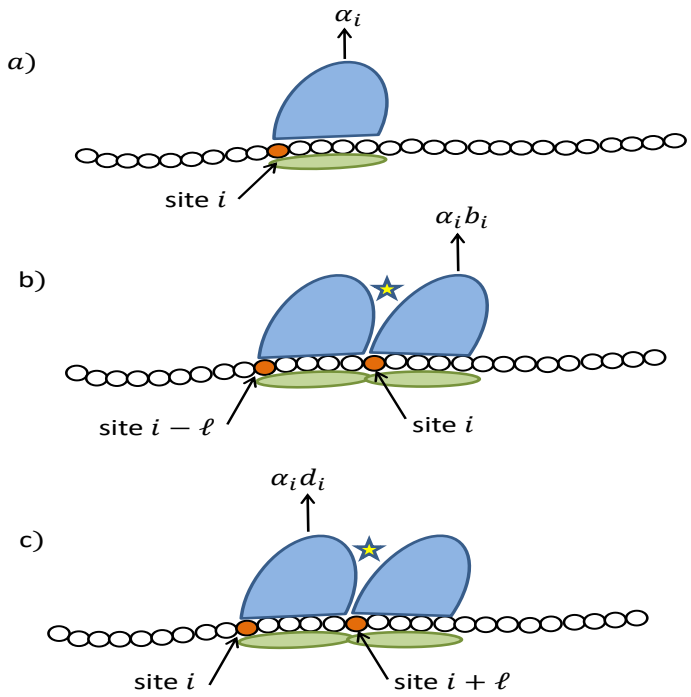

Figure 4.2: Schematic explanation of the detachment of ribosomes from site i. a) When detachment does not depend upon the collisions($a_i = 1$, $b_i = 0$, $c_i = 1$ and $d_i = 0$). b) When detachment occurs due to collision with the trailing ribosome($a_i = 1$, $c_i = 1$ and $d_i = 0$). c) When detachment occurs due to collision with the leading ribosome($a_i = 1$, $b_i = 0$ and $c_i = 0$).

that every reader/coverage density has values in Ψ at time $t = 0$, then this remains true for all $t \geq 0$. Furthermore, all the reader and coverage densities 'immediately' enter and remain in a set that is uniformly separated from the boundary of Ψ, i.e., every site along the mRNA is neither completely full nor completely empty.

4.3.2 Contraction

The next proposition proves that the RFMEOA satisfies SOST (see definition in Chapter 1). Let $|.|_1 : \mathbb{R}^n \to \mathbb{R}_+$ denote the L_1 norm, i.e., for $x \in \mathbb{R}^n$, $|x|_1 = |x_1| + |x_2| + \cdots + |x_n|$.

Proposition 4.3.2. *The RFMEOA is SOST with respect to the L_1 norm, i.e., for each $\epsilon > 0$ and each $\tau > 0$ there exists $\gamma = \gamma(\tau, \epsilon) > 0$ such that*

$$|x(t+\tau, a) - x(t+\tau, b)|_1 \leq (1+\epsilon)\ \exp(-t\gamma)|a-b|_1, \tag{4.7}$$

for all $t \geq 0$ and all $a, b \in \Psi$.

From a biological point of view, this means the following. If we initiate the system with two different ribosomal densities in Ψ. This generates two different solutions

and the distance between these solutions decreases with time at an exponential rate.

4.3.3 Global asymptotic stability

The next result describes the asymptotic property of the RFMEOA that follows from Propositions 4.3.1 and 4.3.2.

Theorem 4.3.1. *The RFMEOA admits a globally asymptotically stable steady-state density* $e \in \text{int}(\Psi)$*, i.e.,* $\lim_{t\to\infty} x(t,a) = e$*, for all* $a \in \Psi$*.*

From a biological point of view, this means that the system always converges to the unique steady-state profile, i.e., perturbations in the distribution of ribosomes on an mRNA will not change the asymptotic behavior of the RFMEOA. The next example demonstrates the stability property.

Example 4.3.1. Consider the RFMEOA with dimension $n = 3$, particle size $\ell = 2$, $\lambda_i = 1$, $i = 0, \ldots, 3$, $\alpha_1 = 0.1$, $\alpha_2 = 0$, $\alpha_3 = 0.1$, $a_1 = 0$, $a_2 = 0$, $a_3 = 1$, $b_i = 0$, $i = 1, \ldots, 3$, $c_1 = 0$, $c_2 = 0$, $c_3 = 1$, $d_1 = 1$, $d_2 = 0$ and $d_3 = 0$. Fig. 4.3 depicts the trajectories for three different initial conditions $[1 \quad 0 \quad 0]'$, $[0 \quad 1 \quad 0]'$, and $[0 \quad 0 \quad 1]'$ in Ψ. It can be seen that the three solutions converge to the same steady-state point.

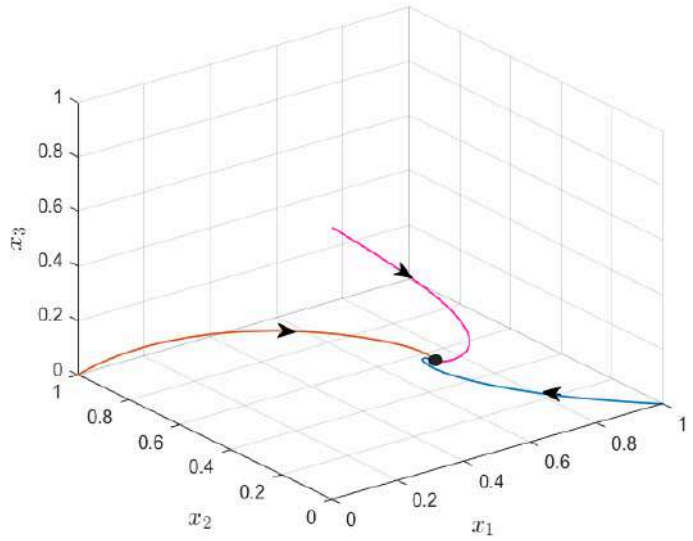

Figure 4.3: Trajectories of RFMEOA for three initial conditions given in Example 4.3.1 as a function of time. The steady-state point is marked by an ellipse.

In the next section, we explore how the steady-state output rate depends on the various parameters of the RFMEOA.

4.4 Effect of parameters

One might naturally expect the steady-state production rate to increase as the initiation rate increases. However, this is not always true in the case of the premature termination of the leading ribosome due to collision with the trailing one. The next example demonstrates this.

Example 4.4.1. Consider the RFMEOA with dimension $n = 10$, particle size $\ell = 3$, $\lambda_i = 1$, $i = 0, \ldots, n$, except $\lambda_4 = 0.1$, $\alpha_i = 0$, except $\alpha_4 = 1$, $a_i = 0$, $i = 1, \ldots, n$, $b_i = 0$, except $b_4 = 0.5$, $c_i = 1$, and $d_i = 0$, $i = 1, \ldots, n$. Fig. 4.4 depicts that the steady-state production rate decreases as the initiation rate increases. As the initiation rate increases, more ribosomes accumulate leading to an increase in ribosome collisions stimulating the abortion of the ribosome at stall site 4 and hence decreasing the production rate.

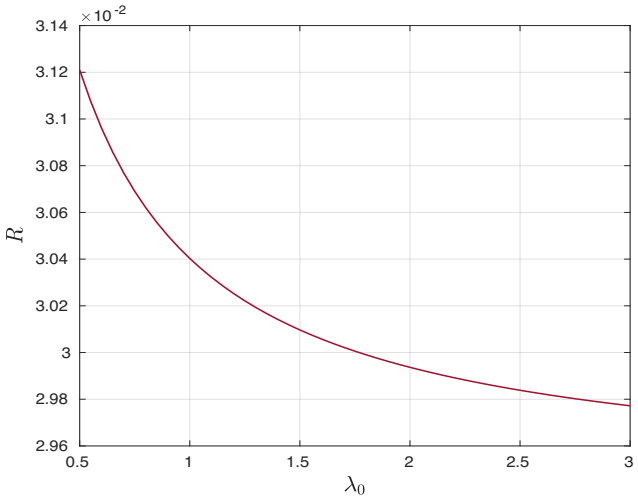

Figure 4.4: The steady-state production rate R as a function of λ_0 for a RFMEOA in Example 4.4.1.

The above example shows that increasing the initiation rate can decrease the protein expression and is consistent with the prediction of the collision-stimulated abortive termination model (CSAT) [116].

In general, to study the effect of parameters on the system dynamics by a theoretical framework is cumbersome. One needs to calculate derivatives of the steady-state point coordinates w.r.t. small changes in the parameters to obtain information on whether the steady-state output rate increases or decreases. The next result shows that these derivatives exist.

Let $p = [\lambda_0 \ \cdots \ \lambda_n \ \ \alpha_1 \ \cdots \ \alpha_n \ \ a_1 \ \cdots \ a_n \ \ b_1 \ \ \cdots \ b_n \ \ c_1 \ \cdots \ c_n \ \ d_1 \ \cdots \ d_n]'$ is the

vector of all the parameters. Consider mapping h from p to the unique steady-state point in $\text{int}(\Psi)$.

Proposition 4.4.1. *The derivative* $(\partial/\partial p_j)h_i(p)$ *exists for all* i, j.

However, there are some special cases for which the steady-state output rate sensitivity to variations in the parameters can be answered theoretically.

4.4.1 The case when $a_i = 1$ and $b_i = 0$ for all i

The next result shows that increasing any of the transition rates along the mRNA increases the steady-state protein production rate. Also, increasing the parameters associated with the detachment rate decreases the steady-state protein production rate.

Proposition 4.4.2. *Consider a RFMEOA with dimension* n, *particle size* ℓ, $a_i = 1$, *and* $b_i = 0$, *for all* i. *Then* $(\partial/\partial\alpha_i)R < 0$ *for all* $i = 1, 2, \ldots, n-1$ *and* $(\partial/\partial\lambda_i)R > 0$ *for* $i = 0, 1, 2, \ldots, n$.

Also, note that $(\partial/\partial c_i)R < 0$ and $(\partial/\partial d_i)R < 0$. In particular, increasing the initiation rate increases the protein production rate. The next example shows this.

Example 4.4.2. Consider the RFMEOA with dimension $n = 6$, particle size $\ell = 2$, $\lambda_i = 1$, $i = 1, \ldots, n$, except $\lambda_4 = 0.1$, $\alpha_i = 1$, except $\alpha_6 = 0$, $a_i = 1$, $b_i = 0$, $i = 1, \ldots, n$, $c_i = 0.1$, and $d_i = 0.1$, $i = 1, \ldots, n$. Fig. 4.5 depicts that the steady-state production rate increases as initiation rate increases.

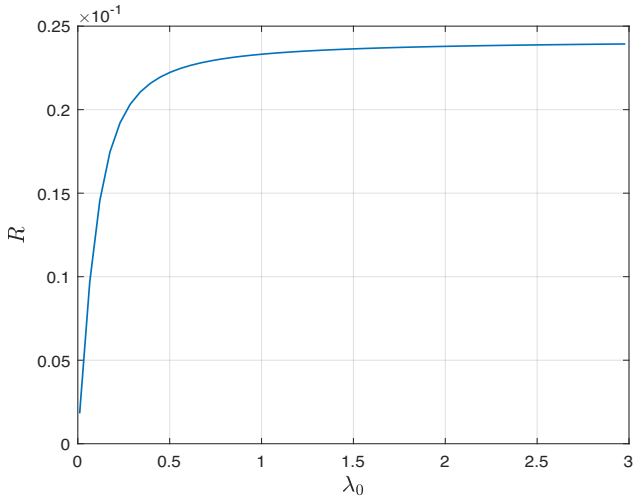

Figure 4.5: The steady-state production rate R as a function of λ_0 for a RFMEOA in Example 4.4.2.

The above example is also consistent with the prediction of the collide and abortive termination model (CAT) [116]. The next result analyzes the RFMEOA under the assumption of constant transition rates, i.e., $\lambda_i := \lambda > 0$, $i = 0, 1, \ldots, n$, and constant parameters $\alpha_i := \alpha > 0$, $i = 1, \ldots, n$.

Proposition 4.4.3. *Consider a RFMEOA with dimension n, particle size ℓ, $\lambda_i = \lambda > 0$, $\alpha_i = \alpha > 0$, $a_i = 1$, and $b_i = 0$ for all i. Then*

$$e_1 > e_2 > \cdots > e_{n-1} > e_n. \tag{4.8}$$

The above proposition implies that steady-state reader densities monotonically decrease between sites 1 and n.

4.4.2 The case when $\ell = 1$

The next result shows that an increase in any of the transition [detachment] rates increases [decreases] the steady-state protein production rate.

Proposition 4.4.4. *Consider a RFMEOA with dimension n, $\ell = 1$, and assume $\alpha_n = 0$. Then $(\partial/\partial\alpha_i)R < 0$ for all $i = 1, 2, \ldots, n-1$ and $(\partial/\partial\lambda_i)R > 0$ for $i = 0, 1, 2, \ldots, n$.*

Consider an RFMEOA in Example 4.4.1 with $\ell = 1$. By the above proposition, we have that increasing λ_0 increases R as shown in Fig. 4.6. This demonstrates the effect of the length on the steady-state output rate for varying the other parameters. Note that this result also holds in the absence of abortions [60].

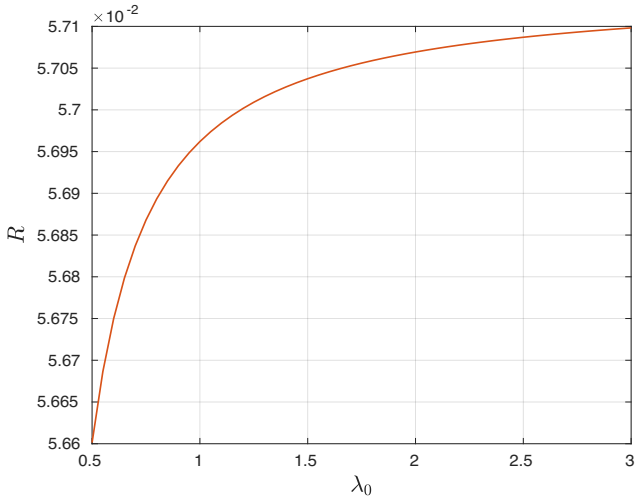

Figure 4.6: The steady-state production rate R as a function of λ_0 for a RFMEOA in Example 4.4.1 with $\ell = 1$.

The next result analyzes the RFMEOA under the assumption of constant transition rates, i.e., $\lambda_i := \lambda > 0$, $i = 0, 1, \ldots, n$.

Proposition 4.4.5. *Consider a RFMEOA with dimension n, $\ell = 1$, and $\lambda_i := \lambda > 0$. Then*

$$e_1 > e_2 > \cdots > e_{n-1} > e_n. \tag{4.9}$$

The above result shows that steady-state reader densities monotonically decrease between sites 1 and n.

4.5 Discussion

It has been observed that a long pause of a ribosome at a site causes a long queue of stalled ribosomes even under normal conditions [79]. In some cases, ribosome stalls result in ribosome collisions that act as the trigger for quality control responses, which act to remove stalled ribosomes from the mRNA. Hence, abortions due to ribosome stalling or ribosome-ribosome collisions play a role in translational regulation as they rescue ribosomes and make them available to translate other mRNAs [123]. The motivation for studying RFMEOA is a recent biological study supporting a model in which the leading stalled ribosome undergoes premature termination after collision with the trailing one [80]. The RFMEOA is a deterministic mathematical model for mRNA translation that incorporates many realistic features: the fact that ribosomes cover several codons and the phenomenon of premature termination of ribosomes from the mRNA strand without synthesis of the full-length protein due to different reasons including ribosome-ribosome collisions, non-availability of elongation factors.

Our main result shows that the RFMEOA is a contractive dynamical system. This implies that it converges to a unique steady state for any set of feasible parameters, i.e., it is robust to the initial conditions. We showed that in the special case, in which trailing ribosomes that collide with the leading ribosomes undergo abortive termination, increasing any of the transition [detachment] rate always increases [decreases] the steady-state protein production rate.

Furthermore, in a computational study, it has been proposed that there is a decrease in gene expression at high initiation rates when ribosome collisions at stalls stimulate premature termination of the leading ribosomes [116]. We also observed this prediction, i.e., increasing the initiation rate may sometimes lead to a decrease in the production rate through simulations of the RFMEOA by considering the parameters that support this scenario.

Translation is a complex process and understanding its various bio-physical

aspects can address numerous biological questions. We believe that the RFMEOA may serve as a basis to consider more sophisticated aspects, for example, mRNA degradation, programmed frameshifts, mRNA secondary structures, to deepen the understanding of the translation process [120]. It could also be generalized to model other biological dynamical processes such as transcription, cellular transport, and more [24]. Another research topic is to incorporate the phenomena of competition for resources and analyze the effect of abortive termination on the total production rate in the entire system.

4.6 Appendix: Proofs

Proof of Proposition 4.3.1: Consider the RFMEOA with $x(0) \in \partial\Psi$. Then there exists an index j such that $x_j(0) \in \{0,1\}$ or $y_j(0) \in \{0,1\}$. We shall consider few cases.

Case 1: Suppose that $y_j(0) = 0$ for some j say the case $j = \ell$. This implies $x_k(0) = 0$ for $k = 1, 2, \ldots, \ell$. We have

$$\dot{y}_\ell(0) = \lambda_0(1-y_\ell(0)) - \lambda_\ell x_\ell(0)(1-y_{2\ell}(0)) - \sum_{i=1}^{\ell} \alpha_i\, x_i(0)(a_i + b_i\, x_{i-\ell}(0))(c_i + d_i\, x_{i+\ell}(0)). \tag{4.10}$$

Now, Eq. (4.10) implies that $\dot{y}_\ell(0) = \lambda_0$ and thus $y_\ell(0^+) > 0$. Therefore, for any $\tau > 0$ $\exists$ $\epsilon(\tau) > 0$ such that $y_\ell(t,a) \geq \epsilon$ for all $t \geq \tau$. Continuing in this way, we have $y_j(t,a) \geq \epsilon$ for all $i \in \{\ell, \ell+1, \ldots, n\}$ and all $t \geq \tau$.

Case 2: Suppose that $x_j(0) = 0$ for some j. Then there exists a minimal index k such that $x_k(0) = 0$. Let $k = n$ then

$$\dot{x}_n(0) = \lambda_{n-1}x_{n-1}(0) - \lambda_n x_n(0) - \alpha_n\; x_n(0)(a_n + b_n\; x_{n-\ell}(0))(c_n + d_n\; x_{n+\ell}(0)). \tag{4.11}$$

Now, Eq. (4.11) implies that $\dot{x}_n(0) = \lambda_{n-1}x_{n-1}(0) > 0$ and thus $x_n(0^+) > 0$. Continuing in this way, we can show that if $x_j(0) = 0$ for some j then $x_j(0^+) > 0$. The analysis for other cases can be done using similar arguments. This shows that for any $a \in \partial\Psi$, $x(t,a) \in \text{int}(\Psi)$, for all $t > 0$.

Now, the proof of the other part of the proposition follows from the fact that Ψ is compact, convex, and with a repelling boundary; see [[48], Theorem 2].

Proof of Proposition 4.3.2: Let $\tau > 0$ be given. By Proposition 4.3.1, $\exists$ $\delta =$

$\delta(\tau) \in (0, 1/2)$ such that for all i and all $t \geq \tau$ we have,

$$\delta \leq x_i(t), y_i(t) \leq 1 - \delta. \tag{4.12}$$

Let

$$\eta_i(t) := \lambda_i(t) \frac{(1 - y_{i+\ell}(t))}{(1 - x_{i+1}(t))}, \quad \text{and} \tag{4.13}$$

$$\Phi_i(t) := \alpha_i(a_i + b_i\ x_{i-\ell}(t))(c_i + d_i\ x_{i+\ell}(t)), \tag{4.14}$$

for $i = 1, 2, \ldots, n$, with $x_i(t) \equiv 0$ for $i < 1$ and $i > n$.
Hence, using notations in Eqs. (4.13) and (4.14), RFMEOA can be written as:

$$\dot{x}_i = \eta_{i-1}(t)x_{i-1}(1 - x_i) - \eta_i(t)x_i(1 - x_{i+1}) - \Phi_i(t)x_i, \tag{4.15}$$

for $i = 1, 2, \ldots, n$ with $x_0 \equiv 0$ and $x_{n+1} \equiv 0$.

Note that the time-varying detachment rates Φ_i's are non-negative. Also, Eq. (4.12) implies that η_i's are uniformly bounded and uniformly separated from zero for all $t \geq \tau$. It follows from Eq. (4.15) that RFMEOA can be interpreted as the MFALK with the time-varying transition and detachment rates with no backward and attachment dynamics for all $t \geq \tau$ [68]. Now, the results in Refs. [68] and [56] imply that RFMEOA is SOST on Ψ.

Proof of Theorem 4.3.1: We can write RFMEOA as $\dot{x} = q(x)$ with $q : \Psi \to \mathbb{R}^n$. Since the compact and convex set Ψ is an invariant set of this dynamical system, it contains the steady-state point e [57]. By Proposition 4.3.1, $e \in \text{int}(\Psi)$ and then the result follows from Proposition 4.3.2.

Proof of Proposition 4.4.1: The argument used in the proof of [[67], Proposition 3] implies that all the derivatives w.r.t. the given parameters are well-defined.

Proof of Proposition 4.4.2: At steady state, the left-hand side of Eq. (4.2) is zero, so

$$f_{i-1}(e) = f_i(e) + g_i(e), \quad i = 1, 2, \ldots, n. \tag{4.16}$$

with f_is and g_is defined in Eqs. (4.3) and (4.4), respectively. Let $R = (\lambda_n + \alpha_n)e_n$ denote the steady-state production rate. From Eq. (4.16), we get

$$R = f_n(e) + g_n(e) = f_i(e) - \sum_{k=i+1}^{n-1} g_k(e), \quad i = 0, 1, \ldots n - 1. \tag{4.17}$$

Given a RFMEOA, pick any $j \in \{0, 1, \ldots, n\}$ and consider a new RFMEOA with $\lambda_j < \bar{\lambda}_j$ and all the other rates unchanged. Let $\bar{e}$ and $\bar{R}$ denote the steady-state

density and production rate in the modified RFMEOA, respectively. We have to show that $R < \bar{R}$. Seeking a contradiction, assume that

$$\bar{R} \leq R. \tag{4.18}$$

We start with the case $j = n$. Combining Eqs. (4.17) and (4.18) with the fact that $\lambda_n < \bar{\lambda}_n$ implies that

$$\bar{e}_n < e_n. \tag{4.19}$$

From Eqs. (4.17) and (4.18) we have, $\bar{e}_{n-1} \leq e_{n-1}$ and $\bar{e}_{n-k} \leq e_{n-k}$, $k = 1, \ldots, \ell - 1$. This implies that

$$\bar{y}_n < y_n. \tag{4.20}$$

Now, from Eqs. (4.17) and (4.18), we have

$$\lambda_{n-\ell}\ \bar{e}_{n-\ell}\ (1 - \bar{y}_n) - \sum_{i=n-\ell+1}^{n-1} \alpha_i\ \bar{e}_i \ \leq\ \lambda_{n-\ell}\ e_{n-\ell}\ (1 - y_n) - \sum_{i=n-\ell+1}^{n-1} \alpha_i\ e_i \tag{4.21}$$

which implies from Eq. (4.20) that $\bar{e}_{n-\ell} < e_{n-\ell}$ and so $\bar{y}_{n-1} < y_{n-1}$. Continuing in this way we have $\bar{e}_k < e_k$, $k = 1, \ldots, n - \ell$ and so $\bar{y}_\ell < y_\ell$. Using Eqs. (4.17) and (4.18), results in $R < \bar{R}$ which is contradiction to Eq. (4.18). So we conclude that $R < \bar{R}$ in the case $\lambda_n < \bar{\lambda}_n$.
Hence, using the same approach for any $j \in \{0, 1, \ldots, n-1\}$, we can conclude that $R < \bar{R}$. So, $(\partial/\partial\lambda_j)R > 0$ for all j. The proof of the other equation in Proposition 4.4.2 is very similar and is thus omitted.

Proof of Proposition 4.4.3: Consider Eq. (4.16) with $\lambda_i = \lambda(> 0)$, $i = 0, 1, \ldots, n$ and $\alpha_i = \alpha(> 0)$, $i = 1, \ldots, n$. Then

$$e_j = \left(\frac{\lambda + \alpha}{\lambda}\right)^{n-j} e_n \quad \text{for} \quad j = n - \ell + 1, \ldots, n \tag{4.22}$$

Since $(\lambda + \alpha) > \lambda$, we have $e_{n-\ell+1} > e_{n-\ell+2} > \cdots > e_n$ and $e_{n-\ell}(1 - y_n) > e_{n-\ell+1}$. Since $y_n \in (0, 1)$, it implies $e_{n-\ell} > e_{n-\ell+1}$ and $y_{n-1} > y_n$. Also from Eq. (4.16), we have

$$\lambda e_{n-\ell-1}(1 - y_{n-1}) = \lambda e_{n-\ell}(1 - y_n) + \alpha(c_{n-\ell} + d_{n-\ell}x_n) \tag{4.23}$$

which implies $e_{n-\ell-1}(1 - y_{n-1}) \geq e_{n-\ell}(1 - y_n)$ and combining this with $y_{n-1} > y_n$ we have $e_{n-\ell-1} > e_{n-\ell}$. Continuing in this manner completes the proof.

Proof of Proposition 4.4.4: Pick any $j \in \{0, 1, \ldots, n\}$ and consider a new RFMEOA with $\lambda_j < \bar{\lambda}_j$ and all the other rates unchanged. Let $\bar{e}$ and $\bar{R}$ denote the steady-state density and production rate in the modified RFMEOA, respectively.

We have to show that $R < \bar{R}$. Seeking a contradiction, assume that

$$\bar{R} \leq R. \tag{4.24}$$

We start with the case $j = n$, i.e., $\lambda_n < \bar{\lambda}_n$. From Eq. (4.24), we have $\bar{e}_n < e_n$. From Eq. (4.17) we have

$$\bar{e}_{n-1} = \frac{\bar{R}}{\lambda_{n-1}(1-\bar{e}_n)} < \frac{R}{\lambda_{n-1}(1-e_n)} = e_{n-1}. \tag{4.25}$$

Now Eqs. (4.17) and (4.25) implies that

$$\begin{aligned}\bar{e}_{n-2} &= \frac{\bar{R} + \alpha_{n-1}a_{n-1}\bar{e}_{n-1}(c_{n-1} + d_{n-1}\bar{e}_n)}{\lambda_{n-2}(1-\bar{e}_{n-1}) - \alpha_{n-1}b_{n-1}\bar{e}_{n-1}(c_{n-1} + d_{n-1}\bar{e}_n)} \\ &< \frac{R + \alpha_{n-1}a_{n-1}e_{n-1}(c_{n-1} + d_{n-1}e_n)}{\lambda_{n-2}(1-e_{n-1}) - \alpha_{n-1}b_{n-1}e_{n-1}(c_{n-1} + d_{n-1}e_n)} = e_{n-2}.\end{aligned} \tag{4.26}$$

Continuing in this way we have $\bar{e}_i < e_i$, $i = 1, \ldots, n$.

We have from Eq. (4.17),

$$\lambda_0(1-\bar{e}_1) \leq \lambda_0(1-e_1). \tag{4.27}$$

This contradicts that $\bar{e}_1 < e_1$ and thus completes the proof. The proof of the other cases is very similar and is thus omitted.

Proof of Proposition 4.4.5: The proof is similar to the proof of Proposition 4.4.3 above and is thus omitted.

Chapter 5

Large-scale mRNA translation and the intricate effects of competition for the finite pool of ribosomes

In this chapter[1], large-scale simultaneous mRNA translation in the cell has been investigated through a mathematical network model that encapsulates important biological features such as competition for shared resources and the possibility of drop-off of ribosomes at different sites along the mRNA. We study the dynamical properties of the model and analyze how state variables get affected by modifying various biological features.

5.1 Introduction

Translation is a fundamental process that takes place in all living cells, from bacteria to humans. Many mRNA molecules are translated in parallel with many ribosomes decoding every mRNA molecule [124]. This implies that the mRNA molecules effectively "compete" for the finite resources in the cell, like tRNA molecules and free ribosomes [72, 125]. The competition for ribosomes may explain important dynamical properties of translation, that are difficult to understand when considering the translation of a single, isolated mRNA molecule. For example, it is known that stalling ribosomes may detach from the mRNA before completing the translation process [81, 75]. This is somewhat surprising, as a ribosome that drops-off from the mRNA before reaching the stop codon fails to complete the synthesis of a full-length protein, and releases a truncated protein, whose accumulation could be detrimental to the cell [112]. However, in the context of competition for free ribosomes, premature drop-off may have a positive effect: it allows stalled ribosomes to join the pool of free ribosomes that can initiate translation in other mRNA molecules. Thus, modeling translation as a network of

[1]The content of this chapter is published as: "Aditi Jain, Michael Margaliot, and Arvind Kumar Gupta. Large-scale mRNA translation and the intricate effects of competition for the finite pool of ribosomes. *Journal of the Royal Society Interface* 19(188): 20220033, 2022."

interconnected processes and taking into account competition for shared resources is important for gaining a deeper understanding of fundamental principles in cellular biophysics.

Typically, translation is initiated by ribosome scanning from the end of the capped mRNA. However, some mRNAs include internal ribosome entry sites (IRESs), that allow for translation initiation in a cap-independent manner. IRESs, first discovered in poliovirus, are common in RNA viruses and allow viral translation even when host translation is inhibited for some reason [126, 127]. If the IRES is located in the $5'$ UTR region then it can be modeled as one of the bio-physical properties that affects the initiation rate of the mRNA. However, certain viruses, like HIV, have IRESs within the open reading frame, downstream of the initiation codon [128]. Cellular growth regulatory genes and genes transcribed in response to stress also contain IRES elements [76]. Also, synthetic biologists often insert IRES sequences into their vectors to allow expressing two or more genes from a single vector [129]. We believe that the effect of IRESs on translation should also take into account the competition for shared resources, like ribosomes. For example, a recent study [130] shows that the non-structural protein 1 (Nsp1), produced by the SARS-CoV-2 virus, binds to the human 40S subunit in ribosomal complexes, and thus interferes with mRNA binding. This aids the virus in "hijacking" the cellular translation machinery.

The RFMNP includes a network of RFMs interconnected via a pool of free ribosomes. The dynamics of RFMNP have been described in Chapter 1. For a recent application of this model to large-scale ribosome traffic engineering, see Ref. [131]. However, the RFMNP cannot model the important features of premature drop-off and IRESs. As we will see below, adding these features to the model generates new, important and perhaps surprising results.

In this chapter, we consider a network of RFMs with an additional Langmuir kinetics (RFMLK). For details of the dynamics of RFMLKs, the reader can refer to chapter 1. This allows modeling drop-off and attachment of ribosomes at any site along the mRNA due to premature drop-off or IRESs, respectively. The RFMLKs are interconnected via a pool of free ribosomes yielding a new model referred to as the *RFM with Langmuir kinetics network* (RFMLKN). This allows modeling simultaneous translation of an arbitrary number of mRNA molecules, with ribosome drop-off from any site along the mRNA molecule to the pool of free ribosomes, and attachment at an IRES at any site along the mRNA. In particular, we use this model to rigorously analyze the effect of ribosome drop-off and/or IRES in one mRNA on the production rate of all the other mRNA molecules. Note that drop-off from [attachment at] site i is modeled by a parameter $\alpha_i \geq 0$ [$\beta_i \geq 0$], such that setting

the parameter to zero implies no drop-off [attachment] at this site.

We use the powerful theory of strictly cooperative dynamical systems with a first integral [132] to prove that the RFMLKN admits a continuum of linearly ordered equilibrium points. Every solution of the system converges to an equilibrium that depends on the network parameters and the total number of ribosomes in the network (that is conserved under the dynamics). This represents a dynamical steady-state where the ribosome flow into and out of every site along any mRNA molecule is equal, and the flows into and out of the pool are also equal. Thus, any two solutions starting from two initial conditions corresponding to an equal total number of ribosomes in the network converge to the same equilibrium point. In other words, the network "forgets" the exact initial condition, except for the total initial density of ribosomes. This qualitative behavior holds for any feasible set of parameters covering many possible biophysical conditions.

More generally, we show that if all the transition rates vary in a periodic manner, with a common period T, then every solution of the RFMLKN converges to a periodic solution with period T. This implies in particular that the protein production rate in all the mRNAs entrains to periodic excitations in the translational machinery.

We use the RFMLKN to analyze quantitatively and qualitatively important questions such as the effect of ribosome drop-off/attachment from/to a site in one mRNA on the steady-state production rate of all the other mRNAs in the network. The analysis highlights how the competition for shared resources generates an indirect and intricate web of mutual effects between the mRNA molecules in the cell. These effects cannot be analyzed using models of translation on a single, isolated mRNA molecule.

The chapter is organized as follows. The next section summarizes the main analysis results and their biological implications. Section 5.3 presents the new mathematical model and demonstrates using several simple examples how it can be used to study questions that are relevant for large-scale translation in the cell. Section 5.4 states our main theoretical results. The following section concludes the section and all the proofs are placed in the Appendix.

5.2 Summary of main results and their biological implications

The RFMLKN encapsulates many fundamental aspects of gene translation. During mRNA translation, ribosomes attach at the $5'$ end of the mRNA and scan it in a

sequential manner. At each elongation step, every sequence of three consecutive nucleotides in the mRNA, called a codon, is decoded into an amino-acid, and this process continues until the ribosome reaches the 3' end of the mRNA [2]. The codon decoding rates may vary among different mRNAs and depend on many transcript features [40].

Several ribosomes may scan the same mRNA molecule in parallel, but a ribosome cannot overtake another ribosome in front of it, thus obeying the simple exclusion principle. Ribosomes may detach from the mRNA molecule before reaching the stop codon due to several reasons like ribosome "traffic jams", the presence of a premature stop codon, ribosome-ribosome interactions due to depletion of aminoacyl tRNA or amino-acid misincorporation, etc. [81, 111]. The RFMLKN also allows to model ribosome attachment at IRESs in mRNA sites where such a feature is relevant. The limited availability of free ribosomes induces indirect coupling due to competition between mRNA molecules (see Fig. 5.1).

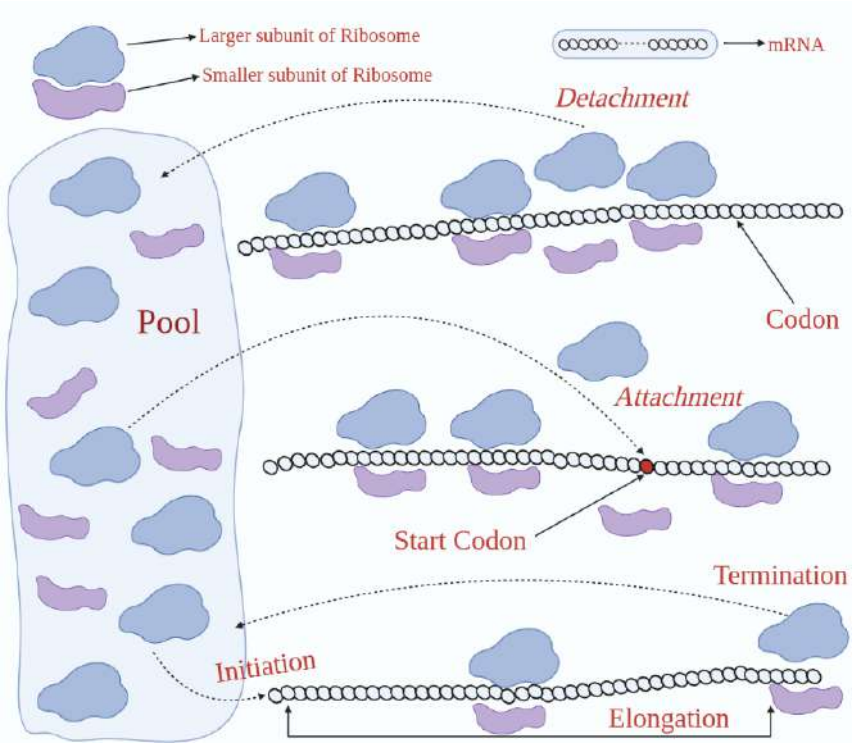

Figure 5.1: Large-scale translation of mRNA molecules in the cell. Several ribosomes may decode the same mRNA. Ribosomes that detach from an mRNA enter the pool of free ribosomes.

We prove that for a given set of elongation, drop-off and attachment rates, and a total number of ribosomes in the network, the RFMLKN admits a unique steady-state, i.e., the ribosomal density profiles on all the mRNAs and in the pool converge to a fixed value, as time goes to infinity. This raises the important question

of how does the steady-state changes if we modify any parameter in the model, e.g. the rate of ribosome drop-off in one site of a specific mRNA.

Our analysis shows that following an increase [decrease] in a drop-off rate in any mRNA molecule, the steady-state ribosome density profile in all the *other* mRNA molecules increases [decreases]. The intuitive explanation for this is as follows: increasing the drop-off rate leads to releasing more ribosomes to the pool of free ribosomes and this increases the initiation rate as well as the attachment rate in all the other mRNA molecules leading to an increase in their ribosome density profile. We also prove the "dual" result, namely, that increasing [decreasing] an attachment rate in a specific site in an mRNA decreases [increases] the steady-state ribosome densities in all the *other* mRNA molecules. However, and perhaps surprisingly, we show that it is very difficult to analytically predict the effect of a variation in one of the rates on the mRNA that is modified, as the effect will depend on the entire network. For example, increasing the attachment rate in one site of a specific mRNA may reduce the pool density and thus decrease the effective attachment rates in other sites along the modified mRNA, leading to an unexpected decrease in the density along this mRNA.

These results highlight the indirect effects of competition for resources, and also the importance of taking competition into account when "tinkering" with the bio-physical features of a single mRNA molecule, e.g. by replacing codons by synonymous codons or using RNA interference (see Ref. [133]).

Our simulations suggest another interesting implication of ribosome drop-off and/or ribosome attachment (e.g. in IRESs). It seems that these phenomena tend to increase the amount of indirect "communication" between the mRNA molecules, through the pool, and thus lead to a higher level of synchronization between the production rates in the mRNAs. This suggests another possible advantage of ribosome drop-off and attachment as tools for regulating the total protein production from different copies of the same mRNA.

5.3 Mathematical Model

Our model is a network of interconnected RFMLKs. We begin by describing the RFMLK with an input and then develop the network of interconnected RFMLKs.

5.3.1 The RFMLK with an input and output

To build a network, we use an RFMLK with an input and output described by

$$\begin{aligned}
\dot{x}_1 &= \lambda_0(1-x_1)u - \lambda_1 x_1(1-x_2) + \beta_1(1-x_1)u - \alpha_1 x_1,\\
\dot{x}_2 &= \lambda_1 x_1(1-x_2) - \lambda_2 x_2(1-x_3) + \beta_2(1-x_2)u - \alpha_2 x_2,\\
&\vdots\\
\dot{x}_n &= \lambda_{n-1} x_{n-1}(1-x_n) - \lambda_n x_n + \beta_n(1-x_n)u - \alpha_n x_n,\\
y &= \lambda_n x_n + \sum_{i=1}^{n} \alpha_i x_i.
\end{aligned} \tag{5.1}$$

The time-varying function $u(t)$ represents the density of ribosomes in the vicinity of the mRNA molecule and thus affects the diffusion of ribosomes to the binding sites along the mRNA. The parameters β_i represent some intrinsic site-specific features, and this modulates the effect of the common $u(t)$. Mathematically, $u(t)$ multiplies the term representing the entry rate into the first site, and also the attachment rates in all the sites. We assume that $u(t) \geq 0$ for any time t. A larger value of $u(t)$ corresponds for example to a larger density of free ribosomes in the vicinity of the mRNA at time t, and consequently, it increases the effective initiation rate in the first site and the attachment rates in all the sites i with $\beta_i > 0$. The output $y(t)$ is the total exit rate of ribosomes from the RFMLK to the environment at time t.

Note that Eq. (5.1) is a nonlinear model, as it includes both products of state-variables and products of state-variables and the control input.

Example 5.3.1. Consider the case $n = 1$. In this special case, Eq. (5.1) becomes the affine control system

$$\dot{x}_1 = -(\lambda_0 u + \lambda_1 + \alpha_1 + \beta_1 u)x_1 + (\lambda_0 + \beta_1)u.$$

Fix $x_1(0) \in [0,1]$. Consider a constant control $u(t) \equiv v$, with $v > 0$, then it is clear that $x_1(t) \in (0,1)$ for all $t > 0$, and that the limit $e_1 := \lim_{t\to\infty} x_1(t)$ exists, and satisfies

$$e_1 = \frac{1}{1 + \frac{\alpha_1+\lambda_1}{(\beta_1+\lambda_0)v}}.$$

In particular, if $v = 0$ then $e_1 = 0$, and if $v \to \infty$ then $e_1 \to 1$. The first case corresponds to no ribosomes in the vicinity of the mRNA, so the single site empties. The second case corresponds to an infinite density of ribosomes, so the site fills up completely. Note also that e_1 is an increasing function of λ_0, β_1, v, and a decreasing function of λ_1, α_1.

The next subsection introduces the RFMLKN.

5.3.2 A network of ribosome flow models with Langmuir kinetics and a pool

To model large-scale translation under competition for the finite pool of ribosomes in the cell, we consider a set of m RFMLKs with input and output, representing m different mRNA molecules in the cell, connected via a pool of free ribosomes.

The ith RFMLK has length n_i, input function u^i, output y^i, and rates λ_0^i, λ_1^i, $\ldots$, $\lambda_{n_i}^i$, β_1^i, β_2^i, $\ldots$, $\beta_{n_i}^i$ and α_1^i, α_2^i, $\ldots$, $\alpha_{n_i}^i$. The dynamics of the m RFMLKs is written as

$$\begin{aligned} \dot{x}^1 &= f(x^1, u^1), \quad y^1 = g(x^1), \\ &\vdots \\ \dot{x}^m &= f(x^m, u^m), \quad y^m = g(x^m). \end{aligned} \tag{5.2}$$

These RFMLKs are interconnected through a pool of free ribosomes, i.e., ribosomes that are not attached to any mRNA. We use the scalar function $z(t) \geq 0$ to denote the density of ribosomes in the pool at time t. The pool feeds the initiation locations as well as the sites in the mRNAs where attachment takes place. Mathematically, this implies that $u^i(t) = G_i(z(t))$, $i = 1, 2, \ldots, m$. We assume that every function $G_i(\cdot) : \mathbb{R}_+ \to \mathbb{R}_+$ satisfies the following two properties:

1. $G_i(0) = 0$;

2. $G_i(\cdot)$ is continuously differentiable with $G_i'(z) > 0$ for all $z \geq 0$.

The first property implies that if the pool is empty then no ribosomes can exit the pool; the second implies that as the number of ribosomes in the pool increases, more ribosomes exit the pool. Note that these properties imply the following:

- There exists $c > 0$ such that $G_i(z) \leq cz$ for all $z > 0$ sufficiently small.

This technical condition will be used later on in the proof of persistence in the RFMLKN.

Functions that satisfy these properties include, for example, the linear function $G(z) = az$, with $a > 0$, and the bounded function $G(z) = a \tanh(bz)$, with $a, b > 0$ [134, 135].

The dynamics of the ith RFMLK in the network is thus given by:

$$\begin{aligned}
\dot{x}_1^i &= \lambda_0^i G_i(z)(1-x_1^i) - \lambda_1^i x_1^i(1-x_2^i) + \beta_1^i G_i(z)(1-x_1^i) - \alpha_1^i x_1^i, \\
\dot{x}_2^i &= \lambda_1^i x_1^i(1-x_2^i) - \lambda_2^i x_2^i(1-x_3^i) + \beta_2^i G_i(z)(1-x_2^i) - \alpha_2^i x_2^i, \\
&\vdots \\
\dot{x}_{n_i}^i &= \lambda_{n_i-1}^i x_{n_i-1}^i(1-x_{n_i}^i) - \lambda_{n_i}^i x_{n_i}^i + \beta_{n_i}^i G_i(z)(1-x_{n_i}^i) - \alpha_{n_i}^i x_{n_i}^i, \\
y^i &= \lambda_{n_i}^i x_{n_i}^i + \sum_{\ell=1}^{n_i} \alpha_\ell^i x_\ell^i.
\end{aligned} \tag{5.3}$$

The output of each RFMLK is fed into the pool. Hence, the pool dynamics is given by:

$$\dot{z} = \sum_{i=1}^{m} \lambda_{n_i}^i x_{n_i}^i + \sum_{i=1}^{m}\sum_{j=1}^{n_i} \alpha_j^i x_j^i - \sum_{i=1}^{m} \lambda_0^i G_i(z)(1-x_1^i) - \sum_{i=1}^{m}\sum_{j=1}^{n_i} \beta_j^i G_i(z)(1-x_j^i). \tag{5.4}$$

In other words, all the ribosomes that exit or drop off the mRNAs feed the pool, and the pool feeds the initiation and attachment sites in all the mRNAs.

Summarizing, the RFMLKN is a dynamical system with $d := 1 + \sum_{i=1}^{m} n_i$ state variables, and dynamics described by Eqs. (5.2), (5.3) and (5.4) (see Fig. 5.2). Eq. (5.4) and our assumptions on the functions G_i imply that if $z(0) \geq 0$ then $z(t) \geq 0$ for all $t \geq 0$, i.e., the pool density is always non-negative.

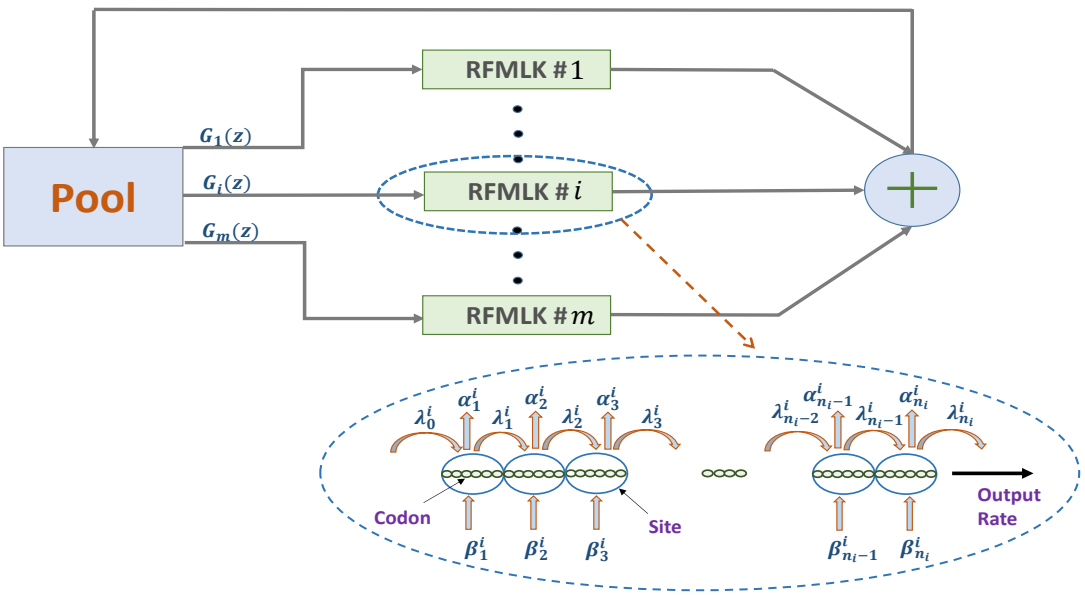

Figure 5.2: Each mRNA is described by an RFMLK with input and output. The output of each RFMLK is fed into the pool, and the pool feeds the initiation and attachment rates in all the RFMLKs.

The feasible set of parameters in the RFMLKN is:

$$\lambda_j^i > 0,\ \beta_j^i \geq 0,\ \alpha_j^i \geq 0,\ \text{for all } i, j.$$

All the theoretical results in this chapter hold for *any* choice of parameter values in this set. In particular, they hold if we set some (or all) of the α_j^i's to zero and/or set some (or all) of the β_j^i's to zero. Thus, the theoretical results remain valid when there is no drop-off from [attachment at] any site, or when there is drop-off from [attachment to] very specific sites. Let

$$H(t) := z(t) + \sum_{i=1}^{m} \sum_{j=1}^{n_i} x_j^i(t).$$

This is the total number of ribosomes in the system at time t. An important property of the RFMLKN is that it is a closed system, so the total number of ribosomes is conserved for all $t \geq 0$. Thus, H is a first integral of the dynamics.

The RFMLKN models the indirect coupling between the mRNA molecules induced by competition for the finite number of ribosomes in the system. For example, if there is a "traffic jam" of ribosomes on one of the mRNAs then the pool density z decreases and thus the initiation and attachment rates to all the mRNAs, that depend on the functions $G_i(z)$, decrease.

We prove in Section 5.4 that all the state variables in the RFMLKN converge to a steady state. The steady-state values depend on the parameter values in all the RFMLKs and the total number of ribosomes in the network. Let $e_j^i \in [0, 1]$ denote the steady-state density at the jth site in the ith RFMLK, and let $e_z \in [0, \infty)$ denote the steady-state pool density.

The RFMLKN provides a versatile and powerful framework for simulating and analyzing the effect of various biological phenomena on large-scale translation in the cell under competition for free ribosomes. In the examples below, we demonstrate how various changes in the network affect the RFMLKN steady-state. These examples are simple and synthetic. Their goal is merely to demonstrate the variety of topics that can be addressed using the new mathematical model.

Our first example demonstrates how the total number of ribosomes in the system affects the ribosomal densities along the mRNAs.

Example 5.3.2. Consider an RFMLKN that includes a single RFMLK with dimension $n_1 = 3$, rates $\lambda_j^1 = 1$, for $j = 0, \ldots, 3$, $\beta_j^1 = 0$, for $j = 1, 3$, $\beta_2^1 = 0.1$, $\alpha_j^1 = 0$, for $j = 1, 3$, and $\alpha_2^1 = 0.01$, and a pool with an output function $G(z) = \tanh(z)$. We simulated this system with the initial condition $x_j^1 = 0$

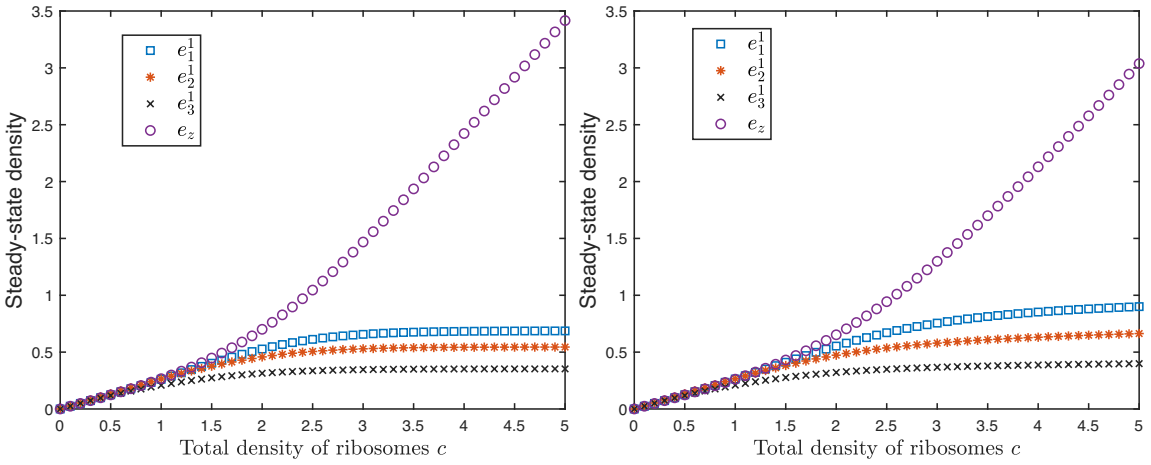

(a) (b)

Figure 5.3: a) Steady-state values in the RFMLKN in Example 5.3.2 as a function of the total number of ribosomes c. (a) when $G(z) = \tanh(z)$; (b) when $G(z) = z$.

for all j, and $z(0) = c$, so that the total number of ribosomes in the system is c, for various values of c. When $c = 0$ there are no ribosomes in the network and the steady-state values are all zero. As c increases, the number of ribosomes along the RFMLK increases. Since $\tanh(z) \to 1$ as $z \to \infty$, ribosomal densities along the mRNA saturate to the values corresponding to initiation rate $\lambda_0^1 = 1$, and attachment rates zero except for $\beta_2^1 = 0.1$. The remaining ribosomes accumulate in the pool (see Fig. 5.3a). Using a different output function, namely, $G(z) = z$, the qualitative behavior is same, but now as c increases, ribosomal densities tend to have higher saturation values, and the remaining ribosomes accumulate in the pool (see Fig. 5.3b).

The next example describes the effect of the drop-off rate of ribosomes along a coding region in one of the mRNA molecules on the steady-state profiles of all the mRNAs in the network. Ref. [81] analyzed the drop-off rate in *E. coli* under normal conditions and estimated it to be 4×10^{-4} drop-off events per codon. This is not negligible. For example, along a coding region of 300 codons (approximately the average coding region length in *E. coli*) then on average, around 10 out of every 100 ribosomes will fail to complete translation of the mRNA. Recent studies suggest that the drop-off rate increases with ribosomal traffic jams [80] and that under stress conditions, such as amino acid starvation or aminoacyl-tRNA depletion due to a high level of recombinant protein expression, ribosome drop-off can substantially affect the efficiency of protein expression [75].

Let

$$a^i := (1/n_i) \sum_{j=1}^{n_i} e_j^i$$

denote the average steady-state density (ASSD) in the ith RFMLK.

Example 5.3.3. Consider an RFMLKN with $m = 3$ RFMLKs with dimensions $n_i = 3$, $i = 1, 2, 3$, and parameters $\lambda_0^1 = 0.8$, $\lambda_0^2 = 1$, $\lambda_0^3 = 1.5$, $\lambda_j^1 = 1$, $\lambda_j^2 = 6.4$, $\lambda_j^3 = 10$, $\alpha_j^1 = \alpha$, $\alpha_j^2 = 0$, $\alpha_j^3 = 0$, $\beta_j^1 = 0$, $\beta_j^2 = 0$, $\beta_j^3 = 0$, for all j, and $G_i(z) = z$, $i = 1, 2, 3$. The initial condition is $x_j^i = 0$, for all i, j, and $z(0) = 2$. We vary the parameter α, i.e., the ribosome drop-off rate from all the sites in the first RFMLK. Fig. 5.4 depicts the ASSD in each RFMLK as a function of α. It can be seen that as α increases, the ASSD in the first RFMLK decreases, whereas the ASSD in all the other RFMLKs increases. Indeed, as the drop-off rate from the first RFMLK increases, the density in the pool increases, and more ribosomes become available for translating the other mRNA molecules, thus increasing the ASSD in the other RFMLKs.

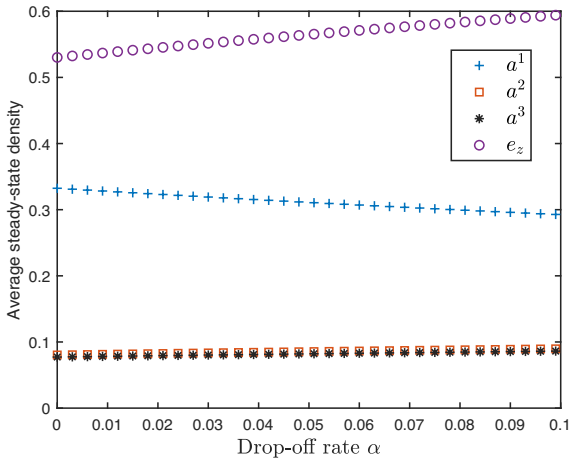

Figure 5.4: Average steady-state density in the RFMLKN in Example 5.3.3 as a function of the drop-off rate α in the first RFMLK.

From a biological perspective, this example corresponds to a situation when due to genetic errors or insufficient availability of charged tRNAs or frameshifting [136], ribosomes start detaching before reaching the stop codon in an mRNA, resulting in truncated protein products. Our results explain why this may still be beneficial to the cell. The ribosome drop-off from one mRNA molecule increases the number of free ribosomes that are now available to translate other mRNAs which in turn increases the corresponding protein production rates. Of course, the effect of drop-off from a single mRNA on the pool may be negligible, but the accumulated drop-off from many mRNAs may be significant.

The next example considers the "dual" case of increasing the attachment rate in one of the mRNA molecules in the network.

Example 5.3.4. Consider an RFMLKN with $m = 2$ RFMLKs with dimensions $n_i = 10$, $i = 1, 2$. The parameter values are $\lambda_0^1 = 0.8$, $\lambda_0^2 = 0.8$, $\lambda_j^1 = 5$, $\lambda_j^2 = 10$, $\alpha_j^1 = 0$,

$\alpha_j^2 = 0$, $\beta_j^1 = \beta$, $\beta_j^2 = 0$, for all j, and $G_i(z) = \tanh(z)$, $i = 1, 2$. The initial condition is $x_j^i = 0$, for all i, j, and $z(0) = 3.5$. Fig. 5.5 depicts the ASSD in each RFMLK as a function of β ranging from 0 to 0.5. It can be seen that as β increases, the ASSD in the first RFMLK increases and the ASSD in the other RFMLK decreases. This is due to the attachment of ribosomes at the first RFMLK leading to a depletion of ribosomes in the pool, and thus to a decrease in the ASSD in the second RFMLK. Note the relatively sharp decrease in the steady-state pool density as β increases. This is due to the fact that the number of sites is $n_i = 10$, so a "traffic jam" in an RFMLK involves many stalled ribosomes along the RFMLK.

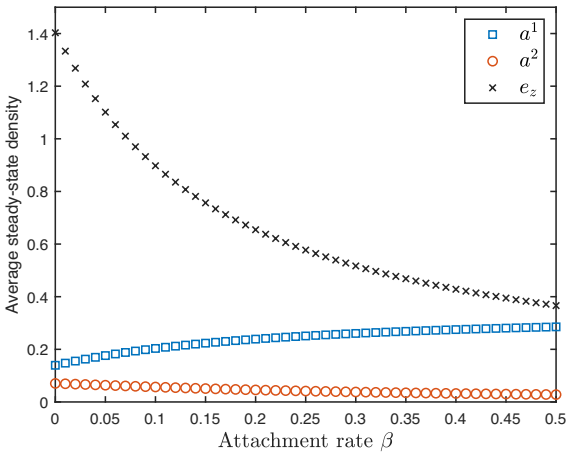

Figure 5.5: Average steady-state density in the RFMLKN in Example 5.3.4 as a function of the attachment rate β in the first RFMLK.

From a biological point of view, the attachment rate may model internal ribosome entry sites (IRESs) that appear in viral mRNAs. The RFMLKN may thus be used to shed more light on how the viral mRNA "overtakes" the pool of free ribosomes and thus: (1) accelerates the translation of viral mRNA, and (2) concomitantly slows down the cellular innate immune response [137]. IRESs have also been used as a biotechnological tool allowing the synthesis of several proteins of interest from one multicistronic mRNA [138, 139, 76]. In this context, the example above shows that the design of such tools should also take into consideration their effect on the pool of free ribosomes.

The next example demonstrates the effect of modifying the length of one mRNA molecule in the network.

Example 5.3.5. Consider an RFMLKN with $m = 2$ RFMLKs with dimensions $n_1 = 5$, and n_2, respectively. The parameter values are $\lambda_0^i = 1$, $\lambda_j^i = 1$, $\alpha_j^i = 0.1$, $\beta_j^i = 0.01$, for all i, j, and $G_i(z) = \tanh(z)$, $i = 1, 2$. The initial condition is $x_j^i = 0$, for all i, j, and $z(0) = 5$. We simulated this network for various values of n_2. As n_2 increases, there is a decrease in the ASSD in both RFMLKs and in the

pool density (see Fig. 5.6). Indeed, increasing n_2 implies that ribosomes that bind to the second RFMLK remain on it for a longer period of time. This decreases the steady-state pool density and, consequently, the steady-state densities in all the RFMLKs.

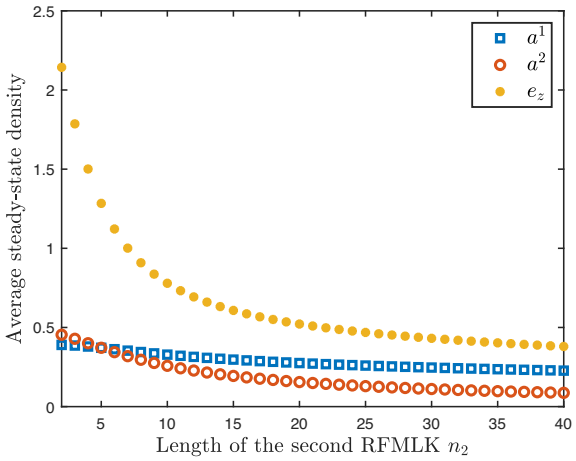

Figure 5.6: ASSD and e_z in Example 5.3.5 as a function of the length n_2 of the second RFMLK.

The next example again studies the effect of increasing n_2 and also compares the RFMLKN and the RFMNP.

Example 5.3.6. Consider an RFMLKN with $m = 2$ RFMLKs with dimensions $n_1 = 5$, and n_2, respectively. The parameters are $\lambda_j^i = \alpha_j^i = \beta_j^i = 1$, for all i, j, and the initial condition is $x_j^i(0) = 0$, for all i, j and $z(0) = 25$. Recall that $e_{n_1}^1$ $[e_{n_2}^2]$ denotes the steady-state density in the last site of the first [second] RFMLK. Let $\rho_{n_1}^1$ $[\rho_{n_2}^2]$ denote the steady-state density in the last site of the first [second] RFMLK, when $\lambda_j^i = 1$, $\alpha_j^i = \beta_j^i = 0$ for all i, j, so the RFMLKs reduce to RFMs. Fig. 5.7 shows that as n_2 increases, the steady-state densities $e_{n_1}^1$ and $e_{n_2}^2$ tend to equal values. However, $\rho_{n_1}^1$ and $\rho_{n_2}^2$ are different. The reason for this may be that the non-zero attachment and detachment rates increase the indirect communication between the RFMLKs (through the pool) leading to better "synchronization".

The next section rigorously analyzes the RFMLK and the RFMLKN using tools from systems and control theory and in particular the theory of cooperative dynamical systems [50].

5.4 Main results

We begin by analyzing the properties of the RFMLK with input and output described in Eq. (5.1), as these are the basic ingredients of the RFMLKN. Recall

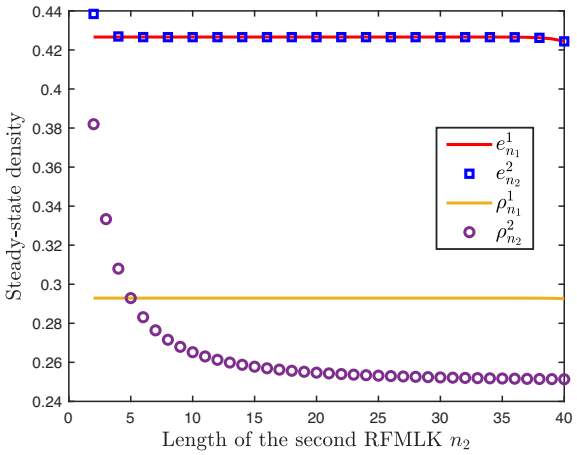

Figure 5.7: Steady-state densities in Example 5.3.6 as a function of the length n_2 of the second RFMLK.

that $x_i(t) \in [0,1]$ for all t, so the state-space of the RFMLK is $C^n := [0,1]^n$. Let $x(t,a)$ denote the solution of Eq. (5.1) at time $t \geq 0$ for the initial condition $a \in C^n$. For the sake of readability, all the proofs are placed in the Appendix.

5.4.1 Persistence

If $u(t) \equiv 0$ then no ribosomes enter the RFMLK and then it is clear that $x(t)$ will converge to zero, that is, the density of ribosomes at each site will go to zero. The next result shows that for any input that is bounded below by a positive number all the state variables remain bounded away from zero and also bounded away from one. In other words, all the sites along the mRNA will never become completely empty nor completely full.

Proposition 5.4.1. *Consider the RFMLK with a control u such that $u(t) \geq s > 0$ for all $t \geq 0$. For any $\tau > 0$ there exists $\epsilon = \epsilon(\tau) > 0$, with $\epsilon(\tau) \to 0$ as $\tau \to 0$, such that for any initial condition $a \in C^n$ the solution of (5.1) satisfies*

$$\epsilon \leq x_i(t,a) \leq 1 - \epsilon, \quad \text{for all } i \in \{1,\ldots,n\} \text{ and all } t \geq \tau.$$

In other words, for any control $u(t)$ that is strictly positive for all $t \geq 0$ we have that after any time $\tau > 0$ all the normalized densities are strictly separated away from zero and from one. In particular, if the densities converge to a steady-state e then $e_i \in (0,1)$ for all i.

5.4.2 Contraction

Contraction theory is a powerful tool for analyzing nonlinear dynamical systems [53, 56], and has found applications in bio-molecular systems, control theory,

synchronization of coupled nonlinear systems [54], reaction-diffusion differential equations [55], mathematical epidemiology [140, 141], and more.

For $x \in \mathbb{R}^n$, let $|.|_1 : \mathbb{R}^n \to \mathbb{R}_+$ denote the L_1 norm. For a non-singular matrix $P \in \mathbb{R}^{n \times n}$, let $|x|_{P,1} := |Px|_1$, i.e., the scaled L_1 norm of x.

Proposition 5.4.2. *Consider the RFMLK with a control u such that $u(t) \geq s > 0$ for all $t \geq 0$, and fix $\tau > 0$. There exist a non-singular matrix $P = P(\tau)$ and $\eta = \eta(\tau) > 0$ such that for any $a, b \in C^n$, we have*

$$|x(t+\tau, a) - x(t+\tau, b)|_{P,1} \leq \exp(-\eta t)|a - b|_{P,1} \text{ for all } t \geq 0.$$

In other words, the RFMLK is contracting with respect to the scaled norm $|\cdot|_{P,1}$ after (the arbitrarily small) time delay τ. From a biological point of view, this implies that the difference between the ribosomal density profiles, corresponding to two different initial ribosomal densities along the mRNA, decreases with time.

Proposition 5.4.2 implies several useful asymptotic properties of the RFMLK. These are described in the following subsections.

5.4.3 Global asymptotic stability

Proposition 5.4.3. *The RFMLK with a constant control $u(t) \equiv s > 0$ admits a unique steady-state $e^s \in \text{int}(C^n)$ that is globally asymptotically stable, i.e.,*

$$\lim_{t \to \infty} x(t, a) = e^s \text{ for any } a \in C^n.$$

In other words, the solution converges to e^s for any initial condition, so the initial condition is "forgotten". The equilibrium e^s represents a dynamic steady-state where the input and output flows from each site in the RFMLK are equal, and thus the densities in each site are constant. From a biological point of view, this implies that the ribosomal density at each site along the mRNA converges to a constant value. This steady-state describes a situation where for each site, the rate of ribosomes entering the site is equal to the rate of ribosomes leaving the site.

5.4.4 Monotone control system

Angeli and Sontag [142] extended the notion of a monotone system to control systems. The next result shows that the RFMLK is a monotone control system. For two vectors $v, w \in \mathbb{R}^n$, we write $v \leq w$ if $v_i \leq w_i$ for all $i = 1, \ldots, n$, and $v \ll w$ if $v_i < w_i$ for all $i = 1, \ldots, n$.

Proposition 5.4.4. *Fix two initial conditions $a, b \in C^n$, with $a \leq b$, and two*

controls $u, v : \mathbb{R}_+ \to \mathbb{R}_+$, *with* $u(t) \leq v(t)$ *for all* $t \geq 0$. *Then the corresponding solutions of the RFMLK satisfy*

$$x(t, a, u) \leq x(t, b, v), \text{ for all } t \geq 0, \tag{5.5}$$

and

$$y(t, a, u) \leq y(t, b, v), \text{ for all } t \geq 0. \tag{5.6}$$

In other words, if we consider two identical RFMLKs: the first with initial densities a_i and the second with initial densities b_i, with $a_i \leq b_i$, for all i, and apply a control u in the first and v in the second, with $u(t) \leq v(t)$, for all $t \geq 0$, then at each time $t \geq 0$ each density in the first RFMLK will be smaller or equal to the corresponding density in the second RFMLK. From a biological point of view, this implies the following. Consider two identical mRNAs. Suppose that for every site, the first mRNA has an initial ribosomal density smaller or equal to the density in the second. Also, the first mRNA is located in a region with a smaller ribosome abundance in the vicinity of the mRNA. Then at each time t, every site in the first mRNA will be less occupied than the corresponding site in the second mRNA.

The next proposition analyzes the relation between the steady-state densities corresponding to constant control values.

Proposition 5.4.5. *Consider the RFMLK with constant controls* $u(t) \equiv s^1$ *and* $v(t) \equiv s^2$ *with* $0 < s^1 < s^2$. *Fix* $a, b \in C^n$, *and let*

$$e^{s^1} := \lim_{t \to \infty} x(t, a, u),$$
$$e^{s^2} := \lim_{t \to \infty} x(t, b, v).$$

Then

$$e^{s^1} \leq e^{s^2}.$$

From a biological point of view this implies the following. Consider two identical mRNAs. Suppose that the first mRNA is located in a region in the cell with a smaller ribosome abundance. Then the ribosomal densities in the mRNAs converge to a steady state, and for each site, the density in the first mRNA will be smaller or equal to the density in the second mRNA.

We now turn to analyze the RFMLKN. Recall that every $x_j^i \in [0, 1]$, and that the pool density satisfies $z \in [0, \infty)$, so the state-space of the RFMLKN is

$$\Omega := [0, 1]^{n_1} \times \cdots \times [0, 1]^{n_m} \times [0, \infty). \tag{5.7}$$

For $a \in \Omega$, let $\begin{bmatrix} x(t,a) \\ z(t,a) \end{bmatrix}$ denote the solution of the RFMLKN at time t with the initial condition a. Let $d := n_1 + \cdots + n_m + 1$, and let 1_d denote a column vector of d ones. For $s \geq 0$, let $L_s := \{a \in \Omega : 1_d' a = s\}$, i.e., the s level set of the first integral H. In other words, L_s is the set of all states in Ω with a total density of ribosomes equal to s.

5.4.5 Invariance and persistence

The next result follows immediately from the equations of the RFMLKN.

Proposition 5.4.6. *The state space Ω in (5.7) is an invariant set for the dynamics of the RFMLKN that is, if $a \in \Omega$ then $\begin{bmatrix} x(t,a) \\ z(t,a) \end{bmatrix} \in \Omega$ for all $t \geq 0$.*

In other words, every trajectory emanating from an initial condition in the state space remains in it for all $t \geq 0$.

The next result shows that trajectories that emanate from an initial condition in Ω become uniformly separated from the boundary of Ω.

Proposition 5.4.7. *Consider the RFMLKN. For any $\tau > 0$ there exists $\epsilon = \epsilon(\tau) > 0$, with $\epsilon(\tau) \to 0$ as $\tau \to 0$, such that for any $a \in \Omega \setminus \{0\}$ we have*

$$\epsilon \leq x_j^i(t,a) \leq 1 - \epsilon \tag{5.8}$$

and

$$\epsilon \leq z(t,a) \tag{5.9}$$

for all $t \geq \tau$, $i \in \{1, 2, \ldots, m\}$, and $j \in \{1, 2 \ldots, n_i\}$.

In other words, after an arbitrarily short time, every density in every RFMLK is in the range $[\epsilon, 1-\epsilon]$, and the pool density is in the range $[\epsilon, \infty)$. From a biological point of view, this implies that after an arbitrarily short time $\tau > 0$ every site along every mRNA is not completely empty nor completely full, and that the pool is not completely empty.

To explain the usefulness of Proposition 5.4.7, note that the Jacobian J of the vector field of the RFMLK with input and output satisfies $J(x,u) = M(x) - D(x,u)$, where $D(x,u)$ is a diagonal matrix with entries

$$\lambda_0 u + \lambda_1(1-x_2) + \alpha_1 + \beta_1 u, \lambda_1 x_1 + \lambda_2(1-x_3) + \alpha_2 + \beta_2 u, \ldots, \lambda_{n-1} x_{n-1} + \lambda_n + \alpha_n + \beta_n u,$$

and

$$M(x) := \begin{bmatrix} 0 & \lambda_1 x_1 & 0 & 0 & \dots & 0 & 0 & 0 \\ \lambda_1(1-x_2) & 0 & \lambda_2 x_2 & 0 & \dots & 0 & 0 & 0 \\ & & & & \ddots & & & \\ 0 & 0 & 0 & 0 & \dots & \lambda_{n-2}(1-x_{n-1}) & 0 & \lambda_{n-1}x_{n-1} \\ 0 & 0 & 0 & 0 & \dots & 0 & \lambda_{n-1}(1-x_n) & 0 \end{bmatrix}.$$

For any $x \in [0,1]^n$ all the entries of $M(x)$ are nonnegative, so (5.3) is a cooperative dynamical system [50]. The matrix $M(x)$ may become reducible for values x on the boundary of $[0,1]^n$. However, $M(x)$ is irreducible for all $x \in (0,1)^n$. Thus, Proposition 5.4.7 guarantees that after an arbitrarily short time the matrix $M(x(t))$ and, thus $J(x(t), u(t))$, becomes an irreducible matrix. This will be used in analyzing the asymptotic properties of the RFMLKN described below.

5.4.6 Stability

The next result shows that every level set contains a unique steady-state ribosome distribution in each mRNA and in the pool. The proof is based on the theory of monotone dynamical systems that admit a first integral, see Ref. [143, 132].

Theorem 5.4.1. *Every level set L_s contains a unique equilibrium point e_{L_s} of the RFMLKN and for any initial condition $a \in L_s$, the solution of the RFMLKN converges to e_{L_s}. Furthermore, for any $0 \leq s < p$,*

$$e_{L_s} \ll e_{L_p}. \tag{5.10}$$

In other words, the RFMLKN admits a continuum of equilibrium points and any two solutions starting from initial conditions in the same level set of the system converge to the same equilibrium point. Thus, the rates λ_j^i, β_j^i, α_j^i and the total number of ribosomes s in the network determine a unique steady-state density profile in the RFMLKs and the pool. Eq. (5.10) implies that for two initial conditions, the first one with a smaller total number of ribosomes than the second one, the corresponding equilibrium points e^1 and e^2 will be completely ordered: every steady-state density in e^1 will be strictly smaller than the corresponding density in e^2.

From a biological point of view, this implies the following. Consider a network of mRNA molecules interconnected via a pool. We compare two scenarios. In the first, the total number of ribosomes in the network is s and in the second it is p, with $p > s$. In both cases, the densities on each mRNA and in the pool converge

to a steady state, and for each site in each mRNA and the pool, the density in the second scenario is larger than in the first one.

Example 5.4.1. To model a gene that is highly expressed with respect to other genes, consider an RFMLKN with a single RFMLK and a pool. Assume that the output function of the pool is $G_1(z) = z$, and that the dimension of the RFMLK is $n_1 = 2$. The equations of the RFMLKN are then

$$\begin{aligned}
\dot{x}_1^1 &= \lambda_0^1 z(1-x_1^1) - \lambda_1^1 x_1^1(1-x_2^1) + \beta_1^1 z(1-x_1^1) - \alpha_1^1 x_1^1, \\
\dot{x}_2^1 &= \lambda_1^1 x_1^1(1-x_2^1) - \lambda_2^1 x_2^1 + \beta_2^1 z(1-x_2^1) - \alpha_2^1 x_2^1, \\
\dot{z} &= \lambda_2^1 x_2^1 - \lambda_0^1 z(1-x_1^1) + \sum_{j=1}^{2} \alpha_j^1 x_j^1 - \sum_{j=1}^{2} \beta_j^1 z(1-x_j^1).
\end{aligned} \tag{5.11}$$

Any equilibrium point $e = \begin{bmatrix} e_1^1 & e_2^1 & e_z \end{bmatrix}' \in L_s$ satisfies

$$\begin{aligned}
\lambda_0^1 e_z(1-e_1^1) &= \lambda_1^1 e_1^1(1-e_2^1) - \beta_1^1 e_z(1-e_1^1) + \alpha_1^1 e_1^1 \\
&= \lambda_2^1 e_2^1 - \sum_{j=1}^{2} \beta_j^1 e_z(1-e_j^1) + \sum_{j=1}^{2} \alpha_j^1 e_j^1,
\end{aligned} \tag{5.12}$$

and

$$e_1^1 + e_2^1 + e_z = s.$$

Fig. 5.8 depicts trajectories of Eq. (5.11) with parameters $\lambda_0^1 = 1$, $\lambda_1^1 = 1$, $\lambda_2^1 = 1$, $\alpha_1^1 = 0.1$, $\alpha_2^1 = 0.1$, $\beta_1^1 = 0.2$, $\beta_2^1 = 0.2$, and three different initial conditions in the level set L_1: $[0.5 \quad 0.5 \quad 0]'$, $[0.5 \quad 0 \quad 0.5]'$, and $[0 \quad 0.5 \quad 0.5]'$. It may be seen that all three solutions converge to the same equilibrium point.

Various intracellular mechanisms may affect the parameters of the translation machinery. For example, the elongation rates depend on the interaction between the nascent peptide and the exit tunnel of the system [144]. Stress conditions increase ribosome abortion and drop-off. Due to competition for the finite pool of ribosomes, any change in the translation speed along a specific mRNA molecule will also indirectly affect the translation of other mRNAs in the network. The variability in the factors that affect translation in the cell requires models that can be used to analyze the sensitivity to parameter values. Another motivation for studying these issues comes from synthetic biology, for example, the recent interest in co-expression of multiple genes at a given desired ratio [108, 145].

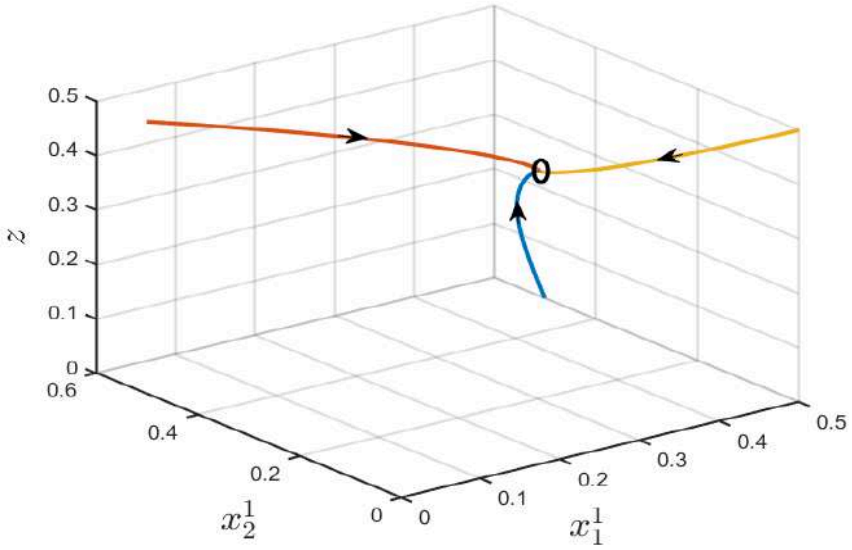

Figure 5.8: Trajectories of the RFMLKN in Example 5.4.1 for three different initial conditions in L_1. The unique equilibrium in L_1 is marked by a circle.

5.4.7 Effect of parameters

Our first result in this subsection analyzes the affect of a modification in the drop-off rate at one site of an mRNA molecule on the entire RFMLKN. We assume, without loss of generality, that the modification is in one of the rates in the first RFMLK.

Theorem 5.4.2. *Consider an RFMLKN with m RFMLKs with dimensions n_i, $i = 1, \ldots, m$, and parameters $\lambda_0^i > 0$, $\lambda_j^i > 0$, $\alpha_j^i \geq 0$, and $\beta_j^i \geq 0$, $i = 1, \ldots, m$ and $j = 1, 2, \ldots, n_i$. Fix $s > 0$. Let $e_j^i \in (0, 1)$, and $e_z \in (0, \infty)$ denote the unique steady-state density in the level set L_s of H. Fix $k \in \{1, \ldots, n_1\}$ and suppose that we modify the RFMLKN by changing α_k^1 to $\bar{\alpha}_k^1$, with $\bar{\alpha}_k^1 > \alpha_k^1$. Let $\bar{e}_j^i \in (0, 1)$, $\bar{e}_z > 0$, denote the steady-state density in the modified RFMLKN. Then*

$$\bar{e}_z > e_z \text{ and } \bar{e}_j^i > e_j^i \text{ for all } i \in \{2, \ldots, m\} \text{ and all } j \in \{1, \ldots, n_i\}. \tag{5.13}$$

From a biological point of view, this implies that an increase in the drop-off rate in one of the mRNAs yields an increase in the steady-state pool density and consequently an increase in the density in each site in all the *other* mRNAs. Of course, the exact quantitative effect may be small or large, depending on various parameters e.g. the ratio between the number of ribosomes that detach from the mRNA and the number of ribosomes in the pool.

Note that Theorem 5.4.2 and also the results below analyze the effect of changing a single parameter in the network. However, they also allow to analyze also specific modifications in several parameters. For example, Theorem 5.4.2 shows

that increasing the drop-off rate in an mRNA molecule increases the steady-state pool density, so it is clear that increasing several drop-off rates will also increase the steady-state pool density.

The effect of increasing α_k^1 on the steady-state in the first RFMLK is non-trivial. It is natural to expect a decrease in the density in each site of the first RFMLK. But, as more ribosomes accumulate in the pool the effective attachment rates in sites along the first RFMLK may also increase, leading to an increase in the density in certain sites. In general, the total effect on the first RFMLK will depend on all the parameters in the RFMLKN, and is thus difficult to predict analytically. The next two examples demonstrate this.

Example 5.4.2. Consider an RFMLKN with $m = 2$ RFMLKs of dimensions $n_1 = 6$ and $n_2 = 3$, parameters $\lambda_0^i = 1$, $\lambda_j^i = 1$, $\alpha_j^i = 0$, $\beta_j^i = 0$, for all i, j, and $G_i(z) = z$, $i = 1, 2$. The initial condition is $x_j^i = 0$, for all i, j, and $z(0) = 5$. We simulated this RFMLKN for several values of the drop-off rate α_3^1 from the third site in RFMLK #1. Figs. 5.9a and 5.9b show that increasing α_3^1 increases e_1^1, and decreases e_i^1 for all $i > 1$. As predicted in Theorem. 5.4.2, it also increases e_z, so more ribosomes accumulate in the pool leading to an increase in e_j^2 for all j.

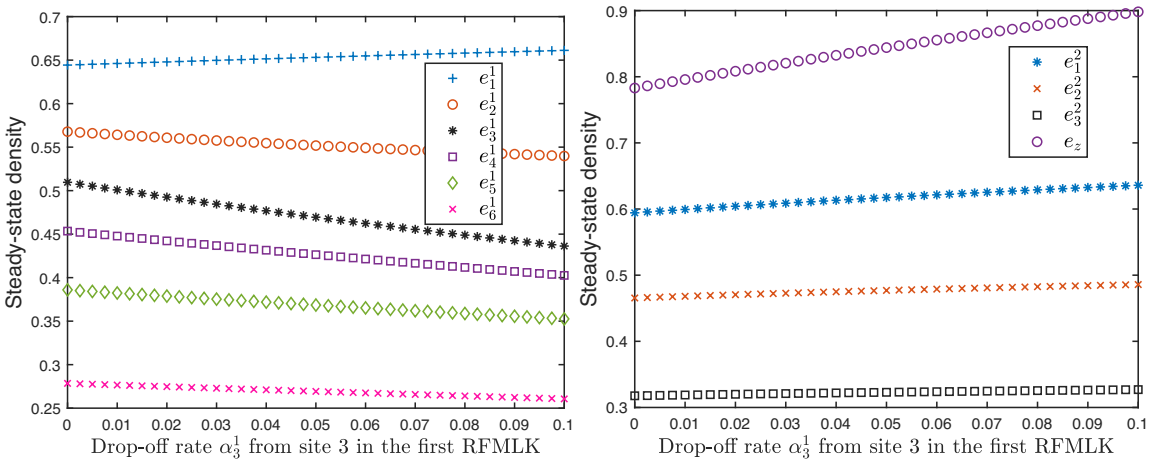

(a) (b)

Figure 5.9: Behavior of the RFMLKN in Example 5.4.2 as a function of α_3^1 when $\beta_4^1 = 0$: a) Steady-state values in RFMLK #1. b) Steady-state values in RFMLK #2 and the pool.

Example 5.4.3. Consider the RFMLKN in Example 5.4.2, but now with $\beta_4^1 = 2$. Fig. 5.10 shows that in this case an increase in the drop-off rate α_3^1 yields an increase in the steady-state values in the sites of RFMLK #1 located after the third site. This is because of an increase in the density of free ribosomes in the pool leading to more ribosomes attaching to the first RFMLK.

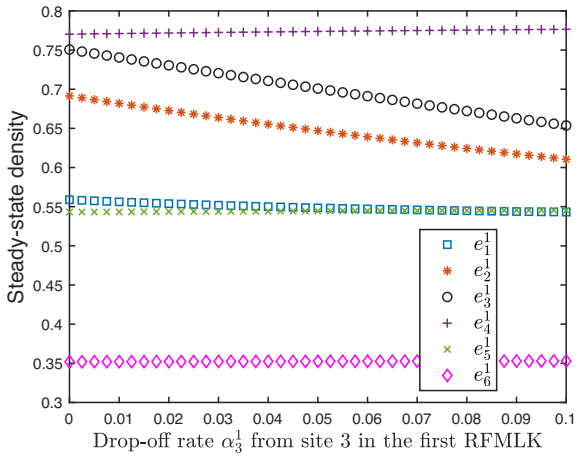

Figure 5.10: Steady-state values in RFMLK #1 in the RFMLKN in Example 5.4.3 as a function of the drop-off rate α_3^1.

It is known that ribosome drop-off from a single RFMLK always decreases the steady-state production rate [68]. The next example demonstrates that ribosome drop-off from one transcript in a network connected via a pool of free ribosomes may still be beneficial for the cell, as it allows ribosomes to detach from slow sites and then attach at the initiation sites of other, less jammed, transcripts. We measure the "usefulness" to the cell using the average steady-state protein production rate in the entire network, defined as

$$R_{av} := \frac{1}{m} \sum_{i=1}^{m} \lambda_{n_i}^i e_{n_i}^i.$$

In other words, this is the total production rate in all the mRNAs (normalized by the number of mRNAs in the network).

Example 5.4.4. We consider a network representing several copies of the *S. cerevisiae* gene YBL025W that encodes the protein RRN10, which is an RNA polymerase I-specific transcription initiation factor. This gene includes 145 codons, excluding the stop codon. It has been modeled using an RFM with length $n = 5$, and rates

$$\begin{bmatrix} \lambda_0 & \dots & \lambda_5 \end{bmatrix} = \begin{bmatrix} 0.1678 & 0.2572 & 0.2758 & 0.2514 & 0.2612 & 0.3002 \end{bmatrix}. \tag{5.14}$$

This model was derived by dividing the 145 codons into 6 groups of consecutive codons, estimating the decoding time d_i for each group based on ribo-seq data, and then setting $\lambda_i = 1/d_i$ (with units of 1/sec). We refer to [46] for the full details.

Consider an RFMLKN with $m = 50$ RFMLKs with dimensions $n_i = 5$, $i \in \{1, 2, \dots, 50\}$. The transition rates are as in Eq. (5.14) in RFMLKs #2 to #50. In RFMLK #1, the transition rates are as in Eq. (5.14), except for $\lambda_2 = 0.001$. Thus,

site 2 in the first RFMLK is a slow site, e.g. due to a stalled ribosome. The other parameters in the network are: $\alpha_j^i = 0$, $\beta_j^i = 0$, and $G_i(z) = z$ for all i, j. The initial condition is $x_j^i = 0$, for all i, j, and $z(0) = 100$. Fig. 5.11 depicts R_{av} as a function of the drop-off rate α_2^1 in the range 0 to 0.01. It can be observed that the total steady-state protein production rate in the network *increases* when ribosomes are allowed to detach from the slow site. The quantitative effect is small, but this is because we modify the drop-off rate in one of the 50 mRNAs. If the drop-off rate is increased in several jammed mRNAs then the effect will be more pronounced.

Increasing α_2^1 from 0 to 0.01 in RFMLK #1 decreases the total density in RFMLK #1 (i.e., the sum of all the densities on the different sites along RFMLK #1) from 2.0002 to 1.8929, increases the total density from 1.9827 to 1.9848 in all the *other* RFMLKs, and increases the pool density from 0.8488 to 0.8506. As the drop-off rate increases more ribosomes accumulate in the pool and become available for *other* RFMLKs, and thus there is an increase in the initiation rates in all the *other* RFMLKs leading to higher production rates. Our simulations suggest that this phenomena takes place only when the number of ribosomes in the pool is rather low, that is, when the pool is "starved". Summarizing, our model suggests that at least in some cases ribosome drop-off from a jammed site may be advantageous to the cell.

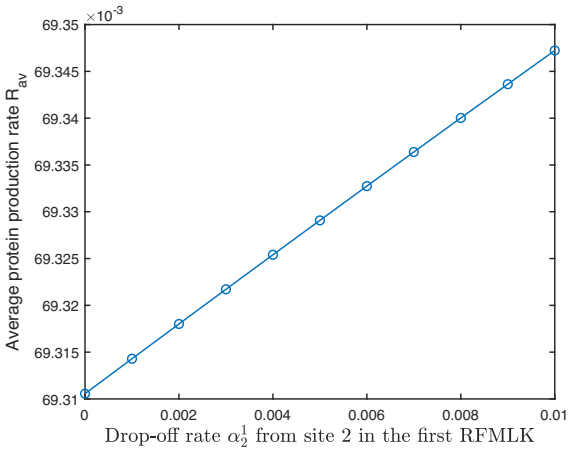

Figure 5.11: Average protein production rate in the RFMLKN in Example 5.4.4 as a function of the drop-off rate α_2^1.

The next result analyzes the "dual" case of the one described in Theorem 5.4.2 i.e., the affect of modifying one of the attachment rates in an RFMLK in the network.

Theorem 5.4.3. *Consider an RFMLKN with m RFMLKs of dimensions n_i, $i = 1, \ldots, m$, and parameters $\lambda_0^i > 0$, $\lambda_j^i > 0$, $\alpha_j^i \geq 0$, and $\beta_j^i \geq 0$, $i = 1, \ldots, m$ and $j = 1, 2, \ldots, n_i$. Fix $s > 0$. Let $e_j^i \in (0, 1)$, and $e_z \in (0, \infty)$ denote the unique steady-state density in the level set L_s of H. Fix $k \in \{1, \ldots, n_1\}$ and suppose that*

we modify the RFMLKN by changing β_k^1 *to* $\bar{\beta}_k^1$*, with* $\bar{\beta}_k^1 > \beta_k^1$*. Let* $\bar{e}_j^i \in (0,1)$*,* $\bar{e}_z > 0$*, denote the steady-state density in the modified RFMLKN. Then*

$$\bar{e}_z < e_z \text{ and } \bar{e}_j^i < e_j^i \text{ for all } i \in \{2,\dots,m\} \text{ and all } j \in \{1,\dots,n_i\}. \tag{5.15}$$

In other words, an increase in the attachment rate in one of the RFMLKs decreases the steady-state pool density and consequently decreases the density in each site in all the *other* RFMLKs.

Example 5.4.5. Consider an RFMLKN with $m = 2$ RFMLKs of dimensions $n_1 = 9$ and $n_2 = 3$, parameters $\lambda_0^i = 1$, $\lambda_j^i = 1$, $\alpha_j^i = 0$, $\beta_j^i = 0$, for all i, j, and $G_i(z) = z$, $i = 1, 2$. The initial condition is $x_j^i = 0$, for all i, j, and $z(0) = 5$. We simulated this RFMLKN for several values of the attachment rate β_3^1. Fig. 5.12b shows that as β_3^1 increases there is a decrease in the steady-state pool density (as more ribosomes bind to the third site of RFMLK #1) and consequently a decrease in the steady-state values in all the sites in RFMLK #2. As shown in Fig. 5.12a, the effect of increasing β_3^1 on RFMLK #1 is non-trivial. A decrease in the pool density decreases e_1^1. However, the increase in the attachment rate in the third site leads to more ribosomes attaching to this site and consequently a higher density in sites $3, \dots, 9$. Also, this creates a "traffic jam" along these sites and thus increases the density in site 2 as well.

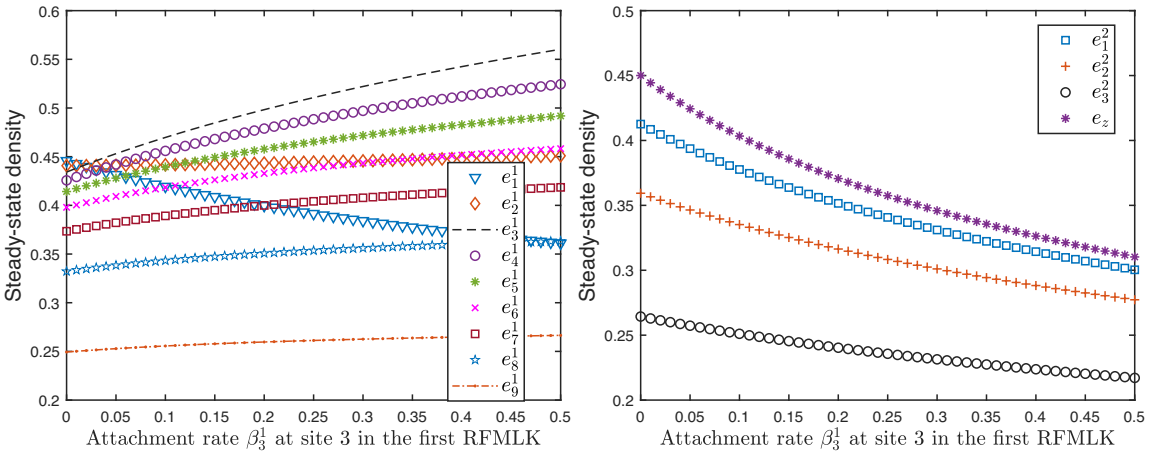

(a) (b)

Figure 5.12: Behavior of the RFMLKN in Example 5.4.5 as a function of the attachment rate β_3^1 : a) Steady-state densities RFMLK #1. b) Steady-state densities in RFMLK #2 and the pool.

Our last result in this subsection analyzes the effect of modifying a hopping rate in one of the RFMLKs in the network.

Theorem 5.4.4. *Consider an RFMLKN with m RFMLKs of dimensions n_i, $i = 1,\ldots,m$, and parameters $\lambda_0^i > 0$, $\lambda_j^i > 0$, $\alpha_j^i \geq 0$ and $\beta_j^i \geq 0$, $i = 1,\ldots,m$, $j = 1,2,\ldots,n_i$. Fix $s > 0$. Let $e_j^i \in (0,1)$, and $e_z \in (0,\infty)$ denote the unique steady-state density in the level set L_s of H. Fix $k \in \{0,\ldots,n_1\}$. Suppose that we modify the RFMLKN by changing λ_k^1 to $\bar{\lambda}_k^1$, with $\bar{\lambda}_k^1 > \lambda_k^1$. Let $\bar{e}_j^i \in (0,1)$, $\bar{e}_z > 0$ denote the steady-state density in the modified RFMLKN. Then one of the following three cases holds. Either*

$$\bar{e}_z > e_z \text{ and } \bar{e}_j^i > e_j^i \text{ for all } i \in \{2,\ldots,m\} \text{ and all } j \in \{1,\ldots,n_i\},$$

or

$$\bar{e}_z = e_z \text{ and } \bar{e}_j^i = e_j^i \text{ for all } i \in \{2,\ldots,m\} \text{ and all } j \in \{1,\ldots,n_i\}, \tag{5.16}$$

or

$$\bar{e}_z < e_z \text{ and } \bar{e}_j^i < e_j^i \text{ for all } i \in \{2,\ldots,m\} \text{ and all } j \in \{1,\ldots,n_i\}.$$

Clearly, this covers all the possible cases for the change in the pool density, and each case shows that the qualitative behavior of all the *other* RFMLKs is the same. From a biological pint of view, this implies that modifying a translation rate in an mRNA affects all the sites in all the *other* mRNAs in the same way. This is natural, as all the mRNAs are fed from the same pool, so if, for example, the steady-state density in the pool increases then all the densities in all the sites in the other mRNAs will increase.

Theorem 5.4.4 does not provide any information on the modified densities in the sites along RFMLK #1. Indeed, it seems that any of these densities may increase or decrease depending upon the parameters in the entire network. The next examples demonstrate this.

Example 5.4.6. Consider an RFMLKN with $m = 2$ RFMLKs of dimensions $n_1 = 9$ and $n_2 = 3$, parameters $\lambda_0^i = 2$, $\lambda_j^i = 2$, for all i,j except for λ_5^1, $\alpha_j^1 = 0.1$, for $j \in \{1,2,\ldots,8\}$, $\alpha_9^1 = 0$, $\alpha_j^2 = 0.1$, for $j = 1,2$, $\alpha_3^2 = 0$, $\beta_j^1 = 0.1$ for all j except for $\beta_1^1 = 0$, $\beta_1^2 = 0$, $\beta_j^2 = 0.1$ for $j = 2,3$ and $G_i(z) = z$, $i = 1,2$. The initial condition is $x_j^i = 0$, for all i,j, and $z(0) = 3$. We simulated this RFMLKN for various values of the elongation rate λ_5^1. Note that when $\lambda_5^1 \ll 2$ it is a bottleneck rate in RFMLK #1. Fig. 5.13b shows that increasing λ_5^1 increases the pool density and thus the densities in all the sites along RFMLK #2. Fig. 5.13a shows that increasing λ_5^1 yields a decrease in sites $3,4,5$ in RFMLK #1, but an increase in all the other sites.

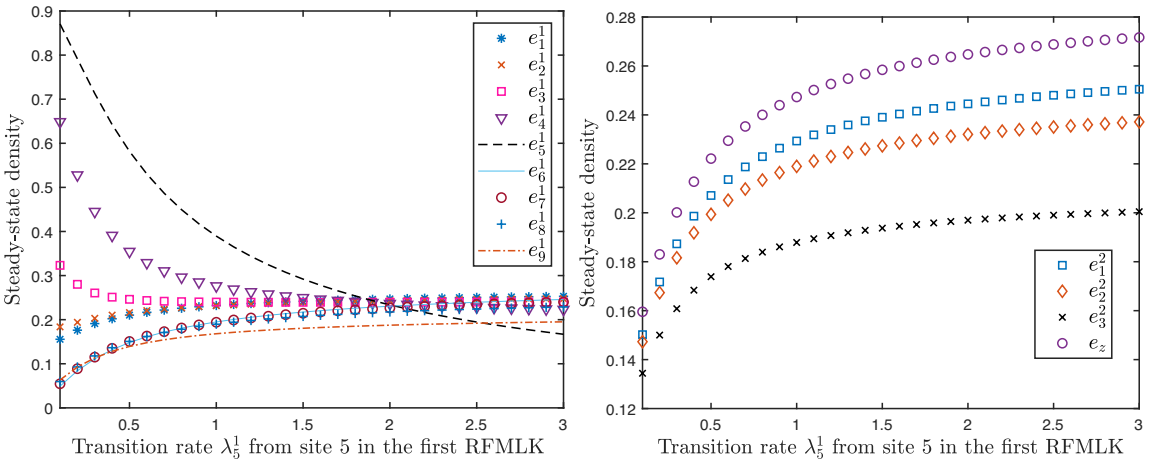

(a) (b)

Figure 5.13: Behavior of the RFMLKN in Example 5.4.6 as a function of the elongation rate λ_5^1: a) Steady-state densities in RFMLK #1. b) Steady-state densities in RFMLK #2 and the pool.

Example 5.4.7. Consider again the RFMLKN in Example 5.4.6, but now the initial condition is $x_j^i = 0$, for all i, j, and $z(0) = 10$. In this case, Fig. 5.14b shows that increasing the elongation rate λ_5^1 leads to a decrease in the steady-state pool density resulting in decreased steady-state densities in RFMLK #2. Fig. 5.14a shows that in this case the effect of increasing λ_5^1 on RFMLK #1 is more intuitive: it decreases the densities in sites $1, \ldots, 5$ and increases the densities in sites $6, \ldots, 9$.

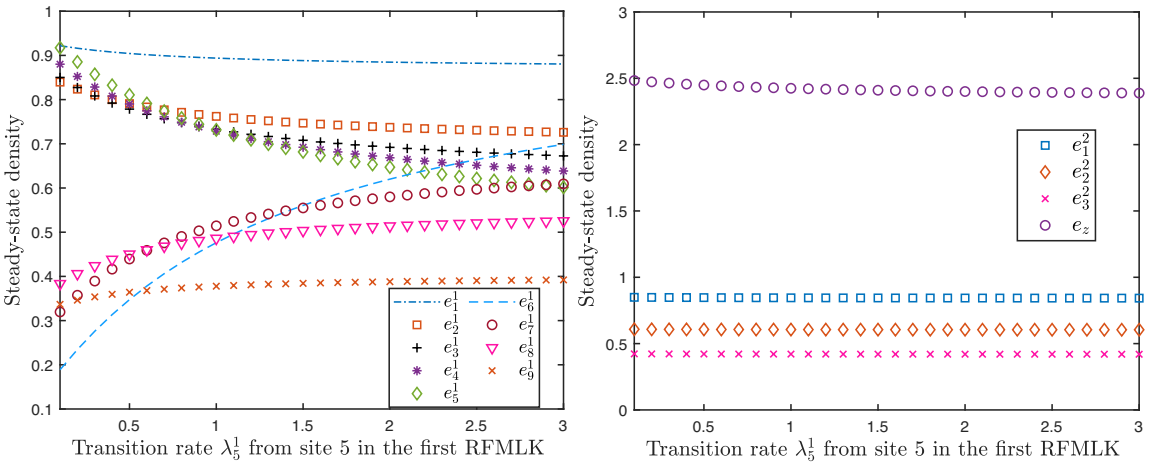

(a) (b)

Figure 5.14: Behavior of the RFMLKN in Example 5.4.7 as a function of the elongation rate λ_5^1: a) Steady-state densities in RFMLK #1. b) Steady-state densities in RFMLK #2 and the pool.

We now analyze several additional mathematical properties of the RFMLKN.

5.4.8 Strong monotonicity

Recall that the dynamical system $\dot{x} = f(x)$ is called cooperative if for any two initial conditions a, b with $a \leq b$ we have $x(t, a) \leq x(t, b)$ for all $t \geq 0$ [50]. In other words, the flow preserves the (partial) ordering between the initial conditions. The next result shows that the RFMLKN is cooperative.

Proposition 5.4.8. *Consider the RFMLKN. Fix two initial conditions $a, b \in \Omega$ with $a \leq b$. Then*

$$x(t, a) \leq x(t, b) \quad \textit{and } z(t, a) \leq z(t, b), \ \textit{for all } t \geq 0.$$

If, furthermore, $a \neq b$ then

$$x(t, a) \ll x(t, b) \quad \textit{and } z(t, a) < z(t, b), \ \textit{for all } t > 0.$$

From a biological point of view, this implies the following. Consider an RFMLKN with two different initial densities. For every site in every mRNA, the first initial density is smaller or equal to the density in the second RFMLKN, and the same holds for the initial pool density. Then at each time $t > 0$, the corresponding solution from these densities still maintain the same ordering between the site densities and the pool density.

The next subsection shows that the flow of the RFMLKN is a non-expansive mapping. For a vector $v \in \mathbb{R}^n$, let $|v|_1 : \mathbb{R}^n \to \mathbb{R}_+$ denote the L_1 norm of v.

5.4.9 Non-expansion

In a contractive system, all solutions converge exponentially to one another. Since the RFMLKN admits more than one equilibrium, it is not a contractive system with respect to any norm. However, the next result shows that the L_1 distance between any two trajectories is non-expansive, i.e., it is bounded by the distance L_1 between the initial conditions.

Proposition 5.4.9. *Consider the RFMLKN. Fix $a, b \in \Omega$. Then*

$$\left| \begin{bmatrix} x(t, a) \\ z(t, a) \end{bmatrix} - \begin{bmatrix} x(t, b) \\ z(t, b) \end{bmatrix} \right|_1 \leq |a - b|_1, \ \textit{for all } t \geq 0. \tag{5.17}$$

In particular, the difference between two "close" ribosomal density profiles will remain close for all $t \geq 0$.

Fix $a \in \Omega$ and let $s =: 1_d' a$. Setting $b = e_{L_s}$ in Eq. (5.17) yields

$$\left| \begin{bmatrix} x(t,a) \\ z(t,a) \end{bmatrix} - e_{L_s} \right|_1 \leq |a - e_{L_s}|_1, \text{ for all } t \geq 0.$$

In other words, the convergence to the equilibrium e_{L_s} is monotone in the sense that the L_1 distance can only decrease with time.

5.4.10 Entrainment

Many biological processes are excited by a periodic input. Proper functioning often requires entraining to the excitation, that is, converging to a periodic pattern with the same period as the excitation. A typical example is the ability of cells to coordinate their growth with the periodic cell-cycle division process. Translation seems to play an important role in this process. It is known for example that expression of the human translation initiation factor eIF3f peaks twice in the cell cycle: in the S and the M phases [146]. An interesting question is whether entrainment in translation may increase the average production rate [147]. Entrainment is also important in the context of synthetic biology, for example, in designing a biological network that is coordinated by a single oscillator producing a common "clock signal" [100].

To study entrainment in the RFMLKN, assume that the parameters $\lambda_j^i, \alpha_j^i, \beta_j^i$ in all the RFMLKs are not constant, but are time-varying functions, that are all jointly periodic with a period $T > 0$. More precisely, we assume that

- There exists a (minimal) $T > 0$ such that all the rate functions $\lambda_j^i(t)$, $\alpha_j^i(t)$ and $\beta_j^i(t)$ are non-negative, continuous, and T-periodic.
- There exists $0 < \delta_1 \leq \delta_2$ such that $\lambda_j^i(t) \in [\delta_1, \delta_2]$, for all i, j and all $t \in [0, T)$.

We then refer to the network as the *periodic RFM with Langmuir kinetics network (PRFMLKN)*. Note that a constant function is T-periodic for any T, so for example, if one parameter in the network is T-periodic and all the others are constant then our assumptions hold.

The next result shows that the PRFMLKN entrains.

Theorem 5.4.5. *Consider the PRFMLKN. Fix $s \geq 0$. There exists a unique function $\phi_s : \mathbb{R}_+ \to \text{int}(\Omega)$, that is T-periodic, and for any initial condition $a = \begin{bmatrix} x(0) \\ z(0) \end{bmatrix} \in L_s$, the solution $\begin{bmatrix} x(t,a) \\ z(t,a) \end{bmatrix}$ of the PRFMLKN converges to ϕ_s as $t \to \infty$.*

In other words, if the rates are T-periodic then all the densities in the mRNAs and the pool converge to a periodic pattern with period T, and thus so will the protein production rate in every mRNA. In particular, if a single parameter in one of the RFMLKs is T-periodic and all the other parameters are constant then the network entrains. Roughly speaking, this can be explained as follows. The T-periodic parameter will generate T-periodic variations in the pool density and this will generate T-periodic patterns in all the mRNA densities, as the pool feeds all the mRNAs. Again, this demonstrates the intricate coupling generated by the competition for shared resources.

Example 5.4.8. Consider a network with $m = 2$ RFMLKs of dimensions $n_1 = 2$ and $n_2 = 3$, and with $G_i(z) = \tanh(z)$, $i = 1, 2$. All the rates in the network are constant and equal to one, except for $\lambda_2^2(t) = 5 + 4\sin(2\pi t)$. Thus all the rates in the network are periodic with a common minimal period $T = 1$. The initial condition is $z(0) = x_j^i(0) = 1/4$ for all i, j. Fig. 5.15 depicts the state-variables and the pool density as a function of t. Note that all the densities converge to a periodic pattern with period one. Note also that since the total number of ribosomes is conserved, maximal peaks in the density along the RFMLKs corresponds to minimal peaks in the pool density, and vice-versa.

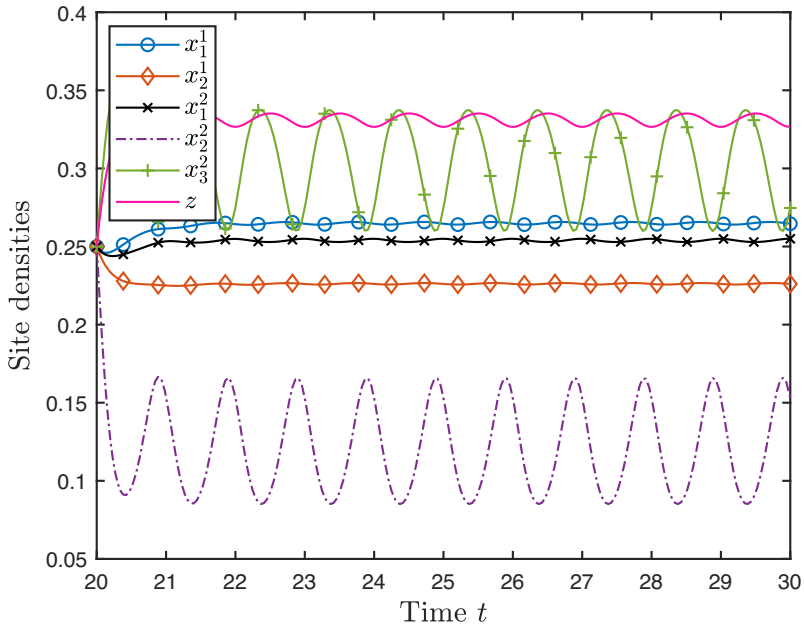

Figure 5.15: Trajectories of PRFMLKN in Example 5.4.8 as a function of time.

5.5 Discussion

We derived and analyzed a novel and general network model of ribosome flow during large-scale translation in the cell. This model encapsulates important cellular

properties like ribosome drop-off, ribosome attachment at IRESs, and competition for a finite pool of free ribosomes. We analyzed the model using tools from systems and control theory, including contraction theory, and the theory of cooperative dynamical systems.

The new model is an irreducible cooperative dynamical system admitting a first integral (the total density of ribosomes in the network). This implies that the system admits a continuum of linearly ordered equilibrium points, and that every trajectory converges to an equilibrium point. The system is also on the "verge of contraction" with respect to the L_1 norm. In addition, we proved that if one or more of the rates in the network are time-varying periodic functions with a common period T, then the densities along all the mRNAs and in the pool converge to a periodic solution with period T, i.e., the system entrains to a periodic excitation.

An important question is the sensitivity of the network steady-state to variations in the mRNA parameters and the density of free ribosomes. We thoroughly analyzed this problem and showed that a modification of a bio-physical property in a specific mRNA has two implications. First, via competition it affects translation in all the other mRNAs in an intuitive manner: if the pool steady-state density increases [decreases] then the density in all other sites in all other mRNAs increases [decreases]. Second, and perhaps surprisingly, it is almost impossible to predict what will be the effect on the densities and protein production rate in the mRNA that is modified, as this depends in a non-trivial way on the interactions between all the mRNAs and the pool. For example, an increase in the drop-off rate in a specific site in an mRNA may increase the pool density, thus increasing the attachment rates along this mRNA and leading to an increase in the density in some sites along this mRNA.

These results highlight that analyzing the effect of any bio-physical property on translation in the cell must take into account the intricate effects of competition, especially when the competition for shared resources plays a major role, e.g. under stressful conditions.

We believe that the new model presented here provides a powerful framework for analyzing and re-engineering the translation process. It may also prove useful for modeling other natural transport phenomena such as gene transcription and intracellular transport, as well as artificial systems. One possible avenue for further research is in developing a quantitative and qualitative understanding of how viral mRNAs hijack the translation machinery and, in particular, whether the indirect effects of competition are enough to hamper the host's immune response.

5.6 Appendix: Proofs

We begin by writing the RFMLK with input and output in the form:

$$\begin{aligned}
\dot{x}_1 &= f_0(x_1, u) - f_1(x_1, x_2) - g_1(x_1, u),\\
\dot{x}_2 &= f_1(x_1, x_2) - f_2(x_2, x_3) - g_2(x_2, u),\\
&\vdots\\
\dot{x}_n &= f_{n-1}(x_{n-1}, x_n) - f_n(x_n) - g_n(x_n, u),\\
y &= h(x),
\end{aligned} \tag{5.18}$$

where $u : \mathbb{R}_+ \to \mathbb{R}_+$ is a scalar input function that takes non-negative values for any time $t \geq 0$, $y : \mathbb{R}_+ \to \mathbb{R}_+$ is a scalar non-negative output function, and

$$\begin{aligned}
f_0(x_1, u) &:= \lambda_0(1 - x_1)u,\\
f_i(x_i, x_{i+1}) &:= \lambda_i x_i(1 - x_{i+1}),\ i = 1, \ldots, n-1,\\
f_n(x_n) &:= \lambda_n x_n,\\
g_i(x_i) &:= \alpha_i x_i - \beta_i(1 - x_i)u,\\
h(x) &:= \lambda_n x_n + \sum_{i=1}^{n} \alpha_i x_i.
\end{aligned} \tag{5.19}$$

The parameters satisfy $\lambda_i > 0, \alpha_i \geq 0$, and $\beta_i \geq 0$ for all i. Recall that every x_i takes values in the interval $[0, 1]$, so the state-space of the RFMLK is $C^n := [0, 1]^n$.

Proof of Proposition 5.4.1: Fix $\delta > 0$. We will show that for any sufficiently small $\triangle > 0$ there exists $K = K(\delta, \triangle) > 0$ such that for every $k \in \{1, \ldots, n\}$ and every $t \geq 0$ the condition

$$x_k \leq \triangle \text{ and } x_i \geq \delta \text{ for all } i \in \{1, \ldots, k-1\}$$

implies that

$$\dot{x}_k \geq K. \tag{5.20}$$

For $k = 1$ the condition is simply $x_1 \leq \triangle$, and then

$$\begin{aligned}
\dot{x}_1 &= f_0(x_1, u) - f_1(x_1, x_2) - g_1(x_1, u)\\
&= (\lambda_0 + \beta_1)(1 - x_1)u - (\lambda_1(1 - x_2) + \alpha_1)x_1\\
&\geq \lambda_0(1 - \triangle)s - (\lambda_1 + \alpha_1)\triangle\\
&=: K_1.
\end{aligned}$$

Note that $K_1 \geq \lambda_0 s/2 > 0$ for any $\triangle > 0$ sufficiently small. For $k \in \{2, \ldots, n-1\}$ we have

$$\begin{aligned}
\dot{x}_k &= f_{k-1}(x_{k-1}, x_k) - f_k(x_k, x_{k+1}) - g_k(x_k, u) \\
&= (\lambda_{k-1} x_{k-1} + \beta_k u)(1 - x_k) - (\lambda_k(1 - x_{k+1}) + \alpha_k) x_k \\
&\geq \lambda_{k-1}\delta(1 - \triangle) - (\lambda_k + \alpha_k)\triangle \\
&=: K_k.
\end{aligned}$$

Note that $K_k \geq \lambda_{k-1}\delta/2 > 0$ for any $\triangle > 0$ sufficiently small. For $k = n$ we have

$$\begin{aligned}
\dot{x}_n &= f_{n-1}(x_{n-1}, x_n) - f_n(x_n) - g_n(x_n, u) \\
&= (\lambda_{n-1} x_{n-1} + \beta_n u)(1 - x_n) - (\lambda_n + \alpha_n) x_n \\
&\geq \lambda_{n-1}\delta(1 - \triangle) - (\lambda_n + \alpha_n)\triangle \\
&=: K_n.
\end{aligned}$$

Note that $K_n \geq \lambda_{n-1}\delta/2 > 0$, for any $\triangle > 0$ sufficiently small. We conclude that Eq. (5.20) holds for $K := \min\{K_1, \ldots, K_n\} \geq \min\{\lambda_0, \ldots, \lambda_n\} \min\{s, \delta\}/2 > 0$. By Ref. [48, Lemma 1], this implies that for any $\tau > 0$ there exists $\epsilon_1 = \epsilon_1(\tau) > 0$, with $\epsilon_1(\tau) \to 0$ as $\tau \to 0$, such that for any $a \in C^n$ the solution of Eq. (5.18) satisfies

$$x_i(t, a) \geq \epsilon_1, \quad \text{for all } i \in \{1, \ldots, n\} \text{ and all } t \geq \tau. \tag{5.21}$$

Let $z_i := 1 - x_{n+1-i}$, $i = 1, \ldots, n$. Then Eq. (5.18) gives

$$\begin{aligned}
\dot{z}_1 &= -f_{n-1}(1 - z_2, 1 - z_1) + f_n(1 - z_1) + g_n(1 - z_1, u), \\
\dot{z}_2 &= -f_{n-2}(1 - z_3, 1 - z_2) + f_{n-1}(1 - z_2, 1 - z_1) + g_{n-1}(1 - z_2, u), \\
&\vdots \\
\dot{z}_n &= -f_0(1 - z_n, u) + f_1(1 - z_n, 1 - z_{n-1}) + g_1(1 - z_n, u).
\end{aligned} \tag{5.22}$$

It is not difficult to verify that this system also satisfies condition Eq. (5.20), so by Ref. [48, Lemma 1], for any $\tau > 0$ there exists $\epsilon_2 = \epsilon_2(\tau) > 0$, with $\epsilon_2(\tau) \to 0$ as $\tau \to 0$, such that for any $a \in C^n$ the solution of Eq. (5.22) satisfies

$$z_i(t, a) \geq \epsilon_2, \quad \text{for all } i \in \{1, \ldots, n\} \text{ and all } t \geq \tau.$$

Combining this with Eq. (5.21) completes the proof of Proposition 5.4.1.

Proof of Proposition 5.4.2: Let f denote the vector field in Eq. (5.18), and

let $J := \frac{\partial}{\partial x} f$ denote its Jacobian. Then

$$J = J_1 - \mathrm{diag}(\alpha_1 + \beta_1 u, , \ldots, \alpha_n + \beta_n u), \tag{5.23}$$

where J_1 is given below

$$\begin{bmatrix} -\lambda_0 u - \lambda_1(1-x_2) & \lambda_1 x_1 & 0 & \ldots & 0 & 0 \\ \lambda_1(1-x_2) & -\lambda_1 x_1 - \lambda_2(1-x_3) & \lambda_2 x_2 & \ldots & 0 & 0 \\ & & & \ddots & & \\ 0 & 0 & 0 & \ldots & -\lambda_{n-2}x_{n-2} - \lambda_{n-1}(1-x_n) & \lambda_{n-1}x_{n-1} \\ 0 & 0 & 0 & \ldots & \lambda_{n-1}(1-x_n) & -\lambda_n x_n \end{bmatrix}.$$

Note that J_1 is the Jacobian of an RFM with a time-varying initiation rate $\lambda_0 u(t) \geq \lambda_0 s$, and that $\alpha_i + \beta_i u(t) \geq 0$ for all t. Note also that for any $x \in \mathrm{int}(C^n)$, all the entries in the super- and sub-diagonal of J_1 are positive, so in particular J_1 (and thus J) is irreducible.

Fix $a, b \in C^n$ and $\tau > 0$. By Proposition 5.4.1, there exists $\epsilon = \epsilon(\tau) > 0$, such that

$$\epsilon \leq x_i(t,a), x_i(t,b) \leq 1 - \epsilon, \qquad \text{for all } i \in \{1, \ldots, n\} \text{ and all } t \geq \tau.$$

Now arguing as in the proof of Ref. [48, Theorem 4] completes the proof of Proposition 5.4.2. *Proof of Proposition 5.4.3:* The RFMLK with a constant input $u(t) \equiv s > 0$ is a time-invariant system that maps the convex and compact state-space $[0,1]^n$ to itself. Hence, it admits an equilibrium e^s. Proposition 5.4.1 implies that $e^s \in (0,1)^n$. Proposition 5.4.2 implies that any solution converges to e^s and this completes the proof of Proposition 5.4.3.

Proof of Proposition 5.4.4: It follows from Eq. (5.23) that J is a Metzler matrix, i.e., every off-diagonal entry of J is non-negative. Also,

$$\begin{aligned} K &:= \frac{\partial}{\partial u} f \\ &= \mathrm{diag}(\frac{\partial}{\partial u} f_0 - \frac{\partial}{\partial u} g_1, -\frac{\partial}{\partial u} g_2, \ldots, -\frac{\partial}{\partial u} g_n) \\ &= \mathrm{diag}(\lambda_0(1-x_1) + \beta_1(1-x_1), \beta_2(1-x_2,), \ldots, \beta_n(1-x_n)), \end{aligned}$$

so every entry of K is non-negative. The results in Ref. [142] imply that the RFMLK is a monotone control system, so Eq. (5.5) holds. Now the definition of the output y implies Eq. (5.6) and this completes the proof of Proposition 5.4.4.

Proof of Proposition 5.4.5: We already know that the limits e^{s^1}, e^{s^2}, and $e := \lim_{t\to\infty} x(t,a,v)$ exist. By monotonicity, $x(t,a,u) \leq x(t,a,v)$, for all $t \geq 0$, and taking the limit as $t \to \infty$ gives $e^{s^1} \leq e$. Since the system is contractive, $e = e^{s^2}$, and this completes the proof of Proposition 5.4.5.

For the sake of simplicity and to avoid cumbersome notation, we provide proofs of the theoretical results when $m = 2$, i.e., a network with two RFMLKs connected via a pool of free ribosomes (the proofs when $m > 2$ are very similar). We write the first RFMLK as

$$\begin{aligned}
\dot{p}_1 &= \lambda_0(1-p_1)u_1 - \lambda_1 p_1(1-p_2) - \alpha_1 p_1 + \beta_1(1-p_1)u_1,\\
\dot{p}_2 &= \lambda_1 p_1(1-p_2) - \lambda_2 p_2(1-p_3) - \alpha_2 p_2 + \beta_2(1-p_2)u_1,\\
&\vdots\\
\dot{p}_n &= \lambda_{n-1} p_{n-1}(1-p_n) - \lambda_n p_n - \alpha_n p_n + \beta_n(1-p_n)u_1,\\
y_1 &= \lambda_n p_n + \sum_{i=1}^{n} \alpha_i p_i,
\end{aligned} \tag{5.24}$$

and the second as

$$\begin{aligned}
\dot{q}_1 &= \eta_0(1-q_1)u_2 - \eta_1 q_1(1-q_2) - \gamma_1 q_1 + \delta_1(1-q_1)u_2,\\
\dot{q}_2 &= \eta_1 q_1(1-q_2) - \eta_2 q_2(1-q_3) - \gamma_2 q_2 + \delta_2(1-q_2)u_2,\\
&\vdots\\
\dot{q}_\ell &= \eta_{\ell-1} q_{\ell-1}(1-q_\ell) - \eta_\ell q_\ell - \gamma_\ell q_\ell + \delta_\ell(1-q_\ell)u_2,\\
y_2 &= \eta_\ell q_\ell + \sum_{i=1}^{\ell} \gamma_i q_i.
\end{aligned} \tag{5.25}$$

The inputs to the RFMLKs are functions of the pool density

$$u_1 = G_1(z), \quad u_2 = G_2(z), \tag{5.26}$$

and the pool dynamics is

$$\dot{z} = y_1 + y_2 - \lambda_0(1-p_1)G_1(z) - \eta_0(1-q_1)G_2(z) - \sum_{i=1}^{n} \beta_i(1-p_i)G_1(z) - \sum_{i=1}^{\ell} \delta_i(1-q_i)G_2(z). \tag{5.27}$$

The state-space of this network is

$$\Omega := [0,1]^n \times [0,1]^\ell \times \mathbb{R}_+.$$

Note that $\sum_{i=1}^{n} \dot{p}_i + \sum_{i=1}^{\ell} \dot{q}_i + \dot{z} = 0$, so

$$H(p,q,z) := \sum_{i=1}^{n} p_i + \sum_{i=1}^{\ell} q_i + z \tag{5.28}$$

is a first integral of the dynamics, that is, $H(p(t), q(t), z(t)) \equiv H(p(0), q(0), z(0))$.

In other words, the total density of ribosomes in the network is conserved. For any $s \geq 0$, we define the s level set of the first integral H by

$$L_s := \{a \in \Omega : \sum_{i=1}^{n+\ell+1} a_i = s\}.$$

Thus, L_s includes all the states in Ω with total density of ribosomes equal to s. Note that for $s = 0$, $L_0 = \{0\}$, and the dynamics emanating from zero remains in zero for all time $t \geq 0$. therefore, we will always consider L_s with $s > 0$.

Proof of Proposition 5.4.7: We now restate and prove the persistence result in Proposition 5.4.7 for the case $m = 2$.

Proposition 5.6.1. *Consider the RFMLKN with $m = 2$. Fix $s > 0$. Then for any $\tau > 0$ there exists $\epsilon(\tau) > 0$, with $\epsilon(\tau) \to 0$ as $\tau \to 0$, such that for any initial condition in L_s and any $t \geq \tau$ the solution of the RFMLKN satisfies*

$$\begin{aligned} \epsilon \leq p_i(t) \leq 1 - \epsilon, \quad & \text{for all } i \in \{1, \ldots, n\}, \\ \epsilon \leq q_j(t) \leq 1 - \epsilon, \quad & \text{for all } j \in \{1, \ldots, \ell\}, \\ 0 < z(t). & \end{aligned}$$

It is useful to denote $p_0 := z$, $p_{n+1} := 0$, and $p_{-1} := p_n$. Using the fact that $y_2 \geq 0$ yields

$$\begin{aligned} \dot{p}_0 \geq \lambda_n p_n + \sum_{i=1}^{n} \alpha_i p_i - \lambda_0(1 - p_1)G_1(p_0) - \eta_0(1 - q_1)G_2(p_0) \\ - \sum_{i=1}^{n} \beta_i(1 - p_i)G_1(p_0) - \sum_{i=1}^{\ell} \delta_i(1 - q_i)G_2(p_0). \end{aligned}$$

We now show that the system with state-variables $p_0, \ldots, p_n$ satisfies the cyclic boundary-repelling (CBR) condition in Ref. [49, Lemma 1], that is, for any $\delta > 0$ and any sufficiently small $\triangle > 0$, there exists $K = K(\delta, \triangle) > 0$ such that for each $k = 0, \ldots, n$ and each $t \geq 0$ the condition

$$p_k(t) \leq \triangle \text{ and } p_{k-1}(t) \geq \delta$$

implies that

$$\dot{x}_k \geq K.$$

Indeed, for $k = 0$ we have

$$\dot{p}_0 \geq \lambda_n p_n - \lambda_0(1-p_1)G_1(p_0) - \eta_0(1-q_1)G_2(p_0) - \sum_{i=1}^{n}\beta_i(1-p_i)G_1(p_0) - \sum_{i=1}^{\ell}\delta_i(1-q_i)G_2(p_0)$$
$$\geq \lambda_n\delta - \lambda_0(1-p_1)G_1(\triangle) - \eta_0(1-q_1)G_2(\triangle) - \sum_{i=1}^{n}\beta_i(1-p_i)G_1(\triangle) - \sum_{i=1}^{\ell}\delta_i(1-q_i)G_2(\triangle),$$

and since $G_i(0) = 0$ and G_i is continuous, $\dot{p}_0 \geq \lambda_n\delta/2$ for all $\triangle > 0$ sufficiently small.

For $k \in \{1, \ldots, n\}$, we have

$$\begin{aligned}\dot{p}_k &= \lambda_{k-1}p_{k-1}(1-p_k) - \lambda_k p_k(1-p_{k+1}) - \alpha_k p_k + \beta_k(1-p_k)G_1(p_0)\\ &\geq \lambda_k\delta(1-\triangle) - \lambda_k\triangle(1-p_{k+1}) - \alpha_k\triangle,\end{aligned}$$

so $\dot{p}_k \geq \lambda_k\delta/2$ for all $\triangle > 0$ sufficiently small.

It is also straightforward to verify that if $p_k(t) > 0$, for some $k \in \{0, \ldots, n\}$ and $t > 0$ then $p_k(r) > 0$, for all $r \geq t$. It now follows from [49, Lemma 1] that for any $\tau > 0$ there exists $\epsilon(\tau) > 0$, with $\epsilon(\tau) \to 0$ as $\tau \to 0$, such that for any initial condition $\begin{bmatrix} p_0(0) & \ldots & p_n(0)\end{bmatrix}^T \neq 0$ and any $t \geq \tau$ the solution of the RFMLKN satisfies

$$\epsilon \leq p_i(t), \quad \text{for all } i \in \{0, \ldots, n\}.$$

Using a similar argument for the q system proves that for any $t \geq \tau$,

$$\epsilon \leq q_i(t), \quad \text{for all } i \in \{1, \ldots, \ell\}.$$

Finally, arguing as in the proof of Proposition 5.4.1 completes the proof of Proposition 5.6.1.

Our next goal is to prove the sensitivity results for the RFMLKN. It is useful to first write equations describing the steady state of the RFMLK for a constant input $u(t) \equiv v$, with $v > 0$. By Eq. (5.1),

$$\begin{aligned} f_0(e_1, v) &= f_1(e_1, e_2) + g_1(e_1, v),\\ f_{j-1}(e_{j-1}, e_j) &= f_j(e_j, e_{j+1}) + g_j(e_j, v), \quad j = 2, \ldots, n-1,\\ f_{n-1}(e_{n-1}, e_n) &= f_n(e_n) + g_n(e_n, v). \end{aligned} \tag{5.29}$$

This yields

$$f_n(e_n) + g_n(e_n, v) = f_0(e_1, v) - \sum_{k=1}^{n-1} g_k(e_k, v)$$
$$= f_j(e_j, e_{j+1}) - \sum_{k=j+1}^{n-1} g_k(e_k, v), \quad j = 1, \ldots, n-1. \tag{5.30}$$

Substituting the expressions for the f_i's and g_i's yields the following result.

Proposition 5.6.2. *Consider the steady state of the RFMLK with $u(t) \equiv v$, where $v > 0$. Then for any $k = 1, \ldots, n-1$, we have*

$$\begin{aligned} e_k &= w_k(e_{k+1}, \ldots, e_n, v) \\ &:= \frac{\lambda_n e_n + \sum_{j=k+1}^{n} \alpha_j e_j - \sum_{j=k+1}^{n} \beta_j v(1-e_j)}{\lambda_k(1-e_{k+1})}, \end{aligned} \tag{5.31}$$

and

$$\begin{aligned} v &= w(e_1, \ldots, e_n) \\ &:= \frac{\lambda_n e_n + \sum_{j=1}^{n} \alpha_j e_j}{\lambda_0(1-e_1) + \sum_{j=1}^{n} \beta_j (1-e_j)}. \end{aligned} \tag{5.32}$$

Note that the function w_k is increasing in $e_{k+1}, \ldots, e_n$ (and strictly increasing in e_{k+1}, e_n), and is decreasing in v. Also, the function w is increasing in $e_1, \ldots, e_n$ (and strictly increasing in e_1, e_n).

Proof of Theorem 5.4.1: It is clear that for $s = 0$, $L_0 = \{e^0\}$, with $e^0 = 0$, and all trajectories converge to e^0. Fix $s > 0$. The Jacobian of the RFMLKN with $m = 2$ is

$$J = \begin{bmatrix} J_{pp} & 0 & v \\ 0 & J_{qq} & w \\ c^T & d^T & r \end{bmatrix}, \tag{5.33}$$

where J_{pp} is the Jacobian of an RFMLK with state-variables $p_1, \ldots, p_n$, rates $\lambda_i, \alpha_i, \beta_i$ and input $u = G_1(z)$ (see Eq. (5.23)), J_{qq} is the Jacobian of an RFMLK with state-variables $q_1, \ldots, q_\ell$, rates $\eta_i, \gamma_i, \delta_i$ and input $u = G_2(z)$ (see Eq. (5.23)),

$$v := \begin{bmatrix} \lambda_0(1-p_1)G_1'(z) + \beta_1(1-p_1)G_1'(z) & \beta_2(1-p_2)G_1'(z) & \ldots & \beta_n(1-p_n)G_1'(z) \end{bmatrix}^T,$$
$$w := \begin{bmatrix} \eta_0(1-q_1)G_2'(z) + \delta_1(1-q_1)G_2'(z) & \delta_2(1-q_2)G_2'(z) & \ldots & \delta_\ell(1-q_\ell)G_2'(z) \end{bmatrix}^T,$$
$$c := \begin{bmatrix} \lambda_0 G_1(z) + \alpha_1 + \beta_1 G_1(z) & \alpha_2 + \beta_2 G_1(z) & \ldots & \lambda_n + \alpha_n + \beta_n G_1(z) \end{bmatrix}^T,$$
$$d := \begin{bmatrix} \eta_0 G_2(z) + \gamma_1 + \delta_1 G_2(z) & \gamma_2 + \delta_2 G_2(z) & \ldots & \eta_\ell + \gamma_\ell + \delta_\ell G_2(z) \end{bmatrix}^T,$$

and

$$r := -\lambda_0(1-p_1)G_1'(z) - \eta_0(1-q_1)G_2'(z) - \sum_{i=1}^{n}\beta_i(1-p_i)G_1'(z) - \sum_{i=1}^{\ell}\delta_i(1-q_i)G_2'(z).$$

These equations imply that for any $\begin{bmatrix} p & q & z \end{bmatrix}^T \in \Omega$ the Jacobian matrix J is Metzler, so the RFMLKN is a cooperative dynamical system. Furthermore, for any $\begin{bmatrix} p & q & z \end{bmatrix}^T \in \text{int}(\Omega)$ all the entries on the super- and sub-diagonals of J_{pp}, J_{qq} are positive, and so are the first entry in v, w, and the first and last entry in c, d. This implies that for any $\begin{bmatrix} p & q & z \end{bmatrix}^T \in \text{int}(\Omega)$ the matrix J is irreducible. Combining this with Proposition 5.6.1 and the results in Ref. [132] on strongly cooperative dynamical systems with a first integral completes the proof of Theorem 5.4.1.

Proof of Theorem 5.4.2: We again prove for the special case $m = 2$, i.e., a network with two RFMLKs and a pool. Let e_i^1, $i \in \{1, \ldots, n\}$, denote the steady-state in the first RFMLK, and e_j^2, $j \in \{1, \ldots, \ell\}$, denote the steady-state in the second RFMLK. Since the initial condition remains the same, we have

$$\sum_{i=1}^{n} e_i^1 + \sum_{j=1}^{\ell} e_j^2 + e_z = \sum_{i=1}^{n} \bar{e}_i^1 + \sum_{j=1}^{\ell} \bar{e}_j^2 + \bar{e}_z. \tag{5.34}$$

We prove that $e_z < \bar{e}_z$ by contradiction. We consider two cases: $e_z = \bar{e}_z$; and $e_z > \bar{e}_z$, and show that each of these cases yields a contradiction.

Case 1. Assume that $e_z = \bar{e}_z$. In this case, there is no change in the input and parameter values in the second RFMLK, so $e_j^2 = \bar{e}_j^2$ for all $j = 1, \ldots, \ell$. Consider the first RFMLK. Since the steady-state input to this RFMLK remains the same, Proposition 7 in Ref. [68], that states that increasing any of the detachment rates (without changing any other parameter) in the RFMLK decreases all the steady-state densities, implies that $\bar{e}_j^1 < e_j^1$, for all j. However, this contradicts Eq. (5.34).

Case 2. Assume that

$$e_z > \bar{e}_z. \tag{5.35}$$

In other words, after increasing α_k^1 to $\bar{\alpha}_k^1$, the steady-state input to each RFMLK is decreased. Then $\bar{e}_j^2 < e_j^2$ for all $j = 1, \ldots, \ell$. Combining this with Eq. (5.34) implies that $e_j^1 < \bar{e}_j^1$ for at least one index j. Let $s \in \{1, \ldots, n\}$ be the *maximal index* such that

$$e_s^1 < \bar{e}_s^1. \tag{5.36}$$

Applying Eq. (5.31) inductively implies that $e_j^1 < \bar{e}_j^1$ for any $j \in \{s, s-1, \ldots, 1\}$

(note that it follows from Eq. (5.31) that increasing α_k^1 can only further increase the corresponding steady-state value $\bar{e}_k^1$). Suppose that

$$s < n. \tag{5.37}$$

Then

$$\begin{aligned} e_j^1 &< \bar{e}_j^1, \quad j = 1, \ldots, s, \\ e_j^1 &\geq \bar{e}_j^1, \quad j = s+1, \ldots, n. \end{aligned} \tag{5.38}$$

By Eq. (5.31),

$$e_s^1 = N/D, \quad \bar{e}_s^1 = \bar{N}/\bar{D}, \tag{5.39}$$

where

$$\begin{aligned} N &:= \lambda_n^1 e_n^1 + \sum_{j=s+1}^{n} \alpha_j^1 e_j^1 - \sum_{j=s+1}^{n} \beta_j^1 G_1(e_z)(1 - e_j^1), \\ D &:= \lambda_s^1 (1 - e_{s+1}^1), \\ \bar{N} &:= \lambda_n^1 \bar{e}_n^1 + \sum_{j=s+1}^{n} \tilde{\alpha}_j^1 \bar{e}_j^1 - \sum_{j=s+1}^{n} \beta_j^1 G_1(\bar{e}_z)(1 - \bar{e}_j^1), \\ \bar{D} &:= \lambda_s^1 (1 - \bar{e}_{s+1}^1), \end{aligned}$$

where $\tilde{\alpha}_k^1 := \bar{\alpha}_k^1$, and $\tilde{\alpha}_i^1 := \alpha_i^1$, for all $i \neq k$. Note that Eq. (5.38) implies that

$$\frac{N}{D} < \frac{\bar{N}}{\bar{D}}. \tag{5.40}$$

By the first equation in Eq. (5.30),

$$\begin{aligned} G_1(e_z) &= \frac{\lambda_n^1 e_n^1 + \sum_{j=1}^{n} \alpha_j^1 e_j^1 - \sum_{j=1}^{n} \beta_j^1 G_1(e_z)(1 - e_j^1)}{\lambda_0^1 (1 - e_1^1)} \\ &= \frac{N + \sum_{j=1}^{s} \alpha_j^1 e_j^1 - \sum_{j=1}^{s} \beta_j^1 G_1(e_z)(1 - e_j^1)}{\lambda_0^1 (1 - e_1^1)}, \end{aligned}$$

and thus

$$G_1(\bar{e}_z) = \frac{\bar{N} + \sum_{j=1}^{s} \tilde{\alpha}_j^1 \bar{e}_j^1 - \sum_{j=1}^{s} \beta_j^1 G_1(\bar{e}_z)(1 - \bar{e}_j^1)}{\lambda_0^1 (1 - \bar{e}_1^1)}.$$

Combining this with Eqs. (5.35) and (5.38) implies that if $\bar{N} \geq N$, then $G_1(\bar{e}_z) \geq G_1(e_z)$, but this contradicts Eq. (5.35), so we conclude that $\bar{N} < N$. Now Eq. (5.40) implies that $\bar{D} < D$, i.e., $\bar{e}_{s+1}^1 > e_{s+1}^1$. However, this contradicts Eq. (5.38), so we conclude that Eq. (5.37) cannot hold, i.e., $s = n$. Applying Eq. (5.31) inductively

implies that

$$e_j^1 < \bar{e}_j^1, \quad j \in \{n, n-1, \ldots, 1\}. \tag{5.41}$$

Eq. (5.32) gives

$$G_1(e_z) = \frac{\lambda_n^1 e_n^1 + \sum_{j=1}^n \alpha_j^1 e_j^1}{\lambda_0^1(1-e_1^1) + \sum_{j=1}^n \beta_j^1(1-e_j^1)},$$
$$G_1(\bar{e}_z) = \frac{\lambda_n^1 \bar{e}_n^1 + \sum_{j=1}^n \tilde{\alpha}_j^1 \bar{e}_j^1}{\lambda_0^1(1-\bar{e}_1^1) + \sum_{j=1}^n \beta_j^1(1-\bar{e}_j^1)},$$

so $G_1(e_z) < G_1(\bar{e}_z)$. This contradicts Eq. (5.35), and we conclude that Case 2 is impossible. This completes the proof of Theorem 5.4.2.

Proof of Theorem 5.4.3: The proof is similar to the proof of Theorem 5.4.2 above.

Proof of Theorem 5.4.4: Clearly, we have three possible cases: $\bar{e}_z = e_z$, or $\bar{e}_z > e_z$, or $\bar{e}_z < e_z$. In the first case, the input to each RFMLK satisfies $G_i(\bar{e}_z) = G_i(e_z)$. Since the parameters in all the RFMLKs, except for RFMLK #1, are unchanged, we conclude that Eq. (5.16) holds. The analysis in the second and third cases is similar. This completes the proof of Theorem 5.4.4.

Proof of Proposition 5.4.8: It was shown in the proof of Theorem 5.4.1 that the RFMLKN is a strongly cooperative dynamical system and the results in Proposition 5.4.8 follow.

Proof of Proposition 5.4.9: Recall that the Jacobian J of the RFMLKN (with $m = 2$) is given in Eq. (5.33). This matrix is Metzler, and a calculation shows that the sum of every column of J is zero. Hence, the L_1 matrix measure of J is zero and this implies Eq. (5.17).

Proof of Theorem 5.4.5: Write the PRFMLKN as $\dot{x} = f(t, x)$. Then $f(t, z) = f(t + T, z)$, for all $t \geq 0$ and $z \in \Omega$, and $H(x)$ is a first integral of the dynamics. Theorem 5.4.5 now follows from the results in Ref. [143]. The fact that $\phi_s \in \text{int}(\Omega)$ follows from the persistence result in Proposition 5.4.7.

Chapter 6

Large-scale closed and generalized networks of ribosome flow model with different site sizes

This chapter[1] presents two large-scale network models that can model concurrent transport processes that give rise to networks comprising multiple tracks. We study several analytical properties related to stability, entrainment, convexity, and more and the results have been explained with plenty of useful but synthetic examples.

6.1 Introduction

Dynamical systems play a key role in understanding the different biophysical aspects of many complex transport phenomena. An important goal in these models is to provide indications on how a change in the parameters affects the system behavior, lead to algorithms for optimizing the flow, uncover underlying mechanisms of the observed complex behavior, enable completing synthetic goals, etc [44, 46].

In the general scenario, multiple transport processes take place concurrently, i.e., flow out of one lattice may enter another lattice or re-enter the same lattice. For example, in each cell, there is a large-scale translation rather than a translation of a single mRNA molecule, vehicular motion on networks of roads, etc [10]. Therefore, it is essential to analyze networks of interconnected transport systems for various objectives such as optimizing the output rate or traffic jams, etc. In this direction, various networks of interconnected RFMs have been developed, including RFM network with a pool [49], network of RFMs with additional features such as ribosome drop-off and attachment [148] and generalized networks of RFMs [149].

Previous studies on the network of RFMs of course analyze transcription, translation, and other cellular processes, but in these studies, the site capacities of all the RFMs are the same. However, from a wider perspective, the capacity of different

[1]The content of this chapter is published as: "Aditi Jain and Arvind Kumar Gupta. Large-scale closed and generalized networks of ribosome flow model with different site sizes. *Physica D: Nonlinear Phenomena* 455: 133881, 2023."

sites can vary. For example, the number of parallel lanes on the roadway varies in a vehicular network, the capacity of buffers differs in linear communication networks, etc. In Ref. [70], RFMD analyzes an important cellular process of modification of proteins by the mechanism of phosphotransfer. Therefore, it is important to analyze networks of RFMDs that provide a framework to understand the network dynamics of such physical and biological systems.

In this chapter, we introduce two large-scale network models that are amenable to mathematical analysis called RFMD network with a pool (RFMDNP) and a generalized network of RFMDs (RFMDN). To facilitate the analysis of a network of RFMDs, we extend the RFMD into a control system by introducing a time-varying non-negative input function. We observe that it is a monotone control system.

The RFMDNP analyzes a closed system consisting of a finite pool of particles feeding a single layer of parallel RFMDs. In the network, the total number of particles is conserved. It explores the interactions induced between the RFMDs as they all compete for a shared resource. The competition couples all the RFMDs and hence, a change in one RFMD affects the others. A system can also exhibit sensitive dependence on the initial conditions or on its parameters [150]. Therefore, it is crucial to analyze the dynamical properties of the network in order to understand its behavior. Utilizing the tools from the theory of cooperative dynamical systems with a first integral, we show that the RFMDNP is an irreducible cooperative system that admits a continuum of linearly ordered steady-state points and it entrains to periodic excitations in the parameters [132, 143, 151]. These stability properties are crucial as they provide a framework to understand how a change in an RFMD affects the network's steady-state behavior. Then we consider the RFMDN to model a network of RFMDs where the flow out of one RFMD is distributed between the inputs of the same or other RFMDs. We prove that for a given set of parameters, the RFMDN always admits a unique steady state i.e., it is robust to the initial conditions. Another important context is to re-engineer the system so that an optimal output rate can be obtained. In this regard, we also show that the problem of maximizing the steady-state output rate of the RFMDN is a convex optimization problem, and thereby we can determine the interconnection weights between the RFMDs using highly efficient algorithms.

Note that the networks of RFMDs we study here are more general than the studies based on the network of RFMs and thus can be utilized to model other transport phenomena such as vehicular traffic flow that cannot be analyzed using a network of RFMs.

The chapter is organized as follows. Section 6.2 reviews the RFMD and presents

the RFMD as an input-output system. Section 6.3 describes the network of RFMDs with a finite pool, details the theoretical results, and analyzes the effect of parameters on the network. The next section introduces a generalized version of network of RFMDs and studies its properties. Section 6.5 contains a discussion of our results and the appendix includes all the mathematical proofs.

6.2 The RFMD with an input and an output

Recall that dynamical equations describing the RFMD are:

$$\dot{x}_i = \lambda_{i-1} x_{i-1}(q_i - x_i) - \lambda_i x_i (q_{i+1} - x_{i+1}), \quad i = 1, \ldots, n, \tag{6.1}$$

where $x_0(t) \coloneqq 1$ and $x_{n+1}(t) \coloneqq 0$.

Also, recall that the relevant state space is: $C \coloneqq \{x \in \mathbb{R}^n : \quad x_i \in [0, q_i], \quad i = 1, 2, \ldots, n\}$. It has been already proved that there exists a unique $e \in \text{int}(C)$ such that for any initial condition in C, the solution belongs to int(C) for all $t > 0$ and $\lim_{t\to\infty} x(t, a) = e$ [70].

Also, recall that the steady-state of the RFMD can be derived from the spectral properties of a parameter-dependent tridiagonal matrix $A_n : \mathbb{R}_+ \to \mathbb{R}^{(n+2)\times(n+2)}$ given by

$$A_n(k) := \begin{bmatrix} 0 & \lambda_0^{-1/2} & 0 & \ldots & 0 \\ \lambda_0^{-1/2} & (1-q_1)k & \lambda_1^{-1/2} & \ldots & 0 \\ 0 & \lambda_1^{-1/2} & (1-q_2)k & \ldots & 0 \\ & & \ddots & & \\ 0 & \ldots & 0 & (1-q_n)k & \lambda_n^{-1/2} \\ 0 & \ldots & 0 & \lambda_n^{-1/2} & 0 \end{bmatrix}.$$

It has been proved that there is an unique value $k^* \in (0, \infty)$ such that $\sigma(A_n(k^*)) = k^*$, where $\sigma(A)$ denotes the maximal eigenvalue (Perron root) of A, and let $\zeta \in \mathbb{R}^{n+2}_{++}$ be the corresponding eigenvector [70]. It has been analyzed that steady-state densities satisfy

$$e_i = \frac{\zeta_{i+2}}{\lambda_i^{1/2} k^* \zeta_{i+1}}, \quad \text{for all} \quad i \in \{1, 2, \ldots, n\} \tag{6.2}$$

and

$$R = \frac{1}{(\sigma(A_n(k^*)))^2}. \tag{6.3}$$

It has also been shown that the steady-state output rate $R(\lambda_0, \lambda_1, \ldots, \lambda_n, q_1, \ldots, q_n)$ is in general a quasi-concave function over $\mathbb{R}^{n+1}_{++} \times (0, 1]^n$

and for fixed q_i's, $R(\lambda_0, \lambda_1, \ldots, \lambda_n)$ is a concave function over $\mathbb{R}^{n+1}_{++}$ [70].

To form a network of RFMDs, we consider the RFMD with a single-input and single-output control system as follows:

$$\begin{aligned}
\dot{x}_1 &= \lambda_0(q_1 - x_1)u - \lambda_1 x_1(q_2 - x_2), \\
\dot{x}_2 &= \lambda_1 x_1(q_2 - x_2) - \lambda_2 x_2(q_3 - x_3), \\
&\vdots \\
\dot{x}_n &= \lambda_{n-1} x_{n-1}(q_n - x_n) - \lambda_n x_n, \quad \text{and} \\
y &= \lambda_n x_n.
\end{aligned} \tag{6.4}$$

The input to the RFMD is a bounded and measurable function $u : \mathbb{R}_+ \to \mathbb{R}_+$ taking non-negative values for all $t \geq 0$. The output rate from the RFMD at time t is represented by $y(t)$. Let $x(t, u, a)$ denote the solution of the RFMD with control function u and initial condition a. The following result shows that given any initial point in C and input function $u(t)$ that takes positive values, the trajectory remains in C for any $t \geq 0$, and after a certain time, all the sites will neither be totally full nor totally empty.

Proposition 6.2.1. *Consider the RFMD with an input u satisfying $u(t) > 0$ for all $t \geq 0$. For every $a \in \text{int}(C)$, the solution $x(t, u, a) \in \text{int}(C)$ for any $t \geq 0$. Moreover, for any $a \in \partial C$ there exists a time τ such that $x(\tau, u, a) \in \text{int}(C)$ for all $t \geq \tau$.*

The above proposition states that for any input function $u(t)$ that is strictly positive, C is an invariant set of the dynamical system (6.4), and all the state variables x_i's get separated from the boundary of C after a certain time τ. The next proposition illustrates the fact that the RFMD is a monotone control system.

Proposition 6.2.2. *Consider two control functions $v, w : \mathbb{R}_+ \to \mathbb{R}_+$ such that $v(t) \leq w(t)$ for all $t \geq 0$ and two starting conditions $a, b \in C$ such that $a \leq b$. Then the respective RFMD solutions satisfy*

$$x(t, v, a) \leq x(t, w, b), \text{ for all } t \geq 0. \tag{6.5}$$

The above result states that given two similar RFMDs, the first with initial densities a_i that are lower than or equal to the initial densities b_i of the second one and with the control input $v(t)$ that is lower than or equal to control input $w(t)$ of the second one for all $t \geq 0$, then the densities in the first RFMD will always be lower than or equal to the respective densities in the second RFMD. Consequently,

the output of the first RFMD will always be lower than or equal to the output of the second RFMD.

In the next section, we describe the dynamics of the RFMDNP and analyze its various mathematical properties.

6.3 A network of RFMDs with a pool

To model RFMDNP, we consider a closed system comprising a finite pool of particles feeding a single-layer parallel set of m RFMDs. These m RFMDs are coupled through a pool and thus the input to each RFMD relies on the pool occupancy. The RFMD $\#i$ has length n_i, parameters λ_0^i, λ_1^i, $\ldots$, $\lambda_{n_i}^i$, q_1^i, q_2^i, $\ldots$, $q_{n_i}^i$, input function u^i, and output y^i (see Fig. 6.1). Thus, the dynamical equations describing the m RFMDs can be written as:

$$\begin{aligned} \dot{x}^1 &= f(x^1, u^1), \quad y^1 = \lambda_{n_1}^1 x_{n_1}^1, \\ &\vdots \\ \dot{x}^m &= f(x^m, u^m), \quad y^m = \lambda_{n_m}^m x_{n_m}^m. \end{aligned} \tag{6.6}$$

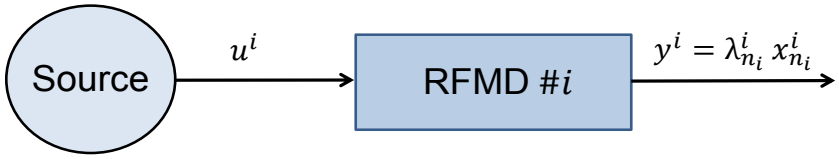

Figure 6.1: An RFMD $\#i$ of length n_i, input u^i from an external source, and output y^i.

The pool's occupancy level at time t is denoted by $z(t)$. The input to each RFMD is supplied by the pool and the output from each RFMD is returned to the pool. We pose the following assumptions: a) if there is no particle in the pool then the effective entry rate into the RFMDs becomes zero, and b) as the number of particles in the pool increases, then the effective entry rate into the RFMDs increases. Mathematically, these can be stated by assuming $u^i(t) = G_i(z(t))$, for $i \in \{1, 2, \ldots, m\}$, where $G_i : \mathbb{R}_+ \to \mathbb{R}_+$ satisfies: a) $G_i(0) = 0$ and b) $G_i(z)$ is continuous and strictly increasing function of z.

Thus, the RFMD $\#i$ dynamics is governed by:

$$\begin{aligned} \dot{x}_1^i &= \lambda_0^i G_i(z)(q_1^i - x_1^i) - \lambda_1^i x_1^i (q_2^i - x_2^i), \\ \dot{x}_2^i &= \lambda_1^i x_1^i (q_2^i - x_2^i) - \lambda_2^i x_2^i (q_3^i - x_3^i), \\ &\vdots \\ \dot{x}_{n_i}^i &= \lambda_{n_i-1}^i x_{n_i-1}^i (q_{n_i}^i - x_{n_i}^i) - \lambda_{n_i}^i x_{n_i}^i, \\ y^i &= \lambda_{n_i}^i x_{n_i}^i, \end{aligned} \tag{6.7}$$

and the pool dynamics is given by:

$$\dot{z} = \sum_{i=1}^{m} y^i - \sum_{i=1}^{m} \lambda_0^i \, G_i(z)(q_1^i - x_1^i). \tag{6.8}$$

The above Eq. (6.8) implies that the flow into the pool is the sum of all the output rates of the RFMDs and the flow out of the pool is the overall flow of particles that binds to the RFMDs. Combining the assumptions on the functions G_i with Eq. (6.8) and given $z(0) \geq 0$, we have $z(t) \geq 0$ for all $t \geq 0$. This implies that the pool density is never negative.

Summing up, the RFMDNP is a nonlinear dynamical system with $\ell := n_1 + \cdots + n_m + 1$ state variables and its dynamics is given by Eqs. (6.6), (6.7) and (6.8) (see Fig. 6.2).

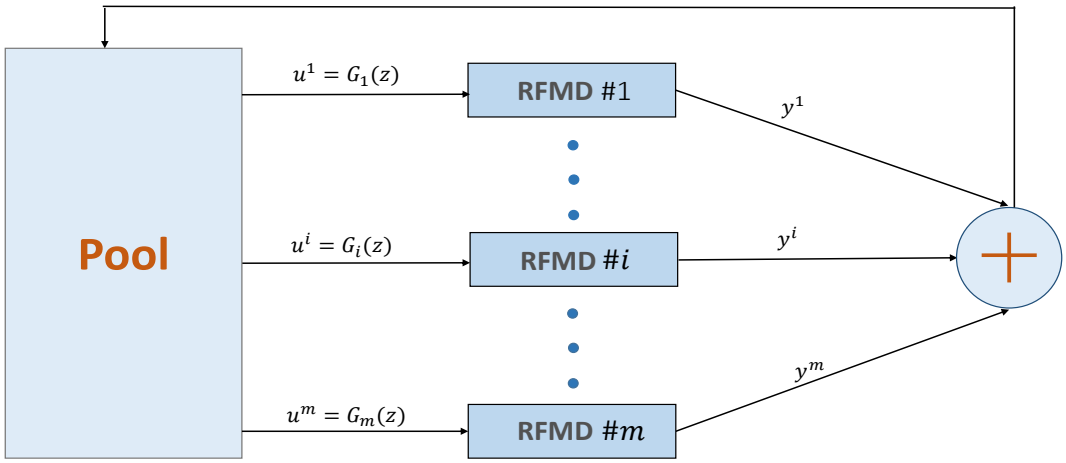

Figure 6.2: A closed network of m RFMDs connected through a pool. The pool feeds the input to each RFMD and the output from each RFMD is fed into the pool.

At any time t, let

$$H(t) := \sum_{i=1}^{m} \sum_{j=1}^{n_i} x_j^i(t) + z(t) \tag{6.9}$$

denote the total density of the particles in the network. Since the RFMDNP is a closed system,

$$H(t) \equiv H(0) \quad \text{for all} \quad t \geq 0. \tag{6.10}$$

In other words, H is a first integral of the dynamical system.

We now analyze some of the mathematical properties of the RFMDNP. Recall that every $x_j^i \in [0, q_j^i]$, and $z \in [0, \infty)$, so the state space of the RFMDNP is

$$\Omega := \Omega_1 \times \cdots \times \Omega_m \times [0, \infty), \tag{6.11}$$

where $\Omega_i := [0, q_1^i] \times [0, q_2^i] \times \cdots \times [0, q_{n_i}^i]$. Let 1_ℓ represent a column vector of ℓ ones. Consider $L_r := \{a \in \Omega : 1_\ell' a = r\}$, which denotes the r level set of the first integral H. For $r = 0$, we have $L_0 = \{0\}$ and the trajectories beginning from zero initial state always stay in zero and thereby, we will always consider $r > 0$. Simply put, L_r is the set containing all the states associated to a total density of r particles in the system. Let $[x(t,a) \quad z(t,a)]'$ denote the solution of the RFMD at time t with the starting point $a \in \Omega$.

6.3.1 Invariance and persistence

The next result shows that any trajectory originating from a point in the state space stays in it at any given time $t \geq 0$.

Proposition 6.3.1. *The state space Ω in Eq. (6.11) is an invariant set for the dynamics of the RFMDNP i.e., if $a \in \Omega$ then $[x(t,a) \quad z(t,a)]' \in \Omega$ for all $t \geq 0$.*

The next proposition states that after an arbitrarily short time, the solution gets uniformly separated from the boundary of the state space.

Proposition 6.3.2. *Given any $\tau > 0$, there exists $\delta = \delta(\tau) > 0$, with $\delta(\tau) \to 0$ as $\tau \to 0$, such that for any $a \in \Omega \setminus \{0\}$ and for all $t \geq \tau$, for all $i \in \{1, 2, \ldots, m\}$, and for all $j \in \{1, 2 \ldots, n_i\}$, we have*

$$\delta \leq x_j^i(t,a) \leq q_j^i - \delta$$

and

$$\delta \leq z(t,a).$$

In particular, after time $\tau > 0$, the density in site j of RFMD $\#i$ is in the range $[\delta, q_j^i - \delta]$ and the pool density is in the range $[\delta, \infty)$. Thus, Proposition 6.3.2 is important in studying the asymptotic behavior of the RFMDNP, as it guarantees that its Jacobian matrix becomes irreducible after an arbitrarily short time.

6.3.2 Stability

The next main result states that the RFMDNP admits a continuum of steady-state points and the trajectories that emanate from the same level set converge to the same steady-state point.

Theorem 6.3.1. *Every level set L_r contains a unique steady-state point e_{L_r} of the RFMDNP and for any starting point $a \in L_r$, the solution of the RFMDNP converges to e_{L_r}. Moreover, for any $0 < r < s$,*

$$e_{L_r} \ll e_{L_s}. \tag{6.12}$$

In particular, every level set admits a unique steady-state particle distribution in each RFMD and the pool. Eq. (6.12) means the following. Consider a network with two scenarios: the total number of particles in the first and second is r and s, respectively, with $r < s$. Then the steady-state densities in the first network are strictly smaller than the corresponding steady-state densities in the second one.

Example 6.3.1. Consider an RFMDNP with a single RFMD of length $n_1 = 2$. Assume that $\lambda_0^1 = 0.1$, $\lambda_1^1 = 1$, $\lambda_2^1 = 1$, $q_1^1 = 0.5$, $q_2^1 = 1$, and $G_1(z) = z$. Fig. 6.3 depicts the trajectories of the RFMDNP with three different starting points in L_2: $[0.5 \quad 0 \quad 1.5]'$, $[0 \quad 1 \quad 1]'$, and $[0.5 \quad 1 \quad 0.5]'$. It can be seen that all three trajectories converge to the same steady-state point.

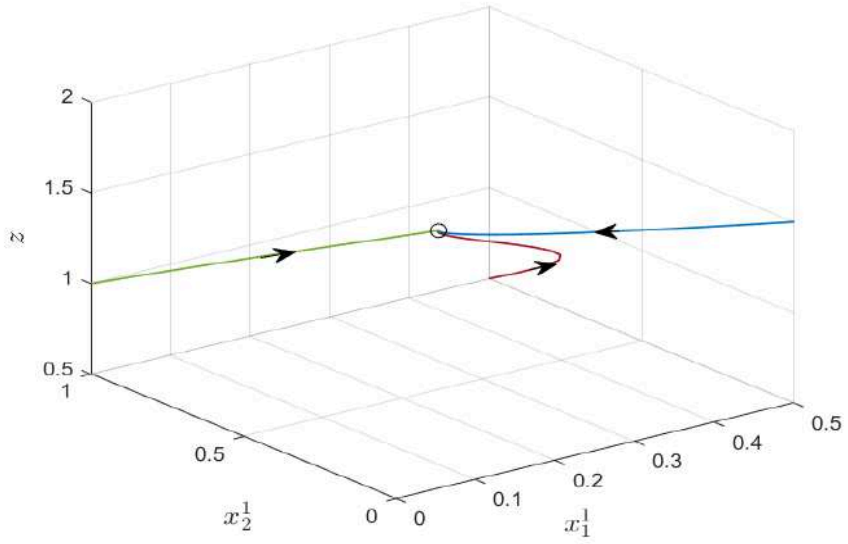

Figure 6.3: Trajectories of the RFMDNP in Example 6.3.1 for three different starting points in L_2. The unique steady-state point in L_2 is marked by an ellipse.

6.3.3 Entrainment

There are periodic excitations in many biological or physical systems, e.g., periodic cell-cycle division in biological organisms, time-varying periodic traffic lights in a road network, oscillations in protein levels, etc. [48, 98]. It is important for dynamical systems to synchronize to periodic oscillations in order to facilitate coordinated movement, e.g., coordinated rhythmic movement is essential for the proper functioning of the human system.

Even seemingly simple, nonlinear systems may not entrain [152]. A natural concern in this context is: how do the steady-state densities in the RFMDNP behave when there is a periodic excitation feeding the network? If $f(t+T) = f(t)$ for all t,

then the function f is T-periodic. In order to consider the periodic excitation in the RFMDNP, we shall assume some or all of the parameters as T-periodic functions. Therefore, we consider the following assumptions:
a) all the transition rates λ_0^i, λ_j^i are positive, continuous, and uniformly bounded functions of time i.e., there exists $0 < \eta_1 \leq \eta_2$ such that $\lambda_0^i(t), \lambda_j^i(t) \in [\eta_1, \eta_2]$ for all $t \geq 0$.
b) the site sizes q_j^i are positive and continuous functions of time i.e., there exists $0 < \delta \leq 1$ such that $q_j^i(t) \in [\delta, 1]$.
c) a minimal $T > 0$ exists such that all the λ_j^i's and the q_j^i's are T-periodic functions.

We call the network with the periodic excitations as the periodic RFMDNP (PRFMDNP). The next result shows that the property of entrainment holds in PRFMDNP.

Theorem 6.3.2. *Consider the PRFMDNP. There exists a unique T-periodic function $\phi_r : \mathbb{R}_+ \to \text{int}(\Omega)$ and for any starting point $a \in L_r$, the solution of the PRFMDNP approaches ϕ_r as $t \to \infty$.*

The above theorem states that every trajectory of the PRFMDNP with an initial density profile L_r converges to a unique T-periodic solution. Thus, the PRFMDNP phase locks to periodic oscillations in the parameters. The following example exhibits this.

Example 6.3.2. Consider the PRFMDNP having $m = 2$ RFMDs of lengths $n_1 = 3$ and $n_2 = 2$. Assume that $\lambda_0^1 = 0.1$, $\lambda_1^1 = 1$, $\lambda_2^1 = 2 + \sin(2\pi t)$, $\lambda_3^1 = 0.5$, $\lambda_0^2 = 0.2$, $\lambda_1^2 = 2$, $\lambda_2^2 = 1$, $q_1^1 = 0.7$, $q_2^1 = 0.3$, $q_3^1 = 1$, $q_1^2 = 1$, , $q_2^2 = 0.3$, and $G_i(z) = \tanh(z)$, $i = 1, 2$. Observe that all the parameters are periodic with a common period $T = 1$. Consider an initial condition $x_j^i(0) = z(0) = 0.1$, for all i, j. Fig. 6.4 shows all the densities as a function of time t and it can be observed that they converge to a periodic pattern with period one.

An important question is what effect would a small variation in one of the parameters in an RFMD has on the steady-state point of the network. The next subsection analyzes this effect on the network.

6.3.4 Effect of parameters

Let $p = [\lambda \quad q \quad H(0)]'$ be the vector of all the parameters and a total number of particles in the network, where λ is the vector of all the transition rates and q is the vector of all the site sizes in the RFMDs. Consider a mapping g from p to the unique steady-state point in int(Ω). The next result allows considering the derivatives of the steady-state point w.r.t. small variations in the parameters.

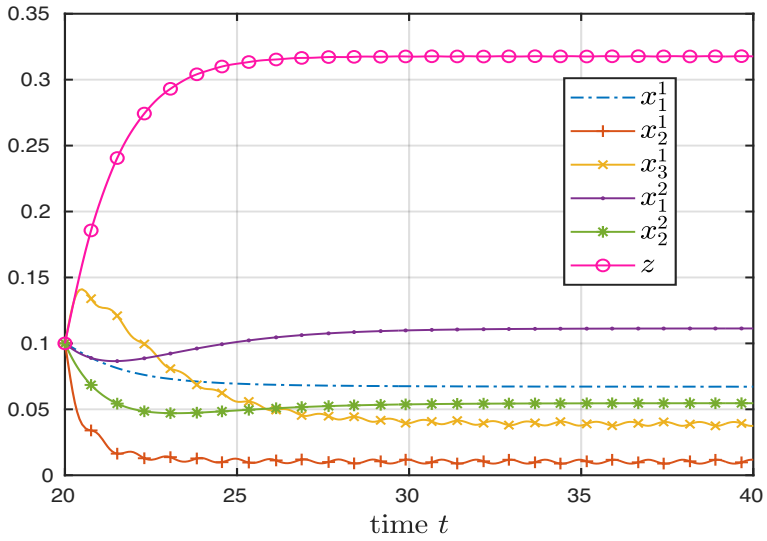

Figure 6.4: Trajectories of the PRFMDNP as a function of time t in Example 6.3.2.

Proposition 6.3.3. *The derivative $(\partial/\partial p_k)g(p)$ exists for all k.*

We next analyze the effect of change in the transition rate at a single site of an RFMD on the whole network. Without loss of generality, we presume that the change is in one of the rates in the RFMD #1.

Theorem 6.3.3. *Consider an RFMDNP with m RFMDs of lengths n_i and parameters $\lambda_0^i > 0$, $\lambda_j^i > 0$, and $q_j^i \in (0,1]$, $i \in \{1,\dots,m\}$ and $j \in \{1,2,\dots,n_i\}$. For the level set L_r of H, let e_j^i, and e_z represents the steady-state density of the RFMDNP. Pick $k \in \{0,1,\dots,n_1\}$, and consider the RFMDNP obtained by modifying λ_k^1 to $\bar{\lambda}_k^1$, with $\bar{\lambda}_k^1 > \lambda_k^1$. Let $\bar{e}_j^i$ and $\bar{e}_z$ represents the steady-state density in this new RFMDNP. We have*

$$\bar{e}_k^1 < e_k^1,\ \bar{e}_j^1 > e_j^1,\ \text{for all } j \in \{k+1,\dots,n_1\}, \tag{6.13}$$

and either one of the following two cases holds:

1. $\bar{e}_z < e_z$ *and* $\bar{e}_j^i < e_j^i$, *for all* $i \neq 1$ *and all* j.
2. $e_z < \bar{e}_z$ *and* $e_j^i < \bar{e}_j^i$, *for all* $i \neq 1$ *and all* j.

Note that increasing the transition rate at site i implies that there is an increase in the flow of particles from site i to site $i+1$. The above theorem states that as λ_k^1 increases; the number of particles in site k of RFMD #1 decreases whereas the number of particles in all the sites $k+1, k+2, \dots, n_1$ of RFMD #1 increases and the other RFMD steady-state densities and the pool density either all increase or all decrease. Observe that changing a transition rate in an RFMD affects the qualitative

behavior of all the other RFMDs and the pool density in a similar manner as they are fed from the same pool. Theorem 6.3.3 does not provide any information about the exact outcome i.e., whether the pool density will increase or decrease as it depends upon various other parameters in the network. However, one can obtain information by computing the derivatives of steady-state point coordinates w.r.t. the rates. Note that the above result is in agreement with the previous result reported in Ref. [49]. The next example demonstrates the case when pool density increases with an increase in a transition rate of an RFMD.

Example 6.3.3. Consider an RFMDNP with $m = 2$ RFMDs of lengths $n_1 = 3$ and $n_2 = 2$. Let $\lambda_0^i = 1$, $\lambda_j^i = 1$, for all i, j except λ_2^1, $q_1^1 = 0.8$, $q_2^1 = 0.4$, $q_3^1 = 0.6$, $q_1^2 = 0.7$, $q_2^2 = 0.5$, and $G_i(z) = \tanh(z)$, $i = 1, 2$. Consider an initial state $x_j^i(0) = 0$ for all i, j and $z(0) = 2$. The simulation for several values of transition rate λ_2^1 is depicted in Figs. 6.5a and 6.5b. It can be seen that as λ_2^1 increases there is a decrease in e_2^1, an increase in e_3^1, an increase in e_z and consequently an increase in e_j^2 for all j. This is because increasing λ_2^1 means that the particles traverse RFMD #1 more easily and hence the particles become more quickly available in the pool.

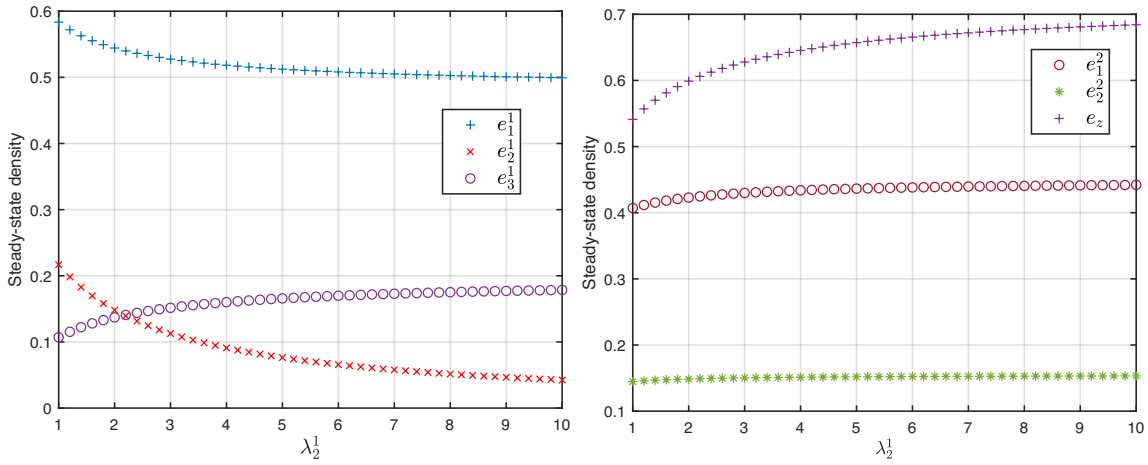

(a) (b)

Figure 6.5: The steady-state densities of the RFMDNP as a function of transition rate λ_2^1 in Example 6.3.3, (a) In RFMD #1, (b) In RFMD #2 and the pool.

The next example illustrates the case when the pool density decreases with an increase in a transition rate of an RFMD.

Example 6.3.4. Consider an RFMDNP with $m = 2$ RFMDs of lengths $n_1 = 7$ and $n_2 = 2$. Let $\lambda_0^i = 1$, $\lambda_j^i = 1$, $q_j^i = 1$ for all i, j except λ_4^1, $q_6^1 = 0.5$ and $G_i(z) = z$, $i = 1, 2$. Assume $x_j^i(0) = 0$ for all i, j and $z(0) = 6$. Figs. 6.6a and 6.6b depict simulations for several values of transition rate λ_4^1. It can be seen that as λ_4^1 increases there is a decrease in e_4^1, an increase in e_k^1 for $k = 5, 6, 7$, a decrease in e_z

and consequently a decrease in e_j^2 for all j. This is because increasing λ_4^1 leads to an increase in a traffic jam due to a small site size in the RFMD #1.

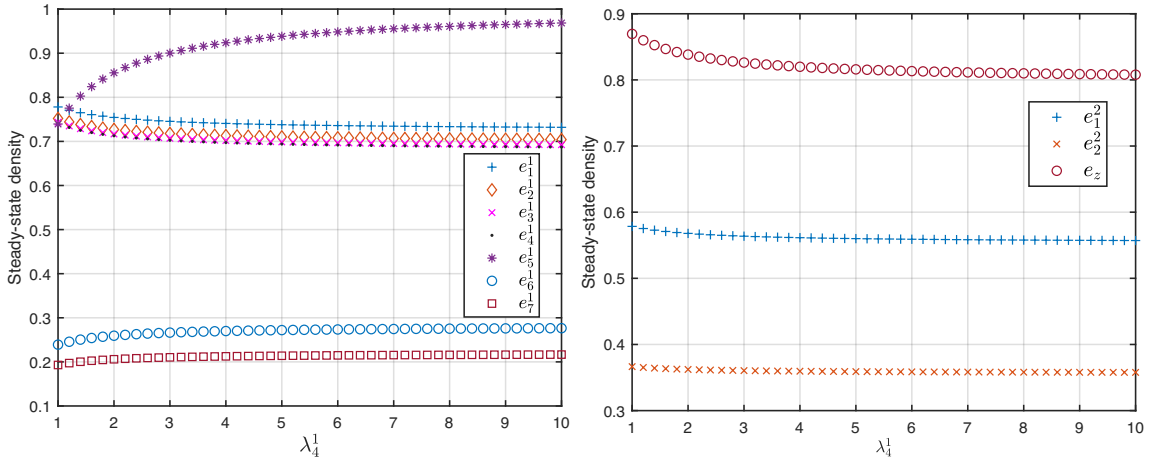

(a) (b)

Figure 6.6: The steady-state densities of the RFMDNP as a function of transition rate λ_4^1 in Example 6.3.4, (a) In RFMD #1, (b) In RFMD #2 and the pool.

The second result shows the effect of change in the site size parameter at one site of an RFMD on the network.

Theorem 6.3.4. *Consider an RFMDNP with m RFMDs of lengths n_i and parameters $\lambda_0^i > 0$, $\lambda_j^i > 0$, and $q_j^i \in (0,1]$, $i \in \{1,\dots,m\}$ and $j \in \{1,2,\dots,n_i\}$. For the level set L_r of H, let e_j^i and e_z represents the steady-state density in the RFMDNP. Pick $k \in \{1,\dots,n_1\}$ and consider the RFMDNP obtained by changing q_k^1 to $\bar{q}_k^1$, with $\bar{q}_k^1 > q_k^1$. Let $\bar{e}_j^i$, $\bar{e}_z$, represents the steady-state density in the new RFMDNP. We have*

$$\bar{e}_{k-1}^1 < e_{k-1}^1, \ \bar{e}_j^1 > e_j^1, \ \textit{for all } j \in \{k,\dots,n_1\}, \tag{6.14}$$

and either one of the following two cases holds:

1. $\bar{e}_z < e_z$ *and* $\bar{e}_j^i < e_j^i$, *for all* $i \neq 1$ *and all* j.
2. $e_z < \bar{e}_z$ *and* $e_j^i < \bar{e}_j^i$, *for all* $i \neq 1$ *and all* j.

An increase in the size of site i results in an increase in the density at site i and consequently increases the densities in all the sites right to it. The above theorem implies that modifying a site size q_k^1 in RFMD #1 decreases the density at site $k-1$ and increases the densities at sites $k, k+1, \dots, n_1$; affects all the sites in all the other RFMDs and the pool density in the same way. Indeed, this theorem does not give any details on the new densities for sites $1, 2, \dots, k-2$ along RFMD #1 and

whether the pool density will increase or decrease as it will depend on various other parameters in the network. The next two examples represent the two cases when the pool density increases and decreases, respectively.

Example 6.3.5. Consider an RFMDNP with $m = 2$ RFMDs of lengths $n_1 = 5$ and $n_2 = 3$. Let $\lambda_0^i = 1$, $\lambda_j^i = 1$, $q_j^i = 1$, for all i, j except q_3^1, and $G_i(z) = z$, $i = 1, 2$. Consider an initial point $x_j^i(0) = 0$, for all i, j and $z(0) = 2$. Figs. 6.7a and 6.7b depict simulations for several values of site size parameter q_3^1. It can be observed that as q_3^1 increases there is a decrease in e_2^1, an increase in e_j^1, for $j = 3, 4, 5$, an increase in e_z and consequently an increase in e_j^2 for all j. This is because increasing q_3^1 means that the particles flow more easily from site 2 to site 3 in RFMD #1 and thus increases the pool density.

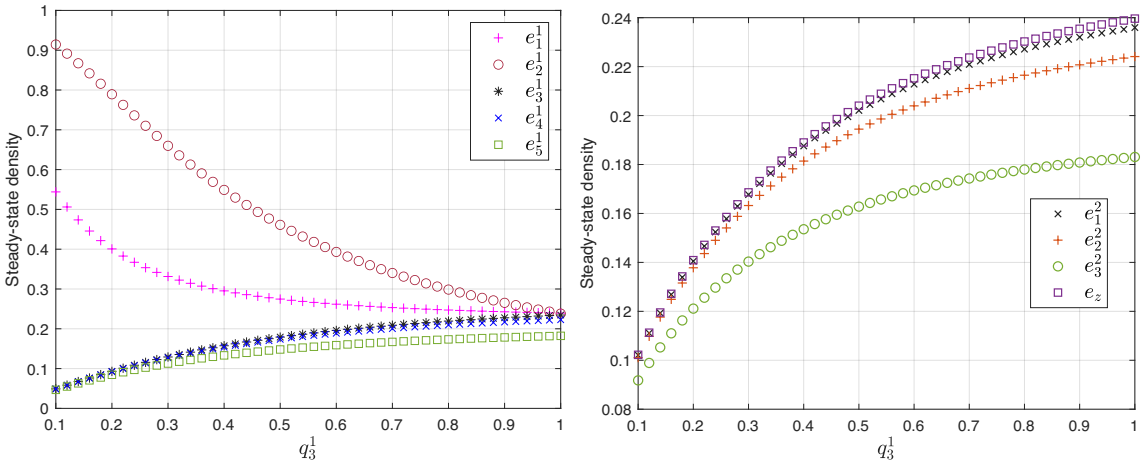

(a) (b)

Figure 6.7: The steady-state densities of the RFMDNP as a function of site size q_3^1 in Example 6.3.5, (a) In RFMD #1, (b) In RFMD #2 and the pool.

Example 6.3.6. Consider an RFMDNP with $m = 2$ RFMDs of lengths $n_1 = 9$ and $n_2 = 3$. Let $\lambda_0^i = 1$, $\lambda_j^i = 1$, $q_j^i = 1$, for all i, j except q_5^1, $q_7^1 = 0.5$, and $G_i(z) = z$, $i = 1, 2$. Consider a starting point $x_j^i(0) = 0$, for all i, j and $z(0) = 6$. Figs. 6.8a and 6.8b depict simulations for several values of site size parameter q_5^1. It can be observed that as q_5^1 increases there is a decrease in e_4^1, an increase in e_k^1 for $k = 5, 6, 7, 8, 9$, a decrease in e_z, and consequently a decrease in e_j^2 for all j. It is because increasing q_5^1 leads to an increase in the flow rate forming a traffic jam due to a bottleneck site size in the RFMD #1 and thus depleting the pool.

Indeed, by modifying the initiation rate λ_0^1 or the site size q_1^1, we obtain all the information about the modified densities along RFMD #1.

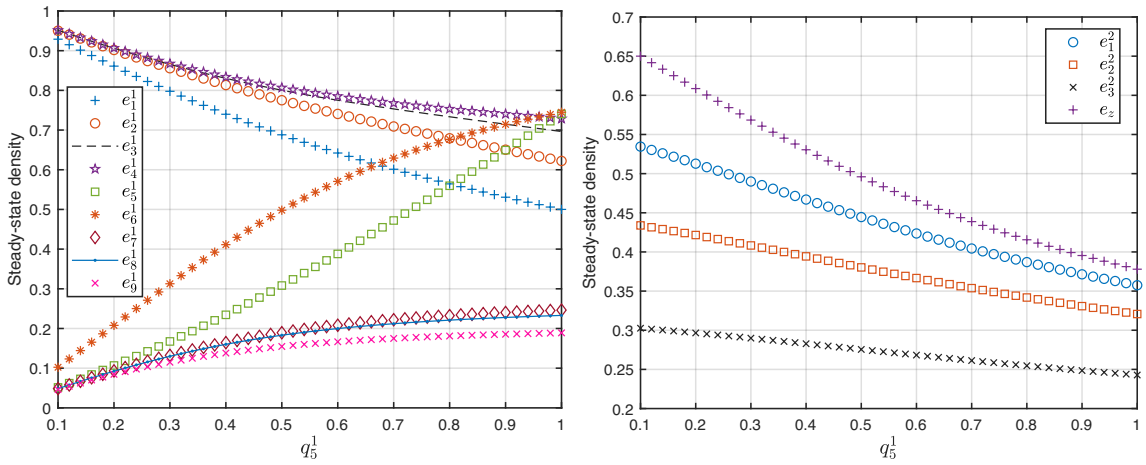

(a) (b)

Figure 6.8: The steady-state densities of the RFMDNP as a function of site size q_5^1 in Example 6.3.6, (a) In RFMD #1, (b) In RFMD #2 and the pool.

Corollary 6.3.4.1. *Suppose that either* λ_0^1 *is modified to* $\bar{\lambda}_0^1$, *with* $\bar{\lambda}_0^1 > \lambda_0^1$ *or* q_1^1 *is modified to* $\bar{q}_1^1$ *with* $\bar{q}_1^1 > q_1^1$. *Then*

$$\bar{e}_j^1 > e_j^1 \text{ for all } j \in \{1, \ldots, n_1\},\ \bar{e}_j^i < e_j^i \text{ for all } i \neq 1,\ j \in \{1, \ldots, n_i\}, \text{and } \bar{e}_z < e_z. \tag{6.15}$$

Note that increasing λ_0^1 or q_1^1 allows more particles to bind to the RFMD #1 more easily and hence this increases the steady-state densities in RFMD #1 and decreases the pool density.

The RFMDNP enables modeling a closed network in which particles are supplied to the RFMDs from a pool whose output function is an increasing function of the density of particles in the pool. This is a specific case of a network of RFMDs that facilitates analyzing competition of shared resources between the RFMDs. In the next section, we analyze a generalized network where the output of an RFMD is distributed into several inputs of other RFMDs including itself. Such networks also allow modeling the optimal division of a resource among several other RFMDs.

6.4 A generalized network of RFMDs

Consider a network of m interconnected RFMDs:

$$\begin{aligned} \dot{x}^1 &= f(x^1, u^1), \quad y^1 = \lambda_{n_1}^1 x_{n_1}^1, \\ &\vdots \\ \dot{x}^m &= f(x^m, u^m), \quad y^m = \lambda_{n_m}^m x_{n_m}^m, \end{aligned} \tag{6.16}$$

with $u^i = \sum_{j=0}^{m} w_j^i y^j$ as the input to RFMD $\#i$ for $i \in \{1, 2, \ldots, m\}$, where $w_0^i > 0$ represent the fixed constant source and $w_j^i \geq 0$ represent the weights describing the output y^j proportion, both feeding the input of RFMD $\#i$. We refer to this as a generalized network of ribosome flow models with different sites network (RFMDN).

Let the total output from the network is:

$$y(t) := \sum_{i=1}^{m} c_i y^i(t), \tag{6.17}$$

where c_i represents the non-negative weights associated with the outputs. Let $\sum_{i=1}^{m} w_k^i \leq 1$ for $k \in \{1, 2, \ldots, m\}$. This kind of network describes a distribution of the output of any RFMD $\#i$ to other RFMDs in the network. We refer to this network as a distributed network of RFMDs.

The state space of the RFMDN is

$$\Omega' := \Omega_1 \times \cdots \times \Omega_m. \tag{6.18}$$

For $a \in \Omega'$, let $x(t, a)$ denote the solution of the RFMDN at time t with the initial condition a. It can be easily shown that the state space is an invariant set of (6.16).

6.4.1 Global asymptotic stability

The following result shows that any trajectory of the RFMDN starting from the boundary of Ω' immediately enters $\text{int}(\Omega')$.

Proposition 6.4.1. *For every $a \in \text{int}(\Omega')$, the solution $x(t, a)$ of the RFMDN stays in $\text{int}(\Omega')$ for any $t \geq 0$. Moreover , for any $a \in \partial\Omega'$, there exists a time τ such that $x(\tau, a) \in \text{int}(\Omega')$ for all $t \geq \tau$.*

The next result guarantees that the general network is a globally asymptotically stable network. The proof of the result is based on the powerful theory of cooperative systems [50].

Theorem 6.4.1. *The RFMDN admits a globally asymptotically stable steady-state density $e \in \text{int}(\Omega')$, i.e., $\lim_{t\to\infty} x(t, a) = e$ for all $a \in \Omega'$.*

In other words, the state variables approach a steady state that only depends on the parameters in the network and is independent of the starting state. Let $y_{ss} := \lim_{t\to\infty} y(t)$ i.e., y_{ss} denotes the steady-state output rate. Note that $w_0^i > 0$ can be replaced by $w_0^i \geq 0$ if the input u^i to RFMD $\#i$ satisfies $u^i(t) > 0$ for all $t > 0$. The following simple example exhibits the dynamic behavior of the RFMDN.

Example 6.4.1. Consider the RFMDN depicted in Fig. 6.9a. Each RFMD has dimension $n_i = 1$ for $i = 1, 2, 3$. Assume that $\lambda_0^i = 1$, $\lambda_j^i = 1$, $q_1^1 = 0.5$, $q_1^2 = 1$ and $q_1^3 = 0.7$. Here the input to RFMD #1 is $u^1 = 0.1 + 0.5y^2 + 0.2y^3$, to RFMD #2 is $u^2 = 0.3y^1 + 0.1y^2 + 0.3y^3$, and to RFMD #3 is $u^3 = 0.7y^1$. The network output is given as $y = 0.4y^2 + 0.5y^3$. Fig. 6.9b depicts the trajectories of the RFMDN with three different starting conditions: $[0.5 \quad 0 \quad 0]'$, $[0 \quad 0.5 \quad 0]'$, and $[0 \quad 0 \quad 0.5]'$. Note that all the state variables and thus the network output converges to a unique steady-state value.

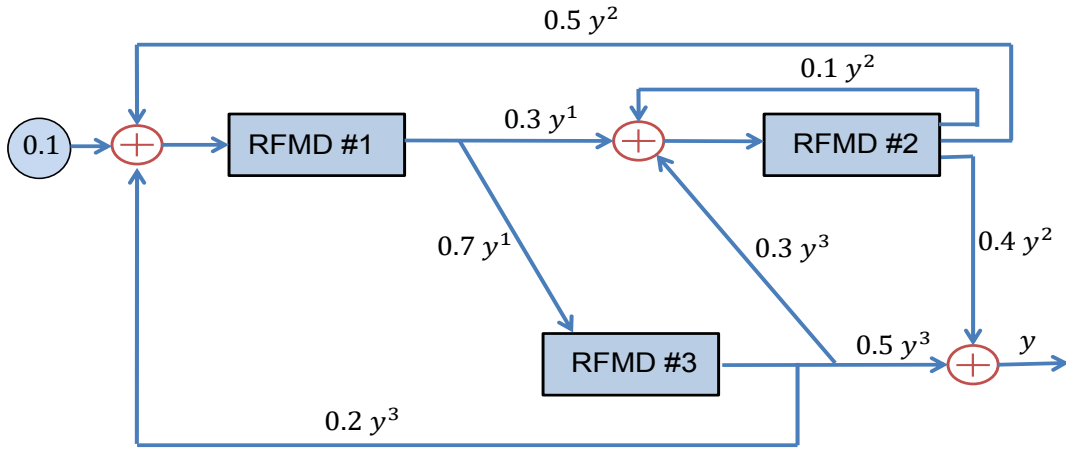

(a)

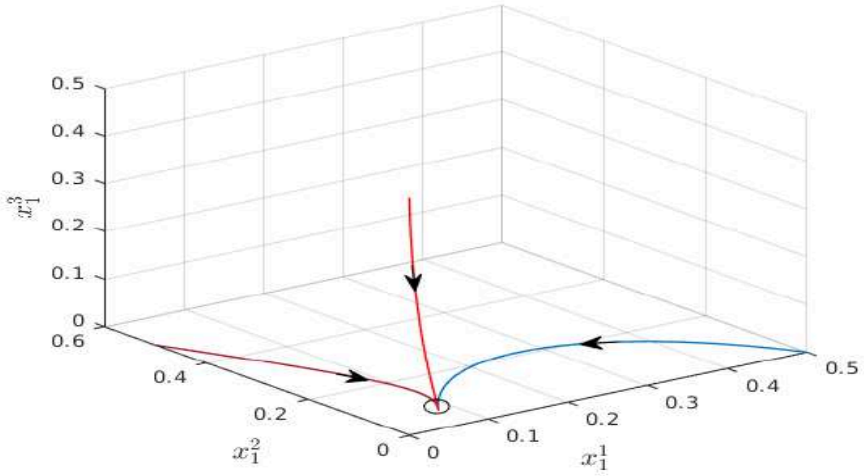

(b)

Figure 6.9: a) The network of the three connected RFMDs in Example 6.4.1. b) Trajectories of the RFMDN in Example 6.4.1 for three different starting points. The unique steady-state point is marked by an ellipse.

Now, we analyze a closed-loop system of an RFMD with positive feedback. In this system, a fixed source is feeding a single RFMD with rate $w_1 > 0$ and $w_2 \geq 0$ describes the weightage of the RFMD output feeding back into the input of the

RFMD (see Fig. 6.10). The main theoretical Theorem 6.4.1 guarantees that this network is globally asymptotically stable. Thus, the dynamics of this network are as follows:

$$\begin{aligned}
\dot{x}_1 &= (w_1 + w_2\lambda_n x_n)(q_1 - x_1) - \lambda_1 x_1(q_2 - x_2),\\
\dot{x}_2 &= \lambda_1 x_1(q_2 - x_2) - \lambda_2 x_2(q_3 - x_3),\\
&\vdots\\
\dot{x}_n &= \lambda_{n-1} x_{n-1}(q_n - x_n) - \lambda_n x_n.
\end{aligned} \tag{6.19}$$

The output rate is $y(t) = \lambda_n x_n(t)$. The next is an intuitive result which implies that increasing any of the feedback parameters w_1 or w_2 increases the output rate.

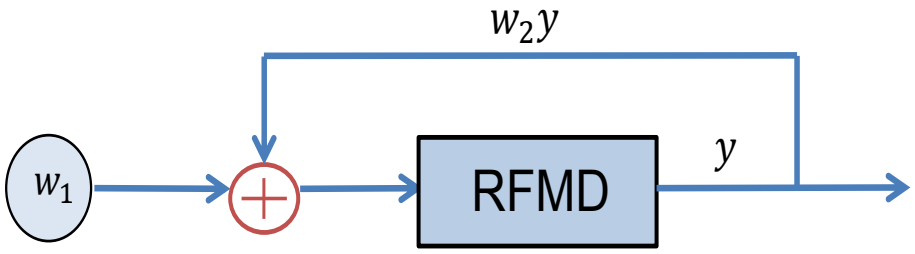

Figure 6.10: The network of closed-loop of an RFMD with positive feedback. The total RFMD input is $u(t) = w_1 + w_2 y$.

Proposition 6.4.2. *Consider the system given by (6.19) and let the parameters λ_i and q_i be fixed. Let y_{ss} and $\bar{y}_{ss}$ denote the steady-state output rate corresponding to the control parameters (w_1, w_2) and $(\bar{w}_1, \bar{w}_2)$ respectively. If $w_1 = \bar{w}_1$ then $y_{ss} < \bar{y}_{ss}$ if and only if $w_2 < \bar{w}_2$. If $w_2 = \bar{w}_2$ then $y_{ss} < \bar{y}_{ss}$ if and only if $w_1 < \bar{w}_1$.*

Example 6.4.2. Consider Eq. (6.19) with $n = 3$, $w_1 = 0.1$, $\lambda_i = 1$, for all i, $q_1 = 1$, $q_2 = 0.5$, $q_3 = 1$. Fig. 6.11 depicts y_{ss} as a function of w_2. It can be observed that y_{ss} increases with w_2.

Further, we analyze a network of RFMDs having no feedback connections i.e., input u^i of RFMD $\#i$, for any i, does not depend on its output directly or indirectly. We refer to it as feed-forward networks of RFMDs. Recall that steady-state densities and the steady-state output rate in a single RFMD can be obtained from the spectral approach removing the requirement to numerically simulate the dynamics until the convergence. The same approach can be applied to a feed-forward network of RFMDs to find the steady state of the whole network. It can be explained as follows. Consider RFMDs that are fed by a constant source only and the steady-state output rate of these RFMDs can be calculated by Eq. (6.3). Now, consider those RFMDs that are fed by the output of the above RFMDs and/or constant sources. Note

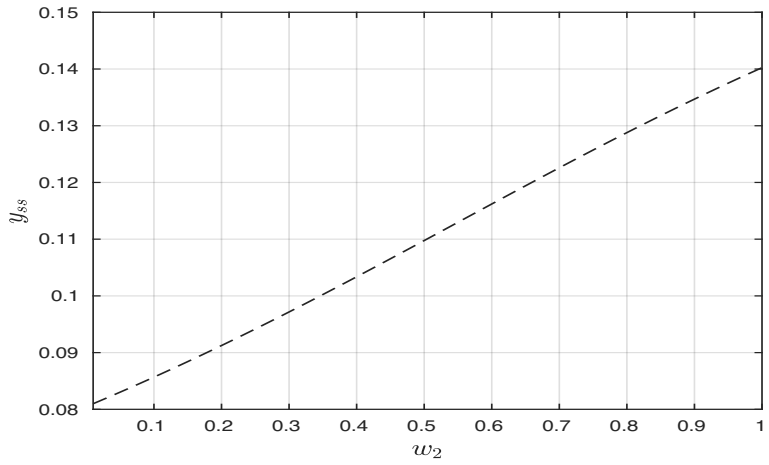

Figure 6.11: The steady-state output rate y_{ss} for the closed-loop network as a function of w_2 in Example 6.4.2.

that the input to these RFMDs converges to a steady-state value and hence with the constant input, the steady-state output rate of these RFMDs can be computed by Eq. (6.3). Continuing in this way, we can find the steady state of the overall network. The next simple example exhibits this.

Example 6.4.3. Consider the network given in Fig. 6.12. It consists of three RFMDs each with dimension $n_i = 1$. Assume that $\lambda_0^1 = 0.5$, $\lambda_1^1 = 1$, $q_1^1 = 0.1$, $\lambda_0^2 = 0.1$, $\lambda_1^2 = 0.5$, $q_1^2 = 1$, $\lambda_0^3 = 0.8$, $\lambda_1^3 = 1$, and $q_1^3 = 0.5$. The spectral representation of the steady-state in RFMD #1 is based on the matrix

$$A_1(k) := \begin{bmatrix} 0 & 1/\sqrt{0.5} & 0 \\ 1/\sqrt{0.5} & 0.9k & 1 \\ 0 & 1 & 0 \end{bmatrix}.$$

After calculations, we have $y^1 = 0.0333$. The spectral representation of the steady-state in RFMD #2 is based on the matrix

$$A_2 := \begin{bmatrix} 0 & 1/\sqrt{0.1} & 0 \\ 1/\sqrt{0.1} & 0 & 1/\sqrt{0.5} \\ 0 & 1/\sqrt{0.5} & 0 \end{bmatrix}.$$

After calculations, we get $y^2 = 0.0833$. Now, the constant input value to RFMD #3 is $y^1 + y^2$. Thus, the spectral representation of RFMD #3 is based on the matrix

$$A_3(k) := \begin{bmatrix} 0 & 1/\sqrt{0.0933} & 0 \\ 1/\sqrt{0.0933} & 0.5k & 1 \\ 0 & 1 & 0 \end{bmatrix}.$$

Hence, the steady-state output rate of the network is $y_{ss} = 0.0427$.

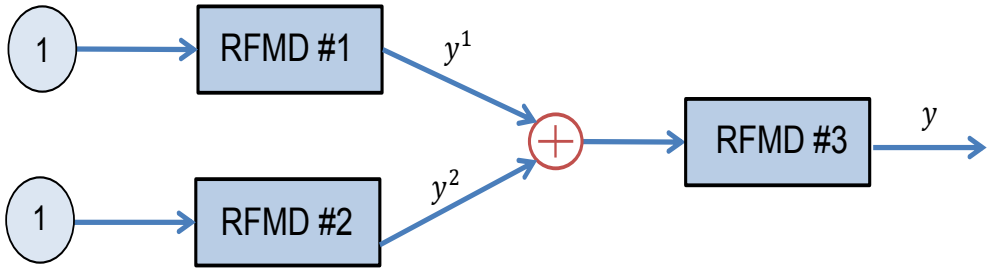

Figure 6.12: The feed-forward network of three RFMDs in Example 6.4.3.

6.4.2 Optimizing the network output rate

It is important to understand how a common resource should be divided into a system comprising several sub-systems such that the overall output measure is optimized. In this section, we study the problem of optimizing the total output rate from the distributed network of RFMDs w.r.t. the connecting weights i.e., how to distribute the output from each RFMD between the RFMDs so that the network output rate is maximized.

Problem 1 Consider an RFMDN consisting of m RFMDs having a total output rate at time t defined as in Eq. (6.17). The optimization problem is to maximize the steady-state network output rate y_{ss} w.r.t. the connection (control) weights w_j^i subject to the constraints:

$$w_j^i \in [0,1] \text{ for all } i \in \{1,2,\ldots,m\} \text{ and } j \in \{0,1,\ldots,m\} \tag{6.20}$$

and

$$\sum_{i=1}^{m} w_k^i = 1 \text{ for all } k \in \{1,2,\ldots,m\}, \tag{6.21}$$

where w_j^i describes the connection weight of output of RFMD $\#j$ to input of RFMD $\#i$. The next result is important as it implies that one can easily determine the optimal weights in Problem 1.

Theorem 6.4.2. *Problem* 1 *can be formulated as a convex optimization problem.*

The next simple example illustrates this.

Example 6.4.4. Consider an RFMDN having only one RFMD of dimension $n_1 = 1$, $\lambda_0^1 = \lambda_1^1 = 1$ and $q_1^1 = 0.5$. Suppose it is fed by a source with the rate 0.1 along with feedback from its output back to the input with proportion v i.e., $u^1 = 0.1 + vy^1$. Let

$y_{ss} = e_1^1(v)$ denote the steady-state output rate of the network. It can be observed in Fig. 6.13 that y_{ss} is not concave in v. Thus, the given optimization problem:

$$\max \;\; y_{ss}(v) \;\; \text{subject to} \;\; v \in [0, 1] \tag{6.22}$$

is not a convex optimization problem. However, with a reparametrization of the input as $u^1 = 0.1 + w$ with $w \in [0, y^1]$, Problem (6.22) becomes a convex optimization problem given as:

$$\max \;\; y_{ss}(w) = \frac{0.5(0.1 + w)}{1.1 + w} \;\; \text{subject to} \;\; 0 \leq w \leq \frac{0.5(0.1 + w)}{1.1 + w}. \tag{6.23}$$

The solution to this problem is achieved at $w^* = 0.0742$ and $y_{ss} = 0.0742$. This concludes that the solution to the Problem (6.22) is $v^* = 1$. Hence, after suitable reparametrization of the Problem (6.22) to (6.23), we can determine the optimal weights.

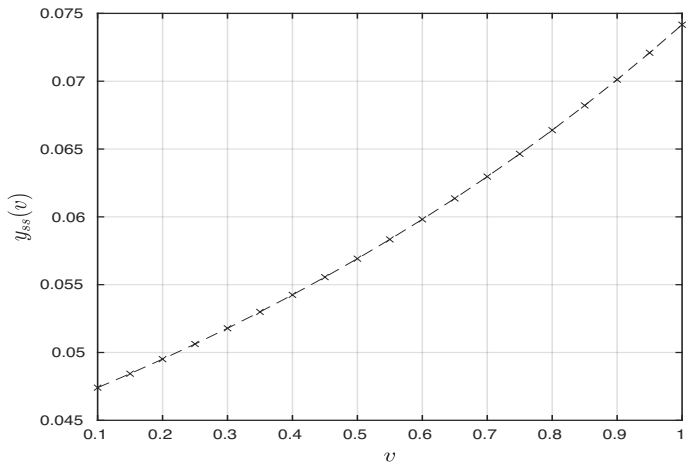

Figure 6.13: The steady-state output rate y_{ss} for the RFMDN as a function of v in Example 6.4.4.

Further, we analyze that in a feed-forward network of RFMDs, Problem 1 can be solved more directly.

Theorem 6.4.3. *Consider a feed-forward network of RFMDs, where w denotes the set of all connection weights. Then the mapping $w \to y_{ss}(w)$ is concave and thus Problem 1 is a convex optimization problem.*

In other words, without any formulation, Problem 1 is a convex optimization problem for feed-forward networks. The next example exhibits this.

Example 6.4.5. Consider an RFMDN consisting of $m = 2$ RFMDs each with dimension $n_i = 10$, $i = 1, 2$. Assume that $\lambda_0^i = 1$, $\lambda_j^i = 1$, and $q_j^i = 1$, for all i, j.

Let a unit resource feed the inputs to RFMD #1 and RFMD #2 with $u^1 = v$ and $u^2 = 1 - v$, respectively, where $v \in [0, 1]$. The sum of the outputs from the two RFMDs is the total network output. The solid line in Fig. 6.14 depicts that the steady-state output rate $y_{ss}(v)$ is a concave function and it attains maximum value at $v = 0.5$. Note that since both the lanes are equivalent, therefore equally dividing the input from the given unit source optimizes the network output. Now, let all the parameters be the same but $q_8^1 = 0.3$, i.e., the site capacity in lane 1 at site 8 is less than the other site capacities. The dashed line in Fig. 6.14 shows that $y_{ss}(v)$ attains maximum value at $v = 0.15$. This can be explained as follows: in order to avoid traffic jams in RFMD #1 due to the presence of a site with less capacity, more resources are dispatched to RFMD #2.

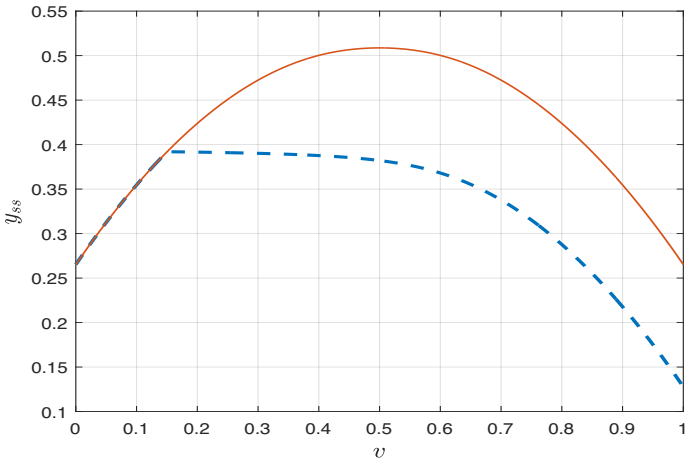

Figure 6.14: The steady-state output rate y_{ss} for the RFMDN as a function of v in Example 6.4.5. The solid line represents the case when $q_j^i = 1$, for all $i.j$ and the dashed line represents the case when $q_j^i = 1$, for all i, j except for $q_8^1 = 0.3$.

6.5 Discussion

Understanding the motion of particles along networks of interconnected tracks has attracted increasing attention in recent years. Dynamical systems play a crucial role in analyzing biological and physical systems. In this chapter, we consider large-scale networks of the dynamical model RFMD which has been developed to model the unidirectional motion of particles along an isolated track having different site sizes. We rigorously study two network models: the RFMDNP which facilitates modeling a network of parallel RFMDs coupled indirectly through a shared finite resource and the RFMDN which models the network of interconnected RFMDs coupled directly through several outputs of other RFMDs or itself.

The RFMDNP is a closed system that consists of several RFMDs interconnected

through a resource, namely, the pool of particles. We establish that the RFMDNP admits a continuum of linearly ordered steady-state points. This steady-state point is independent of the initial profile and depends on all the parameters and the total number of particles in the network. We also show that if all the parameters change periodically in time with a common period T, then every solution of the RFMDNP converges to a periodic trajectory having period T. In other words, the RFMDNP phase locks to periodic parameters with a common period. Furthermore, we study the effect of changing parameters in an RFMD on the steady-state behavior of the network. Our mathematical analysis predicts that an increase in a transition rate or an increase in a size of a site in any one RFMD say RFMD #1 always leads to an increase in the output of RFMD #1. The output rates of all the other RFMDs are affected in the same way i.e., either they all increase or all decrease.

To enable the analysis of important phenomena such as transport on a network of roads comprising sites of different sizes where the flow out from a road may enter (re-enter) another (same) road, we consider a network of interconnected RFMDs (RFMDN), in which the RFMD outputs in the network is connected through some connection weights to the inputs of other RFMDs. We show that the network admits a unique steady state independent of the initial profile. In other words, the network is globally asymptotically stable. In addition, we study the mathematical properties of closed-loop and feed-forward networks and demonstrate them using simple examples. For a feed-forward network of RFMDs, we see that the steady state of the network can be determined using a spectral approach without any requirement to solve the equations of the system numerically. Furthermore, we analyze the problem of how to determine the interconnection weightage between the RFMDs in order to maximize the steady-state output of the network and show that this is a convex optimization problem. These findings are in accordance with the previous results reported in Ref. [149].

We also note that the networks of RFMs analyze essential cellular processes such as protein synthesis, and intracellular transport. We believe this suggests that the networks presented here will also provide a powerful framework to model many natural and artificial processes such as cellular transport, communication networks, vehicular traffic, and more. A possible avenue for future research is modeling the network of RFMDs by considering the weighted connections between the RFMDs as time-varying functions. Another possibility is generalizing these networks to include features like detachment/attachment of particles from internal sites in the lanes.

6.6 Appendix: Proofs

Proof of Proposition 6.2.1: For sake of convenience, let $x(t)$ denote the solution of the system (6.4) for the given input u and initial condition $a = x(0) \in \text{int}(C)$. Seeking a contradiction, assume that there exists a first time $t' > 0$ such that $x(t') \notin \text{int}(C)$. Then $x(t') \in \partial C$, so $x_j(t') \in \{0, q_j\}$ for atleast one index j. We shall consider two cases:

Case 1: Let k be the minimal index such that $x_k(t') = 0$ and $x_j(t') > 0$ for any $j < k$. If $k = 1$, then $\dot{x}_1(t') = \lambda_0 q_1 u > 0$. Since we have $x_1(t) \in (0, q_1)$ for any $t < t'$ and therefore, $x_1(t') > 0$. Therefore, the case $k = 1$ is not possible, so $k > 1$. Now Eq. (6.4) implies that $\dot{x}_k(t') = \lambda_{k-1} x_{k-1}(t') q_k$. We have $x_{k-1}(t') > 0$ and hence, $\dot{x}_k(t') > 0$ which is again a contradiction. Therefore, case 1 is not possible.

Case 2: Let k be the maximal index such that $x_k(t') = q_k$ and $x_j(t') < q_j$ for any $k < j$. If $k = n$, then Eq. (6.4) implies that $\dot{x}_n(t') = -\lambda_n q_n < 0$. Since $x_n(t) \in (0, q_n)$ for any $t < t'$ and therefore, $x_1(t') < q_n$. Therefore, the case $k = n$ is not possible, so $k < n$. Now Eq. (6.4) implies that $\dot{x}_k(t') = -\lambda_k q_k (q_{k+1} - x_{k+1}(t'))$. We have $x_j(t') < q_j$ for any $j > k$, and hence $\dot{x}_k(t') < 0$ and this implies that $x_k(t') < q_k$. Therefore, case 2 also does not hold.

Thus, we get that $\text{int}(C)$ as an invariant state space. To prove the other part, assume that initial point $x(0) \in \partial C$ i.e., $x_j(0) \in \{0, q_j\}$ for atleast one index j. We shall consider two cases:

Case 1: Let k be the minimal index such that $x_k(0) = 0$ and $x_j(0) > 0$ for any $j < k$. We will show that $x_k(\gamma) \in (0, q_k)$, for some $\gamma > 0$. If $k = 1$, then $\dot{x}_1(0) = \lambda_0 q_1 u > 0$, so $x_1(\gamma) \in (0, q_1)$. If $k > 1$, then $\dot{x}_k(0) = \lambda_{k-1} x_{k-1}(0) q_k > 0$, so $x_k(\gamma) \in (0, q_k)$. Thus, $x_i(\gamma) \in (0, q_i)$ for any $i \in \{1, 2, \ldots, k\}$ and for any $t \geq \gamma$. Inductively, there exists a time $\eta > 0$ such that $x_i(\eta) > 0$, for any $i \in \{1, 2, \ldots, n\}$ and for any $t \geq \eta$.

Case 2: Let k be the maximal index such that $x_k(0) = q_k$ and for any $j > k$, $x_j(0) < q_j$. Arguing in the similar manner as in case 1, there exists a time $\psi > 0$ such that $x_i(\psi) < q_i$ for any $i \in \{1, 2, \ldots, n\}$ and for any $t \geq \psi$.

Hence, combining both the cases there exists a time $\tau = \max(\eta, \psi)$ such that $x(\tau) \in \text{int}(C)$ for all $t \geq \tau$.

Proof of Proposition 6.2.2: We first calculate $M := \frac{\partial}{\partial u} f$,

$$\begin{aligned} M &= \text{diag}\left(\frac{\partial}{\partial u} f_1 - \frac{\partial}{\partial u} f_2, -\frac{\partial}{\partial u} f_3, \ldots, -\frac{\partial}{\partial u} f_n\right) \\ &= \text{diag}(\lambda_0(q_1 - x_1), 0, \ldots, 0). \end{aligned}$$

From Proposition 6.2.1, we have every entry of M non-negative. Let $J := \frac{\partial}{\partial x} f$ denote the Jacobian of the dynamics, where f is the vector field. Then J is given

as below

$$\begin{bmatrix} -\lambda_0 u - \lambda_1(q_2 - x_2) & \lambda_1 x_1 & 0 & \dots & 0 \\ \lambda_1(q_2 - x_2) & -\lambda_1 x_1 - \lambda_2(q_3 - x_3) & \lambda_2 x_2 & \dots & 0 \\ 0 & \lambda_2(q_3 - x_3) & -\lambda_2 x_2 - \lambda_3(q_4 - x_4) & \dots & 0 \\ & & \ddots & & \\ 0 & 0 & 0 & \dots & -\lambda_{n-1}x_{n-1} - \lambda_n \end{bmatrix}.$$

It follows from Proposition 6.2.1 that every off-diagonal entry of J is non-negative. Thus, the RFMLK is a monotone control system by using the results in Ref. [142].

We now turn to consider a closed network of RFMDs (RFMDNP).

Proof of Proposition 6.3.2: For the sake of simplicity, consider the case $m = 1$ and the proof in the case when $m > 1$ is similar. The RFMDNP for $m = 1$ is given by:

$$\begin{aligned} \dot{x}_1 &= \lambda_0 G(z)(q_1 - x_1) - \lambda_1 x_1(q_2 - x_2), \\ \dot{x}_2 &= \lambda_1 x_1(q_2 - x_2) - \lambda_2 x_2(q_3 - x_3), \\ &\vdots \\ \dot{x}_n &= \lambda_{n-1} x_{n-1}(q_n - x_n) - \lambda_n x_n, \\ \dot{z} &= \lambda_n x_n - \lambda_0\ G(z)(q_1 - x_1). \end{aligned} \tag{6.24}$$

Let $x_0 := z$ and $x_{-1} := x_n$. Now, we will prove that given any $\epsilon > 0$ and any sufficiently small $\triangle > 0$, there exists $P = P(\epsilon, \triangle) > 0$ such that for each $k \in \{0, \dots, n\}$ and each $t \geq 0$ the condition

$$x_k(t) \leq \triangle \text{ and } x_{k-1}(t) \geq \epsilon$$

implies that

$$\dot{x}_k \geq P.$$

For $k = 0$ we have

$$\begin{aligned} \dot{x}_0 &\geq \lambda_n x_n - \lambda_0(q_1 - x_1)G(x_0) \\ &\geq \lambda_n \epsilon - \lambda_0(q_1 - x_1)G(\triangle), \end{aligned}$$

and hence, $\dot{x}_0 \geq \lambda_n \epsilon/2$ for all $\triangle > 0$ sufficiently small. For $k \in \{1, \dots, n\}$ we have

$$\begin{aligned} \dot{x}_k &= \lambda_{k-1} x_{k-1}(q_k - x_k) - \lambda_k x_k(q_{k+1} - x_{k+1}) \\ &\geq \lambda_k \epsilon(q_k - \triangle) - \lambda_k \triangle(q_{k+1} - x_{k+1}), \end{aligned}$$

so $\dot{x}_k \geq \lambda_k q_k \epsilon/2$, for all $\triangle > 0$ sufficiently small. Also, if $x_k(t) > 0$ for some $k \in$

$\{0,\ldots,n\}$ and $t>0$, then $x_k(t')>0$ for all $t'\geq t$. Now, it follows from Lemma 1 in Ref. [49] that for any $\tau>0$ there exists $\delta(\tau)>0$, with $\delta(\tau)\to 0$ as $\tau\to 0$, such that

$$\delta \leq x_i(t), \quad \text{for all } i\in\{0,\ldots,n\}, \quad \text{for any } a, \text{ and any } t\geq\tau. \tag{6.25}$$

Now define $p_i(t) \coloneqq q_{n+1-i} - x_{n+1-i}(t)$, for $i\in\{1,2,\ldots,n\}$ and $p_{n+1}\coloneqq z$. We have,

$$\begin{aligned}
\dot{p}_1 &= \lambda_n(q_n-p_1)-\lambda_{n-1}p_1(q_{n-1}-p_2),\\
\dot{p}_2 &= \lambda_{n-1}p_1(q_{n-1}-p_2)-\lambda_{n-2}p_2(q_{n-2}-p_3),\\
&\vdots\\
\dot{p}_n &= \lambda_1 p_{n-1}(q_1-p_n)-\lambda_0 p_n G(p_{n+1}),\\
\dot{p}_{n+1} &= \lambda_n(q_n-p_1)-\lambda_0 p_n G(p_{n+1}).
\end{aligned} \tag{6.26}$$

From Eq. (6.25), we have $p_{n+1}\geq\delta$ for all $t\geq\tau$. Note that the first n equations of Eq. (6.26) are an RFMD with time-varying exit rate $\lambda_0 G(p_{n+1})$ and therefore, $\exists\ \delta_1(\tau)>0$ such that

$$\delta_1 \leq p_i(t), \quad \text{for all } i\in\{1,\ldots,n\} \quad \text{and any} \quad t\geq\tau. \tag{6.27}$$

Combining this with Eq. (6.25) proves the proposition.

Proof of Theorem 6.3.1: The Jacobian of the RFMDNP is

$$J(x,z) := \begin{bmatrix}
J_1^1 & 0 & \ldots & 0 & J_{m+1}^1\\
0 & J_2^2 & 0 & \ldots & J_{m+1}^2\\
 & & \ddots & & \\
0 & 0 & \ldots & J_m^m & J_{m+1}^m\\
J_1^{m+1} & J_2^{m+1} & \ldots & J_m^{m+1} & J_{m+1}^{m+1}
\end{bmatrix}$$

where J_i^i is the Jacobian of RFMD $\#i$ given by

$$\begin{bmatrix}
-\lambda_0^i G_i(z)-\lambda_1^i(q_2^i-x_2^i) & \lambda_1^i x_1^i & 0 & 0\\
\lambda_1^i(q_2^i-x_2^i) & -\lambda_1^i x_1^i-\lambda_2^i(q_3^i-x_3^i) & \lambda_2^i x_2^i & 0\\
 & & \ddots & \\
0 & 0 & 0 & \lambda_{n_i-1}^i x_{n_i-1}^i\\
0 & 0 & 0 & -\lambda_{n_i-1}^i x_{n_i-1}^i-\lambda_{n_i}^i
\end{bmatrix},$$

$J_i^{m+1}=[\lambda_0^i G_i(z)\ \ 0\ldots 0\ \ \lambda_{n_i}^i]$, $J_{m+1}^i=[\lambda_0^i G_i'(z)(q_1^i-x_1^i)\ \ 0\ldots\ \ 0]'$, $i\in\{1,2,\ldots,m\}$, and

$J^{m+1}_{m+1} = -\sum_{i=1}^{m} \lambda^i_0 G'_i(z)(q^i_1 - x^i_1)$. For any point in Ω, every off-diagonal entry of J is non-negative, so the RFMDNP is a cooperative dynamical system. Also for any point in $\text{int}(\Omega)$, we have $x^i_j \in (0, q^i_j)$ and $z > 0$ for all $t \geq 0$ which implies that every term on the sub and super-diagonal of J^i_i is positive and $G_i(z) > 0$, $i = 1, 2, \ldots, m$. Hence, J is an irreducible matrix. Now, combining Proposition 6.3.2 with the results in Ref. [153] completes the proof of this theorem.

Proof of Theorem 6.3.2: We can write the PRFMDNP as $\dot{x} = f(t, x)$. Then $f(t, y) = f(t + T, y)$ for all $t \geq 0$, $y \in \Omega$. Now, $\phi_r \in \text{int}(\Omega)$ follows from the Proposition 6.3.2 and the results in Ref. [143] proves the theorem.

Proof of Proposition 6.3.3: We can write the RFMDNP as $\dot{x} = f(x)$, where x represents the vector consisting of state variables and the pool density, with initial condition $x(0) = x_0$. Then $\delta\dot{x} = J(x)\delta x$, where $J \coloneqq \frac{\partial f}{\partial x}$ is the Jacobian of the dynamics. Note that from Proposition 6.3.2, the given system is a strongly cooperative system of ODEs having a first integral with positive gradient. Hence, the results in Ref. [154] shows that $\exists$ a norm depending on x such that for all $t > 0$, we have $|\delta(x(t))|_{x(t)} < |\delta x_0|_{x_0}$. At the unique steady-state point e, we have $|\exp(J(e)t)\delta(x_0)|_e < |\delta x_0|_e$ for all $t > 0$. Hence, the matrix obtained by restricting $J(e)$ to the integral manifold is Hurwitz matrix, and thereby the mapping h is analytic using the implicit function theorem.

Proof of Theorem 6.3.3: We shall prove it for the case $m = 2$ (the proof of the case when $m > 2$ is similar) i.e.,

$$\bar{e}^1_k < e^1_k \text{ and } \bar{e}^1_j > e^1_j, \text{ for all } j \in \{k + 1, \ldots, n_1\} \tag{6.28}$$

and

$$\text{sign}(\bar{e}^2_j - e^2_j) = \text{sign}(\bar{e}_z - e_z), \text{ for all } j \in \{1, 2, \ldots, n_2\}. \tag{6.29}$$

Since, the initial condition remains the same, therefore

$$\sum_{i=1}^{n_1} e^1_i + \sum_{j=1}^{n_2} e^2_j + e_z = \sum_{i=1}^{n_1} \bar{e}^1_i + \sum_{j=1}^{n_2} \bar{e}^2_j + \bar{e}_z = H(0) \tag{6.30}$$

At the steady-state, the RFMDNP equations yield:

$$\begin{aligned}\lambda_0^1 G_1(e_z)(q_1^1 - e_1^1) &= \lambda_1^1 e_1^1 (q_2^1 - e_2^1),\\ &= \lambda_2^1 e_2^1 (q_3^1 - e_3^1),\\ &\vdots\\ &= \lambda_{n_1-1}^1 e_{n_1-1}^1 (q_{n_1}^1 - e_{n_1}^1)\\ &= \lambda_{n_1}^1 e_{n_1}^1,\end{aligned} \tag{6.31}$$

$$\begin{aligned}\lambda_0^2 G_2(e_z)(q_1^2 - e_1^2) &= \lambda_1^2 e_1^2 (q_2^2 - e_2^2),\\ &= \lambda_2^2 e_2^2 (q_3^2 - e_3^2),\\ &\vdots\\ &= \lambda_{n_2-1}^2 e_{n_2-1}^2 (q_{n_2}^2 - e_{n_2}^2)\\ &= \lambda_{n_2}^2 e_{n_2}^2,\end{aligned} \tag{6.32}$$

,

$$\lambda_{n_1}^1 e_{n_1}^1 + \lambda_{n_2}^2 e_{n_2}^2 = \lambda_0^1 G_1(e_z)(q_1^1 - e_1^1) + \lambda_0^2 G_2(e_z)(q_1^2 - e_1^2). \tag{6.33}$$

The last equality in Eq. (6.32) gives

$$e_{n_2-1}^2 = \frac{\lambda_{n_2}^2 e_{n_2}^2}{\lambda_{n_2-1}^2 (q_{n_2}^2 - e_{n_2}^2)}. \tag{6.34}$$

It can be observed that if $e_{n_2}^2$ increases with an increase in λ_k^1 then the numerator and denominator of the Eq. (6.34) increases and decreases, respectively, and hence the left side of Eq. (6.34) is increasing. Similarly, if $e_{n_2}^2$ decreases with an increase in λ_k^1, then the numerator and denominator of the Eq. (6.34) decreases and increases, respectively, and hence the left side of Eq. (6.34) is decreasing. Therefore,

$$\text{sign}(\bar{e}_{n_2-1}^2 - e_{n_2-1}^2) = \text{sign}(\bar{e}_{n_2}^2 - e_{n_2}^2). \tag{6.35}$$

Using the same argument above and by Eq. (6.32) we have

$$\text{sign}(\bar{e}_1^2 - e_1^2) = \text{sign}(\bar{e}_2^2 - e_2^2) = \cdots = \text{sign}(\bar{e}_{n_2-1}^2 - e_{n_2-1}^2) = \text{sign}(\bar{e}_{n_2}^2 - e_{n_2}^2). \tag{6.36}$$

Again by Eq. (6.32), we have

$$G_2(e_z) = \frac{\lambda_{n_2}^2 e_{n_2}^2}{\lambda_0^2 (q_1^2 - e_1^2)}. \tag{6.37}$$

Since $G_i(z)$ for $i = 1, 2$ is a strictly increasing function of z, therefore combining this with Eq. (6.36), proves the Eq. (6.29).

Arguing as above and using Eq. (6.31), we have:

$$\text{sign}(\bar{e}^1_{k+1} - e^1_{k+1}) = \text{sign}(\bar{e}^1_{k+2} - e^1_{k+2}) = \cdots = \text{sign}(\bar{e}^1_{n_1} - e^1_{n_1}). \tag{6.38}$$

By Eq. (6.31), we have

$$e^1_k = \frac{\lambda^1_{n_1} e^1_{n_1}}{\lambda^1_k (q^1_{k+1} - e^1_{k+1})}. \tag{6.39}$$

Now, if $\text{sign}(\bar{e}^1_{n_1} - e^1_{n_1}) < 0$ i.e., $\bar{e}^1_{n_1} < e^1_{n_1}$, then combining this with Eqs. (6.38) and (6.39) and the fact that $\lambda^1_k < \bar{\lambda}^1_k$ yields

$$\text{sign}(\bar{e}^1_k - e^1_k) = \text{sign}(\bar{e}^1_{k+1} - e^1_{k+1}) = \cdots = \text{sign}(\bar{e}^1_{n_1} - e^1_{n_1}). \tag{6.40}$$

Arguing as above and using Eqs. (6.31) and (6.40) we have

$$\text{sign}(\bar{e}_z - e_z) = \text{sign}(\bar{e}^1_1 - e^1_1) = \text{sign}(\bar{e}^1_2 - e^1_2) = \cdots = \text{sign}(\bar{e}^1_{n_1} - e^1_{n_1}). \tag{6.41}$$

By Eqs. (6.29) and (6.41), we get a contradiction to Eq. (6.30). Hence, $\text{sign}(\bar{e}^1_{n_1} - e^1_{n_1}) > 0$ i.e., $e^1_{n_1} < \bar{e}^1_{n_1}$ and from Eq. (6.38), we get

$$e^1_j < \bar{e}^1_j, \text{ for all } j \in \{k+1, \ldots, n_1\}. \tag{6.42}$$

Now if $e^1_k < \bar{e}^1_k$, we again get Eq. (6.40) and hence $e^1_j < \bar{e}^1_j$, for all $j \in \{1, \ldots, n_1\}$ and $e_z < \bar{e}_z$ and this implies that $e^2_j < \bar{e}^2_j$, for all $j \in \{1, \ldots, n_2\}$ which is again a contradiction to Eq. (6.30). Hence, $\bar{e}^1_k < e^1_k$.

Next, we turn to consider a generalized network of RFMDs (RFMDN).

Proof of Proposition 6.4.1: The proof is based on similar arguments as in the proof of the Proposition 6.2.1 and is thus omitted.

Proof of Theorem 6.4.1: We can write the RFMDN as $\dot{x} = f(x)$. Let $J := \frac{\partial}{\partial x} f$ denote the Jacobian of the dynamics. Since the input to each RFMD is positive, therefore each RFMD is a monotone control system and the other non-diagonal terms are non-negative in J as all the connection weights w^i_j's are non-negative, and hence the network is a cooperative system.

At steady-state, the equations of the RFMDN yield:

$$\begin{aligned}\lambda_0^i u^i(q_1^i - e_1^i) &= \lambda_1^i e_1^i(q_2^i - e_2^i),\\ &= \lambda_2^i e_2^i(q_3^i - e_3^i),\\ &\vdots\\ &= \lambda_{n_i-1}^i e_{n_i-1}^i(q_{n_i}^i - e_{n_i}^i)\\ &= \lambda_{n_i}^i e_{n_i}^i.\end{aligned} \tag{6.43}$$

Note that $e_{n_i}^i$ uniquely determines e_1^i, e_2^i,...,$e_{n_i-1}^i$. Let us assume that $\bar{e} \neq e$ is another steady-state point of the network. Then $\bar{e}_{n_k}^k \neq e_{n_k}^k$ for some k. Without loss of generality, suppose that $e_{n_1}^1 < \bar{e}_{n_1}^1$. Then by Eq. (6.43), we have

$$\lambda_{n_1-1}^1 e_{n_1-1}^1(q_{n_1}^1 - e_{n_1}^1) < \lambda_{n_1-1}^1 \bar{e}_{n_1-1}^1(q_{n_1}^1 - \bar{e}_{n_1}^1) \tag{6.44}$$

which implies

$$e_{n_1-1}^1 < \bar{e}_{n_1-1}^1. \tag{6.45}$$

Continuing in this manner, we get

$$e_j^1 < \bar{e}_j^1 \quad \text{for all} \quad j \in \{1, 2, \ldots, n_1\}. \tag{6.46}$$

Also by Eq. (6.43), we have

$$\begin{aligned}\bar{e}_1^1 - e_1^1 &= q_1 - \frac{\lambda_{n_1}^1 \bar{e}_{n_1}^1}{\lambda_0^1 \bar{u}^1} - q_1 + \frac{\lambda_{n_1}^1 e_{n_1}^1}{\lambda_0^1 u^1},\\ &= \frac{\lambda_{n_1}^1(e_{n_1}^1 \bar{u}^1 - \bar{e}_{n_1}^1 u^1)}{\lambda_0^1 u^1 \bar{u}^1},\\ &= \frac{\lambda_{n_1}^1}{\lambda_0^1 u^1 \bar{u}^1}\Big(w_0^1(e_{n_1}^1 - \bar{e}_{n_1}^1) + \sum_{j=2}^{m} w_j^1 \lambda_{n_j}^j (e_{n_1}^1 \bar{e}_{n_j}^j - \bar{e}_{n_1}^1 e_{n_j}^j)\Big).\end{aligned} \tag{6.47}$$

Since the left-hand side is positive and the first term on the right-hand side is negative, therefore atleast one of the terms of the summation must be positive. Again, without loss of generality, we can assume that $e_{n_1}^1 \bar{e}_{n_2}^2 - \bar{e}_{n_1}^1 e_{n_2}^2 > 0$. So

$$\frac{\bar{e}_{n_1}^1}{e_{n_1}^1} < \frac{\bar{e}_{n_2}^2}{e_{n_2}^2}, \tag{6.48}$$

which implies

$$e_j^2 < \bar{e}_j^2 \quad \text{for all} \quad j \in \{1, 2, \ldots, n_2\}. \tag{6.49}$$

By Eq. (6.43), we have

$$\bar{e}_1^2 - e_1^2 = \frac{\lambda_{n_2}^2}{\lambda_0^2 u^2 \bar{u}^2}\Big(w_0^2(e_{n_2}^2 - \bar{e}_{n_2}^2) + w_1^2\lambda_{n_1}^1(e_{n_2}^2\bar{e}_{n_1}^1 - \bar{e}_{n_2}^2 e_{n_1}^1) + \sum_{j=3}^{m} w_j^2\lambda_{n_j}^j(e_{n_2}^2\bar{e}_{n_j}^j - \bar{e}_{n_2}^2 e_{n_j}^j)\Big). \tag{6.50}$$

By Eqs. (6.48) and (6.49), we must have atleast one of the terms in the summation should be positive. Again, without loss of generality assume that $e_{n_2}^2\bar{e}_{n_3}^3 - \bar{e}_{n_2}^2 e_{n_3}^3 > 0$ which implies

$$\frac{\bar{e}_{n_2}^2}{e_{n_2}^2} < \frac{\bar{e}_{n_3}^3}{e_{n_3}^3}. \tag{6.51}$$

Hence, continuing in this way we get

$$1 < \frac{\bar{e}_{n_1}^1}{e_{n_1}^1} < \frac{\bar{e}_{n_2}^2}{e_{n_2}^2} < \cdots < \frac{\bar{e}_{n_m}^m}{e_{n_m}^m} \tag{6.52}$$

which implies that

$$e_j^i < \bar{e}_j^i, \quad \text{for all} \;\; i \in \{1, 2, \ldots, m\} \;\; \text{and} \;\; j \in \{1, 2, \ldots, n_i\}. \tag{6.53}$$

Using Eq. (6.43), we have

$$\bar{e}_1^m - e_1^m = \frac{\lambda_{n_m}^m}{\lambda_0^m u^m \bar{u}^m}\Big(w_0^m(e_{n_m}^m - \bar{e}_{n_m}^m) + \sum_{j=1}^{m-1} w_j^m\lambda_{n_j}^j(e_{n_m}^m\bar{e}_{n_j}^j - \bar{e}_{n_m}^m e_{n_j}^j)\Big). \tag{6.54}$$

By Eqs. (6.52) and (6.53), the left-hand side of the above equation is positive and the right-hand side is negative which gives us a contradiction. Hence, there exists a unique steady-state point of the network.

By Proposition 6.4.1 and the results in Ref. [155] implies that the network admits a globally asymptotically stable steady-state point.

Proof of Proposition 6.4.2: Suppose $w_2 < \bar{w}_2$. To the contrary, let $\bar{y}_{ss} \leq y_{ss}$. Then we have $\bar{e}_n \leq e_n$. From the arguments given in the above proposition, we get $\bar{e}_i \leq e_i$ for all $i \in \{1, 2, \ldots, n-1\}$. Now,

$$\begin{aligned} \bar{e}_1^1 - e_1^1 &= \frac{\lambda_n e_n}{\lambda_0(w_1 + w_2\lambda_n e_n)} - \frac{\lambda_n \bar{e}_n}{\lambda_0(w_1 + \bar{w}_2\lambda_n\bar{e}_n)} \\ &= \frac{\lambda_n}{\lambda_0}\Big(w_1(e_n - \bar{e}_n) + \lambda_n e_n\bar{e}_n(\bar{w}_2 - w_2)\Big). \end{aligned} \tag{6.55}$$

This implies $\bar{e}_1 > e_1$ which is a contradiction. Hence, $y_{ss} < \bar{y}_{ss}$. The other part of the proposition can be proved in a similar way.

Proof of Theorem 6.4.2: Let $v_j^i := w_j^i y^i$. Then the inputs can be written as

$u^i = w_0^i + \sum_{j=1}^{m} v_j^i$. Also, we know that the steady-state output of an RFMD with fixed site sizes is a concave function of the transition rates and hence, $y_{ss}^i = g_i(u^i)$ for some concave function g_i. Then the constraints become $w_0^i \geq 0$, $v_j^i \geq 0$ and $\sum_{i=1}^{m} v_j^i = g_j(u^j)$. These constraints define a convex set of w_0^i and v_j^i. Note that the steady-state network output rate is a weighted sum of the concave functions. Hence, the formulation of Problem 1 is a convex optimization problem [156].

Proof of Theorem 6.4.3: Consider a graph of m nodes where each RFMD represents a node and there is a directed edge from RFMD $\#i$ to RFMD $\#j$ if the flow out of the former feeds the later. Then the graph of feed-forward network of m RFMDs is a directed acyclic graph [157]. Hence, the steady-state input to any RFMD $\#i$ will be a weighted sum of steady-state outputs of RFMDs. Also, we know that for fixed site sizes, the output y^i is a concave function of the transition rates and in particular the input rate, and hence the mapping $w \rightarrow y_{ss}(w)$ is concave. The constraints already define a convex set and hence this completes the proof.

Chapter 7

A mathematical framework for analyzing particle flow in a network with multiple pools

This chapter[1] introduces a network model of ribosome flow models (RFMs) having multiple pools where each RFM captures the dynamics of particle flow in a lane and competes for the finite resources present at the nearby pool. We study a ribosome flow model network with two pools (RFMNTP) and show that the network always admits a steady state. We then analyze the behavior of the RFMNTP with respect to modifying the transition rate through a theoretical framework. Finally, we illustrate how these results can provide insights into studying a network with multiple pools.

7.1 Introduction

Movement is a vital aspect of life. Various cellular and physical processes involve the movement of particles along tracks. These processes generally take place in parallel and they compete for the available limited resources. For example, during gene expression all DNA (mRNA) molecules simultaneously compete for the limited amount of RNAPs (ribosomes) [1, 158, 72]. This competition generates a network in which an indirect coupling induces interactions among the lanes even in the absence of explicit connections [159, 160]. Hence, it is of considerable interest to analyze such networks in the presence of these interactions and also, to design several resource-sharing synthetic gene networks [161, 162]. In physical systems such as vehicular flow, the number of vehicles moving along the roads is finite. The entry rate of the vehicles along the road is affected due to the queue of vehicles waiting to enter a road, where each vehicle competes with other vehicles for limited space on the road [163]. This requires modeling the complex road network to comprehend the traffic flow thereby, reducing travel time, and preventing traffic deadlocks [164, 165].

[1]The content of this chapter is published as "Aditi Jain and Arvind Kumar Gupta. A mathematical framework for analysing particle flow in a network with multiple pools. *Royal Society Open Science* 11: 231588, 2024."

Several computational and mathematical models have been developed to study resource-sharing networks [166, 167, 168]. One such model includes the set of totally asymmetric simple exclusion processes (TASEPs) that are interconnected to each other via a pool of free particles [169, 170, 171]. The TASEP and its networks have been used to model and analyze various natural and artificial systems, including mRNA translation, vehicular traffic flow, and more [5, 22, 172]. Regardless of its simple description, rigorous analysis of networks of TASEPs is complex, exact solutions exist for simplified cases and most non-homogeneous cases are studied via numerical methods or extensive Monte Carlo simulations [33, 34, 173]. Hence, understanding the effect of parameters on the dynamics of a system through TASEP-based models has proved challenging. There are lattice hydrodynamic models that utilize ordinary differential equations to model the flow of vehicles along the lanes[174, 175, 176]. Therefore, the framework of RFM that also describes the flow of particles can serve as the basis for understanding the dynamics of vehicular traffic.

An RFM network in Ref. [149] is a generalized network that analyzes various network topologies using a set of interconnected RFMs. It models the static connections between the RFMs and hence, the input to each RFM is a source (maybe pools of free ribosomes in the cell) whose output rate is a constant or proportion of the output of other RFMs. Here, the pool supplies a constant input source and hence, it does not take into account the competition effects on the network's behavior due to finite resources.

Almost all prior research has provided an understanding of biological activities constrained by a single pool. However, taking into account the concept of multiple pools helps one to comprehend the participation of particles in the vicinity of their targets. For instance, in the context of introducing synthetic circuit genes, a network model called Orthogonal Ribosome Flow Model (ORFM) was introduced where the ribosome pool has been divided by use of orthogonal ribosomes and the introduced genes are only translated by mutated ribosomes [177]. The concept of orthogonal ribosomes was used to increase the protein output by decoupling circuit genes from the host pool of ribosomes. The concept of multiple pools also provides a useful framework to model vehicular flow between different cities where each pool represents each city.

In this chapter, we study the idea that the entry rate of the particles on lanes is affected by the occupancy of the nearby pool. Studying a minimal model of a two-pool network is a useful strategy for gaining insights into the behavior of more complex systems with multiple pools. We present our theoretical investigation of a two-pool network and then illustrate how one can generalize it to study a network

with multiple pools. We introduce a new model called the ribosome flow model network with two pools (RFMNTP) that includes several RFMs interconnected via two dynamical pools of free particles. It captures the feature that the particles located far away from RFMs will not impact the initiation rates of these RFMs. Therefore, each RFM can be associated with two pools of particles, one pool containing particles impacting the initiation rate of the RFM, and the other pool receiving its output. The whole system being closed conserves the number of particles. This two-pool network then models vehicular flow between the two cities where each pool represents each city. Similarly, pedestrian flow involving the movement of people between two places is reminiscent of the fact that it can be studied by incorporating two pools in the network.

By utilizing the theory of cooperative dynamical systems with a first integral, we prove that the RFMNTP admits a continuum of steady-state points [132, 143, 153]. Therefore, the same steady-state point is attained by any two solutions starting from initial conditions corresponding to an equal total number of particles in the network, and hence, the network can be analyzed by the steady-state density profile. This theoretical analysis can also be easily extended to prove the stability results for multiple pools. Next, we study how a change in one RFM affects the dynamics of the network. The change in the steady-state with respect to changing the rate of a site in a specific RFM, say R, can be any one of the following outcomes: a) steady-state pool densities can both increase (decrease) simultaneously, b) a decrease in the steady-state pool density that is feeding R and an increase in the steady-state density of the other pool. The results hold for any set of parameters in the network.

The structure of this chapter is organized as follows. The next section introduces the network of ribosome flow models with multiple pools. Section 7.3 describes a two-pool network and then describes our main mathematical results. Section 7.4 illustrates the idea of understanding the dynamics of a network with multiple pools. The final section summarizes and suggests some directions for further research. The proofs of the results are provided in the Appendix for ease of reading.

7.2 The mathematical framework

We first review the spectral properties of the RFM that have been described in Chapter 1.

7.2.1 Ribosome flow model

Recall that the state-space of the RFM is C^n. It has also been proved that RFM admits a steady-state e [39]. In Ref. [44], it has been shown that there exists a

spectral representation for the mapping from λ_0, λ_1,..., λ_n to steady-state e given by $(n+2)\times(n+2)$ Jacobi matrix

$$A := \begin{bmatrix} 0 & \lambda_0^{-1/2} & 0 & \dots & 0 \\ \lambda_0^{-1/2} & 0 & \lambda_1^{-1/2} & \dots & 0 \\ 0 & \lambda_1^{-1/2} & 0 & \dots & 0 \\ & & \ddots & & \\ 0 & \dots & 0 & 0 & \lambda_n^{-1/2} \\ 0 & \dots & 0 & \lambda_n^{-1/2} & 0 \end{bmatrix}.$$

Note that A admits a unique maximal eigenvalue $\sigma > 0$ and the entries of a corresponding eigenvector $\zeta \in \mathbb{R}^{n+2}$ are all positive for all $i \in \{1, 2, \dots, n+2\}$ [83]. It has also been proved in Ref. [44] that the steady-state values of the RFM satisfy

$$e_j = \frac{\zeta_{j+2}}{\lambda_j^{1/2}\sigma\zeta_{j+1}}, \quad \text{for} \quad j = 1, 2, \dots, n \tag{7.1}$$

and the steady-state output rate satisfy

$$R = \frac{1}{\sigma^2}. \tag{7.2}$$

To build a network of interconnected RFMs, the first step is to extend the RFM into a single-input single-output (SISO) system. This is done by adding a time-varying measurable and bounded function $v : \mathbb{R}_+ \to \mathbb{R}_+$ to the RFM [61]. In the context of translation, the function v represents the flow of ribosomes into the mRNA from the cell environment. The equations describing the RFM with input and output are as follows:

$$\begin{aligned} \dot{x}_1 &= \lambda_0 v(1 - x_1) - \lambda_1 x_1(1 - x_2), \\ \dot{x}_2 &= \lambda_1 x_1(1 - x_2) - \lambda_2 x_2(1 - x_3), \\ &\vdots \\ \dot{x}_n &= \lambda_{n-1} x_{n-1}(1 - x_n) - \lambda_n x_n, \\ \text{and} \quad R(t) &= \lambda_n x_n(t). \end{aligned} \tag{7.3}$$

The system given by (7.3) is a monotone control system [142]. It can also be seen that C^n is an invariant set of the dynamics i.e., any trajectory emanating from any point in C^n shall remain in it for all time $t \geq 0$.

7.2.2 Network of ribosome flow models with multiple pools

Now, we provide some insights into the dynamics of the flow of particles on several lanes connected via multiple pools. Consider a network consisting of M pools and N RFMs. Each pool is connected to at least one RFM that receives its input from the pool and at least one other RFM that feeds its output to the pool. The particles that are not attached to any RFM are present in the pools. The topology of this network can be represented using a directed multigraph where each node represents the pool and the directed edges represent the RFMs that indicate the flow of particles from one pool to the other pool (see Fig. 7.1).

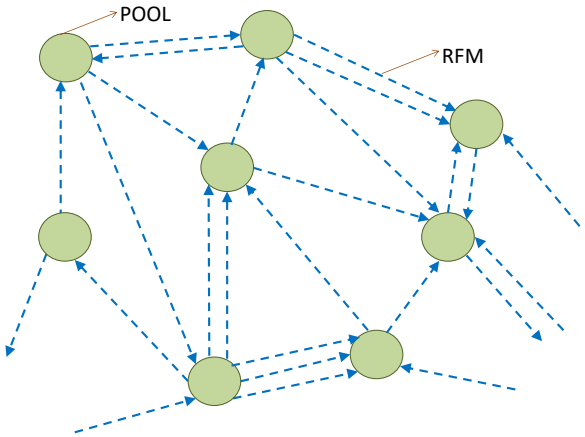

Figure 7.1: The graph representation of the network with multiple pools where each node (circle) represents the pool and the directed edges (dashed lines having arrows) represent a chain of sites on which particles undergo RFM dynamics. The arrow of the edge pointing to the pool represents that the output of the RFM is feeding the pool.

Let RFM $\#i$ be described by the tuple $\mathcal{A}_i := \{n_i, G_i, x^i_j, \lambda^i_k\}$ for $i = 1, 2, \ldots, N$, $j = 1, 2 \ldots, n_i$, $k = 0, 1, \ldots, n_i$, where n_i is the dimension of RFM $\#i$; $G_i : \mathbb{R}_+ \to \mathbb{R}_+$ is the input function of the RFM $\#i$; x^i_j's are the state variables and λ^i_k's are the positive transition rates along RFM $\#i$. Let Pool $\#j$ density is described by $z_j(t)$ for $j = 1, 2, \ldots, M$ where z_j represent the average number of particles in the pool. Assume that Pool $\#j$ is feeding the input to the RFM $\#k$, $k \in \mathcal{I}$ where $\mathcal{I}$ is a subset of the set $\{1, 2, \ldots, N\}$ and let RFM $\#k'$, $k' \in \mathcal{I}'$ where $\mathcal{I}'$ is a subset of the set $\{1, 2, \ldots, N\} \setminus \mathcal{I}$, is feeding its output to the Pool $\#j$. Thus, the dynamics of the RFM $\#k$ is described by the following ODEs:

$$\begin{aligned}
\dot{x}^k_1 &= \lambda^k_0 G_k(z_j)(1 - x^k_1) - \lambda^k_1 x^k_1 (1 - x^k_2), \\
\dot{x}^k_2 &= \lambda^k_1 x^k_1 (1 - x^k_2) - \lambda^k_2 x^k_2 (1 - x^k_3), \\
&\vdots \\
\dot{x}^k_{n_k} &= \lambda^k_{n_k - 1} x^k_{n_k - 1} (1 - x^k_{n_k}) - \lambda^k_{n_k} x^k_{n_k},
\end{aligned} \tag{7.4}$$

and the dynamics is described by the following balance equation for each Pool $\#j$:

$$\dot{z}_j = \sum_{k' \in \mathcal{I}'} \lambda^{k'}_{n_{k'}} x^{k'}_{n_{k'}} - \sum_{k \in \mathcal{I}} \lambda^k_0 G_k(z_j)(1 - x^k_1). \tag{7.5}$$

The entry rate of particles into the RFMs is modulated by the occupancy level of the nearby pool. Note that there is no direct link between the RFMs in the network and the interconnections are via the pool of particles. The pool outflow functions G_k describe the likelihood that the particles will attach to the RFMs. In other words, these functions model the competition for particles between the RFMs. Therefore, RFM having a more effective initiation rate $\lambda^k_0 G_k(z_j)$ have more influx of particles into them.

Each state variable x^i_j represents the normalized particle density and G_i gives non-negative output. Therefore, the state space of the network is

$$\Omega = [0,1]^{n_1} \times [0,1]^{n_2} \ldots [0,1]^{n_N} \times [0,\infty)^M. \tag{7.6}$$

Let

$$F(t) := \sum_{j=1}^{M} z_j(t) + \sum_{i=1}^{N} \sum_{j=1}^{n_i} x^i_j(t) \tag{7.7}$$

describe the total occupancy of particles in the network at any time t. Since it is a closed system, $F(t)$ is a first integral of the dynamics. Note that all the particles can be accommodated in any of the pools.

Analyzing such networks requires information about interconnected RFMs and the pools and therefore, a minimal model of a two-pool network provides a useful starting point for studying the behavior of particle flow in a network with multiple pools. We now shall begin our study with a new model RFMNTP that considers two dynamic pools in the network. The proposed model considers the dynamics of particles on various tracks, wherein on some tracks particles are recruited from one pool and return to the other pool, and vice versa. This is a primary study of a system having two pools in the framework of a network of RFMs. The findings can be generalized to complex systems with multiple pools.

7.3 The ribosome flow model network with two pools

We consider a network model consisting of several RFMs and two finite pools: Pool I and Pool II and this model the dynamics of the flow of particles on several lanes

interconnected via two pools (see Fig. 7.2a). We represent those RFMs, say $m \geq 1$ in number, whose input is received through Pool I and output is supplied to Pool II as RFMXs. For the reverse case, the RFMs, say $n \geq 1$ in number, whose input is received through Pool II and output is supplied to Pool I are referred to as RFMYs. We call this network a ribosome flow model network with two pools (RFMNTP) (see Fig. 7.2b). Let RFMX # i is described by the tuple $\mathcal{E}_i := \{\ell_i, G_i, x_j^i, \lambda_k^i\}$ for $i = 1, 2, \ldots, m$, $j = 1, 2 \ldots, \ell_i$, $k = 0, 1, \ldots, \ell_i$, where ℓ_i is the dimension of RFMX # i; $G_i : \mathbb{R}_+ \to \mathbb{R}_+$ is the ith input function; x_j^i's are the state variables and λ_k^i's are the positive transition rates along RFMX # i. Similarly, consider RFMY # i represented by the tuple $\mathcal{F}_i := \{p_i, H_i, y_j^i, \eta_k^i\}$ for $i = 1, 2, \ldots, n$, $j = 1, 2 \ldots, p_i$, $k = 0, 1, \ldots, p_i$, where p_i is the dimension of RFMY # i; $H_i : \mathbb{R}_+ \to \mathbb{R}_+$ is the ith input function; y_j^i's are the state variables and η_k^i's are the positive transition rates along RFMY # i. The Pool I and Pool II density at time t is modeled by $z_1(t)$ and $z_2(t)$, respectively.

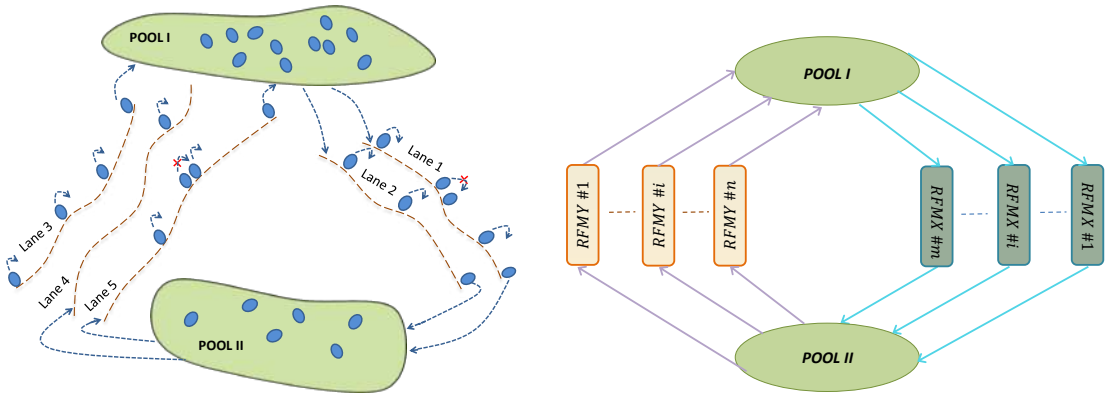

(a) (b)

Figure 7.2: (a) Topology of the network with two pools and 5 lanes: Particles from Pool I (Pool II) transverse lanes 1,2 (3,4,5) and join the Pool II (Pool I) and then transverse lanes 3,4,5 (1,2) and again join Pool I (Pool II). Hence, Pool I (Pool II) supplies its input to lanes 1,2 (3,4,5) and receives its output from lanes 3,4,5 (1,2). In the case of vehicular traffic, particle/lane/pool represents the car/road/city. (b) Topology of the RFMNTP: the m RFMXs receive their input from Pool I and supply their output to Pool II and the n RFMYs receive their input from Pool II and supply their output to Pool I.

Thus, the RFMX #i dynamics is described by the following equations:

$$\begin{aligned}
\dot{x}_1^i &= \lambda_0^i G_i(z_1)(1 - x_1^i) - \lambda_1^i x_1^i (1 - x_2^i), \\
\dot{x}_2^i &= \lambda_1^i x_1^i (1 - x_2^i) - \lambda_2^i x_2^i (1 - x_3^i), \\
&\vdots \\
\dot{x}_{\ell_i}^i &= \lambda_{\ell_i - 1}^i x_{\ell_i - 1}^i (1 - x_{\ell_i}^i) - \lambda_{\ell_i}^i x_{\ell_i}^i,
\end{aligned} \tag{7.8}$$

and its output rate of exit of particles is given by $\lambda^i_{\ell_i} x^i_{\ell_i}$.

The dynamics of RFMY $\#i$ is described by the following equations:

$$\begin{aligned}
\dot{y}^i_1 &= \eta^i_0 H_i(z_2)(1-y^i_1) - \eta^i_1 y^i_1(1-y^i_2),\\
\dot{y}^i_2 &= \eta^i_1 y^i_1(1-y^i_2) - \eta^i_2 y^i_2(1-y^i_3),\\
&\vdots\\
\dot{y}^i_{p_i} &= \eta^i_{p_i-1} y^i_{p_i-1}(1-y^i_{p_i}) - \eta^i_{p_i} y^i_{p_i},
\end{aligned} \tag{7.9}$$

and its output rate of exit of particles is given by $\eta^i_{p_i} y^i_{p_i}$.

Pool I feeds all the RFMXs and the output of each RFMY is supplied into Pool I, so the change in z_1 is given by the following balance equation:

$$\dot{z}_1 = \sum_{i=1}^{n} \eta^i_{p_i} y^i_{p_i} - \sum_{i=1}^{m} \lambda^i_0 \; G_i(z_1)(1-x^i_1). \tag{7.10}$$

Also, Pool II feeds all the RFMYs, and the output of each RFMX is supplied into Pool II, so the change in z_2 is given by the following balance equation:

$$\dot{z}_2 = \sum_{i=1}^{m} \lambda^i_{\ell_i} x^i_{\ell_i} - \sum_{i=1}^{n} \eta^i_0 \; H_i(z_2)(1-y^i_1). \tag{7.11}$$

It can be observed that if the pools are empty then no particles can attach to the respective lanes, and as the pools become fuller more particles can attach to the lanes. Therefore these properties are satisfied by imposing the following assumptions on G_i and H_i: a) $G_i(0) = 0$ and $H_i(0) = 0$, b) $G_i(z_1)$ and $H_i(z_2)$ are continuous and strictly increasing functions of z_1 and z_2, respectively. Let

$$Q(t) := z_1(t) + z_2(t) + \sum_{i=1}^{m}\sum_{j=1}^{\ell_i} x^i_j(t) + \sum_{i=1}^{n}\sum_{j=1}^{p_i} y^i_j(t) \tag{7.12}$$

describe the total occupancy of particles in the network at any time t. Since the RFMNTP is a closed system, $Q(t)$ is a first integral of the dynamics, i.e., $Q(t) = Q(0)$ for all $t \geq 0$. Note that both pool densities are bounded by $Q(0)$. Summing up, the RFMNTP is a dynamical system with $s = \sum_{i=1}^{m} \ell_i + \sum_{i=1}^{n} p_i + 2$ state variables whose dynamics are given by Eqs. (7.8), (7.9), (7.10) and (7.11). The next section rigorously analyzes the mathematical aspect of the RFMNTP.

7.3.1 Dynamical properties of the RFMNTP

Given two vectors u, $v \in \mathbb{R}^n$, we define order relation $u \ll v$ if $u_i < v_i$ for all i. Recall that every x_j^i and y_j^i represent normalized particle density and the assumptions on G_i and H_i imply that the pool densities are always non-negative. Therefore, the state space of the RFMNTP is

$$\mathcal{B} = [0,1]^{\ell_1} \times [0,1]^{\ell_2} \times \dots [0,1]^{\ell_m} \times [0,1]^{p_1} \times [0,1]^{p_2} \times \dots [0,1]^{p_n} \times [0,\infty) \times [0,\infty). \quad (7.13)$$

Let $[x(t,a) \;\; y(t,a) \;\; z_1(t,a) \;\; z_2(t,a)]'$ denote the solution of the RFMNTP at time t for the initial condition $a \in \mathcal{B}$, where x and y is the vector consisting of all the state variables of RFMXs and RFMYs, respectively. For $r \geq 0$, let $L_r \coloneqq \{a \in \mathcal{B} : \sum_{i=1}^{s} a_i = r\}$ i.e., L_r represent all states in $\mathcal{B}$ corresponding to total occupancy of particles equal to r in the network.

7.3.2 Invariance

The following result states that for any initial condition $a \in \mathcal{B}$, the trajectory of the RFMNTP stays in $\mathcal{B}$ for all $t \geq 0$.

Proposition 7.3.1. *The state space $\mathcal{B}$ is an invariant set of the RFMNTP, i.e., $0 \leq x_j^i(t,a) \leq 1$, $0 \leq y_j^i(t,a) \leq 1$, $z_i(t,a) \in [0,\infty)$ for any $t \geq 0$, and any initial condition $a \in \mathcal{B}$.*

We shall now show that the proposed nonlinear system of differential equations is a cooperative system. This property guarantees the monotonicity (order-preserving property) of the flow with respect to the partial ordering in the phase space (refer to Chapter 1). Now, the Jacobian matrix J of the vector field of the RFMNTP is:

$$J(x,y,z_1,z_2) = \begin{bmatrix} X_1 & 0 & 0 & 0 & 0 & 0 & \dots & 0 & U_1 & 0 \\ 0 & X_2 & 0 & 0 & 0 & 0 & \dots & 0 & U_2 & 0 \\ \vdots & & \ddots & \vdots & \vdots & \vdots & & \vdots & \vdots & \vdots \\ 0 & 0 & \dots & X_m & 0 & 0 & \dots & 0 & U_m & 0 \\ 0 & 0 & \dots & 0 & Y_1 & 0 & \dots & 0 & 0 & V_1 \\ 0 & 0 & \dots & 0 & 0 & Y_2 & \dots & 0 & 0 & V_2 \\ \vdots & \vdots & & \vdots & \vdots & & \ddots & \vdots & \vdots & \vdots \\ 0 & 0 & \dots & 0 & 0 & 0 & \dots & Y_n & 0 & V_n \\ A_1 & A_2 & \dots & A_m & B_1 & B_2 & \dots & B_n & Z_1 & 0 \\ C_1 & C_2 & \dots & C_m & D_1 & D_2 & \dots & D_n & 0 & Z_2 \end{bmatrix}$$

where X_i represents the Jacobian matrix of RFMX $\#i$ and is given by

$$\begin{bmatrix} -\lambda_0^i G_i(z_1) - \lambda_1^i(1-x_2^i) & \lambda_1^i x_1^i & 0 & \dots & 0 \\ \lambda_1^i(1-x_2^i) & -\lambda_1^i x_1^i - \lambda_2^i(1-x_3^i) & \lambda_2^i x_2^i & \dots & 0 \\ & & \ddots & & \\ 0 & 0 & 0 & \dots & \lambda_{\ell_i-1}^i x_{\ell_i-1}^i \\ 0 & 0 & 0 & \dots & -\lambda_{\ell_i-1}^i x_{\ell_i-1}^i - \lambda_{\ell_i}^i \end{bmatrix},$$

and Y_i represents the Jacobian matrix of RFMY $\#i$ and is given by

$$\begin{bmatrix} -\eta_0^i H_i(z_2) - \eta_1^i(1-y_2^i) & \eta_1^i y_1^i & 0 & \dots & 0 \\ \eta_1^i(1-y_2^i) & -\eta_1^i y_1^i - \eta_2^i(1-y_3^i) & \eta_2^i y_2^i & \dots & 0 \\ & & \ddots & & \\ 0 & 0 & 0 & \dots & \eta_{p_i-1}^i y_{p_i-1}^i \\ 0 & 0 & 0 & \dots & -\eta_{p_i-1}^i y_{p_i-1}^i - \eta_{p_i}^i \end{bmatrix},$$

$A_i = [\lambda_0^i G_i(z_1) \;\; 0 \dots 0 \;\; 0]$, $B_i = [0 \dots 0 \;\; 0 \;\; \eta_{p_i}^i]$, $C_i = [0 \dots 0 \;\; 0 \;\; \lambda_{\ell_i}^i]$, $D_i = [\eta_0^i H_i(z_2) \;\; 0 \dots 0 \;\; 0]$, $U_i = [\lambda_0^i G_i'(z_1)(1-x_1^i) \;\; 0 \dots \;\; 0]'$, $V_i = [\eta_0^i H_i'(z_2)(1-y_1^i) \;\; 0 \dots \;\; 0]'$, $Z_1 = -\sum_{i=1}^m \lambda_0^i G_i'(z_1)(1-x_1^i)$ and $Z_2 = -\sum_{i=1}^n \eta_0^i H_i'(z_2)(1-y_1^i)$. Clearly, by Proposition 7.3.1 we get that the Jacobian matrix J is Metzler for any initial condition in $\mathcal{B}$, and thus the RFMNTP is a cooperative dynamical system.

7.3.3 Persistence

The next result proves that the property called persistence holds which implies that any trajectory becomes uniformly separated from the boundary of $\mathcal{B}$.

Proposition 7.3.2. *For any $\delta > 0$ there exists $\epsilon > 0$ depending on δ with $\epsilon \to 0$ as $\delta \to 0$ such that $\epsilon \leq x_j^i(t,a) \leq 1-\epsilon$, for $i \in \{1,2,\dots,m\}$, $j \in \{1,2,\dots,\ell_i\}$, $\epsilon \leq y_j^i(t,a) \leq 1-\epsilon$, for $i \in \{1,2,\dots,n\}$, $j \in \{1,2,\dots,p_i\}$ and $\epsilon \leq z_i(t,a)$ for $i \in \{1,2\}$ for all $a \in (\mathcal{B} \setminus \{0\})$ and all $t \geq \delta$.*

In other words, all the densities are smaller than one and larger than zero, and the pool occupancies are strictly positive. This result guarantees that the Jacobian matrix of the dynamics becomes irreducible after an arbitrarily short time [83]. Thus, the RFMNTP is a cooperative irreducible system of ODEs. Next, we analyze the asymptotic behavior of the RFMNTP.

7.3.4 Stability

The following result shows that each level set of the first integral has a unique intersection with the ordered set of fixed points.

Theorem 7.3.1. *The RFMNTP admits a unique steady-state point in every level set L_r, say e_r, and for any initial condition $a \in L_r$, the trajectory converges to e_r. Furthermore, for any $0 \leq r_1 < r_2$, we have $e_{r_1} \ll e_{r_2}$.*

The above theorem implies that the rates λ_j^i, η_j^i, and the total density of particle r determine a unique steady-state point of the network. Moreover, the continuum of the steady state points $\{e_r : r \in [0, \infty)\}$ are linearly ordered. Combining Proposition 7.3.2 and Theorem 7.3.1 follows that for any $r > 0$, $e_r \in \text{int}(\mathcal{B})$ i.e., the steady-state profile will never include densities of RFMXs and RFMYs that are either zero or one and the Pool I, and the Pool II steady-state densities are always strictly positive. The following example demonstrates the Theorem 7.3.1.

Example 7.3.1. Consider an RFMNTP with $m = 1$ RFMX and $n = 1$ RFMY each with dimension 2. Assume that $\lambda_0^1 = 0.8$, $\lambda_1^1 = 1$, $\lambda_2^1 = 1.2$, $\eta_0^1 = 1$, $\eta_1^1 = 2$, $\eta_2^1 = 1$, $G_1(z_1) = \tanh(z_1)$, and $H_1(z_2) = z_2$. By Theorem 7.3.1, there exist an unique equilibrium point e in L_2 and after simulating the dynamical system, we have $e = [0.3589 \quad 0.2302 \quad 0.1909 \quad 0.2763 \quad 0.6023 \quad 0.3414]'$. Figures 7.3a and 7.3b depict trajectories of RFMNTP for initial conditions in the level set L_2: $[0.5\ 0.5\ 0.5\ 0.5\ 0\ 0]'$ and $[0\ 0\ 0\ 0\ 1\ 1]'$, respectively. It can be observed that each of these trajectories converges to e.

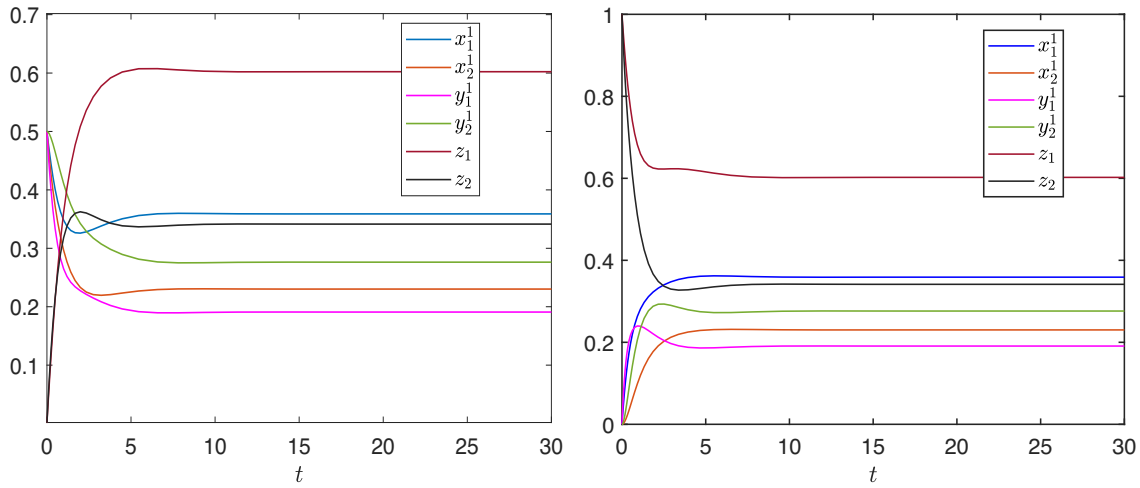

(a) (b)

Figure 7.3: Trajectories of the RFMNTP in Example 7.3.1: (a) For initial condition $[0.5\ 0.5\ 0.5\ 0.5\ 0\ 0]'$ and (b) For initial condition $[0\ 0\ 0\ 0\ 1\ 1]'$.

For ease of notation, let $e = [e_x \quad e_y \quad e_{z_1} \quad e_{z_2}]'$ where $e_x := [e_{x_1}^1 \quad e_{x_2}^1 \cdots e_{x_{\ell_1}}^1 \quad e_{x_1}^2 \quad e_{x_2}^2 \cdots e_{x_{\ell_2}}^2 \cdots e_{x_1}^m \quad e_{x_2}^m \cdots e_{x_{\ell_m}}^m]$ and $e_y := [e_{y_1}^1 \quad e_{y_2}^1 \cdots e_{y_{p_1}}^1 \quad e_{y_1}^2 \quad e_{y_2}^2 \cdots e_{y_{p_2}}^2 \cdots e_{y_{p_1}}^n \quad e_{y_{p_2}}^n \cdots e_{y_{p_n}}^n]$ denote the unique steady-state point of the RFMNTP in the level set L_r of Q. At steady-state, the change in all

the state variables and the pool variables w.r.t. time t becomes zero and thereby Eq. (7.8) implies

$$\lambda_0^i G_i(e_{z_1})(1-e_{x_1}^i) = \lambda_1^i e_{x_1}^i (1-e_{x_2}^i) = \cdots = \lambda_{\ell_i}^i e_{x_{\ell_i}}^i. \tag{7.14}$$

Similarly, at steady-state, Eq. (7.9) yields

$$\eta_0^i H_i(e_{z_2})(1-e_{y_1}^i) = \eta_1^i e_{y_1}^i (1-e_{y_2}^i) = \cdots = \eta_{p_i}^i e_{y_{p_i}}^i. \tag{7.15}$$

Again at steady-state, Eq. (7.10) implies that

$$\sum_{i=1}^{n} \eta_{p_i}^i e_{y_{p_i}}^i = \sum_{i=1}^{m} \lambda_0^i \; G_i(e_{z_1})(1-e_{x_1}^i). \tag{7.16}$$

We can also express the above equation as:

$$\sum_{i=1}^{n} \eta_{p_i}^i e_{y_{p_i}}^i = \sum_{i=1}^{m} \lambda_{\ell_i}^i e_{x_{\ell_i}}^i. \tag{7.17}$$

Eq. (7.17) implies that the total output of all the RFMXs is equal to the total output of all the RFMYs.

Next, we provide an analysis of how the spectral approach can obtain the steady-state e of the network without any numerical simulations of the dynamics. Consider an RFMNTP with m RFMXs where each RFMX has dimension ℓ_i, $i = 1, 2, \ldots, m$ and n RFMYs where each RFMY has dimension p_k, $k = 1, 2, \ldots, n$. We also assume that the transition rates in RFMX $\#i$ are represented by λ_j^i and in RFMY $\#k$ by η_k^i. The input to RFMX $\#i$ is given by G_i and to RFMY $\#k$ by H_k. Consider the total density of particles in the network to be r.

The steady-state values of each RFMX $\#i$ satisfy

$$e_{x_j}^i = \frac{\zeta_{j+2}^i}{\sqrt{\lambda_j^i \sigma_x^i \zeta_{j+1}^i}}, \quad j = 1, 2, \ldots, \ell_i, \tag{7.18}$$

where σ_x^i is the Perron eigenvalue and ζ^i is the corresponding Perron eigenvector of

the $(\ell_i + 2) \times (\ell_i + 2)$ Jacobi matrix A_i given by

$$A_i := \begin{bmatrix} 0 & (\lambda_0^i G_i(e_{z_1}))^{-1/2} & 0 & \dots & 0 \\ (\lambda_0^i G_i(e_{z_1}))^{-1/2} & 0 & (\lambda_1^i)^{-1/2} & \dots & 0 \\ 0 & (\lambda_1^i)^{-1/2} & 0 & \dots & 0 \\ & & \ddots & & \\ 0 & \dots & 0 & 0 & (\lambda_{\ell_i}^i)^{-1/2} \\ 0 & \dots & 0 & (\lambda_{\ell_i}^i)^{-1/2} & 0 \end{bmatrix}.$$

The steady-state values of each RFMY $\#k$ satisfy

$$e_{y_j}^k = \frac{\xi_{j+2}^k}{\sqrt{\eta_j^k \sigma_y^k \xi_{j+1}^k}}, \quad j = 1, 2, \dots, p_k, \tag{7.19}$$

where σ_y^k is the Perron eigenvalue and ξ^k is the corresponding Perron eigenvector of the $(p_k + 2) \times (p_k + 2)$ Jacobi matrix B_k given by

$$B_k := \begin{bmatrix} 0 & (\eta_0^k H_k(e_{z_2}))^{-1/2} & 0 & \dots & 0 \\ (\eta_0^k H_k(e_{z_2}))^{-1/2} & 0 & (\eta_1^k)^{-1/2} & \dots & 0 \\ 0 & (\eta_1^k)^{-1/2} & 0 & \dots & 0 \\ & & \ddots & & \\ 0 & \dots & 0 & 0 & (\eta_{p_k}^k)^{-1/2} \\ 0 & \dots & 0 & (\eta_{p_k}^k)^{-1/2} & 0 \end{bmatrix}.$$

It follows from Eq. (7.12) that

$$e_{z_1} + e_{z_2} + \sum_{i=1}^{m} \sum_{j=1}^{\ell_i} e_{x_j}^i(e_{z_1}) + \sum_{k=1}^{n} \sum_{j=1}^{p_k} e_{y_j}^k(e_{z_2}) = r. \tag{7.20}$$

Also, Eq. (7.17) implies

$$\sum_{i=1}^{n} \eta_{p_i}^i e_{y_{p_i}}^i(e_{z_2}) = \sum_{i=1}^{m} \lambda_{\ell_i}^i e_{x_{\ell_i}}^i(e_{z_1}). \tag{7.21}$$

Combining Eqs. (7.20) and (7.21) gives the expression of e_{z_1} and e_{z_2} in terms of number of particles r. Thus, the entire steady-state profile of the network can then be calculated by plugging the values of r in the expression. Note that this approach also allows one to obtain an expression of densities for any unknown transition parameter and we only need to plug the values to obtain the entire steady-state profile without any numerical simulations of the dynamics. However, one has to choose stable algorithms to solve the system of nonlinear equations (7.20) and (7.21).

7.3.5 Entrainment

Many important dynamical processes are periodic such as the cell-cycle division process, gene regulation, circadian rhythm, 24-hour solar day, and more [178, 179, 180]. Proper functioning often requires such processes to vary periodically with the same period. For example, a person's lack of synchronization to day and night can have health consequences [181]. For nonlinear systems, a periodic input signal does not guarantee that the response of the system will also be periodic as their behavior can be quasi-periodic or chaotic [182, 59]. Therefore, a natural question is whether the RFMNTP synchronizes with the periodic excitations or not. To answer this question, we assume that some or all the parameters in the RFMNTP are not constants but periodic and continuous functions of time with a common period $T > 0$, and satisfy the condition $0 < \delta_1 < \lambda_j^i \leq \delta_2$ and $0 < \delta_3 < \eta_j^i \leq \delta_4$. In this case, we call the network model the *periodic* RFMNTP (PRFMNTP). The next result shows that all the trajectories approach a periodic pattern with the same period T.

Theorem 7.3.2. *Consider the PRFMNTP. Fix $r > 0$. Then a unique T-periodic function $\phi_r : \mathbb{R}_+ \to \text{int}(\mathcal{B})$ exists and for any $a \in L_r$, the solution of the PRFMNTP converges to ϕ_r.*

In particular, PRFMNTP entrains to the periodic excitations in the parameters. As an additional point, if we examine the RFMNTP model for vehicular traffic between two cities, it enables a continuous flow of traffic while coordinating with the traffic lights. In simpler terms, when the traffic lights (rates) change periodically, the traffic density (state variables) will gradually settle into a recurring pattern with the same period. The following example illustrates the dynamic behavior of the PRFMNTP model.

Example 7.3.2. Consider a PRFMNTP with $m = 1$ RFMX with dimension $\ell_1 = 3$ and $n = 1$ RFMY with dimensions $p_1 = 2$. Assume that $\lambda_0^1 = 0.8$, $\lambda_1^1 = 3$, $\lambda_2^1 = 3 + 2\sin(2\pi t)$, $\lambda_3^1 = 3 - 2\sin(2\pi t)$, $\eta_0^1 = 1.2$, $\eta_1^1 = 4 - 2\sin(2\pi t)$, $\eta_2^1 = 1$, $G_1(z_1) = z_1$, and $H_1(z_2) = z_2$. Let initial condition be $x_j^i = 0$, $y_j^i = 0$, $z_1(0) = 0$ and $z_2(0) = 1$. Note that all the parameters are periodic with a common period $T = 1$. It can be seen in Fig. 7.4 that every trajectory converges to a periodic function with period one.

7.3.6 Effect of parameters

In this subsection, we analyze the effect of change in parameters on the network using a theoretical framework that is well explained through simple examples.

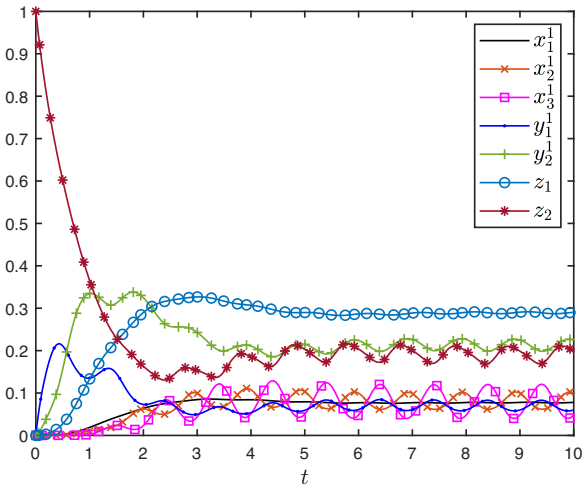

Figure 7.4: Trajectories of the PRFMNTP in Example 7.3.2 as a function of time. Each state variable converges to a periodic solution having period one.

Without loss of generality, we analyze the effect of change in the transition rate at a single site of an RFMX on the steady-state point of the network and presume that the change is in one of the transition rates in the RFMX #1. Let $\lambda \coloneqq [\lambda_0^1 \cdots \lambda_{\ell_1}^1 \;\; \lambda_0^2, \cdots \lambda_{\ell_2}^2 \cdots \lambda_0^m \cdots \lambda_{\ell_m}^m]$ and $\eta \coloneqq [\eta_0^1 \cdots \eta_{p_1}^1 \;\; \eta_0^2 \cdots \eta_{p_2}^2 \cdots \eta_0^n \cdots \eta_{p_n}^n]$.

Theorem 7.3.3. *Consider an RFMNTP with m RFMXs having dimensions $\ell_1, \ell_2, \ldots, \ell_n$ and n RFMYs having dimensions $p_1, p_2, \ldots, p_n$. Let $\mathcal{P} = [\lambda \;\; \eta]'$ denote the set of all parameters of the RFMNTP. Fix $r > 0$ and let e denote the unique steady-state point of the RFMNTP in the level set L_r of Q. Pick $k \in \{0, 1, \ldots, \ell_1\}$ and suppose that we modify λ_k^1 to $\bar{\lambda}_k^1$ with $\lambda_k^1 < \bar{\lambda}_k^1$. Let $\bar{e}$ denote the steady-state point in the new RFMNTP. Then*

$$\bar{e}_{x_k}^1 < e_{x_k}^1 \quad \text{and} \quad e_{x_j}^1 < \bar{e}_{x_j}^1 \quad \text{for all} \quad j \in \{k+1, \ldots, \ell_1\}. \tag{7.22}$$

Also, either one of the following cases holds:

1. $e_{z_1} < \bar{e}_{z_1}$, $e_{z_2} < \bar{e}_{z_2}$, $e_{x_j}^i < \bar{e}_{x_j}^i$ *for all* $i \in \{2, 3, \ldots, m\}$, $j \in \{1, 2, \ldots, \ell_i\}$ *and* $e_{y_j}^i < \bar{e}_{y_j}^i$ *for all* $i \in \{1, 2, \ldots, n\}$, $j \in \{1, 2, \ldots, p_i\}$.

2. $\bar{e}_{z_1} < e_{z_1}$, $e_{z_2} < \bar{e}_{z_2}$, $\bar{e}_{x_j}^i < e_{x_j}^i$ *for all* $i \in \{2, 3, \ldots, m\}$, $j \in \{1, 2, \ldots, \ell_i\}$ *and* $e_{y_j}^i < \bar{e}_{y_j}^i$ *for all* $i \in \{1, 2, \ldots, n\}$, $j \in \{1, 2, \ldots, p_i\}$.

3. $\bar{e}_{z_1} < e_{z_1}$, $\bar{e}_{z_2} < e_{z_2}$, $\bar{e}_{x_j}^i < e_{x_j}^i$ *for all* $i \in \{2, 3, \ldots, m\}$, $j \in \{1, 2, \ldots, \ell_i\}$ *and* $\bar{e}_{y_j}^i < e_{y_j}^i$ *for all* $i \in \{1, 2, \ldots, n\}$, $j \in \{1, 2, \ldots, p_i\}$.

4. $e_{z_1} = \bar{e}_{z_1}$, $e_{z_2} < \bar{e}_{z_2}$, $e_{x_j}^i = \bar{e}_{x_j}^i$ *for all* $i \in \{2, 3, \ldots, m\}$, $j \in \{1, 2, \ldots, \ell_i\}$ *and* $e_{y_j}^i < \bar{e}_{y_j}^i$ *for all* $i \in \{1, 2, \ldots, n\}$, $j \in \{1, 2, \ldots, p_i\}$.

5. $\bar{e}_{z_1} < e_{z_1}$, $e_{z_2} = \bar{e}_{z_2}$, $\bar{e}^i_{x_j} < e^i_{x_j}$ *for all* $i \in \{2, 3, \ldots, m\}$, $j \in \{1, 2, \ldots, \ell_i\}$ *and* $e^i_{y_j} = \bar{e}^i_{y_j}$ *for all* $i \in \{1, 2, \ldots, n\}$, $j \in \{1, 2, \ldots, p_i\}$.

Clearly, the above theorem lists all the possible cases of the effect of modifying the transition rate λ^1_k on the steady-state densities of the remaining RFMXs, all the RFMYs, and the pools. However, it does not give any information on the modified steady-state densities in sites $\{1, \ldots, k-1\}$ of RFMX #1. Note that the theorem also exhibits how the output rates in all the RFMXs and RFMYs change. The next example demonstrates the scenario when modifying a slow site increases the output rates of all lanes.

Example 7.3.3. Consider an RFMNTP with $m = 1$ RFMX with dimension $\ell_1 = 10$ and $n = 2$ RFMYs with dimensions $p_i = 5$ for $i = 1, 2$. Assume that $\lambda^1_j = 1$ for $i = 1$, $j = 1, 2, \ldots, \ell_i$, $\eta^i_j = 1$ for $i = 1, 2$ and $j = 1, 2, \ldots, p_i$, $G_1(z_1) = z_1$, and $H_i(z_2) = z_2$ for $i = 1, 2$. Let initial point is $x^i_j = 0$, $y^i_j = 0$, $z_1(0) = 0.2$ and $z_2(0) = 0.2$. We simulate the system until steady-state for a range of values of λ^1_5. It can be seen in Fig. 7.5a that we have $e_{z_1} < \bar{e}_{z_1}$ and $e_{z_2} < \bar{e}_{z_2}$. Note that when λ^1_5 is small it is the only bottleneck rate in the RFMX and increasing it allows more particles to traverse RFMX more quickly. Hence, this increases the output flow rate of the RFMX, and subsequently, the Pool II density increases. This further increases the output rates of all the RFMYs and thus increases the Pool I density.

It has been previously reported that due to environmental change, stress conditions, or pathological conditions, there could be particle stalling leading to an increase in a traffic jam in a track resulting in a decrement in output rates of other tracks [49]. However, in our model, resource sharing is based on the concept that the entry rate is impacted by the neighboring particles and this can lead to both effects: a decrease in output rates from some of the tracks and an increase in output rates from others. The next example demonstrates this.

Example 7.3.4. Consider an RFMNTP with $m = 1$ RFMX with dimension $\ell_1 = 20$ and $n = 1$ RFMY with dimension $p_1 = 10$. Assume that $\lambda^1_j = 1$ for $i = 1$, $j = 1, 2, \ldots, \ell_i$ except $\lambda^1_7 = 0.1$, $\eta^i_j = 1$ for $i = 1$ and $j = 1, 2, \ldots, p_i$, $G_1(z_1) = z_1$, and $H_1(z_2) = z_2$. Consider an initial condition $x^i_j = 0$, $y^i_j = 0$, $z_1(0) = 4$ and $z_2(0) = 4$. We simulate the system until steady-state for a range of values of λ^1_5. It can be seen in Fig. 7.5b that we have $\bar{e}_{z_1} < e_{z_1}$ and $e_{z_2} < \bar{e}_{z_2}$. This can be explained as follows. Note that, when λ^1_7 is the bottleneck rate in the RFMX, increasing λ^1_5 only generates more traffic jams along RFMX. This depletes the Pool I density. However, in this case, the number of particles increases on the RFMX and thus the output flow rate of the RFMX increases, and subsequently, the Pool II density increases.

The following example exhibits the scenario in which increasing any of the transition rates in a specific lane yields an increase in the output rate of this lane, and the output rates in the other lanes all decrease.

Example 7.3.5. Consider an RFMNTP with $m = 2$ RFMX with dimensions $\ell_1 = 10$, $\ell_2 = 5$ and $n = 2$ RFMYs with dimensions $p_i = 5$ for $i = 1, 2$. Assume that $\lambda_j^i = 1$ for $i = 1, 2$, $j = 1, 2, \ldots, \ell_i$, $\eta_j^i = 1$ for $i = 1, 2$ and $j = 1, 2, \ldots, p_i$, $G_i(z_1) = z_1$, and $H_i(z_2) = z_2$ for $i = 1, 2$. Consider an initial condition $x_j^i = 0$, $y_j^i = 0$, $z_1(0) = 4$ and $z_2(0) = 4$. We simulate the system until steady-state for a range of values of λ_5^1. It can be seen in Fig. 7.5c that we have $\bar{e}_{z_1} < e_{z_1}$ and $\bar{e}_{z_2} < e_{z_2}$. This can be understood by the following explanation. Increasing λ_5^1 leads to the formation of traffic jams along RFMX #1 due to the bottleneck rate λ_7^1. This depletes Pool I and decreases the output rate of RFMX #2. So, there is a trade-off between the output values of both RFMXs i.e., whether the rate of increment of the output of RFMX #1 is higher than the rate of decrement of RFMX #2. Depending upon the parameters of the RFMNTP, it can be seen in Fig. 7.5c that Pool II density decreased due to the overall decrease in the total output rates from both RFMXs.

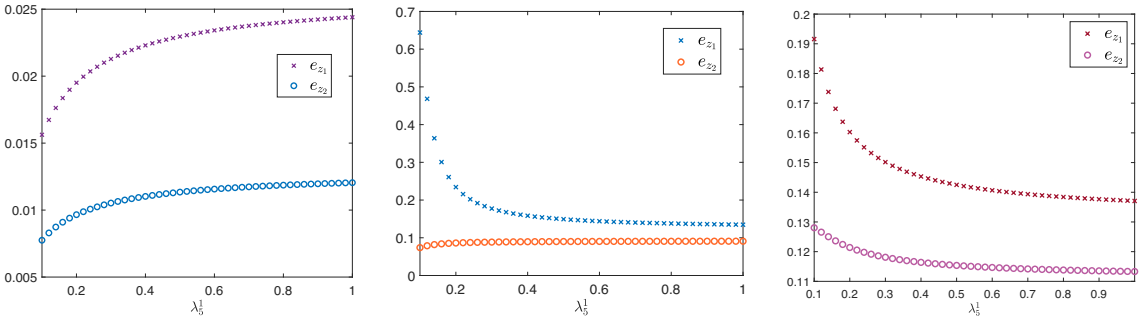

(a) (b) (c)

Figure 7.5: The steady-state pool densities for various values of transition rate λ_5^1 in the RFMX #1 of the RFMNTP considered in (a) Example 7.3.3 (b) Example 7.3.4 (c) Example 7.3.5.

The next result provides specific information for the case when there is a single RFMX in the network.

Corollary 7.3.3.1. *Consider an RFMNTP with $m = 1$ RFMX and n RFMYs. Pick $k \in \{0, 1, \ldots, \ell_1\}$ and suppose that λ_k^1 is changed to $\bar{\lambda}_k^1$ with $\lambda_k^1 < \bar{\lambda}_k^1$. Then*

$$\bar{e}_{x_k}^1 < e_{x_k}^1 \quad \text{and} \quad e_{x_j}^1 < \bar{e}_{x_j}^1 \quad \text{for all} \quad j \in \{k+1, \ldots, \ell_1\}, \tag{7.23}$$

$$e_{z_2} < \bar{e}_{z_2}, \quad \text{and} \quad e_{y_j}^i < \bar{e}_{y_j}^i \quad \text{for all} \quad i \in \{1, 2, \ldots, n\}, j \in \{1, 2, \ldots, p_i\}. \tag{7.24}$$

The following result implies that we can study steady-state properties of a

network of m identical RFMXs and m identical RFMYs by a much simpler network consisting of only a single RFMX and a single RFMY.

Proposition 7.3.3. *Consider the following two RFMNTPs:*
(a) An RFMNTP with m identical RFMXs each having length ℓ, rates $\lambda_0, \lambda_1 \ldots, \lambda_\ell$ and m identical RFMYs each having length p, rates $\eta_0, \eta_1 \ldots, \eta_p$. Let the output function G of Pool I and H of Pool II be homogeneous functions of degree 1. Let $r > 0$ be the total density of particles in the network and e denote its steady-state point.
(b) An RFMNTP with a single RFMX of length ℓ, rates $(m\lambda_0), \lambda_1 \ldots, \lambda_\ell$ and a single RFMY of length p, rates $(mn\eta_0), \eta_1 \ldots, \eta_p$. Let the output function G of Pool I and H of Pool II be homogeneous functions of degree 1. Let r/m be the total density of particles in the network and $\tilde{e} = [\tilde{e}_{x_1} \;\; \tilde{e}_{x_2} \cdots \tilde{e}_{x_\ell} \;\; \tilde{e}_{y_1} \;\; \tilde{e}_{y_2} \cdots \tilde{e}_{y_p} \;\; \tilde{e}_{z_1} \;\; \tilde{e}_{z_2}]'$ denote its steady-state point.
Then we have

$$e^i_{x_j} = \tilde{e}_{x_j} \quad \textit{for all} \quad i = 1, 2, \ldots, m, j = 1, 2, \ldots \ell, \tag{7.25}$$

$$e^i_{y_j} = \tilde{e}_{y_j} \quad \textit{for all} \quad i = 1, 2, \ldots, m, j = 1, 2, \ldots p, \tag{7.26}$$

and

$$e_{z_1} = m\tilde{e}_{z_1} \;\; \textit{and} \;\; e_{z_2} = m\tilde{e}_{z_2}. \tag{7.27}$$

7.3.7 Mapping of the RFMNP to RFMNTP

In this section, we show that the RFMNP is a special case of our model RFMNTP. The RFMNP has been used for analyzing the competition of ribosomes in the translation process. It assumes that the ribosomes that are located far away will also impact the initiation rates of the mRNAs and therefore include several RFMs interconnected via a single pool of free particles. All the RFMs feed the pool and the pool feeds the entry locations in all the RFMs. In this section, we show that the model RFMNP can be studied by the model RFMNTP i.e., we can construct the model RFMNP through RFMNTP as illustrated in the next paragraph.

Consider an RFMNP having m RFMs with dimensions ℓ_i, rates λ^i_j, state variables x^i_j, a pool with density z, and the first integral having value $(1/2)Q(0)$. Construct an RFMNTP having m RFMXs and m RFMYs with the assumption $\ell_i = p_i$ for all $i = 1, 2, \ldots, m$, $\lambda^i_j = \eta^i_j$ for all $i = 1, 2, \ldots, m$, $j = 0, 1, \ldots, \ell_i$, $G_i = H_i$ for each $i = 1, 2 \ldots, m$ and having the first integral $Q(0)$. We shall show that both Pool I and Pool II steady-state density value is the same i.e., $e_{z_1} = e_{z_2}$. Suppose on the contrary $e_{z_1} < e_{z_2}$. Note that G_i is well defined and strictly increasing function and this implies $G_i(e_{z_1}) < G_i(e_{z_2})$ for all i. Since each RFMY is a copy of an

RFMX, respectively, therefore, we have $e^i_{x_{\ell_i}} < e^i_{y_{\ell_i}}$ for all i and this implies that $\sum_{i=1}^{m} \lambda^i_{\ell_i}(e^i_{y_{\ell_i}} - e^i_{x_{\ell_i}}) > 0$ which is a contradiction to Eq. (7.17) in our case. Hence, $e_{z_1} = e_{z_2}$ which implies that the steady-state densities of each RFMX $\#i$ are the same as of each RFMY $\#i$, respectively. Therefore, our system becomes equivalent to the given one-pool network RFMNP.

7.3.8 Monte Carlo simulations(MCs)

It has been shown that RFM and Monte Carlo simulations (TASEP with parallel update rule) provide highly correlated predictions for a large set of parameters [38]. In this section, we compare the steady states of the RFMNTP with the Monte Carlo simulations. This supports the modeling of the network of RFMs with two pools.

We validate our model by performing Monte Carlo simulations with a parallel update scheme. Each site is occupied with atmost one particle and the particle advances to the consecutive site if it is time to hop. The hopping times between consecutive sites of lanes receiving inputs from Pool I is exponentially distributed with parameters $\lambda^i_1, \lambda^i_2, \ldots, \lambda^i_{\ell_i}$, i.e., the next hopping time at site j of lane i is $t + e(\lambda^i_j)$ where t is the current time and $e(\lambda^i_j)$ is randomly generated from the exponential distribution with mean parameter λ^i_j and the hopping time for the particle to hop to site 1 of lane i is calculated as $t + e(\lambda^i_0 G_i(z_1))$ where z_1 is the number of particles present in Pool I at time t. Similarly, the hopping times between consecutive sites of lanes receiving inputs from Pool II are exponentially distributed with parameters $\eta^i_1, \eta^i_2, \ldots, \eta^i_{p_i}$ the hopping time for the particle to hop to site 1 of lane i is calculated as $t + e(\lambda^i_0 H_i(z_2))$ where z_2 is the number of particles present in Pool II at time t. A simulation begins with an empty chain with all the particles distributed arbitrarily in the pools and continues for 10^7 time steps. After removing the initial 10^4 steps from the calculation, the steady-state density of each site is calculated as the number of time steps it was occupied divided by the overall simulation runtime. In the example below, we show that simulations match the model RFMNTP.

Example 7.3.6. Consider an RFMNTP with $m = 2$ RFMXs having dimensions $\ell_1 = 10$, $\ell_2 = 15$, $n = 1$ RFMY having dimension $p_1 = 15$, $\lambda^i_0 = 1$, $\lambda^1_j = 1 + \theta_j$, where θ_j is a random variable uniformly distributed in the interval $(0, 1)$, $\lambda^2_j = 2 + \theta_j$, $\eta^1_0 = 1$, $\eta^1_j = 5 + \theta_j$, $G_i(z_1) = z_1$, $H_i(z_2) = z_2$, and first integral having value 7. It can be observed in Fig. 7.6 that the steady-state density profile of the RFMNTP and the Monte Carlo simulations match well with each other.

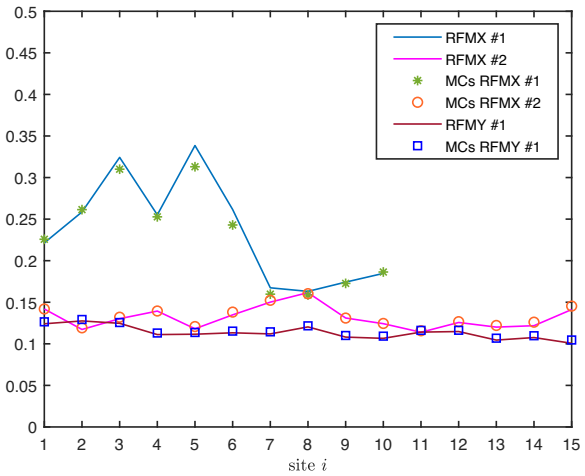

Figure 7.6: The steady-state density as a function of the site number for RFMXs and RFMYs in the RFMNTP in Example 7.3.6. Solid lines and symbols denote numerically simulated RFMNTP and Monte Carlo simulations, respectively.

7.4 Analyzing a network with multiple pools

Consider a network consisting of M pools and N RFMs having interconnections via the pools. One can extend the analysis done in the section §7.3.1 to show that the network admits a continuum of steady-state points. The following example demonstrates the dynamic behavior of the network with three pools.

Example 7.4.1. Consider a network of three RFMs, each with dimension 2, having three pools. Suppose RFM #1 receives its input from Pool #1 and supplies its output to Pool #2, RFM #2 receives its input from Pool #2 and supplies its output to Pool #3, and RFM #3 receives its input from Pool #3 and supplies its output to Pool #1. Assume that $\lambda_0^1 = 0.8$, $\lambda_1^1 = 1$, $\lambda_2^1 = 2$, $\lambda_0^2 = 1$, $\lambda_1^2 = 1.2$, $\lambda_2^2 = 0.1$, $\lambda_0^3 = 0.1$, $\lambda_1^3 = 0.5$, $\lambda_2^3 = 1$, $G_1(z_1) = \tanh(z_1)$, $G_2(z_2) = \tanh(z_2)$, and $G_3(z_3) = z_3$. There exist an unique equilibrium point e in L_4 and after calculation we have $e = [0.09514 \quad 0.04541 \quad 0.8249 \quad 0.9082 \quad 0.1998 \quad 0.0908 \quad 0.12613 \quad 0.5745 \quad 1.1350]'$. Figures 7.7a and 7.7b depict trajectories of RFMNTP for initial conditions in the level set L_4: $[0.5\ 0.5\ 0.5\ 0.5\ 0.5\ 0.5\ 0\ 0\ 1]'$ and $[0\ 0\ 0\ 0\ 0\ 0\ 1.5\ 1.5\ 1]'$, respectively. It can be observed that each of these trajectories converges to e.

Next, we understand the effect of modifying a transition rate of a site in an RFM on the entire network by analyzing the steady-state densities.
Eq. (7.4) at steady-state e is given as:

$$\lambda_0^k G_k(e_{z_j})(1 - e_{x_1}^k) = \lambda_1^k e_{x_1}^k (1 - e_{x_2}^k) = \cdots = \lambda_{n_k}^k e_{x_{n_k}}^k. \tag{7.28}$$

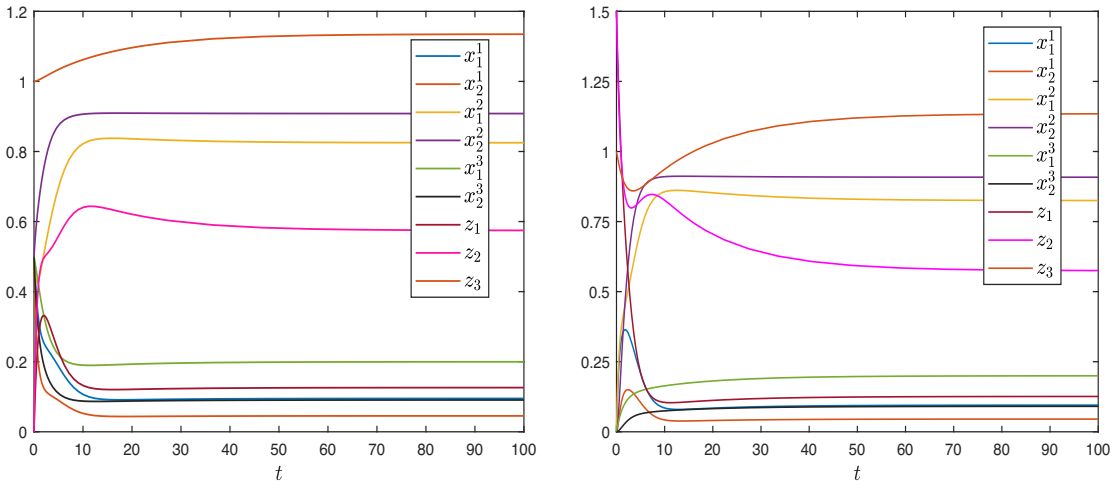

(a) (b)

Figure 7.7: Trajectories of the network with three pools in Example 7.4.1: (a) For initial condition $[0.5\ 0.5\ 0.5\ 0.5\ 0.5\ 0.5\ 0\ 0\ 1]'$ and (b) For initial condition $[0\ 0\ 0\ 0\ 0\ 0\ 1.5\ 1.5\ 1]'$.

Eq. (7.5) at steady-state e is given as

$$\sum_{k' \in \mathcal{I}'} \lambda_{n_{k'}}^{k'} e_{x_{n_{k'}}}^{k'} = \sum_{k \in \mathcal{I}} \lambda_0^k G_k(e_{z_j})(1 - e_{x_1}^k). \tag{7.29}$$

Rewriting the above equation we get,

$$\sum_{k' \in \mathcal{I}'} \lambda_{n_{k'}}^{k'} e_{x_{n_{k'}}}^{k'} = \sum_{k \in \mathcal{I}} \lambda_{n_k}^{k} e_{x_{n_k}}^{k}. \tag{7.30}$$

WLOG, we assume that Pool #1 is feeding the RFM #1 and there is an increment in the rate λ_k^1 of RFM #1. Let $\bar{e}$ represent the steady state of the modified network. Then by arguing similarly as in the proof of the Theorem 7.3.3, we get the information that $\bar{e}_{x_k}^1 < e_{x_k}^1$ and $e_{x_j}^1 < \bar{e}_{x_j}^1$ for all $j \in \{k+1, \ldots, n_1\}$. The steady-state densities of the RFMs and the pools associated directly with Pool #1 follow the cases mentioned in the Theorem 7.3.3 depending on the various parameter values. The change in the steady-state densities of the other pools depends on the total input it is receiving from the RFMs and can be analyzed through Eq. (7.30). Also, the case when $e_{z_1} < \bar{e}_{z_1}$ and $\bar{e}_{z_j} < e_{z_j}$ for any $j \in \{1, 2, \ldots, M\}$ is not possible as argued in Theorem 7.3.3. This is a brief outline to gain an understanding of how the network with multiple pools behaves as the exact scenario will be more clear when we know the interconnections between the RFMs via the pools.

In order to verify that the high correlation between the model and Monte Carlo simulations holds for a large set of parameters, we ran 250 tests, wherein each test a new set of rates are drawn randomly.

Example 7.4.2. Consider a network with $M = 3$ pools and $N = 3$ RFMs having dimensions $n_1 = 20$, $n_2 = 30$, $n_3 = 40$, where RFM #1/RFM #2/RFM #3 receives its input from Pool #1/Pool #2/Pool #3 and supplies its output to Pool #2/Pool #3/Pool #1. Assume that $\lambda_0^i = 1$, $\lambda_j^1 = 0.5 + \theta_j$, $\lambda_j^2 = 2 + \theta_j$, $\lambda_j^3 = 1 + \theta_j$ where θ_j is a random variable uniformly distributed in the interval $(0, 1)$, $G_i(z_j) = z_j$, and first integral having value 6. Fig. 7.8 depicts the correlations between the steady-state mean densities (ρ) of the RFMs and the steady-state mean densities (σ) calculated through Monte Carlo simulations. It can be seen that the correlation between the two is high ($r \simeq 0.919633$).

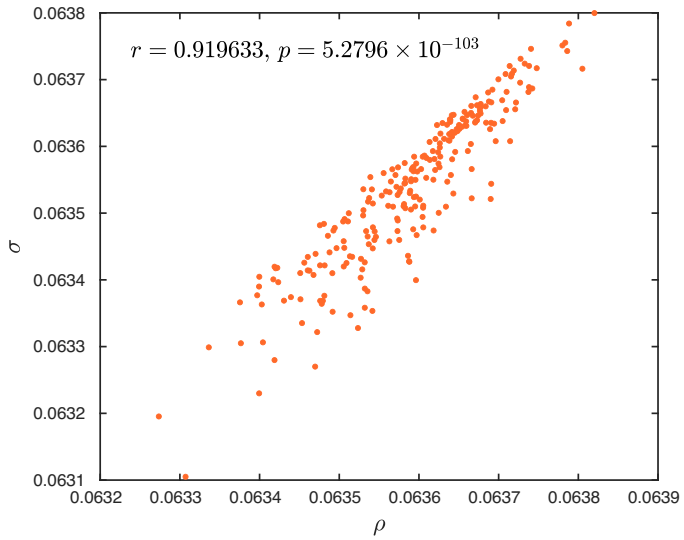

Figure 7.8: Steady-state mean densities (numerically simulated ρ and Monte Carlo simulated σ) , and the corresponding Pearson's correlation coefficient r and p-value in Example 7.4.2.

7.5 Discussion

Various transport phenomena involve the movement of particles along some tracks, for example, there is movement of RNA polymerases along DNA molecules, movement of ribosomes along mRNA molecules, motor proteins move along microtubules in order to transport cargo from one location to another, data packets move along buffers, there is the movement of vehicles along roads and many more. In all these systems, the particles are moving on a network of interconnected lanes in several transport systems. A common attribute in such phenomena is the presence of finite resources generating a closed network. The RFM was developed for analyzing the excluded flow of particles along a one-dimensional isolated track and it provides a useful and versatile modeling component that helps to understand the complex networks of the cellular as well as physical processes.

The network models consisting of a single pool are used to describe the behavior of the system when the particles are distributed uniformly throughout the system. These single-pool models, however, do not take into account the distribution of particles in a local neighborhood and hence are not been able to model the movement of resources between different pools, for instance, the movement of cars (resources) between the two cities (pools). We introduced a new network model, RFMNTP, composed of several RFMs that focused on analyzing how the network behaves when only the nearby resources impact the entry rates of its target. The RFMNTP is a closed network consisting of RFMs strategically connected to two pools such that Pool I (Pool II) feeds the input of some of the RFMs (remaining RFMs) and the output of them is fed into Pool II (Pool I). In other words, the first sites of some of the lanes and the last sites of the remaining lanes are connected to the same pool.

Understanding the stability of a system is a fundamental and foremost aspect of analyzing systems in various fields of study. In this context, it is important to understand the stability of our network to predict its long-term behavior. We prove that the RFMNTP is a cooperative irreducible dynamical system that admits a non-trivial first integral and thus enjoys several dynamical properties. In particular, The RFMNTP admits a continuum of steady-state points and it entrains to periodic excitations in the parameters. Our theoretical analysis shows that an increase in the transition rate of a site in an RFM has a non-trivial effect on the output rates of the other RFMs. It can lead to any of the scenarios: the output rate of all the other RFMs increase or decrease; an increase in output rates of some of the RFMs and a decrease in output rates of the other RFMs. The specific outcome can be predicted by simulating the RFMNTP.

A noteworthy observation is that there could be a simultaneous increase in the output rates of some of the RFMs and a decrease in the output rates of the other RFMs. In the previous network model [49], we have seen that an increase in a transition rate in an RFM in the presence of a bottleneck rate leads to a decrease in the output rate of the other RFMs, whereas we can see in Example 3.4 that this may not hold due to aspect of local sharing of particles incorporated through two pools. Next, we have illustrated how to gain an understanding of how the changes in an RFM affect other RFMs and the overall behavior of the network with multiple pools.

The model described here can be generalized to capture more complicated features. For example, the output of the shorter lanes can be fed back into the same pool. This phenomenon may be studied by adding its output rate to the same pool. The RFM also provides an analytical framework for modeling and analyzing linear communication networks [45]. In this context, the moving particles are data

packets, the chain of sites is a one-dimensional chain of ordered buffers, and the decreasing entry rate to a fuller buffer represents a kind of decentralized backpressure flow control. Another research direction is to analyze networks, comprising multiple flows that share common nodes, using a set of interconnected RFMs, constraining the link capacities in the communication networks. An applicability of our model can be to analyze a network topology where a common source node is linked to several chains of ordered buffers. The output of these chains at the destination node can be a source node for other sets of chains of ordered buffers and so on. One may also generalize RFMNTP by considering nearest-neighbor interactions in the network as seen in molecular motor traffic. Another interesting direction is to try and validate our predictions about the local behavior of the cellular environment experimentally.

7.6 Appendix: Proofs

Proof of Proposition 7.3.2: For simplicity, we consider RFMNTP with one RFMX and one RFMY. Let $x_j^1 \coloneqq x_j$ and $y_j^1 \coloneqq y_j$. Also, let $x_0 \coloneqq z_1$, $x_{\ell+1} \coloneqq z_2$, $x_{\ell+j+1} \coloneqq y_j$ for $j = 1, 2, \ldots, p$ and $x_{-1} \coloneqq x_{\ell+p+1}$. We now show that the system with state-variables $x_0, \ldots, x_{\ell+p+1}$ satisfies the cyclic boundary-repelling (CBR) property described in Chapter 1 (i.e., for any $\delta > 0$ and any sufficiently small $\triangle > 0$, $\exists\ P = P(\delta, \triangle) > 0$ such that for each $k = 1, \ldots, \ell + p + 1$ and each $t \geq 0$ the condition $x_k(t) \leq \triangle$ and $x_{k-1}(t) \geq \delta$ implies that $\dot{x}_k \geq P$).

For $k = 0$, we have $\dot{x}_0 = \eta_p x_{\ell+p+1} - \lambda_0 G(x_0)(1 - x_1) \geq \eta_p \delta - \lambda_0 G(\triangle)(1 - x_1)$, and we have $G(0) = 0$, G is a continuous function and thus $\dot{x}_0 \geq \eta_p \delta/2$ for all $\triangle > 0$ sufficiently small.

Now for $k = 1$, we have $\dot{x}_1 = \lambda_0 G(z_1)(1 - x_1) - \lambda_1 x_1(1 - x_2) \geq \lambda_0 G(\delta)(1 - \triangle) - \lambda_1 \triangle(1 - x_2)$, so $\dot{x}_1 \geq \lambda_0 G(\delta)/2$ for all $\triangle > 0$ sufficiently small.

For $k \in \{2, \ldots, \ell\}$, we have $\dot{x}_k = \lambda_{k-1} x_{k-1}(1 - x_k) - \lambda_k x_k(1 - x_{k+1}) \geq \lambda_k \delta(1 - \triangle) - \lambda_k \triangle(1 - x_{k+1})$, and therefore $\dot{x}_k \geq \lambda_k \delta/2$ for all $\triangle > 0$ sufficiently small.

For $k = \ell+1$, we have $\dot{x}_{\ell+1} = \lambda_\ell x_\ell - \eta_0 H(x_{\ell+1})(1 - x_{\ell+2}) \geq \lambda_\ell \delta - \eta_0 H(\triangle)(1 - x_{\ell+2})$, and we have $H(0) = 0$, H is a continuous function and thus $\dot{x}_{\ell+1} \geq \lambda_\ell \delta/2$ for all $\triangle > 0$ sufficiently small.

Now for $k = \ell + 2$, we have $\dot{x}_{\ell+2} = \eta_0 H(z_2)(1 - x_{\ell+2}) - \eta_1 x_{\ell+2}(1 - x_{\ell+3}) \geq \eta_0 H(\delta)(1 - \triangle) - \eta_1 \triangle(1 - x_{\ell+3})$, so $\dot{x}_{\ell+2} \geq \eta_0 H(\delta)/2$ for all $\triangle > 0$ sufficiently small.

For $k \in \{\ell + 3, \ldots, \ell + p + 1\}$ we have $\dot{x}_k = \eta_{k-1} x_{k-1}(1 - x_k) - \eta_k x_k(1 - x_{k+1}) \geq \eta_k \delta(1 - \triangle) - \eta_k \triangle(1 - x_{k+1})$, and therefore $\dot{x}_k \geq \eta_k \delta/2$ for all $\triangle > 0$ sufficiently small. Thus, the RFMNTP satisfies CBR.

Also, observe that that if $x_k(t) > 0$ and $t > 0$ then $x_k(T) > 0$ for all $T \geq t$. It now follows from the result [Lemma 1] on repelling boundaries and persistence in Ref. [49]) that for any $\tau > 0$ there exists $\epsilon_1(\tau) > 0$, with $\epsilon_1(\tau) \to 0$ as $\tau \to 0$, such that for any non-zero initial condition and any $t \geq \tau$ the solution of the RFMNTP satisfies

$$\epsilon_1 \leq x_i(t), \quad \text{for all } i \in \{0, \ldots, \ell + p + 1\}. \tag{7.31}$$

For the other part of the equality, define $u_i(t) \coloneqq 1 - x_{\ell+1-i}(t)$ for $i = 1, 2, \ldots, \ell$ and $v_i(t) \coloneqq 1 - y_{p+1-i}(t)$ for $i = 1, 2, \ldots, p$. From Eq. (7.31), we have $z_1 \geq \epsilon_1$ and $z_2 \geq \epsilon_1$ for all $t \geq \tau$. Note that the system with state variables $u_1, u_2, \ldots, u_\ell$ are an RFM having time-varying exit rate $\lambda_0 G(z_1)$ and the system with state variables $v_1, v_2, \ldots, v_p$ are an RFM having time-varying exit rate $\eta_0 H(z_2)$. Therefore, $\exists\ \epsilon_2(\tau) > 0$ and $\epsilon_3(\tau) > 0$ such that any $t \geq \tau$, we have $\epsilon_2 \leq u_i(t)$, for all $i \in \{1, \ldots, \ell\}$ and $\epsilon_3 \leq v_i(t)$, for all $i \in \{1, \ldots, p\}$. Combining this with the definition of u_i and v_i completes the proof.

Proof of Theorem 7.3.1: We have that the RFMNTP is a cooperative irreducible system on $\text{int}(\mathcal{B})$ with a non-trivial first integral. Combining this with Proposition 7.3.2 and the results in Ref. [153][see Theorems 10 and 11] completes the proof of this theorem.

Proof of Theorem 7.3.2: From the Proposition 7.3.2, it follows that $\phi_r \in \text{int}(\mathcal{B})$ and the results in Ref. [143] [see Theorem 3.1] prove this theorem.

Proof of Theorem 7.3.3: At steady-state we have

$$\sum_{i=1}^{m}\sum_{j=1}^{\ell_i} e^i_{x_j} + \sum_{i=1}^{n}\sum_{j=1}^{p_i} e^i_{y_j} + e_{z_1} + e_{z_2} = r \tag{7.32}$$

and this also holds for the modified network since the initial condition is the same i.e.,

$$\sum_{i=1}^{m}\sum_{j=1}^{\ell_i} \bar{e}^i_{x_j} + \sum_{i=1}^{n}\sum_{j=1}^{p_i} \bar{e}^i_{y_j} + \bar{e}_{z_1} + \bar{e}_{z_2} = r. \tag{7.33}$$

Pick $k \in \{1, 2, \ldots, \ell_1 - 1\}$. Let us assume that

$$\bar{e}^1_{x_{\ell_1}} \leq e^1_{x_{\ell_1}}. \tag{7.34}$$

Then the Eq. (7.14) implies that

$$\lambda^1_{\ell_1-1}\bar{e}^1_{x_{\ell_1-1}}(1 - \bar{e}^1_{x_{\ell_1}}) \leq \lambda^1_{\ell_1-1}e^1_{x_{\ell_1-1}}(1 - e^1_{x_{\ell_1}}). \tag{7.35}$$

From Eq. (7.34), the above equation implies that $\bar{e}^1_{x_{\ell_1-1}} \leq e^1_{x_{\ell_1-1}}$. Continuing this way, we have

$$\bar{e}^1_{x_j} \leq e^1_{x_j} \quad \text{for all } j = k+1, k+2, \ldots, \ell_j. \tag{7.36}$$

Now, from Eq. (7.14) consider

$$\bar{\lambda}^1_k \bar{e}^1_{x_k}(1 - \bar{e}^1_{x_{k+1}}) \leq \lambda^1_k e^1_{x_k}(1 - e^1_{x_{k+1}}). \tag{7.37}$$

We have $\lambda^1_k < \bar{\lambda}^1_k$, thereby Eq. (7.37) implies that

$$\bar{\lambda}^1_k \bar{e}^1_{x_k}(1 - \bar{e}^1_{x_{k+1}}) < \bar{\lambda}^1_k e^1_{x_k}(1 - e^1_{x_{k+1}}). \tag{7.38}$$

which implies $\bar{e}^1_{x_k} < e^1_{x_k}$. From Eq. (7.14) we have

$$\lambda^1_{k-1} \bar{e}^1_{x_{k-1}}(1 - \bar{e}^1_{x_k}) < \lambda^1_{k-1} e^1_{x_{k-1}}(1 - e^1_{x_k}). \tag{7.39}$$

Now, since $\bar{e}^1_{x_k} < e^1_{x_k}$, we must have $\bar{e}^1_{x_{k-1}} < e^1_{x_{k-1}}$. Continuing in this way, we get

$$\bar{e}^1_{x_j} < e^1_{x_j} \quad \text{for all } j = 1, 2, \ldots, k-2. \tag{7.40}$$

This also implies that $\bar{e}_{z_1} < e_{z_1}$. Since RFMX is a monotone control system and therefore we have

$$\bar{e}^i_{x_{\ell_j}} < e^i_{x_{\ell_j}} \quad \text{for all } i = 2, 3, \ldots, m \quad \text{and } j = 1, 2, \ldots, \ell_i. \tag{7.41}$$

Note that all the RFMYs are interconnected through the pool variable z_2 and hence all are affected in the same manner. From Eqs. (7.17),(7.34) and (7.41), we have

$$\bar{e}^i_{y_{\ell_j}} < e^i_{y_{\ell_j}} \quad \text{for all } i = 1, 2, \ldots, n \quad \text{and } j = 1, 2, \ldots, p_i. \tag{7.42}$$

and this implies $\bar{e}_{z_2} < e_{z_2}$ which yields the contradiction to the Eq. (7.33). Hence, $e^1_{x_{\ell_1}} < \bar{e}^1_{x_{\ell_1}}$. Now if $e^1_{x_k} \leq \bar{e}^1_{x_k}$, this implies that $e_{z_1} < \bar{e}_{z_1}$ which further implies $e^i_{y_{\ell_j}} < \bar{e}^i_{y_{\ell_j}}$ for all $i = 1, 2, \ldots, n$ and $j = 1, 2, \ldots, p_i$ and $e_{z_2} < \bar{e}_{z_2}$. This is again a contradiction to Eq. (7.33). Also, note that the case e_{z_1} is increasing and e_{z_2} is decreasing is not possible as this will lead to the contradiction to Eq. (7.17).
Now, consider $k = 0$. Let us assume that

$$\bar{e}^1_{x_{\ell_1}} \leq e^1_{x_{\ell_1}}. \tag{7.43}$$

Continuing as above we have

$$\bar{e}^1_{x_j} \leq e^1_{x_j} \quad \text{for all } j = 1, 2, \ldots, \ell_1 - 1. \tag{7.44}$$

Now, from Eq. (7.14) consider

$$\bar{\lambda}_0^1 G_1(\bar{e}_{z_1})(1-\bar{e}_{x_1}^1) \leq \lambda_0^1 G_1(e_{z_1})(1-e_{x_1}^1). \tag{7.45}$$

We have $\lambda_0^1 < \bar{\lambda}_0^1$ and thereby Eqs. (7.44) and (7.45) implies $\bar{e}_{z_1} < e_{z_1}$. Again using the above arguments we get the contradiction to Eq. (7.43).
Now, consider $k = \ell_1$. Then we have to show that $\bar{e}_{x_{\ell_1}}^1 < e_{x_{\ell_1}}^1$. Seeking a contradiction, assume

$$e_{x_{\ell_1}}^1 \leq \bar{e}_{x_{\ell_1}}^1. \tag{7.46}$$

Then Eq. (7.14) with the fact that $\lambda_{\ell_1}^1 < \bar{\lambda}_{\ell_1}^1$ implies that

$$\lambda_{\ell_1-1}^1 e_{x_{\ell_1-1}}^1 (1-e_{x_{\ell_1}}^1) < \lambda_{\ell_1-1}^1 \bar{e}_{x_{\ell_1-1}}^1 (1-\bar{e}_{x_{\ell_1}}^1). \tag{7.47}$$

From Eq. (7.46), the above equation implies that $e_{x_{\ell_1-1}}^1 < \bar{e}_{x_{\ell_1-1}}^1$. Continuing this way, we have

$$e_{x_j}^1 < \bar{e}_{x_j}^1 \quad \text{for all } j = 1, 2, \ldots, \ell_1 - 2. \tag{7.48}$$

This also implies that $e_{z_1} < \bar{e}_{z_1}$. Since RFMX is a monotone control system and therefore we have

$$e_{x_{\ell_j}}^i < \bar{e}_{x_{\ell_j}}^i \quad \text{for all } i = 2, 3, \ldots, m \quad \text{and } j = 1, 2, \ldots, \ell_i. \tag{7.49}$$

Note that all the RFMYs are interconnected through the pool variable z_2 and hence all are affected in the same manner. From Eqs. (7.17), (7.46), (7.49) and the fact that $\lambda_{\ell_1}^1 < \bar{\lambda}_{\ell_1}^1$, we have $e_{y_{\ell_j}}^i < \bar{e}_{y_{\ell_j}}^i$ for all $i = 1, 2, \ldots, n$ and $j = 1, 2, \ldots, p_i$. This implies $e_{z_2} < \bar{e}_{z_2}$ which yields the contradiction to the Eq. (7.33). Hence, $\bar{e}_{x_{\ell_1}}^1 < e_{x_{\ell_1}}^1$. This completes the proof of this theorem.

Proof of Proposition 7.3.3: The network considered in part (a) has identical RFMXs and hence the steady-state density profile of the RFMXs are same and similarly this holds for RFMYs. Without loss of generality, consider the steady-state equations for the RFMX #1 in (a):

$$\lambda_0 G(e_{z_1})(1-e_{x_1}^1) = \lambda_1 e_{x_1}^1 (1-e_{x_2}^1) = \cdots = \lambda_\ell e_{x_\ell}^1, \tag{7.50}$$

and the steady-state equation for the RFMY #1 in (a) is as follows:

$$\eta_0 H(e_{z_2})(1-e_{y_1}^1) = \eta_1 e_{y_1}^1 (1-e_{y_2}^1) = \cdots = \eta_p e_{y_p}^1. \tag{7.51}$$

Similarly, the steady-state equation for RFMX in (b):

$$m\lambda_0 G(\tilde{e}_{z_1})(1-\tilde{e}_{x_1}) = \lambda_1\tilde{e}_{x_1}(1-\tilde{e}_{x_2}) = \cdots = \lambda_\ell\tilde{e}_{x_\ell}, \tag{7.52}$$

and the steady-state equation for the RFMY in (b) is as follows:

$$m\eta_0 H(\tilde{e}_{z_2})(1-\tilde{e}_{y_1}) = \eta_1\tilde{e}_{y_1}(1-\tilde{e}_{y_2}) = \cdots = \eta_p\tilde{e}_{y_p}. \tag{7.53}$$

Now, consider Eqs. (7.50) and (7.52), suppose we have

$$\lambda_\ell e^1_{x_\ell} = \lambda_\ell\tilde{e}_{x_\ell} \tag{7.54}$$

$$\implies e^1_{x_i} = \tilde{e}_{x_i} \quad \text{for all} \quad i \tag{7.55}$$

and also

$$\lambda_0 G(e_{z_1})(1-e^1_{x_1}) = m\lambda_0 G(\tilde{e}_{z_1})(1-\tilde{e}_{x_1}) \tag{7.56}$$

$$\implies e_{z_1} = m\tilde{e}_{z_1}. \tag{7.57}$$

Similarly, we get

$$e^1_{y_i} = \tilde{e}_{y_i} \quad \text{for all} \quad i \quad \text{and } e_{z_2} = m\tilde{e}_{z_2}. \tag{7.58}$$

Now, the steady-state Eq. (7.12) for the network (a) is

$$m(e^1_{x_1} + e^1_{x_2} + \cdots + e^1_{x_\ell}) + m(e^1_{y_1} + e^1_{y_2} + \cdots + e^1_{y_p}) + e_{z_1} + e_{z_2} = r. \tag{7.59}$$

By Eqs. (7.55), (7.57) and (7.58), we get

$$\tilde{e}_{x_1} + \tilde{e}_{x_2} + \cdots + \tilde{e}_{x_\ell} + \tilde{e}_{y_1} + \tilde{e}_{y_2} + \cdots + \tilde{e}_{y_p} + \tilde{e}_{z_1} + \tilde{e}_{z_2} = r/m. \tag{7.60}$$

and this completes the proof of the proposition.

Chapter 8

Conclusion and future scopes

Numerous cellular processes involve the transportation of particles to different locations for material transport or cellular product synthesis. Gene translation, a fundamental process, entails ribosomes moving along mRNA molecules to generate functional proteins, making it one of the most energy-consuming processes. Predicting protein synthesis rates, ribosome densities, and related parameters has garnered significant interest among theoretical biologists. Models for translation analysis are introduced with diverse formulations at various levels of abstraction. A recent approach, the ribosome flow model (RFM), is a deterministic, continuous-time mathematical model for particle interaction flow. Its advantage lies in its amenability to rigorous mathematical analysis using systems and control theory tools, offering an improved predictive framework for systems and synthetic biology applications. Additionally, it finds utility in describing biological and physical processes such as molecular motor traffic, pedestrian dynamics, and vehicular traffic flow.

While the RFM serves as a foundational model, numerous generalizations have been developed to incorporate observed realistic features, including interactions between molecular motors, particle abortion along tracks, finite resource availability, extended particle size, and various stochasticity types within cells. However, the scope for extending these models is extensive, as several realistic features must be integrated to deepen our understanding of the process. Motivated by several experimentally observed features, this thesis focuses on model development and understanding the impact of these features on system dynamics. Dynamical properties such as invariance, persistence, stability, and entrainment are studied within this context, employing tools from cooperative dynamical systems, contraction theory, and random matrix theory.

8.1 Summary of results

The contents of Chapter 2 consider the variability in rates in a generalized version of RFM, called RFMD, which incorporates feature of different site sizes. The RFMD analyzes the motion of particles along a lattice having different size capacities

through a system of ordinary differential equations. Firstly, we analyze stochasticity in RFMD by assuming parameters as independent and identically distributed (i.i.d.) random variables. In this context, we prove that given a constant homogeneous site size [transition rate] as the dimension of the RFMD increases, the steady-state flow rate depends only on the size [rate] and the minimal value of the random variables modeling the transition rates [size sites]. Furthermore, in the case of finite dimension, the bounds for the steady-state flow rate are provided when transition rates [site sizes] are drawn from i.i.d. random variables and also in the most general case when the transition rates or site sizes are drawn from different distributions.

The next model introduced in Chapter 3 is a deterministic framework to study cellular phenomena involving interacting particles and is called the excluded flow of extended interacting objects with drop-off effect (EFEIOD). This model incorporates many biologically observed features including extended length of the particles, nearest-neighbor interactions, and the fact that particles can detach along the lattice. Using tools from contraction theory, we show that the model admits a unique steady state and entrains to periodic excitations in the parameters. Simulations of the EFEIOD demonstrate several useful observations. For instance, in the presence of weak repulsions, increasing the length of the particles can increase the output rate. Another observation is that an increase in detachment rates can increase the output rate. In the absence of interactions, we analyze the effect of parameters on the output rate through a theoretical framework and prove that increasing transition [detachment] rates always increase the output rate. In this context further, we consider the model as a control system after introducing two parameters that represent the constant input source and recycling rate of particles, respectively. It has been shown that increasing any of these parameters leads to an increase in the output rate.

Next, Chapter 4 addresses the biological phenomenon of abortions of ribosomes due to collision mechanisms in the gene translation process through a mathematical model called ribosome flow model with extended length and abortions (RFMEOA). It is a deterministic framework that also incorporates the fact that ribosomes cover several codons. We show that the RFMEOA admits a unique steady-state using tools from contraction theory. Furthermore, the effect of parameters in a special case, in which trailing ribosomes undergo abortive termination, is investigated through a theoretical framework. In this respect, we prove that increasing any of the transition [detachment] rates always increases [decreases] the output rate. Next, we observe that an increase in the initiation rate may sometimes lead to a decrease in the output rate.

In Chapter 5, we investigate simultaneous mRNA translation in the cell through

a mathematical network model that encapsulates important biological features such as competition for shared resources and the possibility of attachment/detachment of ribosomes at different sites along the mRNA. We utilize the powerful theory of strictly cooperative dynamical systems with a first integral to prove that the model always converges to a steady state that depends on the parameters and the total number of ribosomes in the network. Furthermore, we study how this steady state is affected by modifying various biological features. One of our findings is that when the number of free ribosomes is small, increasing the drop-off rate in an mRNA that is "jammed" by ribosomes can increase the total protein production rate in the network. This is because the ribosomes that drop off from the jammed mRNA can initiate translation in other mRNAs.

The contents of Chapter 6 describe two large-scale network models called an RFMD network with a pool (RFMDNP) and a generalized network of RFMDs (RFMDN). These models represent the fact that the entry rate of particles into the lanes may be influenced indirectly due to finite resources or directly by feedback/feed-forward mechanisms, respectively. We show that the RFMDNP admits a continuum of linearly ordered steady-state points. Furthermore, an increase in transition rates [site sizes] in an RFMD increases the output rate of this RFMD and the output rate in other RFMDs all increase or decrease. Next, utilizing tools from cooperative theory we show that the RFMDN is globally asymptotically stable. Determining the interconnection weights between the RFMDs to optimize the output rate is a convex optimization problem.

The final Chapter 7 introduces a two-pool RFM network (RFMNTP), where each RFM competes for finite resources at nearby pools. We prove that the RFMNTP is a cooperative irreducible dynamical system that admits a non-trivial first integral. Our theoretical analysis shows that an increase in a transition rate of a site in an RFM has a non-trivial effect on the output rates of the other RFMs. It can lead to any of the scenarios: the output rate of all the other RFMs increase or decrease; an increase in output rates of some of the RFMs; and a decrease in output rates of the other RFMs. Simulations reveal counterintuitive results such as altering transition rates can simultaneously increase the output of some of the RFMs while decreasing another. This emphasizes the non-trivial role of local particle sharing. Finally, these analyses have been extended to understand the network of RFMs with multiple pools.

8.2 Future scopes

Integration of the ribosome flow model into systems biology frameworks can enhance predictive modeling of cellular behavior. By incorporating ribosome dynamics into mathematical models of cellular processes, researchers can gain a more comprehensive understanding of cellular function and behavior. Advancements in experimental techniques such as single-molecule imaging, ribosome profiling, and high-throughput sequencing provide opportunities to validate the RFM and its generalizations.

There are many open problems related to RFM dynamics. One can formulate a more sophisticated mathematical model taking into account the programmed frameshifting of ribosomes while moving along an mRNA template. In the RFM, it has been shown that the steady-state output rate is related to the maximal eigenvalue of a certain matrix with elements that are transition rates of the ribosomes. An intriguing avenue of investigation involves determining if RFMLK can similarly be analyzed using a linear algebraic methodology. One can further generalize the RFMD model to capture more complicated features such as attachment/detachment of particles.

Another possible avenue for further research is modeling a generalized network of RFMs incorporating the feature of attachment/detachment of ribosomes. Prior network models primarily adjusted the entry rate of particles based on pool occupancy, leaving exit rates unchanged. Exploring this direction entails formulating a model to examine network dynamics when RFM outflow to the pool is constrained by pool capacities. Another research problem is assessing the impact of abortive termination on overall production rates across the system. This analysis could be pursued by integrating resource competition phenomena within the RFMEOA framework.

In conclusion, the ribosome flow model holds promise for advancing our understanding of protein synthesis dynamics, gene expression regulation, and cellular behavior. Its future scope encompasses diverse areas of research with the potential to impact various fields and contribute to the development of new therapies and biotechnologies.

References

[1] Francis Crick. Central dogma of molecular biology. *Nature*, 227(5258):561–563, 1970.

[2] B Alberts, A Johnson, J Lewis, M Raff, K Roberts, and P Walter. Molecular biology of the cell, 5th edn, garland science, new york. *ISBN*, 1174808063: 1392, 2007.

[3] Lee D Kapp and Jon R Lorsch. The molecular mechanics of eukaryotic translation. *Annual review of biochemistry*, 73(1):657–704, 2004.

[4] Jonathon Howard. Mechanics of motor proteins. In *Physics of bio-molecules and cells. Physique des biomolécules et des cellules: session LXXV. 2–27 July 2001*, pages 69–94. Springer, 2002.

[5] Debashish Chowdhury, Ludger Santen, and Andreas Schadschneider. Statistical physics of vehicular traffic and some related systems. *Physics Reports*, 329(4-6):199–329, 2000.

[6] Abbas El Gamal and Young-Han Kim. *Network information theory*. Cambridge university press, 2011.

[7] Marina Chekulaeva and Markus Landthaler. Eyes on translation. *Molecular cell*, 63(6):918–925, 2016.

[8] Joshua W Shaevitz, Elio A Abbondanzieri, Robert Landick, and Steven M Block. Backtracking by single rna polymerase molecules observed at near-base-pair resolution. *Nature*, 426(6967):684–687, 2003.

[9] Evgeny Nudler. Rna polymerase backtracking in gene regulation and genome instability. *Cell*, 149(7):1438–1445, 2012.

[10] Yoav Arava, Yulei Wang, John D Storey, Chih Long Liu, Patrick O Brown, and Daniel Herschlag. Genome-wide analysis of mrna translation profiles in saccharomyces cerevisiae. *Proceedings of the National Academy of Sciences*, 100(7):3889–3894, 2003.

[11] Ada Yonath. Ribosomes: ribozymes that survived evolution pressures but is paralyzed by tiny antibiotics. In *Macromolecular Crystallography: Deciphering the Structure, Function and Dynamics of Biological Molecules*, pages 195–208. Springer, 2011.

[12] Stefan Klumpp and Terence Hwa. Traffic patrol in the transcription of ribosomal rna. *RNA biology*, 6(4):392–394, 2009.

[13] Cécile Leduc, Kathrin Padberg-Gehle, Vladimir Varga, Dirk Helbing, Stefan Diez, and Jonathon Howard. Molecular crowding creates traffic jams of kinesin motors on microtubules. *Proceedings of the National Academy of Sciences*, 109 (16):6100–6105, 2012.

[14] Manfred Schliwa and Günther Woehlke. Molecular motors. *Nature*, 422(6933): 759–765, 2003.

[15] Jonathan R Warner and Kerri B McIntosh. How common are extraribosomal functions of ribosomal proteins? *Molecular cell*, 34(1):3–11, 2009.

[16] Jennifer L Ross. The impacts of molecular motor traffic jams. *Proceedings of the National Academy of Sciences*, 109(16):5911–5912, 2012.

[17] Scott A Small, Sabrina Simoes-Spassov, Richard Mayeux, and Gregory A Petsko. Endosomal traffic jams represent a pathogenic hub and therapeutic target in alzheimer's disease. *Trends in neurosciences*, 40(10):592–602, 2017.

[18] Reinhart Heinrich and Tom A Rapoport. Mathematical modelling of translation of mrna in eucaryotes; steady states, time-dependent processes and application to reticulocytest. *Journal of theoretical biology*, 86(2):279–313, 1980.

[19] Alexandra Dana and Tamir Tuller. Efficient manipulations of synonymous mutations for controlling translation rate: an analytical approach. *Journal of Computational Biology*, 19(2):200–231, 2012.

[20] Tobias von der Haar. Mathematical and computational modelling of ribosomal movement and protein synthesis: an overview. *Computational and structural biotechnology journal*, 1(1):e201204002, 2012.

[21] Yun-Bo Zhao and J Krishnan. mrna translation and protein synthesis: an analysis of different modelling methodologies and a new pbn based approach. *BMC systems biology*, 8:1–24, 2014.

[22] Debashish Chowdhury, Andreas Schadschneider, and Katsuhiro Nishinari. Physics of transport and traffic phenomena in biology: from molecular motors and cells to organisms. *Physics of Life reviews*, 2(4):318–352, 2005.

[23] Richard A Blythe and Martin R Evans. Nonequilibrium steady states of matrix-product form: a solver's guide. *Journal of Physics A: Mathematical and Theoretical*, 40(46):R333, 2007.

[24] Shlomit Edri, Eran Gazit, Eyal Cohen, and Tamir Tuller. The rna polymerase flow model of gene transcription. *IEEE Transactions on Biomedical Circuits and Systems*, 8(1):54–64, 2014.

[25] John H Lagergren, John T Nardini, G Michael Lavigne, Erica M Rutter, and Kevin B Flores. Learning partial differential equations for biological transport models from noisy spatio-temporal data. *Proceedings of the Royal Society A*, 476(2234):20190800, 2020.

[26] Jeremy Gunawardena. Models in systems biology: the parameter problem and the meanings of robustness. *Elements of computational systems biology*, pages 19–47, 2010.

[27] Shankar Mukherji, Margaret S Ebert, Grace XY Zheng, John S Tsang, Phillip A Sharp, and Alexander Van Oudenaarden. Micrornas can generate thresholds in target gene expression. *Nature genetics*, 43(9):854–859, 2011.

[28] Ziv Bar-Joseph, Anthony Gitter, and Itamar Simon. Studying and modelling dynamic biological processes using time-series gene expression data. *Nature Reviews Genetics*, 13(8):552–564, 2012.

[29] Domitilla Del Vecchio, Yili Qian, Richard M Murray, and Eduardo D Sontag. Future systems and control research in synthetic biology. *Annual Reviews in Control*, 45:5–17, 2018.

[30] Carolyn T MacDonald, Julian H Gibbs, and Allen C Pipkin. Kinetics of biopolymerization on nucleic acid templates. *Biopolymers: Original Research on Biomolecules*, 6(1):1–25, 1968.

[31] Andreas Schadschneider, Debashish Chowdhury, and Katsuhiro Nishinari. *Stochastic transport in complex systems: from molecules to vehicles*. Elsevier, 2010.

[32] Hadas Zur and Tamir Tuller. Predictive biophysical modeling and understanding of the dynamics of mrna translation and its evolution. *Nucleic acids research*, 44(19):9031–9049, 2016.

[33] Anatoly B Kolomeisky. Asymmetric simple exclusion model with local inhomogeneity. *Journal of Physics A: Mathematical and General*, 31(4):1153, 1998.

[34] Tom Chou and Greg Lakatos. Clustered bottlenecks in mrna translation and protein synthesis. *Physical review letters*, 93(19):198101, 2004.

[35] JiaJia Dong, Beate Schmittmann, and Royce KP Zia. Inhomogeneous exclusion processes with extended objects: The effect of defect locations. *Physical Review E*, 76(5):051113, 2007.

[36] Chris A Brackley, David S Broomhead, M Carmen Romano, and Marco Thiel. A max-plus model of ribosome dynamics during mrna translation. *Journal of Theoretical Biology*, 303:128–140, 2012.

[37] Yun-Bo Zhao and J Krishnan. Probabilistic boolean network modelling and analysis framework for mrna translation. *IEEE/ACM transactions on computational biology and bioinformatics*, 13(4):754–766, 2015.

[38] Shlomi Reuveni, Isaac Meilijson, Martin Kupiec, Eytan Ruppin, and Tamir Tuller. Genome-scale analysis of translation elongation with a ribosome flow model. *PLoS computational biology*, 7(9):e1002127, 2011.

[39] Michael Margaliot and Tamir Tuller. Stability analysis of the ribosome flow model. *IEEE/ACM Transactions on Computational Biology and Bioinformatics*, 9(5):1545–1552, 2012.

[40] Tamir Tuller, Isana Veksler-Lublinsky, Nir Gazit, Martin Kupiec, Eytan Ruppin, and Michal Ziv-Ukelson. Composite effects of gene determinants on the translation speed and density of ribosomes. *Genome biology*, 12(11):1–18, 2011.

[41] John A Jacquez and Carl P Simon. Qualitative theory of compartmental systems. *Siam Review*, 35(1):43–79, 1993.

[42] Fred Brauer. Compartmental models in epidemiology. *Mathematical epidemiology*, pages 19–79, 2008.

[43] J Cividini, HJ Hilhorst, and C Appert-Rolland. Exact domain wall theory for deterministic tasep with parallel update. *Journal of Physics A: Mathematical and Theoretical*, 47(22):222001, 2014.

[44] Gilad Poker, Yoram Zarai, Michael Margaliot, and Tamir Tuller. Maximizing protein translation rate in the non-homogeneous ribosome flow model: a convex optimization approach. *Journal of The Royal Society Interface*, 11 (100):20140713, 2014.

[45] Yoram Zarai, Oz Mendel, and Michael Margaliot. Analyzing linear communication networks using the ribosome flow model. In *2015 IEEE International Conference on Computer and Information Technology;*

Ubiquitous Computing and Communications; Dependable, Autonomic and Secure Computing; Pervasive Intelligence and Computing, pages 755–761. IEEE, 2015.

[46] Yoram Zarai, Michael Margaliot, and Tamir Tuller. Optimal down regulation of mrna translation. *Scientific reports*, 7(1):41243, 2017.

[47] Clark Robinson. *Dynamical systems: stability, symbolic dynamics, and chaos*. CRC press, 1998.

[48] Michael Margaliot, Eduardo D Sontag, and Tamir Tuller. Entrainment to periodic initiation and transition rates in a computational model for gene translation. *PloS one*, 9(5):e96039, 2014.

[49] Alon Raveh, Michael Margaliot, Eduardo D Sontag, and Tamir Tuller. A model for competition for ribosomes in the cell. *Journal of The Royal Society Interface*, 13(116):20151062, 2016.

[50] Hal L Smith. *Monotone dynamical systems: an introduction to the theory of competitive and cooperative systems: an introduction to the theory of competitive and cooperative systems*. Number 41. American Mathematical Soc., 2008.

[51] John Smillie. Competitive and cooperative tridiagonal systems of differential equations. *SIAM journal on mathematical analysis*, 15(3):530–534, 1984.

[52] Jerrold E Marsden and Anthony Tromba. *Vector calculus*. Macmillan, 2003.

[53] Winfried Lohmiller and Jean-Jacques E Slotine. On contraction analysis for non-linear systems. *Automatica*, 34(6):683–696, 1998.

[54] Giovanni Russo, Mario Di Bernardo, and Eduardo D Sontag. Global entrainment of transcriptional systems to periodic inputs. *PLoS computational biology*, 6(4):e1000739, 2010.

[55] Zahra Aminzare and Eduardo D Sontagy. Contraction methods for nonlinear systems: A brief introduction and some open problems. In *53rd IEEE Conference on Decision and Control*, pages 3835–3847. IEEE, 2014.

[56] Michael Margaliot, Eduardo D Sontag, and Tamir Tuller. Contraction after small transients. *Automatica*, 67:178–184, 2016.

[57] David Richeson and Jim Wiseman. A fixed point theorem for bounded dynamical systems. *Illinois Journal of Mathematics*, 46(2):491–495, 2002.

[58] LA Zadeh. Desoer, ca: Linear system theory–the state space approach, 1963.

[59] Evgeni V Nikolaev, Sahand Jamal Rahi, and Eduardo D Sontag. Subharmonics and chaos in simple periodically forced biomolecular models. *Biophysical journal*, 114(5):1232–1240, 2018.

[60] Gilad Poker, Michael Margaliot, and Tamir Tuller. Sensitivity of mrna translation. *Scientific Reports*, 5(1):12795, 2015.

[61] Michael Margaliot and Tamir Tuller. Ribosome flow model with positive feedback. *Journal of the Royal Society Interface*, 10(85):20130267, 2013.

[62] Yoram Zarai, Michael Margaliot, and Tamir Tuller. Maximizing protein translation rate in the ribosome flow model: the homogeneous case. *IEEE/ACM Transactions on Computational Biology and Bioinformatics*, 11 (6):1184–1195, 2014.

[63] Yoram Zarai, Alexander Ovseevich, and Michael Margaliot. Optimal translation along a circular mrna. *Scientific reports*, 7(1):1–16, 2017.

[64] Michael Margaliot, Wasim Huleihel, and Tamir Tuller. Variability in mrna translation: a random matrix theory approach. *Scientific Reports*, 11(1):1–14, 2021.

[65] Hubert Stanley Wall. *Analytic theory of continued fractions*. Courier Dover Publications, 2018.

[66] Z Bai and Jack Silverstein. *Spectral Analysis of Large Dimensional Random Matrices*. 2010. ISBN 978-1-4419-0660-1. doi: 10.1007/978-1-4419-0661-8.

[67] Yoram Zarai, Michael Margaliot, and Anatoly B Kolomeisky. A deterministic model for one-dimensional excluded flow with local interactions. *Plos one*, 12 (8):e0182074, 2017.

[68] Yoram Zarai, Michael Margaliot, and Tamir Tuller. A deterministic mathematical model for bidirectional excluded flow with langmuir kinetics. *PloS one*, 12(8):e0182178, 2017.

[69] Yoram Zarai, Michael Margaliot, and Tamir Tuller. Ribosome flow model with extended objects. *Journal of The Royal Society Interface*, 14(135):20170128, 2017.

[70] Eyal Bar-Shalom, Alexander Ovseevich, and Michael Margaliot. Ribosome flow model with different site sizes. *SIAM Journal on Applied Dynamical Systems*, 19(1):541–576, 2020.

[71] Jonathan R Warner. The economics of ribosome biosynthesis in yeast. *Trends in biochemical sciences*, 24(11):437–440, 1999.

[72] Jesper Vind, Michael A Sørensen, Michael D Rasmussen, and Steen Pedersen. Synthesis of proteins in escherichia coli is limited by the concentration of free ribosomes: expression from reporter genes does not always reflect functional mrna levels. *Journal of molecular biology*, 231(3):678–688, 1993.

[73] Gretchen A Rice, Michael J Chamberlin, and Caroline M Kane. Contacts between mammalian rna polymerase ii and the template dna in a ternary elongation complex. *Nucleic acids research*, 21(1):113–118, 1993.

[74] Michael A Gilchrist and Andreas Wagner. A model of protein translation including codon bias, nonsense errors, and ribosome recycling. *Journal of theoretical biology*, 239(4):417–434, 2006.

[75] Pierre Bonnin, Norbert Kern, Neil T Young, Ian Stansfield, and M Carmen Romano. Novel mrna-specific effects of ribosome drop-off on translation rate and polysome profile. *PLoS computational biology*, 13(5):e1005555, 2017.

[76] Christopher UT Hellen and Peter Sarnow. Internal ribosome entry sites in eukaryotic mrna molecules. *Genes & development*, 15(13):1593–1612, 2001.

[77] Wouter H Roos, Otger Campas, Fabien Montel, Günther Woehlke, Joachim P Spatz, Patricia Bassereau, and Giovanni Cappello. Dynamic kinesin-1 clustering on microtubules due to mutually attractive interactions. *Physical biology*, 5(4):046004, 2008.

[78] Cecile Appert-Rolland, Maximilian Ebbinghaus, and Ludger Santen. Intracellular transport driven by cytoskeletal motors: General mechanisms and defects. *Physics Reports*, 593:1–59, 2015.

[79] Peixun Han, Yuichi Shichino, Tilman Schneider-Poetsch, Mari Mito, Satoshi Hashimoto, Tsuyoshi Udagawa, Kenji Kohno, Minoru Yoshida, Yuichiro Mishima, Toshifumi Inada, et al. Genome-wide survey of ribosome collision. *Cell reports*, 31(5):107610, 2020.

[80] Michael A Ferrin and Arvind R Subramaniam. Kinetic modeling predicts a stimulatory role for ribosome collisions at elongation stall sites in bacteria. *Elife*, 6:e23629, 2017.

[81] Celine Sin, Davide Chiarugi, and Angelo Valleriani. Quantitative assessment of ribosome drop-off in e. coli. *Nucleic acids research*, 44(6):2528–2537, 2016.

[82] William J Blake, Mads Kærn, Charles R Cantor, and James J Collins. Noise in eukaryotic gene expression. *Nature*, 422(6932):633–637, 2003.

[83] Roger A Horn and Charles R Johnson. *Matrix analysis*. Cambridge university press, 2012.

[84] Martin Haenggi. Outage, local throughput, and capacity of random wireless networks. *IEEE Transactions on Wireless Communications*, 8(8):4350–4359, 2009. doi: 10.1109/TWC.2009.090105.

[85] Silvia Noschese, Lionello Pasquini, and Lothar Reichel. Tridiagonal toeplitz matrices: properties and novel applications. *Numerical linear algebra with applications*, 20(2):302–326, 2013.

[86] Nicolaas Godfried Van Kampen. *Stochastic processes in physics and chemistry*, volume 1. Elsevier, 1992.

[87] Gabriella Piazzesi, Leonardo Lucii, and Vincenzo Lombardi. The size and the speed of the working stroke of muscle myosin and its dependence on the force, 2002.

[88] Ivo A Telley, Peter Bieling, and Thomas Surrey. Obstacles on the microtubule reduce the processivity of kinesin-1 in a minimal in vitro system and in cell extract. *Biophysical journal*, 96(8):3341–3353, 2009.

[89] Hamid Teimouri, Anatoly B Kolomeisky, and Kareem Mehrabiani. Theoretical analysis of dynamic processes for interacting molecular motors. *Journal of Physics A: Mathematical and Theoretical*, 48(6):065001, 2015.

[90] Alex H Williams, Cian O'Donnell, Terrence J Sejnowski, and Timothy O'Leary. Dendritic trafficking faces physiologically critical speed-precision tradeoffs. *Elife*, 5:e20556, 2016.

[91] Tripti Midha, Luiza VF Gomes, Anatoly B Kolomeisky, and Arvind Kumar Gupta. Theoretical investigations of asymmetric simple exclusion processes for interacting oligomers. *Journal of Statistical Mechanics: Theory and Experiment*, 2018(5):053209, 2018.

[92] Karsten Kruse and Frank Jülicher. Oscillations in cell biology. *Current opinion in cell biology*, 17(1):20–26, 2005.

[93] Tamir Tuller, Yedael Y Waldman, Martin Kupiec, and Eytan Ruppin. Translation efficiency is determined by both codon bias and folding energy. *Proceedings of the national academy of sciences*, 107(8):3645–3650, 2010.

[94] Sumita Das, Tomoki P Terada, and Masaki Sasai. Single-molecular and ensemble-level oscillations of cyanobacterial circadian clock. *Biophysics and physicobiology*, 15:136–150, 2018.

[95] Anze Zupanic, Catherine Meplan, Sushma N Grellscheid, John C Mathers, Tom BL Kirkwood, John E Hesketh, and Daryl P Shanley. Detecting translational regulation by change point analysis of ribosome profiling data sets. *RNA*, 20(10):1507–1518, 2014.

[96] Jeroen R Mesters, Anatolij P Potapov, J Martien De Graaf, and Barend Kraal. Synergism between the gtpase activities of ef-tu· gtp and ef-g· gtp on empty ribosomes: Elongation factors as stimulators of the ribosomal oscillation between two conformations. *Journal of molecular biology*, 242(5):644–654, 1994.

[97] Yoram Zarai and Tamir Tuller. Computational analysis of the oscillatory behavior at the translation level induced by mrna levels oscillations due to finite intracellular resources. *PLoS computational biology*, 14(4):e1006055, 2018.

[98] Milana Frenkel-Morgenstern, Tamar Danon, Thomas Christian, Takao Igarashi, Lydia Cohen, Ya-Ming Hou, and Lars Juhl Jensen. Genes adopt non-optimal codon usage to generate cell cycle-dependent oscillations in protein levels. *Molecular systems biology*, 8(1):572, 2012.

[99] Kelly Dong, Earl Goyarts, Antonella Rella, Edward Pelle, Yung Hou Wong, and Nadine Pernodet. Age associated decrease of mt-1 melatonin receptor in human dermal skin fibroblasts impairs protection against uv-induced dna damage. *International journal of molecular sciences*, 21(1):326, 2020.

[100] Ahmad S Khalil and James J Collins. Synthetic biology: applications come of age. *Nature Reviews Genetics*, 11(5):367–379, 2010.

[101] Frank Buttgereit and Martin D Brand. A hierarchy of atp-consuming processes in mammalian cells. *Biochemical Journal*, 312(1):163–167, 1995.

[102] Nicholas T Ingolia, Sina Ghaemmaghami, John RS Newman, and Jonathan S Weissman. Genome-wide analysis in vivo of translation with nucleotide resolution using ribosome profiling. *science*, 324(5924):218–223, 2009.

[103] Shiping Zhang, Emanuel Goldman, and Geoffrey Zubay. Clustering of low usage codons and ribosome movement. *Journal of theoretical biology*, 170(4): 339–354, 1994.

[104] Tamir Tuller, Asaf Carmi, Kalin Vestsigian, Sivan Navon, Yuval Dorfan, John Zaborske, Tao Pan, Orna Dahan, Itay Furman, and Yitzhak Pilpel. An evolutionarily conserved mechanism for controlling the efficiency of protein translation. *Cell*, 141(2):344–354, 2010.

[105] Namiko Mitarai, Kim Sneppen, and Steen Pedersen. Ribosome collisions and translation efficiency: optimization by codon usage and mrna destabilization. *Journal of molecular biology*, 382(1):236–245, 2008.

[106] Alon Diament, Anna Feldman, Elisheva Schochet, Martin Kupiec, Yoav Arava, and Tamir Tuller. The extent of ribosome queuing in budding yeast. *PLoS computational biology*, 14(1):e1005951, 2018.

[107] J Ross Buchan and Ian Stansfield. Halting a cellular production line: responses to ribosomal pausing during translation. *Biology of the Cell*, 99(9):475–487, 2007.

[108] Ziqing Liu, Olivia Chen, J Blake Joseph Wall, Michael Zheng, Yang Zhou, Li Wang, Haley Ruth Vaseghi, Li Qian, and Jiandong Liu. Systematic comparison of 2a peptides for cloning multi-genes in a polycistronic vector. *Scientific reports*, 7(1):2193, 2017.

[109] Lisa M Lindqvist, Kristofferson Tandoc, Ivan Topisirovic, and Luc Furic. Cross-talk between protein synthesis, energy metabolism and autophagy in cancer. *Current opinion in genetics & development*, 48:104–111, 2018.

[110] Bhavya Mishra, Gunter M Schütz, and Debashish Chowdhury. Slip of grip of a molecular motor on a crowded track: Modeling shift of reading frame of ribosome on rna template. *Europhysics Letters*, 114(6):68005, 2016.

[111] Gong Zhang, Ivan Fedyunin, Oskar Miekley, Angelo Valleriani, Alessandro Moura, and Zoya Ignatova. Global and local depletion of ternary complex limits translational elongation. *Nucleic acids research*, 38(14):4778–4787, 2010.

[112] Egor Svidritskiy, Gabriel Demo, and Andrei A Korostelev. Mechanism of premature translation termination on a sense codon. *Journal of Biological Chemistry*, 293(32):12472–12479, 2018.

[113] Sinéad O'Loughlin, Mark C Capece, Mariia Klimova, Norma M Wills, Arthur Coakley, Ekaterina Samatova, Patrick BF O'Connor, Gary Loughran, Jonathan S Weissman, Pavel V Baranov, et al. Polysomes bypass a 50-nucleotide coding gap less efficiently than monosomes due to attenuation

of a 5' mrna stem–loop and enhanced drop-off. *Journal of molecular biology*, 432(16):4369–4387, 2020.

[114] Min Shi, Heng Zhang, Lantian Wang, Changlan Zhu, Ke Sheng, Yanhua Du, Ke Wang, Anusha Dias, She Chen, Malcolm Whitman, et al. Premature termination codons are recognized in the nucleus in a reading-frame-dependent manner. *Cell discovery*, 1(1):1–20, 2015.

[115] CG Kurland. Translational accuracy and the fitness of bacteria. *Annual review of genetics*, 26(1):29–50, 1992.

[116] Heungwon Park and Arvind R Subramaniam. Inverted translational control of eukaryotic gene expression by ribosome collisions. *PLoS biology*, 17(9): e3000396, 2019.

[117] Elina Nürenberg and Robert Tampé. Tying up loose ends: ribosome recycling in eukaryotes and archaea. *Trends in biochemical sciences*, 38(2):64–74, 2013.

[118] Maxim A Skabkin, Olga V Skabkina, Christopher UT Hellen, and Tatyana V Pestova. Reinitiation and other unconventional posttermination events during eukaryotic translation. *Molecular cell*, 51(2):249–264, 2013.

[119] E Marshall, I Stansfield, and MC Romano. Ribosome recycling induces optimal translation rate at low ribosomal availability. *Journal of the Royal Society Interface*, 11(98):20140589, 2014.

[120] Philip J Farabaugh. Programmed translational frameshifting. *Microbiological reviews*, 60(1):103–134, 1996.

[121] Szymon Juszkiewicz, Shaun H Speldewinde, Li Wan, Jesper Q Svejstrup, and Ramanujan S Hegde. The asc-1 complex disassembles collided ribosomes. *Molecular cell*, 79(4):603–614, 2020.

[122] Taolan Zhao, Yan-Ming Chen, Yu Li, Jia Wang, Siyu Chen, Ning Gao, and Wenfeng Qian. Disome-seq reveals widespread ribosome collisions that promote cotranslational protein folding. *Genome biology*, 22(1):1–35, 2021.

[123] Carrie L Simms, Liewei L Yan, and Hani S Zaher. Ribosome collision is critical for quality control during no-go decay. *Molecular cell*, 68(2):361–373, 2017.

[124] Nicholas T Ingolia, Gloria A Brar, Silvia Rouskin, Anna M McGeachy, and Jonathan S Weissman. The ribosome profiling strategy for monitoring translation in vivo by deep sequencing of ribosome-protected mrna fragments. *Nature protocols*, 7(8):1534–1550, 2012.

[125] Chris A Brackley, M Carmen Romano, and Marco Thiel. The dynamics of supply and demand in mrna translation. *PLoS Computational Biology*, 7(10): e1002203, 2011.

[126] Andrew E Firth and Ian Brierley. Non-canonical translation in rna viruses. *The Journal of general virology*, 93(Pt 7):1385, 2012.

[127] Derek Walsh, Michael B Mathews, and Ian Mohr. Tinkering with translation: protein synthesis in virus-infected cells. *Cold Spring Harbor perspectives in biology*, 5(1):a012351, 2013.

[128] Nicolas Locker, Nathalie Chamond, and Bruno Sargueil. A conserved structure within the hiv gag open reading frame that controls translation initiation directly recruits the 40s subunit and eif3. *Nucleic acids research*, 39(6): 2367–2377, 2011.

[129] SM Ngoi, AC Chien, and CGL Lee. Exploiting internal ribosome entry sites in gene therapy vector design. *Current gene therapy*, 4(1):15–31, 2004.

[130] Katharina Schubert, Evangelos D Karousis, Ahmad Jomaa, Alain Scaiola, Blanca Echeverria, Lukas-Adrian Gurzeler, Marc Leibundgut, Volker Thiel, Oliver Mühlemann, and Nenad Ban. Sars-cov-2 nsp1 binds the ribosomal mrna channel to inhibit translation. *Nature structural & molecular biology*, 27 (10):959–966, 2020.

[131] Hadas Zur, Rachel Cohen-Kupiec, Sophie Vinokour, and Tamir Tuller. Algorithms for ribosome traffic engineering and their potential in improving host cells' titer and growth rate. *Scientific reports*, 10(1):21202, 2020.

[132] Janusz Mierczyński. Strictly cooperative systems with a first integral. *SIAM journal on mathematical analysis*, 18(3):642–646, 1987.

[133] Maxim V Gerashchenko, Mikhail V Nesterchuk, Elena M Smekalova, Joao A Paulo, Piotr S Kowalski, Kseniya A Akulich, Roman Bogorad, Sergey E Dmitriev, Steven Gygi, Timofei Zatsepin, et al. Translation elongation factor 2 depletion by sirna in mouse liver leads to mtor-independent translational upregulation of ribosomal protein genes. *Scientific reports*, 10(1):15473, 2020.

[134] RKP Zia, JJ Dong, and B Schmittmann. Modeling translation in protein synthesis with tasep: A tutorial and recent developments. *Journal of Statistical Physics*, 144(2):405–428, 2011.

[135] DA Adams, B Schmittmann, and RKP Zia. Far-from-equilibrium transport with constrained resources. *Journal of Statistical Mechanics: Theory and Experiment*, 2008(06):P06009, 2008.

[136] Jingwei Li and Yunxin Zhang. Translation with frameshifting of ribosome along mrna transcript. *arXiv preprint arXiv:1502.02109*, 2015.

[137] Noam Stern-Ginossar, Sunnie R Thompson, Michael B Mathews, and Ian Mohr. Translational control in virus-infected cells. *Cold Spring Harbor perspectives in biology*, 11(3):a033001, 2019.

[138] Xiaoli Qin and Peter Sarnow. Preferential translation of internal ribosome entry site-containing mrnas during the mitotic cycle in mammalian cells. *Journal of Biological Chemistry*, 279(14):13721–13728, 2004.

[139] Alex V Kochetov, Shandar Ahmad, Vladimir Ivanisenko, Oxana A Volkova, Nikolay A Kolchanov, and Akinori Sarai. uorfs, reinitiation and alternative translation start sites in human mrnas. *FEBS letters*, 582(9):1293–1297, 2008.

[140] Michael Y Li and James S Muldowney. Global stability for the seir model in epidemiology. *Mathematical biosciences*, 125(2):155–164, 1995.

[141] Chengshuai Wu, Ilya Kanevskiy, and Michael Margaliot. k-contraction: Theory and applications. *Automatica*, 136:110048, 2022.

[142] David Angeli and Eduardo D Sontag. Monotone control systems. *IEEE Transactions on automatic control*, 48(10):1684–1698, 2003.

[143] Baorong Tang, Yang Kuang, and Hal Smith. Strictly nonautonomous cooperative system with a first integral. *SIAM journal on mathematical analysis*, 24(5):1331–1339, 1993.

[144] Renana Sabi and Tamir Tuller. A comparative genomics study on the effect of individual amino acids on ribosome stalling. *BMC genomics*, 16:1–12, 2015.

[145] Kyuri Lee, Soo Young Kim, Yunmi Seo, Hyokyung Kwon, Young Jik Kwon, and Hyukjin Lee. Multicistronic ivt mrna for simultaneous expression of multiple fluorescent proteins. *Journal of Industrial and Engineering Chemistry*, 80:770–777, 2019.

[146] Ana E Higareda-Mendoza and Marco A Pardo-Galván. Expression of human eukaryotic initiation factor 3f oscillates with cell cycle in a549 cells and is essential for cell viability. *Cell division*, 5(1):1–13, 2010.

[147] M Ali Al-Radhawi, Michael Margaliot, and Eduardo D Sontag. Maximizing average throughput in oscillatory biochemical synthesis systems: an optimal control approach. *Royal Society open science*, 8(9):210878.

[148] Aditi Jain, Michael Margaliot, and Arvind Kumar Gupta. Large-scale mrna translation and the intricate effects of competition for the finite pool of ribosomes. *Journal of the Royal Society Interface*, 19(188):20220033, 2022.

[149] Itzik Nanikashvili, Yoram Zarai, Alexander Ovseevich, Tamir Tuller, and Michael Margaliot. Networks of ribosome flow models for modeling and analyzing intracellular traffic. *Scientific reports*, 9(1):1–14, 2019.

[150] Ying-Cheng Lai and Raimond L Winslow. Extreme sensitive dependence on parameters and initial conditions in spatio-temporal chaotic dynamical systems. *Physica D: Nonlinear Phenomena*, 74(3-4):353–371, 1994.

[151] Jiang Ji-Fa. Periodic monotone systems with an invariant function. *SIAM Journal on Mathematical Analysis*, 27(6):1738–1744, 1996.

[152] Harry L Swinney. Observations of order and chaos in nonlinear systems. *Physica D: Nonlinear Phenomena*, 7(1-3):3–15, 1983.

[153] Janusz Mierczyński. Cooperative irreducible systems of ordinary differential equations with first integral. *arXiv preprint arXiv:1208.4697*, 2012.

[154] Janusz Mierczyński. A class of strongly cooperative systems without compactness. In *Colloquium Mathematicae*, volume 62, pages 43–47, 1991.

[155] Jiang Ji-Fa. On the global stability of cooperative systems. *Bulletin of the London Mathematical Society*, 26(5):455–458, 1994.

[156] Stephen Boyd, Stephen P Boyd, and Lieven Vandenberghe. *Convex optimization*. Cambridge university press, 2004.

[157] Rangaswami Balakrishnan and Kanna Ranganathan. *A textbook of graph theory*. Springer Science & Business Media, 2012.

[158] Gordon Churchward, Hans Bremer, and R Young. Transcription in bacteria at different dna concentrations. *Journal of bacteriology*, 150(2):572–581, 1982.

[159] Andras Gyorgy and Domitilla Del Vecchio. Limitations and trade-offs in gene expression due to competition for shared cellular resources. In *53rd IEEE Conference on Decision and Control*, pages 5431–5436. IEEE, 2014.

[160] Timothy Frei, Federica Cella, Fabiana Tedeschi, Joaquín Gutiérrez, Guy-Bart Stan, Mustafa Khammash, and Velia Siciliano. Characterization and mitigation of gene expression burden in mammalian cells. *Nature communications*, 11(1):4641, 2020.

[161] Yili Qian and Domitilla Del Vecchio. Effective interaction graphs arising from resource limitations in gene networks. In *2015 American Control Conference (ACC)*, pages 4417–4423. IEEE, 2015.

[162] Alexander PS Darlington, Juhyun Kim, José I Jiménez, and Declan G Bates. Dynamic allocation of orthogonal ribosomes facilitates uncoupling of co-expressed genes. *Nature communications*, 9(1):695, 2018.

[163] Meesoon Ha and Marcel Den Nijs. Macroscopic car condensation in a parking garage. *Physical Review E*, 66(3):036118, 2002.

[164] Dietrich E Wolf, Michael Schreckenberg, and Achim Bachem. *Traffic and granular flow*. World Scientific, 1996.

[165] Arvind Giridhar and PR Kumar. Scheduling automated traffic on a network of roads. *IEEE Transactions on Vehicular Technology*, 55(5):1467–1474, 2006.

[166] L Jonathan Cook and RKP Zia. Competition for finite resources. *Journal of Statistical Mechanics: Theory and Experiment*, 2012(05):P05008, 2012.

[167] William H Mather, Jeff Hasty, Lev S Tsimring, and Ruth J Williams. Translational cross talk in gene networks. *Biophysical journal*, 104(11): 2564–2572, 2013.

[168] Renana Sabi and Tamir Tuller. Modelling and measuring intracellular competition for finite resources during gene expression. *Journal of the Royal Society Interface*, 16(154):20180887, 2019.

[169] L Jonathan Cook and RKP Zia. Feedback and fluctuations in a totally asymmetric simple exclusion process with finite resources. *Journal of Statistical Mechanics: Theory and Experiment*, 2009(02):P02012, 2009.

[170] Philip Greulich, Luca Ciandrini, Rosalind J Allen, and M Carmen Romano. Mixed population of competing totally asymmetric simple exclusion processes with a shared reservoir of particles. *Physical Review E*, 85(1):011142, 2012.

[171] Izaak Neri, Norbert Kern, and Andrea Parmeggiani. Totally asymmetric simple exclusion process on networks. *Physical review letters*, 107(6):068702, 2011.

[172] Tom Chou, Kirone Mallick, and Royce KP Zia. Non-equilibrium statistical mechanics: from a paradigmatic model to biological transport. *Reports on progress in physics*, 74(11):116601, 2011.

[173] JJ Dong, B Schmittmann, and RKP Zia. Towards a model for protein production rates. *Journal of Statistical Physics*, 128:21–34, 2007.

[174] Michael Herty, Axel Klar, and AK Singh. An ode traffic network model. *Journal of computational and applied mathematics*, 203(2):419–436, 2007.

[175] Arvind Kumar Gupta and Poonam Redhu. Analyses of the driver's anticipation effect in a new lattice hydrodynamic traffic flow model with passing. *Nonlinear Dynamics*, 76:1001–1011, 2014.

[176] Md Anowar Hossain and Jun Tanimoto. A microscopic traffic flow model for sharing information from a vehicle to vehicle by considering system time delay effect. *Physica A: Statistical Mechanics and its Applications*, 585:126437, 2022.

[177] Jared Miller, M Ali Al-Radhawi, and Eduardo D Sontag. Mediating ribosomal competition by splitting pools. *IEEE Control Systems Letters*, 5(5):1555–1560, 2020.

[178] Steven M Reppert and David R Weaver. Coordination of circadian timing in mammals. *Nature*, 418(6901):935–941, 2002.

[179] Michael Polymenis and Rodolfo Aramayo. Translate to divide: control of the cell cycle by protein synthesis. *Microbial Cell*, 2(4):94, 2015.

[180] Philipp Eser, Carina Demel, Kerstin C Maier, Björn Schwalb, Nicole Pirkl, Dietmar E Martin, Patrick Cramer, and Achim Tresch. Periodic mrna synthesis and degradation co-operate during cell cycle gene expression. *Molecular systems biology*, 10(1):717, 2014.

[181] William H Walker, James C Walton, A Courtney DeVries, and Randy J Nelson. Circadian rhythm disruption and mental health. *Translational psychiatry*, 10 (1):28, 2020.

[182] Yuri A Kuznetsov and Yuri A Kuznetsov. Numerical analysis of bifurcations. *Elements of applied bifurcation theory*, pages 505–585, 2004.